# A Microparticle Engineering Approach to Enhance the Potency of Mesenchymal Stem Cells

by

James Allen Ankrum

M.Phil, Engineering Design
Cambridge University, 2008

B.S.E, Biomedical Engineering
University of Iowa, 2007



SUBMITTED TO THE DIVISION OF HEALTH SCIENCES AND TECHNOLOGY
IN PARTIAL FULFILLMENT OF THE REQUIREMENTS FOR THE DEGREE OF

DOCTOR OF PHILOSOPHY IN MEDICAL ENGINEERING
AT THE
MASSACHUSETTS INSTITUTE OF TECHNOLOGY

September 2013



Signature of Author .....
Division of Health Sciences & Technology
August 7, 2013

Certified by .....
Jeffrey M. Karp
Associate Professor of Medicine, Harvard Medical School
Thesis Supervisor

Accepted by.....
Emery N. Brown
MD, PhD/Director, Harvard-MIT Program in Health Sciences and Technology/Professor of Computational Neuroscience and Health Sciences and Technology

# A Microparticle Engineering Approach to Enhance the Potency of Mesenchymal Stem Cells

by

James Allen Ankrum

M.Phil, Engineering Design, Cambridge University, 2008

B.S.E, Biomedical Engineering, University of Iowa, 2007

SUBMITTED TO THE DIVISION OF HEALTH SCIENCES AND TECHNOLOGY ON AUGUST 7, 2013 IN PARTIAL FULFILLMENT OF THE REQUIREMENTS FOR THE DEGREE OF DOCTOR OF PHILOSOPHY IN MEDICAL ENGINEERING

ABSTRACT

Cell-based therapies, which rely on transplanted cells to restore function to damaged tissues, are currently under investigation in clinical trials. Stem and progenitor cells, including mesenchymal stem cells (MSCs), have shown potential in pre-clinical models to treat diseases ranging from connective tissue defects, through differentiating into bone or cartilage forming cells, to inflammatory conditions, through suppressing activated immune cells. While the ability of stem cells to differentiate into multiple lineages, secrete trophic factors, and modulate inflammatory processes has made them applicable to many diseases, these diverse functions also pose challenges in controlling their phenotype. In this thesis a new platform technology to influence the phenotype of cells is described and used to solve three critical challenges in MSC-based therapies, controlling MSC differentiation, tracking cells, and enhancing MSC's immunomodulatory potency. MSCs were found to efficiently and stably internalize micron-sized biodegradable particles. The platform can be tuned to specific applications through incorporation of phenotype altering drugs or other payloads into particles. In the first study, particles were loaded with a small molecule drug, dexamethasone (DEX), that induces MSC osteogenic differentiation. Modification of MSCs with DEX-particles resulted in differentiation of particle-laden cells to the same extent as those grown in osteogenic media. Furthermore, DEX was released from the cells in sufficient quantities to influence neighboring and distant cells demonstrating the particle platform can influence both the modified cell and its microenvironment. Next, the platform was adapted to address the need for longitudinal tracking of MSCs. Loading iron oxide nanoparticles in the microparticles resulted in enhanced tracking of MSCs by MRI from 6 days with nanoparticles alone to beyond 12 days with iron oxide microparticles. Finally, the novel discovery that glucocorticoid steroids significantly increase the immunomodulatory potency of MSCs by up-regulating expression of indoleamine-2,3-dioxygenase (IDO) is reported. Loading MSCs with particles containing the glucocorticoid steroid, budesonide, doubled their potency in suppressing activated peripheral blood mononuclear cell co-cultures in an IDO dependent manner. While the platform presented here was used to control, track, and augment MSCs, it can easily be tailored to control the function of other therapeutically relevant cells to develop next-generation cell-based therapies.

Thesis Supervisor: Jeffrey M Karp
Title: Associate Professor of Medicine, Harvard Medical School

BIOGRAPHICAL NOTE

Throughout my PhD I had the privilege of working on a breadth of projects, both in MIT courses and in Prof. Jeffrey Karp's research lab. A number of fellowships and awards, along with my advisor's support, allowed me to explore the full breadth of my interests without obligation to work on a specific grant. The list of awards, publications, patents, book chapters, and presentations below represent the sum total of my public contribution to science during my PhD. While the majority of the topics listed below are discussed in great detail in the chapters and appendices of the thesis that follows, it is my hope that this list of references will be of use in locating the published manuscripts and acknowledging the peers and mentors that made this work possible.

**Honors & Awards**

- 2011 & 2012 Hugh Hampton Young Memorial Fellowship
- 2011 Lindau Nobel Laureate Participant
- 2011 MIT 100K Elevator Pitch Semifinalist (Life Sciences and Products and Services)
- 2008-2011 NSF Graduate Research Fellowship
- 2008 MIT Presidential Fellowship
- 2008 HST Medical Engineering Fellowship

**Publications**

1. **Ankrum J**, Ong, JF, Karp J. *MSCs are not immune privileged, but immune evasive: A historical perspective*. Submitted.

2. **Ankrum J**, Miranda O, Sarkar D, Xu C, Karp J. *A protocol for modification of mesenchymal stem cells with intracellular microparticles*. Submitted.

3. **Ankrum J**, Dastidar R, Ong, JF, Levy O, Karp J. *Enhanced Mesenchymal Stem cell immunomodulatory potency through intracellular budesonide microparticles*. Submitted.

4. Vemula PK, Wiradharma N, **Ankrum J**, Miranda OR, John G, Karp JM. *Prodrugs as self-assembled hydrogels: a new paradigm for biomaterials*. Current Opinion in Biotechnology (2013), 24, 1-9 (Invited review).

5. Cho W, **Ankrum J**, Guo D, Chester S, Kashyap A, Campbell G, Rijal R, Wood R, Karnik R, Langer R, Karp J. *Microstructured Barbs on the North American Porcupine Quill Enable Easy Tissue Penetration and Difficult Removal. Proceedings of the National Academy of Sciences* (2012), 109(52), 21289-21294.
   Work towards mimicking porcupine quills featured as cover image of PNAS and in media stories on Science Now, Nature, NPR, Discovery, Popular Mechanics, The Smithsonian, BBC, and the MIT homepage.

6. Teo G, **Ankrum** J, Martinelli R, Boetto S, Simms K, Sciuto T, Dvorak A, Karp J, Carman C. *Multipotent Stromal Cells Transmigrate Between and Directly Through TNF-a-activated Endothelial Cells*. Stem Cells (2012), 30(11), pp 2472-2486.

7. Xu CJ, Miranda-Nieves D, **Ankrum J**, Matthiesen M, Phillips J, Roes I, Wojtkiewicz G, Kultima J, Zhao W, Vemula P, Lin C, Nahrendorf M, Karp J. *Tracking Mesenchymal Stem Cells with Iron Oxide Nanoparticle Loaded Poly(lactide-co-glycolide) Microparticles*. Nano Letters (2012), 12(8), pp 4131–4139.

8. Xu CJ, Mu L, Roes I, Miranda-Nieves D, Nahrendorf M, **Ankum** J, Zhao W, Karp JM. *Nanoparticle-based Monitoring of Cell Therapy*. Nanotechnology (2011) vol 22(49) pp 494001.

9. **Ankrum J,** Olechowski A, Canseco J, Greenblatt E, Roberts M. *Nasogastric Tube Design to Reduce Clogging and Simplify Flushing*. Journal of Medical Devices (2011) vol 5(2) pp 027510.

10. Sarkar D*, **Ankrum J***, Teo G, Carman C, Karp J. *Cellular and Extracellular Programming of Cell Fate through engineered intracrine-, paracrine-, and endocrine-like mechanisms*. Biomaterials (2011) vol. 32(11) pp. 2053-61.
*__co-first authors__. Work toward programmable cells featured in 2011 press release that in turn was published by funder (NSF) and resulted in many media stories.

11. **Ankrum J**, Karp J. *Mesenchymal stem cell therapy: Two steps forward, one step back.* Trends in molecular medicine (2010), 16-5, pp. 203-209.

**Book Chapters**

1. Zhao W, **Ankrum, J**, Sarkar D, Teo W, Kumar N, Karp J. *Stem Cell Homing to Sites of Injury and Inflammation*. "Stem Cells Revascularization Therapies." Taylor & Francis, (Invited) (2011), 217

2. Zhao W, Sarkar D, **Ankrum J**, Hall S, Loh W, Teo G, Karp J. *Therapeutic applications of mesenchymal stem/multipotent stromal cells*. "Stem Cells & Regenerative Medicine." Springer (2011).

3. Sarkar D, Zhao W, Schaefer S, **Ankrum J**, Teo G, Karp J. *Applications of Biomaterials in Functional Tissue Engineering*. "BIOMATERIALS SCIENCE: An Introduction to materials in Medicine 3RD EDITION." Invited for publication by Academic Press (2012).

**Patents**

1. **Ankrum J**, Olechowski A, Canseco J, Greenblatt E, Roberts M. 2012. *Medical Aspiration Apparatus*. International Publication Number WO 2012/109198A1, filed 7 February 2012. Patent Pending.

2. Karp J, Cho W, Laulicht, B, **Ankrum J**, Karnik R, Langer R. *Deployable Barbed Microneedle Array and Uses Thereof.* International Publication Number WO 2012/100002, filed 18 January 2012. Patent Pending.

**Public Posters & Presentations**

1. **Ankrum J,** Dastidar R, Ong JF, Levy O, Karp J. *Modulation of mesenchymal stem cell IDO activity through intracellular drug doped particles*. Presented as a poster presentation at the 2013 International Society for Stem Cell Research Meeting, June 12-15th 2013 in Boston, MA

2. **Ankrum J,** Dastidar R, Ong JF, Levy O, Karp J. *Enhanced mesenchymal stem cell immunomodulatory potency through intracellular budesonide microparticles*. Presented as a poster presentation at the 2013 Brigham and Women's Hospital Regenerative Medicine Symposium, June 11th, 2013 in Boston, MA

3. **Ankrum J,** Dastidar R, Ong JF, Levy O, Karp J. *Control of Mesenchymal Stem Cell Phenotype and Microenvironment through Intracellular Particles*. Presented as an Oral Presentation at the 2013 Society for Biomaterials Meeting, April 10-13th 2013 in Boston, MA

4. **Ankrum J**. *Engineered Cell Therapy and Bioinspired Medical Devices*. Presented at the Lemelson-MIT Student Prize Applicant Showcase, March 5, 2013 in Cambridge, MA.

5. **Ankrum J**, Sarkar S, Xu C, Miranda-Nieves D, Ong JF,Carman C, Karp J. *Monitoring and Controlling Mesenchymal Stem Cells Through Intracellular Microparticles*. Presented as a Poster at the BMES Cellular and Molecular Bioengineering Conference, January 5, 2013 in Waimea, HI

6. **Ankrum J**, Sarkar S, Teo G, Carman C, Karp J. *Controlling Cell Fate: A Biomaterials Approach*. Presented as a Poster at the 25th HST Research Forum, April 19, 2012 in Boston, MA.

7. **Ankrum J,** Sarkar S, Teo G, Carman C, Karp J. *Controlling Cell Fate: A Biomaterials Approach.* Oral presentation given as part of the HST.590 Biomedical Engineering Seminar Series, March 1, 2012 in Cambridge, MA.

8. **Ankrum J,** Sarkar S, Teo G, Carman C, Karp J. *A Biomaterials Approach for Programming Cell Fate*. Presented as an Oral Presentation at the 2011 Society for Biomaterials Meeting, April 13-16th 2011 in Orlando, FL.

9. **Ankrum J,** Olechowski A, Canseco J, Greenblatt E, Roberts M. *Nasogastric Tube Design to Reduce Clogging and Simplify Flushing*. Presented as a poster at the 2011 Design of Medical Devices Conference, April 12-14, 2011 in Minneapolis, MN.

10. **Ankrum J,** Cuevas P, Melgri R, Urban L. 6.979: NextLab I: *Designing Mobile Technologies for the Next Billion Users: Thrive in 5 Baby Blog*, Fall 2008. (Massachusetts Institute of Technology: MIT OpenCourseWare), http://ocw.mit.edu

ACKNOWLEDGEMENTS

Pursuing a graduate degree has been a family affair. The work described herein, and maintenance of my sanity, would not have been possible without the love and support of my wife, Laura. She is always there at the end of the day, whether the experiments go poorly or exactly as planned. She has supported me through long days at lab, critiqued my presentations, and joined me in the lab for weekend experiments. I count myself blessed to have gone through this journey with such a wonderful companion.

Next I would like to thank my advisor Jeff Karp for his belief in me since we first met back in January of 2009. Despite my never touching a pipette or culturing cells, he invested in me and took me on as his first graduate student. I have learned a tremendous amount from Jeff over the past five years and am deeply grateful to have had an advisor who invests in my research and my professional development. I would also like to thank my thesis committee, Prof. Dan Anderson, Dr. Augustine Choi for their critical feedback and for pushing me to reach my full potential.

The Karp Lab has been a fun and stimulating environment and I have had the privilege of learning from some of the brightest scientists I know. To the post-docs I worked with: Weian, Debanjan, Chenjie, Wookyung, Oren, Oscar, thank you for all that you have taught me and making Karp Lab a great place to work. To my undergraduate students, Riddhi, Faii, Thula, and Krishnan, thank you for laboring with me through all the experiments, your desire for knowledge has pushed me to deepen my own understanding. To Grace, Kelvin, and the rest of Karp Lab thank you for being there to commiserate in the difficult times and celebrate in the good times. Some of our best ideas have come out of our casual Friday afternoon brain storming sessions and your input has helped me to grow as a scientist and shaped the thesis you see here.

Outside of lab, my family and friends have always been there to live life with me through the ups and downs of the past five years. My mom and brother have been steadfast in their support for me, and inspire me to weather any storm. My father passed away in the months prior to my arrival at MIT, but he was so excited I chose to come to Harvard-MIT and would have loved to see all that I got to be a part of. My in-laws, Kevin and Mary, have been our most frequent visitors to Boston and a constant source of encouragement. Last but not least, my community at City on a Hill Church has been ever present and like a family to Laura and me during our time in Boston. To all of you, thank you for your support and know while this is the end of my PhD, it is not the end of our memories, friendships, and collaborations.

TABLE OF CONTENTS

# Chapter 1 Preface

The purpose of this chapter is to introduce the reader to mesenchymal stem cells (MSCs), the state of MSC based therapies at the beginning of my thesis research. Included is a thorough introduction to MSC phenotype including cell surface markers, differentiation potential, and expression of therapeutic factors, as well as citations to seminal papers in the field. Data regarding when, where, and how MSCs are being used in clinical trials is also included to orient the reader to the context in which MSC therapy is in use. The chapter closes with a list of outstanding questions regarding MSC therapy that have served as a driving force for my research during my PhD.

This article is an adaptation of a peer-reviewed article published on March 23, 2010 in *Trends and Molecular Medicine*. Reprinted with permission.

Ankrum J, Karp J. (2010). Mesenchymal stem cell therapy: Two steps forward, one step back. Trends Mol Med, 16(5), 203–9.

**Glossary of Terms**

Allogeneic: Cells originate from a donor of the same species as the recipient

Autologous: Donor cells originate from the recipient

Xenograft: Cells originate from a donor of a different species than the recipient

Alu Sequences: A repetitive sequence of several hundred base pairs that occur frequently in primate genomes

Endocrine Signaling: Secreted factors exert effect on distant cells

Paracrine Signaling: Secreted factors exert effect on neighboring cells

# Chapter 1: Mesenchymal Stem Cell Therapy: Two steps forward, one step back


## Abstract

Mesenchymal stem cell (MSC) therapy is poised to establish a new clinical paradigm, however, recent trials have produced mixed results. While MSC were originally considered to treat connective tissue defects, preclinical studies revealed potent immunomodulatory properties that prompted the use of MSC to treat numerous inflammatory conditions. Unfortunately, while clinical trials have met safety endpoints, efficacy has not been demonstrated. We believe the challenge to demonstrate efficacy can be attributed in part to an incomplete understanding of the fate of MSC following infusion. Here, we highlight the clinical status of MSC therapy and discuss the importance of cell-tracking techniques, which have advanced our understanding of the fate and function of systemically infused MSC and might improve clinical application.


## Introduction to MSC Therapy

Imagine a simple intravenous cell therapy that can restore function to damaged or diseased tissue, avoid host rejection and reduce inflammation throughout the body without the use of immunosuppressive drugs. Such a breakthrough would revolutionize medicine. Fortunately, pending regulatory approval, this approach might not be far off. Specifically, cell therapy utilizing adult mesenchymal stem cells (MSC), multipotent cells with the capacity to promote angiogenesis, differentiate to produce multiple types of connective tissue and downregulate an inflammatory response, are the focus of a multitude of clinical studies currently underway. MSC are being explored to regenerate damaged tissue and treat inflammation, resulting from cardiovascular disease and myocardial infarction (MI), brain and spinal cord injury, stroke, diabetes, cartilage and bone injury, Crohn's disease and graft versus host disease (GvHD) (*1*). The problems, however, are that some recent late stage clinical trials have failed to meet primary

endpoints, and the fate of MSC following systemic infusion as well as the mechanisms through which they impact host biology are largely unknown(*2*).

In this chapter, we will highlight the recent paradigm shift that has occurred in therapeutic use of MSC based on their immunomodulatory properties as opposed to their multilineage differentiation capacity. We discuss the clinical state of MSC therapy in addition to cell-tracking techniques that have been developed with *in vivo* models to elucidate the mechanisms through which MSC provide a therapeutic effect.

## MSC Phenotype

While they have donned many names, i.e. mesenchymal stem cells, mesenchymal stromal cells, multipotent stromal cells, marrow stromal cells, and colony-forming unit-fibroblastic, MSC were originally described as adherent cells from bone marrow that form colonies(*3*). Later these cells were found to have multilineage differentiation potential as they could form connective tissue cell types capable of producing bone, adipose and cartilage (*4*). The International Society for Cellular Therapy (ISCT) defines human MSC as tissue culture plastic adherent cells capable of osteogenesis, adipogenesis and chondrogenesis that are positive for CD73, CD90, and CD105 but negative for CD11b, CD14, CD34, CD45, CD79a, and HLA-DR surface markers (*5*). Despite these guidelines, characterizing and defining the MSC phenotype represents an ongoing challenge (*2*, *6*, *7*). Bone marrow-derived MSC are a heterogeneous population of cells and MSC characteristics such as surface marker expression, proliferation rate and differentiation potential are dependent on passage, cell density and the cell culture media(*7*). The discovery of MSC in fat and virtually all other mature tissues(*8*) has introduced additional nuances in that MSC properties seem to depend on the tissue from which they are isolated (*7*). Although MSC were initially considered for therapy based on their multi-lineage differentiation capacity, their ability to secrete cytokines and growth factors that are anti-apoptotic, pro-angiogenic and have the potential to reduce scarring and inflammation have positioned MSC for a broader spectrum of clinical applications (*9*). In particular, the use of MSC to down-regulate inflammation offers significant therapeutic potential for treating inflammatory diseases. Specifically, MSC possess the ability to reduce B-cell proliferation, monocyte maturation

and secretion of interferon (INF)-γ and TNF-α while promoting T-regulatory cell induction and secretion of IL-10 (*10*, *11*). Table 1 presents a summary of MSC traits and properties.

**Table 1. Reported MSC Characteristics** (Adapted from (*12*))

| Surface Markers | Differentiation Potential | Therapeutic Factors |
|---|---|---|
| CD44+<br>CD73 +<br>CD90 +<br>CD105 +<br>CD11b -<br>CD14 -<br>CD34 -<br>CD45 -<br>CD79a -<br>HLA-DR -<br>(*5*, *13*) | Osteogenic<br>Adipogenic<br>Chondrogenic<br>Myogenic<br>Endothelial<br>Epithelail<br>Neuronal<br>(*1*, *4*, *7*) | VEGF, Ang-1, SDF-1, PDGF, TSG-6, bFGF, FGF-7, IL-1ra, IL-6, PIGF, MCP-1, TGFβ, PGE-2, IDO, M-CSF, HGF, MMP-9, Sfrp, Thymosin β4, Plasminogen activator, Tenacin C, Thrombospondin 1<br>(*9-11*, *14*, *15*) |

## Paradigm shift in the use of MSC for therapy

While the initial applications conceived for MSC therapy focused on their multilineage differentiation capacity, and more specifically on the potential of MSC to differentiate into osteogenic cells that produce bone tissue as a treatment for fractures, osteogenesis imperfecta or spinal fusion, recent clinical trials have focused almost entirely on the ability of MSC to exert their biological function through trophic mechanisms, including the secretion of cytokines that might serve both paracrine and endocrine functions (*14-17*). This shift stemmed from observations that MSC therapy resulted in reduction of inflammation, apoptosis and fibrosis in numerous disease models despite a lack of MSC differentiation and engraftment in the injured tissue. Thus it was hypothesized that regeneration must be due to trophic factors rather than

differentiation as reviewed by van Poll et al (*18*). This paradigm shift towards utilizing trophic properties of MSC for therapy also included a shift from local delivery of MSC to systemic administration, which is less invasive and more convenient, especially for multiple dosing regimens. However, similar to bone marrow transplantation, where a small percentage of the total hematopoietic stem cells that are infused reach the bone marrow (*19*, *20*), only a small percentage of the infused MSC (often <1%) reach the target tissue with cell entrapment commonly observed in capillaries within the liver, spleen and lung (*1*).

## Clinical State of MSC Therapy

Mixed results from recent clinical trials have evoked promise and discouragement from both the scientific and clinical communities. Early studies demonstrating that MSC modulate immune function in human (*21*) and mouse (*22*) *in vitro* cultures and within rodent models generated optimism for the prospect of treating some of the most chronic and elusive inflammatory conditions in the developed world. For example, numerous groups have shown reduced scarring and increased cardiac output following MSC therapy in animal models of MI (*23-25*). A recently completed phase I trial, using a single infusion of allogeneic MSC (Osiris Therapeutics, Inc. Prochymal™ product) in patients within 10 days of acute MI corroborates these findings (*26*). In the randomized placebo-controlled, dose-escalating trial, patients receiving MSC experienced a 4-fold decrease in arrythmias and premature ventricular contractions (PVC), and showed improved overall health compared to patients receiving placebo. Magnetic resonance imaging of a subset of patients one year post-treatment revealed a significant increase in left ventricular ejection fraction (LVEF). Interestingly, an increase in the dose of MSC reduced the rate of PVC but not any of the other metrics. Importantly, there were no significant adverse events, and thus, this trial validated the safety of allogeneic MSC; however, the viability of MSC post-treatment and the role of MSC in the recovery of cardiac function remain to be elucidated. These results should be considered with cautious optimism; the BOOST trial, which assessed intracoronary delivery of MSC, initially showed significant improvement in LVEF over control, but this difference was not significant after 18 months (*27*), thus long-term follow

up of intravenous MSC therapy is needed. A phase II trial using MSC to treat GvHD reported a reduced 2-year mortality rate (*28*). These promising results provided significant motivation for large-scale, placebo-controlled clinical trials. While phase I and II safety trials progressed without severe adverse events, the phase III randomized, placebo-controlled trials failed to reach their primary endpoints. These trials utilized MSC as a first- and second-line therapy to treat GvHD and steroid–refractory GvHD, respectively (*29*). Interestingly, these trials illuminated the significant placebo effect that is common with stem cell-based therapies. It is important to consider that the placebo effect has the potential to mask modest therapeutic efficacy. Treatment resulted in a statistically significant improvement over those receiving placebo in patients with steroid-refractory liver or gastrointestinal GvHD and a clinically significant improvement over controls among pediatric patients(*29*). Further analysis of the data is ongoing. A trial targeting Chronic Obstructive Pulmonary Disease (COPD) with Prochymal™ is underway and preliminary data (gathered 6 months after treatment) showed reduced systemic inflammation compared to controls as measured by C-reactive protein, but there was no significant improvement in pulmonary function (*30*). Although the mixed clinical data could be considered a major setback to the entire MSC field, these trials extended initial phase I safety data to thousands of patients, and we believe this should be considered a critical milestone, especially given that typical doses include hundreds of millions of allogenic MSC. It is also important to consider that it took several decades to optimize bone marrow transplantation before it became a standard of care. Thus, we need to focus on reaching the challenges that were highlighted by these clinical trials, which likely stem from our lack of understanding of the fate of MSC following systemic infusion. Enhanced understanding of fundamental MSC biology should allow more systematic engineering approaches to reduce variability and achieve higher efficacy.

It is possible that the inability to meet primary clinical endpoints resulted from a low efficiency of engrafted cells, which is often described in animal models(*2*), that reduces the potential for long-term availability of immunomodulatory cytokines. Intriguingly, positive data have emerged from clinical trials despite the lack of data supporting long-term survival and engraftment of systemically delivered MSC. This could result from the dominant use of allogenic MSC in animal studies and human trials

(see Table 2 for the source of MSC used in clinical trials), which may be recognized and quickly disposed of by the host immune system. Hare and colleagues (University of Miami, FL) are currently recruiting patients to determine if autologous MSC exhibit enhanced therapeutic efficacy compared to allogeneic MSC in a National Institutes of Health-funded study for heart failure. In addition to these considerations, it is also possible that once introduced into the body, MSC do not secrete the same repertoire or concentration of cytokines that have been observed *in vitro*. The lack of data supporting long-term engraftment and the limited knowledge of cell fate for systemically administered MSC could be due to a lack of sufficient technologies to monitor MSC fate *in vivo*, an area we believe deserves attention.

## Monitoring MSC fate *in vivo*

A large fraction of systemically infused MSC typically become trapped within the lungs as emboli due to their large size and their repertoire of cell-surface adhesion receptors (*31-34*). Alternatively, they arrest and interrupt blood flow during the first pass through the precapillary level (*35*). Such passive arrest prevents the majority of infused MSC from homing to damaged or diseased tissues. Despite these complications, numerous animal studies and some clinical trials have reported favorable outcomes following systemic infusion of MSC (*23*, *28*, *36-38*). The lack of specific homing is perhaps why high dosing is used in clinical trials; 150-300 million MSC are typically administered with each infusion (*39*). This prompts the questions: can entrapped MSC transmigrate through the endothelium; how long do the entrapped MSC survive; and can they provide benefit to distant organs? Several recent publications have attempted to address these questions.

Lee and colleagues used a cross-species experimental design and real-time PCR (rtPCR) to track the fate of systemically administered human MSC in a mouse model(*15*). rtPCR analysis for human-specific Alu sequences in blood samples showed that within 5 minutes of MSC infusion through the tail vein, 99% of MSC were cleared from the circulation. Within 10-30 minutes, a resurgence of ~2-3% of the infused MSC was observed within the blood stream. Tissue samples from various organs revealed

that the majority of cells were initially found in the lung, which was consistent with previous studies(*31*, *33*). Fifteen minutes after infusion, 83% of the human DNA was

**Table 2. State of Clinical Trials Using Exogenous MSCs** (Adapted from (*12*))

| Condition by Organ System | Trials[a](Patients) | Allogeneic | Autogeneic | Trophic[b] | Differentiate[b] | IV[c] | Local[c] | IA[c] |
|---|---|---|---|---|---|---|---|---|
| Multiple Systems | 18 (1067) | | | | | | | |
| *GvHD* | *16 (1027)* | *15* | *1* | *16* | | *16* | | |
| *Sjgren's Syndrome* | *1 (20)* | *1* | | *1* | | *1* | | |
| *SLE(Lupus)* | *1 (20)* | *1* | | *1* | | *1* | | |
| Bone/Cartilage | 26 (1487) | | | | | | | |
| *Arthritis-Foot Fusion* | *1 (100)* | *1* | | | *1* | | *1* | |
| *Bone Fracture* | *2 (210)* | | *2* | | *2* | | *2* | |
| *Bone Neoplasms* | *1 (50)* | *1* | | | *1* | | *1* | |
| *Cartilage Defects* | *4 (185)* | *1* | *3* | | *4* | | *4* | |
| *Meniscectomy* | *2 (110)* | *2* | | | *2* | | *2* | |
| *Osteodysplasia* | *2 (58)* | *1* | *1* | | *2* | *1* | *1* | |
| *Osteogenesis Imperfecta* | *3 (35)* | *3* | | | *3* | *3* | | |
| *Osteonecrosis* | *2 (51)* | *1* | *1* | | *2* | *1* | *1* | |
| *Periodontitis* | *1 (10)* | *1* | | | *1* | | *1* | |
| *Spinal Fusion* | *8 (678)* | *8* | | | *8* | | *8* | |
| Cardiovascular | 19 (951) | | | | | | | |
| *Dilated Cardiomyopathy* | *2 (80)* | | *2* | *2* | | | *2* | |
| *Heart Failure* | *3 (200)* | *2* | *1* | *2* | *1* | | *3* | |
| *Ischemic Heart Disease* | *3 (160)* | | *3* | *2* | *1* | | *3* | |
| *Myocardial Infarction* | *7 (428)* | *4* | *3* | *6* | *1* | *3* | *4* | |
| *Limb Ischemia* | *4 (83)* | *3* | *1* | *4* | | | *3* | *1* |
| Gastrointestinal | 3 (480) | | | | | | | |
| *Crohn's* | *3 (480)* | *3* | | *3* | | *3* | | |
| Kidney | 6 (136) | | | | | | | |
| *Acute Kidney Injury* | *1 (15)* | *1* | | *1* | | | | *1* |
| *Kidney Transplant* | *4 (101)* | *2* | *2* | *4* | | *4* | | |
| *Lupus Nephritis* | *1 (20)* | | *1* | *1* | | *1* | | |
| Liver | *7 (204)* | | | | | | | |
| *Cirrhosis* | *6 (203)* | | *6* | *3* | *3* | *2* | *4* | |
| *Fam. Hypercholesterolemia* | *1 (1)* | *1* | | | *1* | | *1* | |
| Lung | 1 (60) | | | | | | | |
| *COPD* | *1 (60)* | *1* | | *1* | | *1* | | |
| Nervous | 12 (294) | | | | | | | |
| *Multiple System Atrophy* | *1 (NA)* | | *1* | *1* | | | | *1* |
| *Neuroblastoma* | *1 (15)* | *1* | | *1* | | *1* | | |
| *Spinal Cord Injury* | *2 (103)* | | *2* | *2* | | | *2* | |
| *Multiple Sclerosis* | *4 (84)* | *1* | *3* | *4* | | *3* | *1* | |
| *Parkinson's Disease* | *1 (5)* | | *1* | | *1* | | *1* | |
| *ALS* | *1 (24)* | | *1* | *1* | | | *1* | |
| *Stroke* | *2 (63)* | | *2* | *1* | *1* | *2* | | |
| Pancreas | 4 (210) | | | | | | | |
| *Type 1 Diabetes* | *3 (110)* | *2* | *1* | *3* | | *3* | | |
| *Type 2 Diabetes* | *1 (100)* | | *1* | *1* | | | | *1* |
| Skin | 5 (455) | | | | | | | |
| *Diabetic Wounds* | *3 (360)* | | *3* | *2* | *1* | | *3* | *1* |
| *Systemic Sclerosis* | *1 (20)* | *1* | | *1* | | *1* | | |
| *Epidermolysis Bullosa* | *1 (75)* | *1* | | *1* | | *1* | | |
| Total | 101 (5,344) | 59 (3,385) | 42 (1,959) | 65 (3,588) | 36 (1,756) | 48 (2,495) | 49 (2,683) | 5 (166) |

| *Completed trials (n=21)* | | | *Scheduled for completion (n = 63)* | | | | | | | |
|---|---|---|---|---|---|---|---|---|---|---|
| 2005 | 2006 | 2007 | 2008 | 2009 | 2010 | 2011 | 2012 | 2013 | 2014 | Not specified/other |
| 1 | 1 | 2 | 8 | 8 | 21 | 20 | 13 | 5 | 1 | 17/4 |

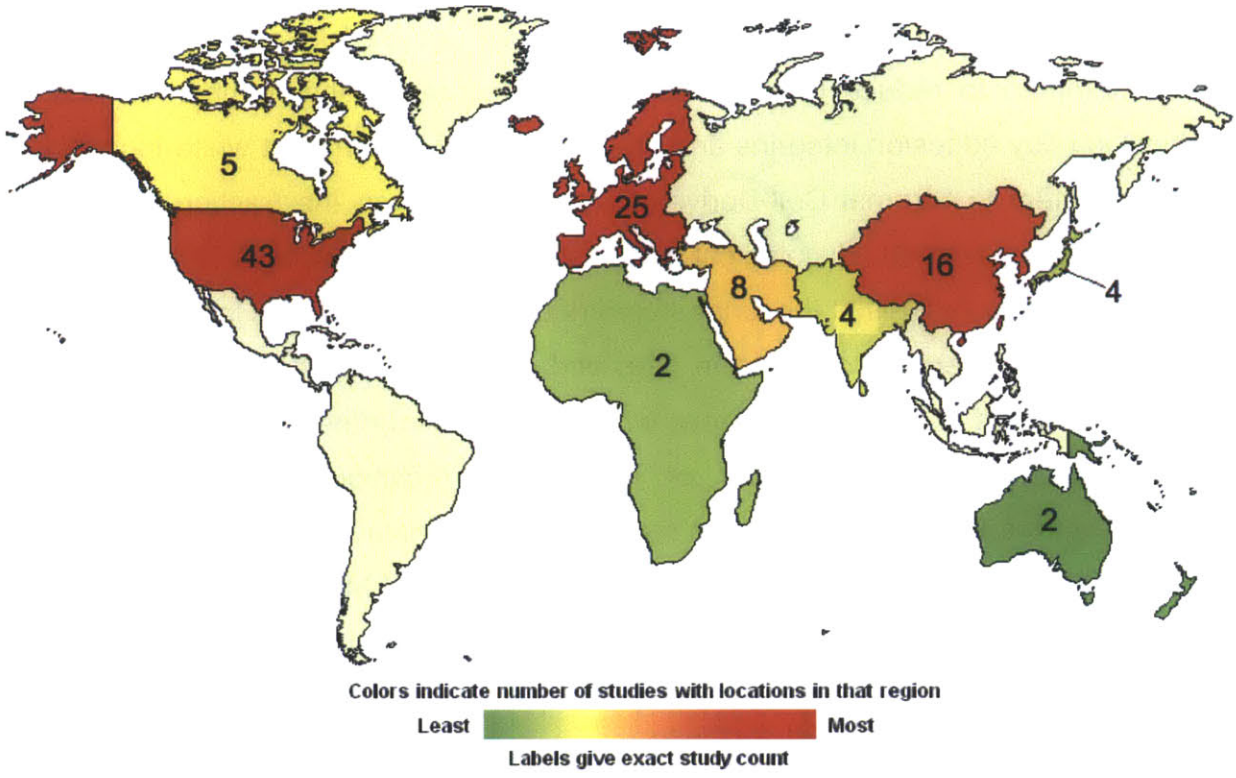


*Studies with multiple locations are reported in each region containing a location.

[a]Data collected from ClinicalTrials.gov registry on 13 March, 2010. Searches for 'Mesenchymal Stem Cells', 'Mesenchymal Stromal Cells', 'Multipotent stromal cells', 'bone marrow stromal cells', 'Stem cells for Spinal Fusion', 'Prochymal', and 'connective tissue progenitor' returned 142 unique results, and of those the 101 reported here used exogenous delivery of MSCs. Based on information provided in the trial summary, it is estimated that approximately 85% of trials utilize culture expanded cells. Excluded trials involved expanded access to existing trials, recruitment of endogenous MSCs to sites of injury, and others that did not pertain to MSC therapy.

[b]Trials were categorized as Trophic, if the rationale for the study was dependent on MSC's pro-angiogenic, anti-apoptotic, or immune modulating properties. Trials were categorized as Differentiate if the rationale depended on the differentiation of delivered MSCs.

[c]IV, intravenous; IA, intra-arterial; Local, delivered in scaffold or injected directly into target tissue.

[d]Map above displays global distribution of MSC clinical trials

detected in the lung while only trace amounts were detected in other tissues. The authors attempted to reduce lung entrapment by decreasing the number of infused cells, blocking key adhesion integrins and pretreating the MSC with rat white-blood cells (to sensitize them to Stromal Cell-Derived Factor-1); however, the fraction of trapped MSC remained unchanged. Histological analysis revealed that the MSC formed emboli in the afferent blood vessels of the lung, a common finding for systemic infusion of other cell types including hematopoietic stem cells and endothelial progenitor cells (*20*, *40*). No MSC were found in the bone marrow, which contradicted other studies(*32*, *41*) and highlighted a potential shortcoming of PCR-based techniques, which could be approximately 10-fold less sensitive than radiolabeling techniques (*42-44*).

Despite mass entrapment of systemically administered MSC within the lung and other tissues, tail vein injection in rodent models of MI still provides a functional improvement that is typically evidenced by decreased scar size and increased cardiac output. In the seminal paper by Lee *et al.*, a paracrine factor that is released by embolized MSC was identified; this factor promotes tissue regeneration through a systemic effect, similar to the action of a conventionally administered drug (*15*). A transcriptome analysis of embolized MSC from the lungs generated a list of 451 upregulated transcripts with rtPCR analysis showing that TSG-6, a known anti-inflammatory protein, had the largest increase in mRNA levels(*15*). TSG-6, which was originally discovered by secretome analysis of skin fibroblasts following incubation with tumor necrosis factor (TNF)-$\alpha$ (*45*), is a 30 kDa protein that inhibits neutrophil migration and the production and activity of both plasmin and matrix-metalloproteinases (MMPs)(*46*). Interestingly, MSC secretion of TSG-6 was 120-fold greater than that of fibroblasts obtained from the same human donor (*15*). Two infusions of recombinant TSG-6 following MI (without administration of MSC) decreased infarct size, reduced scaring and improved cardiac function, yet not to the same extent as MSC. MSC with TSG-6 knock down by RNA interference did not impact infarct size. The authors hypothesized that the embolism of the MSC in the lung creates a local injury that activates the MSC to secrete TSG-6, which enters circulation and downregulates the inflammatory process at the site of MI. MI is characterized by invasion of neutrophils, monocytes, and macrophages that secrete MMPs, breaking down the dead myocardium

to replace it with a fibrous scar (*23*). MSC secretion of TSG-6 and infusion of recombinant TSG-6 interrupted this process during the initial 48 hours of wound healing, resulting in a reduced inflammatory process and improved regeneration of the infarcted tissue. This study utilized xenografts; human MSC were injected into a murine model. Xenografts have different distribution kinetics than allogeneic MSC in murine models (*43*) (allogenic MSC are the standard for human clinical trials). Because Lee *et al.'s* proposed mechanism for enhanced therapeutic efficacy depends on entrapment and activation of xenogenic MSC in the lungs, allogeneic MSC, which have been shown in mouse models to disperse from the lungs within hours of infusion, might produce substantially different results.

In addition to PCR-based techniques for tracking the fate of systemically administered MSC, alternative approaches leverage the advantages of light and fluorescent microscopy that are well suited for small animal models. Lin's group has characterized tumor-cell, hematopoietic stem cell, and MSC trafficking in the skull of living mice using *in vivo* confocal and two-photon microscopy, which provide high-resolution spatial delineation of a cell's location (*32*, *47*, *48*). Similarly, Toma and colleagues utilized intravital microscopy, which permits detailed real-time and serial imaging of *in vivo* phenomenon, to examine the entrapment of MSC within a microvascular bed (*35*). In this model, the cremaster muscle of the rats was exposed and fluorescently labeled MSC were injected into the iliac artery. The density of MSC in varying depths of the vasculature was monitored over time using differential interference contrast and fluorescence imaging. All MSC arrested within 5 minutes of injection with 92% of the injected MSC entrapped during the first pass within the cremaster muscle. However, MSC were only trapped at the precapillary level, resulting in blockage of blood flow to the capillary bed. The number of viable MSC in the cremaster muscle decreased drastically over the next 72 hours; only 14% of those originally entrapped survived, as determined by preserved nuclear morphology. As intravital microcopy is best suited for monitoring cells within a pre-selected location, redistribution of the MSC to other tissues is challenging to evaluate.

One method that can address this is bioluminescence imaging, which lacks single-cell resolution, but enables whole-organism tracking of cell distribution. For

example, Wang *et al.* used MSC expressing a firefly-luciferase reporter gene in combination with bioluminescence imaging in a metastatic breast cancer model (*49*). This allowed non-invasive whole-animal tracking of intravenously injected MSC and their progeny over the course of several days. In healthy controls, MSC were initially found in the pulmonary capillaries but quickly dispersed after one day. The reduction of signal in the lungs can be attributed both to redistribution of MSC to other tissues as well as to cell death. Bioluminescence can be extremely valuable in characterizing MSC affinity and tropism for inflammatory and tumor microenvironments as has been reviewed by Spaeth *et al.* (*50*).

Recent cell tracking studies have provided valuable insight into the distribution of MSC following systemic infusion and have begun to help elucidate the process of cell localization within specific tissues. However, it is critical to note that whole-animal imaging techniques such as bioluminescence lack the resolution to determine if cells remain in the vasculature or have undergone transendothelial migration. Aside from passive cell entrapment, which appears to be a dominant mechanism through which infused MSC reach their final destination, characterization of the host vasculature is required to better understand active homing mechanisms. The vascular expression of adhesion molecules and endothelial presentation of cytokines can vary substantial within a vascular bed (*48*). Thus, future studies should aim to employ multiple methods, summarized in Table 3, to assess the final destination of the infused cells through both macroscopic distribution and microscopic spatial localization analysis.

## Therapeutic implications and concluding remarks

The results from multiple clinical trials using systemically administered MSC illuminate critical challenges that must be addressed; yet provide the young field of MSC therapy with rationale for additional 'steps' forward. Importantly, work has already begun to identify the fate and function of MSC following systemic infusion. With evidence for massive cell entrapment in the lungs and in capillary beds of other tissues, approaches are being developed to enhance cell homing to target tissues through genetic and chemical engineering approaches(*2*, *54*). It is possible that targeted delivery of cells is unnecessary for certain applications, as the therapeutic effects of MSC are systemic,

**Table 3. Cell Monitoring Techniques** (adapted from *(12)*)

| Technique | Detected Agent | Detection Limit | Temporal Resolution | Whole Animal |
|---|---|---|---|---|
| PCR(*44*) | Sequence unique to donor | 50,000 cells | Requires sacrifice | Yes |
| Radiolabeling (SPECT)(*44*) | Isotope | 5,000 cells | 30 sec/projection | Yes |
| Intravital Microscopy(*13, 51*) | Fluorescent marker, ie. reporter gene, antibody, quantum dots | Single Cell | <1 sec | No |
| In vivo confocal(*52*) | Fluorescent marker | Single Cell | <1 sec | No |
| Bioluminescence Microscopy(*53*) | Luciferase gene + substrate | 10 Cells | <1 min | Yes |
| MRI(*43*) | Magnetic nanoparticles | 10-20 cells/voxel | >10 min depending on size of region | Yes |

however, enhanced delivery to specific tissues could increase the efficiency of cell therapy and reduce the number of infused cells, potentially reducing the cost of developing a therapeutic product. Conventional wisdom suggests that promoting transmigration and longevity of MSC, perhaps even non-specifically, could increase therapeutically relevant systemic effects (i.e. where engrafted cells continue to secrete cytokines that are released into the circulation). Furthermore, extensive research is needed to determine if the few MSC that have been reported to engraft in target tissues(*55*) mediate regeneration through the alternate mechanism of differentiation and whether or not these grafted cells integrate and coordinate with the native tissue to restore function. With the discovery of secreted TSG-6 by MSC entrapped within the lungs and knowledge of several other MSC-secreted immunomodulatory factors (Box 1), there is now evidence that the therapeutic effects could in part be due to systemic (endocrine) effects in addition to previously described (local) paracrine signaling and direct cell-cell interactions. For example, Nemeth *et al.* demonstrated that MSC in direct contact with macrophages secrete prostaglandin E2 (PGE2), which reprograms macrophages to increase production of the potent anti-inflammatory cytokine interleukin-10 (IL-10) (*10*, *11*).

The heterogeneity of the MSC population presents a challenge for generalizing findings from different groups, as it is known that differences in culture conditions, source, passage and cell density all impact MSC phenotype (*56*). Moving forward, it is important to characterize the conditions needed to develop therapeutically relevant cells, and in tandem, cell-tracking techniques that can be performed in large animal models and in humans, which would enhance understanding of MSC engraftment, allow long-term assessment of cell phenotype and ultimately increase therapeutic potential (See Table 4 for outstanding questions in MSC therapy.). Furthermore, development of such tracking technologies for animal models could make it possible to monitor cells following systemic infusion into patients. Unlike conventional drugs, which are designed to act through a known pathway, cell therapies are living therapeutics, which can multiply, senesce, undergo necrosis or apoptosis, or alter their phenotype, and thereby drastically change their therapeutic potential. The ability to track the location of cells and monitor viability and functional characteristics (e.g. differentiation state) could provide

**Table 4. Outstanding Questions** (Apapted from (*12*))

| |
|---|
| ***MSC Homing*** |
| • **Which adhesion molecules mediate MSC homing?** |
| ***MSC Engraftment*** |
| • **How should MSC engraftment be defined?** |
| • **Do MSC persist long term and how can this time frame be extended?** |
| • **Which tissue microenvironments provide favorable sites for MSC engraftment?** |
| **MSC Monitoring** |
| • **What are the best approaches to monitor MSC therapy and how might these approaches be connected to clinical interventions to improve the therapeutic outcome?** |
| • **How should MSC distribution and phenotype be monitored in animals and in humans?** |
| **MSC Function** |
| • **What are the kinetics of cytokine secretion and how does this change as MSC differentiate into more mature progeny?** |
| • **In addition to TSG-6, which MSC-secreted cytokines have systemic effects?** |
| **Therapy Optimization** |
| • **What are the optimal conditions to develop therapeutically relevant cells (with increased homing potential and/or increased cytokine production)?** |
| • **Can MSC be replaced by MSC supernatant and how might the supernatant be standardized?** |
| • **Can MSC therapy be improved by shifting the balance between systemic (endocrine) and local (paracrine or cell-cell contact) activity? How might this change for treatment of different diseases?** |
| • **How can patients be stratified to select those who would be most responsive?** |
| • **What is the optimal dosing regimen?** |

feedback for potential clinical interventions and for the development of a consistently efficacious treatment. Despite an incomplete explanation of their role in regeneration, there are multiple clinical trials being performed. As shown in Table 2, the ClinicalTrials.gov registry currently lists 85 trials that are using exogenous MSC to treat a wide range of damaged, diseased or inflammed tissues. Because only 20 of these trials have been completed, we can anticipate an abundance of new human data in the near future for a wide range of therapeutic applications (17 trials are scheduled to be completed in 2010 and 17 trials in 2011). Through investigation of MSC biology, discovery of their therapeutic mechanisms within animal models and testing their therapeutic potential within human trials, we will hopefully achieve many more steps forward to make MSC therapy a new clinical paradigm.

## Acknowledgements

This work was supported by National Institute of Health grant DE019191 and by the American Heart Association grant #0970178N to Jeffrey M Karp and a National Science Foundation Graduate Research Fellowship to James Ankrum.

## References


1. D. G. Phinney, D. J. Prockop, Concise review: mesenchymal stem/multipotent stromal cells: the state of transdifferentiation and modes of tissue repair--current views, *Stem Cell* **25**, 2896–2902 (2007).

2. J. M. Karp, G. S. Leng Teo, Mesenchymal stem cell homing: the devil is in the details, *Cell Stem Cell* **4**, 206–216 (2009).

3. A. Friedenstein, J. Gorskaja, N. Kulagina, Fibroblast precursors in normal and irradiated mouse hematopoietic organs, *Exp Hematol* (1976).

4. A. I. Caplan, Why are MSCs therapeutic? New data: new insight, *J. Pathol.* **217**, 318–324 (2009).

5. M. Dominici *et al.*, Minimal criteria for defining multipotent mesenchymal stromal cells. The International Society for Cellular Therapy position statement, *Cytotherapy* **8**, 315–317 (2006).

6. P. Bianco, P. G. Robey, P. J. Simmons, Mesenchymal stem cells: revisiting history, concepts, and assays, *Cell Stem Cell* **2**, 313–319 (2008).

7. D. Prockop, Repair of Tissues by Adult Stem/Progenitor Cells (MSCs): Controversies, Myths, and Changing Paradigms, *Mol Ther* (2009), doi:10.1038/mt.2009.62.

8. L. Da Silva Meirelles, P. Chagastelles, Mesenchymal stem cells reside in virtually all post-natal organs and tissues, *Journal of cell science* (2006).

9. J. S. Burchfield, S. Dimmeler, Role of paracrine factors in stem and progenitor cell mediated cardiac repair and tissue fibrosis, *Fibrogenesis Tissue Repair* **1**, 4 (2008).

10. A. J. Nauta, W. E. Fibbe, Immunomodulatory properties of mesenchymal stromal cells, *Blood* **110**, 3499–3506 (2007).

11. K. Németh *et al.*, Bone marrow stromal cells attenuate sepsis via prostaglandin E(2)-dependent reprogramming of host macrophages to increase their interleukin-10 production, *Nat Med* **15**, 42–49 (2009).

12. J. Ankrum, J. Karp, Mesenchymal stem cell therapy: Two steps forward, one step back, *Trends Mol Med* **16**, 203–209 (2010).

13. B. Rüster *et al.*, Mesenchymal stem cells display coordinated rolling and adhesion behavior on endothelial cells, *Blood* **108**, 3938–3944 (2006).

14. L. A. Ortiz *et al.*, Interleukin 1 receptor antagonist mediates the antiinflammatory and antifibrotic effect of mesenchymal stem cells during lung injury, *Proc Natl Acad Sci USA* **104**, 11002–11007 (2007).

15. R. H. Lee *et al.*, Intravenous hMSCs Improve Myocardial Infarction in Mice because

Cells Embolized in Lung Are Activated to Secrete the Anti-inflammatory Protein TSG-6, *Cell Stem Cell* **5**, 54–63 (2009).

16. Y. Iso *et al.*, Multipotent human stromal cells improve cardiac function after myocardial infarction in mice without long-term engraftment, *Biochem Biophys Res Commun* **354**, 700–706 (2007).

17. F. Tögel *et al.*, Vasculotropic, paracrine actions of infused mesenchymal stem cells are important to the recovery from acute kidney injury, *Am J Physiol Renal Physiol* **292**, F1626–35 (2007).

18. D. van Poll, B. Parekkadan, I. H. M. B. Rinkes, A. W. Tilles, M. L. Yarmush, Mesenchymal Stem Cell Therapy for Protection and Repair of Injured Vital Organs, *Cell Mol Bioeng* **1**, 42–50 (2008).

19. P. B. van Hennik, A. E. de Koning, R. E. Ploemacher, Seeding efficiency of primitive human hematopoietic cells in nonobese diabetic/severe combined immune deficiency mice: implications for stem cell frequency assessment, *Blood* **94**, 3055–3061 (1999).

20. J. Cui *et al.*, Bone marrow cell trafficking following intravenous administration, *Br J Haematol* **107**, 895–902 (1999).

21. M. Di Nicola *et al.*, Human bone marrow stromal cells suppress T-lymphocyte proliferation induced by cellular or nonspecific mitogenic stimuli, *Blood* **99**, 3838–3843 (2002).

22. M. Krampera *et al.*, Bone marrow mesenchymal stem cells inhibit the response of naive and memory antigen-specific T cells to their cognate peptide, *Blood* **101**, 3722–3729 (2003).

23. M. Laflamme, C. Murry, Regenerating the heart, *Nat Biotechnol* (2005).

24. A. A. Mangi *et al.*, Mesenchymal stem cells modified with Akt prevent remodeling and restore performance of infarcted hearts, *Nat Med* **9**, 1195–1201 (2003).

25. K. Schuleri *et al.*, Autologous mesenchymal stem cells produce reverse remodelling in chronic ischaemic cardiomyopathy, *Eur Heart J* (2009), doi:10.1093/eurheartj/ehp265.

26. J. M. Hare *et al.*, A randomized, double-blind, placebo-controlled, dose-escalation study of intravenous adult human mesenchymal stem cells (prochymal) after acute myocardial infarction, *J Am Coll Cardiol* **54**, 2277–2286 (2009).

27. G. P. Meyer *et al.*, Intracoronary bone marrow cell transfer after myocardial infarction: eighteen months' follow-up data from the randomized, controlled BOOST (BOne marrOw transfer to enhance ST-elevation infarct regeneration) trial, *Circulation* **113**, 1287–1294 (2006).

28. K. Le Blanc *et al.*, Mesenchymal stem cells for treatment of steroid-resistant, severe, acute graft-versus-host disease: a phase II study, *Lancet* **371**, 1579–1586 (2008).

29. C. R. Mills, Osiris Therapeutics Announces Preliminary Results for PRochymal Phase III GvHD Trials*Osiris Press Release* (2009) (available at http://files.shareholder.com/downloads/OSIR/2468414599x0x317779/7677da46-286a-47c4-865d-36c148119a1a/OSIR_News_2009_9_8_General.pdf).

30. C. R. Mills, Osiris Therapeutics Reports Interim Data for COPD Stem Cell Study*Osiris Press Release* (2009) (available at http://files.shareholder.com/downloads/OSIR/2468414599x0x302507/36275c0d-85b9-4726-a51a-708830588b08/OSIR_News_2009_6_23_General.pdf).

31. S. Schrepfer *et al.*, Stem cell transplantation: the lung barrier, *Transplant Proc* **39**, 573–576 (2007).

32. R. Sackstein, J. Merzaban, D. Cain, N. Dagia, Ex vivo glycan engineering of CD44 programs human multipotent mesenchymal ..., *Nat Med* (2008).

33. J. Gao, J. E. Dennis, R. F. Muzic, M. Lundberg, A. I. Caplan, The dynamic in vivo distribution of bone marrow-derived mesenchymal stem cells after infusion, *Cells Tissues Organs (Print)* **169**, 12–20 (2001).

34. I. M. Barbash *et al.*, Systemic delivery of bone marrow-derived mesenchymal stem cells to the infarcted myocardium: feasibility, cell migration, and body distribution, *Circulation* **108**, 863–868 (2003).

35. C. Toma, W. R. Wagner, S. Bowry, A. Schwartz, F. Villanueva, Fate Of Culture-Expanded Mesenchymal Stem Cells in The Microvasculature: In Vivo Observations of Cell Kinetics, *Circ Res* **104**, 398–402 (2009).

36. K. Le Blanc *et al.*, Treatment of severe acute graft-versus-host disease with third party haploidentical mesenchymal stem cells, *Lancet* **363**, 1439–1441 (2004).

37. A. Giordano, U. Galderisi, I. R. Marino, From the laboratory bench to the patient's bedside: an update on clinical trials with mesenchymal stem cells, *J Cell Physiol* **211**, 27–35 (2007).

38. S.-L. Chen *et al.*, Improvement of cardiac function after transplantation of autologous bone marrow mesenchymal stem cells in patients with acute myocardial infarction, *Chin Med J* **117**, 1443–1448 (2004).

39. NIH, Evaluation of PROCHYMAL Adult Human Stem Cells for Treatment-resistant Moderate-to-severe Crohn's Disease (2007) (available at http://clinicaltrials.gov/ct2/show/NCT00482092?term=NCT00482092&rank=1).

40. P. A. Smits *et al.*, Distribution of circulation-derived endothelial progenitors following systemic delivery, *Endothelium* **14**, 1–5 (2007).

41. W. Rombouts, R. Ploemacher, Primary murine MSC show highly efficient homing to the bone marrow but lose homing ability following culture, *Leukemia* **17**, 160–170 (2003).

42. D. L. Kraitchman, Dynamic Imaging of Allogeneic Mesenchymal Stem Cells Trafficking to Myocardial Infarction, *Circulation* **112**, 1451–1461 (2005).

43. D. L. Kraitchman *et al.*, In vivo magnetic resonance imaging of mesenchymal stem cells in myocardial infarction, *Circulation* **107**, 2290–2293 (2003).

44. M. F. Pittenger, B. J. Martin, Mesenchymal stem cells and their potential as cardiac therapeutics, *Circ Res* **95**, 9–20 (2004).

45. T. H. Lee, H. G. Wisniewski, J. Vilcek, A novel secretory tumor necrosis factor-inducible protein (TSG-6) is a member of the family of hyaluronate binding proteins, closely related to the adhesion receptor CD44, *J Cell Biol* **116**, 545–557 (1992).

46. C. M. Milner, V. A. Higman, A. J. Day, TSG-6: a pluripotent inflammatory mediator? *Biochem Soc Trans* **34**, 446–450 (2006).

47. C. L. Celso *et al.*, Live-animal tracking of individual haematopoietic stem/progenitor cells in their niche, *Nature* **457**, 92–96 (2009).

48. D. A. Sipkins *et al.*, In vivo imaging of specialized bone marrow endothelial microdomains for tumour engraftment, *Nature* **435**, 969–973 (2005).

49. H. Wang *et al.*, Trafficking Mesenchymal Stem Cell Engraftment and Differentiation in Tumor-Bearing Mice by Bioluminescence Imaging, *Stem Cell* **27**, 1548–1558 (2009).

50. E. Spaeth, A. Klopp, J. Dembinski, M. Andreeff, F. Marini, Inflammation and tumor microenvironments: defining the migratory itinerary of mesenchymal stem cells, *Gene Ther* **15**, 730–738 (2008).

51. B. S. Shah, P. A. Clark, E. K. Moioli, M. A. Stroscio, J. J. Mao, Labeling of mesenchymal stem cells by bioconjugated quantum dots, *Nano Lett* **7**, 3071–3079 (2007).

52. J. M. Runnels *et al.*, Imaging molecular expression on vascular endothelial cells by in vivo immunofluorescence microscopy, *Mol Imaging* **5**, 31–40 (2006).

53. S. Kidd *et al.*, Direct evidence of mesenchymal stem cell tropism for tumor and wounding microenvironments using in vivo bioluminescent imaging, *Stem Cell* **27**, 2614–2623 (2009).

54. J. Wagner, T. Kean, R. Young, J. E. Dennis, A. I. Caplan, Optimizing mesenchymal stem cell-based therapeutics, *Curr. Opin. Biotechnol.* **20**, 531–536 (2009).

55. H. C. Quevedo *et al.*, Allogeneic mesenchymal stem cells restore cardiac function in

chronic ischemic cardiomyopathy via trilineage differentiating capacity, *Proc Natl Acad Sci USA* **106**, 14022–14027 (2009).

56. R. H. Lee *et al.*, The CD34-like protein PODXL and alpha6-integrin (CD49f) identify early progenitor MSCs with increased clonogenicity and migration to infarcted heart in mice, *Blood* **113**, 816–826 (2009).

# Chapter 2 Preface

In this chapter a method of engineering MSCs with intracellular polymeric microparticles in introduced. As highlighted in Chapter 1, cells used in cell therapy are very responsive to their surroundings, and as such control of cell phenotype and function is often relinquished following administration into patients. With this work, we aimed to establish a method to influence cell phenotype even after injection into a patient. In this chapter I present a summary of the development of particle-modified MSCs and demonstrate the utility of the platform by controlling MSC differentiation into bone forming cells *in vitro*.

This chapter is an adaptation of a peer-reviewed article published on April 1, 2011 in *Biomaterials*. Reprinted with permission.
Sarkar D[1], Ankrum J[1], Teo GSL, Carman CV, Karp JM. (2011). Cellular and extracellular programming of cell fate through engineered intracrine-, paracrine-, and endocrine-like mechanisms. Biomaterials, 32(11), 3053–61.
[1] Co-first authors

Figures 11, 12 and the section "Application of platform technology for enhanced MRI imaging," have been adapted from a peer-reviewed article published on July 12 ,2012 in *Nano Letters*. Adapted with permission, Copyright 2012, American Chemical Society. For a complete version of the manuscript, please see Appendix I.
Xu C, Miranda-Nieves D, Ankrum J, Matthiesen ME, Phillips JA, Roes I, Wojtkiewicz GR, Juneja V, Kultima JR, Zhao W, Vemula PK, Lin CP, Nahrendorf M, and Karp JM. (2012). Tracking Mesenchymal Stem Cells with Iron Oxide Nanoparticle Loaded Poly(lactide-co-glycolide) Microparticles. Nano Lett , 12(8), 4131–9.

### Glossary of Terms

Microenvironment: Local environment around each individual cell
Osteogenesis: Generation of bone forming cells from immature progenitor cells
Intracrine Signaling: Soluble factors released within a cell that act within the same cell

# Chapter 2: Cellular and Extracellular Programming of Cell Fate through Intracrine-, Paracrine-, and Endocrine-like Mechanisms

## Abstract

A cell's fate is tightly controlled by its microenvironment. Key factors contributing to this microenvironment include physical contacts with the extracellular matrix and neighboring cells, in addition to soluble factors produced locally or distally. Alterations to these cues can drive homeostatic processes, such as tissue regeneration/wound healing, or may lead to pathologic tissue dysfunction. *In vitro* models of cell and tissue microenvironments are desirable for enhanced understanding of the biology and ultimately for improved treatment. However, mechanisms to exert specific control over cellular microenvironments remain a significant challenge. Genetic modification has been used but is limited to products that can be manufactured by cells and release kinetics of therapeutics cannot easily be controlled. Herein we describe a non-genetic approach to engineer cells with an intracellular depot of phenotype altering agent/s that can be used for altering cell fate via intracrine-, paracrine-, and endocrine-like mechanisms. Specifically, we show that human mesenchymal stem cells (MSCs) can be engineered with poly(lactic-co-glycolic acid) (PLGA) particles containing dexamethasone, which acts on a cytoplasmic receptor. The controlled release properties of these particles allowed for sustained intracellular and extracellular delivery of agent to promote differentiation of particle carrying cells, as well as neighboring cells and distant cells that do not contain particles.

## Introduction

Control of cell fate and its extracellular environment is critical for tissue regeneration and cell therapy. During development, for example, cells are instructed by a complex set of microenvironmental cues, comprising soluble mediators and direct

contacts with extracellular matrix and neighboring cells that are precisely regulated in time and space (*1*). Consequently, when the microenvironmental balance is altered, cells may be activated toward homeostatic responses, such as regeneration of damaged tissues, or pathologic changes in cell phenotype leading to aberrant cell growth or loss of function. To better understand these processes, engineer tissues, develop *in vitro* tissue models, and develop cell therapies, one must be able to exert localized control over the cell microenvironment.

Current methods to control cell fate in culture include: i) genetic manipulation of cells to program a desired phenotype, ii) addition of drugs or growth factors to the culture media, and iii) presentation of an engineered extracellular environment. Genetic modification has been used to program cell fate in culture to promote expression of specific cell surface receptors and to drive production of therapeutic peptides and proteins (*2-7*). However, these modifications often exhibit a long-term impact on the cells, are limited to agents that can be manufactured by cells, and aside from use of genetic switches, there is an inability to finely tune the release kinetics of these agents. Drugs or growth factors can be added to culture media to mimic a tissue microenvironment, however all cells receive essentially the same signal, and application of soluble factors for controlling the fate of transplanted cells is limited to pre-conditioning regimens. Alternatively, scaffolds or 2D/3D micro/nano-engineered substrates are useful to create multiple distinct microenvironments within a single culture system. These types of substrates have been used extensively to study cell-cell interactions, transplant cells, or mimic stem cell niches *in vitro* through support of cell proliferation, differentiation, or migration *via* controlled presentation of soluble cues, adhesive interactions, or surface stiffness and topology (*8-12*). In addition, cues such as growth factors can be chemically immobilized to the substrate, providing specific locations to modulate cell behavior (*13-15*). However, all of these strategies require cells to be on, or in close proximity to the substrate. Engineering substrates to control cell phenotype and function often involves a complex manufacturing methodology and there are several circumstances under which it is desirable to infuse cells *in vivo* without the use of a carrier or substrate (e.g. systemic cell infusion) (*2-7*, *16*).

Thus, there is a need to exert control over cells and their microenvironment without genetic modification or the use of an engineered substrate. Such a strategy would be useful to create *in vitro* models of regenerative or disease microenvironments that recapitulate critical cell-cell signaling events *in situ*. This approach could also be applied to control the fate of cells following transplantation or control specific *in vivo* microenvironments without the need for a cell carrier.

Here we propose a method to control the cellular microenvironment through a simple biomaterial-based cell modification approach independent of genetic manipulation or the presence of an artificial substrate. Rather than immobilizing cells on a biomaterial to control the cellular microenvironment, we present a strategy in which readily internalized biodegradable particles containing phenotype altering agents can be used to control cell fate (Fig. 1A). Upon modification of the cells, intracellular and extracellular release of agents was characterized. Assays were developed to test whether the released agents could promote osteogenic differentiation of particle-carrying cells as well as neighboring and distant cells (Fig. 1B). Furthermore, *in vitro* and *in vivo* applications of the cell modification approach are discussed.

## Results and Discussion

To exert control over cells without genetic modification or engineered substrates, we conceived of a strategy utilizing a controlled drug delivery approach. Specifically, we envisioned that cells could be modified with a depot containing drugs or differentiation factors that could impact the modified cells and their cellular microenvironment through diffusion or transport of agents out of the carrier cell. Although strategies for modifying the surface of cells with nanoparticles exist, achieving stability beyond minutes or hours requires chemical modification of the cell surface (*17*, *18*). To develop an approach that does not require chemical modification of the cell, we considered utilizing biodegradable particles which are readily internalized by multiple cell types. Particles formulated with poly(lactic-co-glycolic acid) (PLGA) enable a nontoxic and efficient system for sustained intracellular delivery of small molecles directly to the cytoplasm. While the efficiency is particle formulation dependent, PLGA particles have been reported to undergo rapid endo-lysosomal escape, further facilitating delivery to the cytoplasm(*19*). PLGA is a

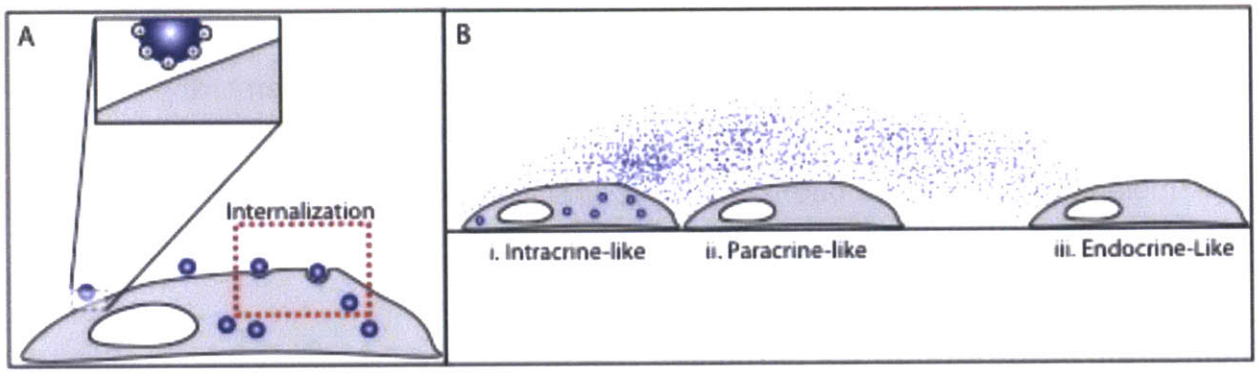


**Figure 1.** Controlling cell fate through internalized biodegradable particles. (A) Schematic illustration of functionalizing cells with biodegradable particles to generate cells with internalized particles. (B) The encapsulated agent can control the cell and neighboring microenvironment in three distinct ways. The release of the agent can control the fate of the (i) particle-carrying cell through intracrine-like signaling, (ii) neighboring cell, through paracrine-like signaling, (iii) and distant cells through endocrine-like signaling. (Adapted from (*20*))

polyester that hydrolyzes into biologically compatible and metabolizable moieties (lactic acid and glycolic acid). While small molecules such as dexamethasone (DEX), a commonly utilized osteogenic differentiation factor, can freely cross membranes of cells such as MSCs to engage intracellular receptors (*21*, *22*), many exogenously supplied large or acidic molecules (i.e. added to the culture media) have limited ability to transverse membranes unless the membranes are permeabilized (*23*, *24*). For agents that cannot passively transverse the cell membrane, active processes including gap junctions and permeability glycoproteins can be utilized (*25*, *26*). Thus, we hypothesized that particle based carriers could be used to deliver high intracellular concentrations of agents leading to either passive or active transport across the cell membrane to impact the extracellular environment. For proof of concept of this approach, we focused on small molecules that have been shown to freely cross cell membranes including dexamethasone and rhodamine dye.

**Engineering MSCs with PLGA particles**

Although MSCs readily internalize nano-sized particles (*27*), small particles (<1μm) that are typically endocytosed (*28*) have been shown in other cell types to be rapidly exocytosed unless they are conjugated to the cell membrane (*19*, *29-31*). To reduce the potential for exocytosis, PLGA particles with a diameter of 1-2 μm were fabricated (Fig. 2A & B) and found to be internalized irrespective of the surface chemistry, likely via phagocytosis (*28*) (Fig. 2C). However, the kinetics of internalization was increased by modifying the surface with a positive charge or with an antibody directed towards an MSC surface antigen (e.g. CD90) (Fig. 2C). Thus positively charged particles were selected for further experimentation. Confocal microscopy demonstrated that ~95% of the PLGA particles were internalized following a 12 hr incubation (Fig. 2D). Importantly, in contrast to previous reports of nanoparticle exocytosis, the 1-2μm particles were stable inside the cell for at least 7 days (Fig. 2E & F). Additionally, internalization of particles was confirmed with transmission electron microscopy (Fig. 3A). While MSCs were found to internalize numerous particles ranging from 0.5-3 μm in diameter (Fig. 3B-C), the modification procedure did not significantly impact cell phenotype including viability, adhesion, proliferation (Fig. 4) or multilineage

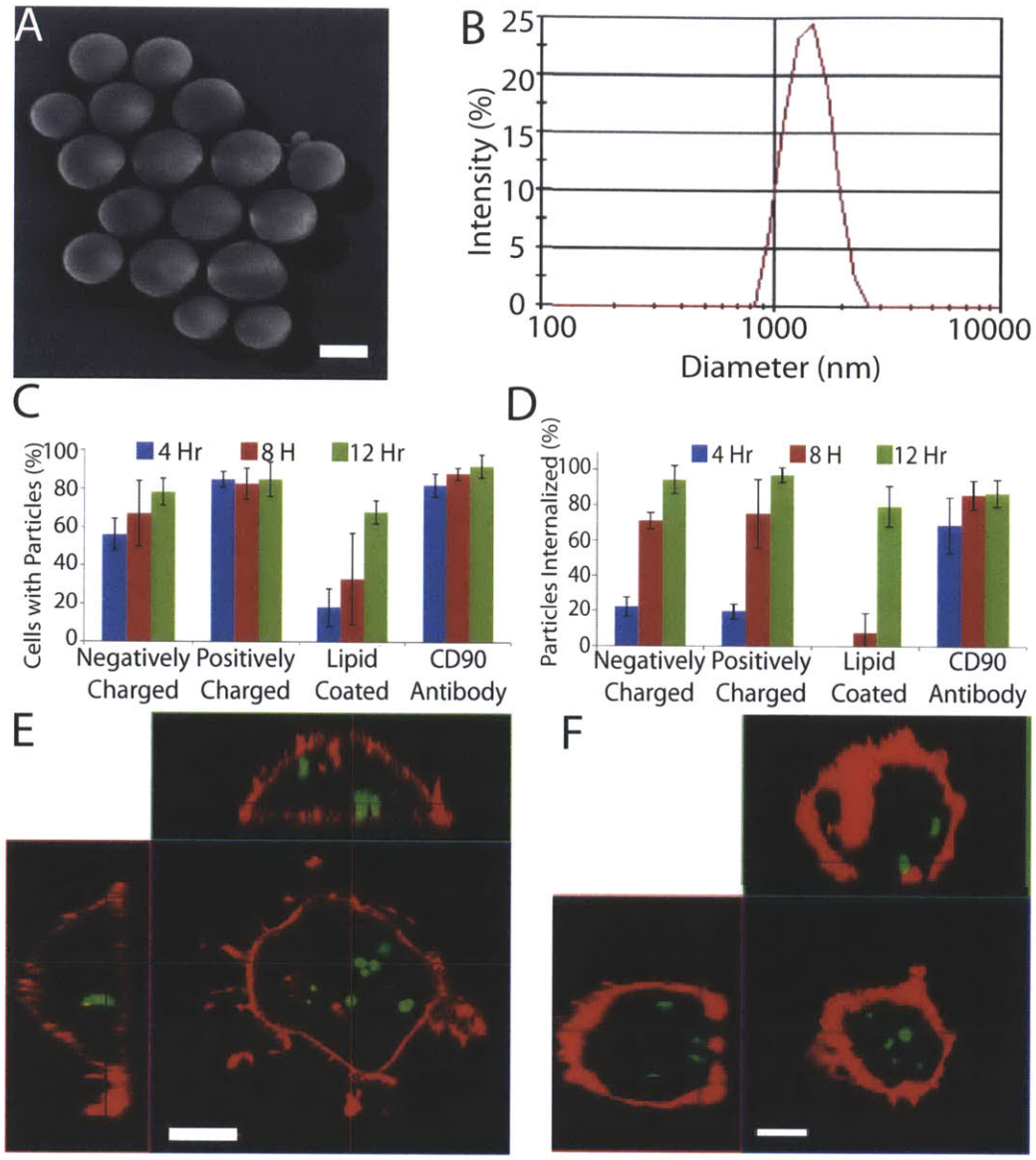


**Figure. 2**. Particle morphology, size, uptake and stability. (A) Scanning electron microscope image of PLGA particles reveals particles are spherical with a smooth pin-hole free surface (Scale bar: 1 μm). (B) Representative distribution of particle diameter as determined by dynamic light scattering. (C) Particle interaction/binding with cells was moderately affected by changes in surface chemistry, yet after 12 hr the majority of cells contained bound particles regardless of surface chemistry. (D) Kinetics of particle internalization as a function of particle surface chemistry. (E,F) Stability of internalized particles within DiD stained MSCs (red) as analyzed by confocal microscopy. Representative orthogonal confocal images (E) 1 day, and (F) 7 days after incubation with DiO loaded PLGA particles (green). (Scale bar: 10 μm) (Adapted from (*20*))

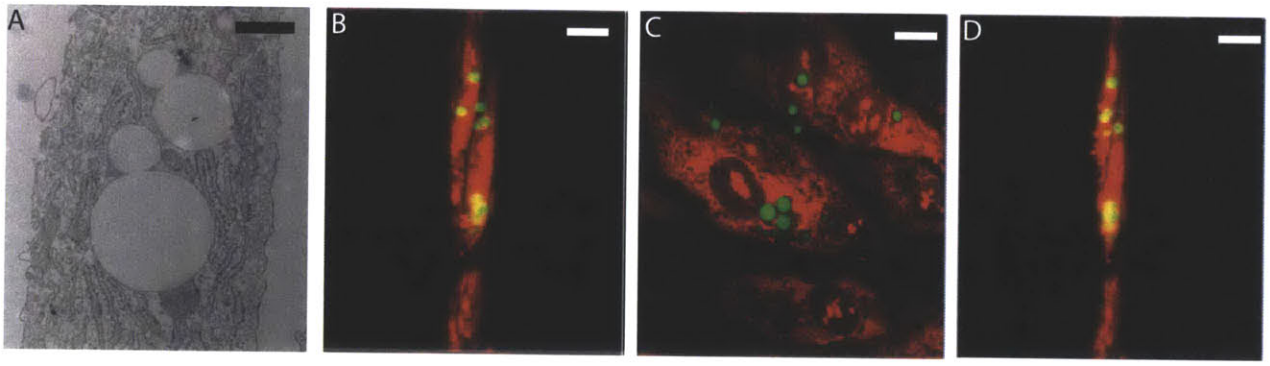


**Figure 3**. MSC internalization of polydisperse particles. MSCs were incubated with polydisperse DiO loaded PLGA particles, 300 nm - 5 μm, for 24 hr, fixed and prepared for transmission electron microscopy and confocal microscopy. (A) PLGA particles were observed in the intracellular space next to the rough endoplasmic reticulum (Scale bar: 500 nm). (B-D) Three 3D projections of a single confocal z-stack reveals 500 nm to 3 μm sized particles were internalized by MSCs at 24 hr (Scale bar: 10 μm). (Adapted from (*20*))

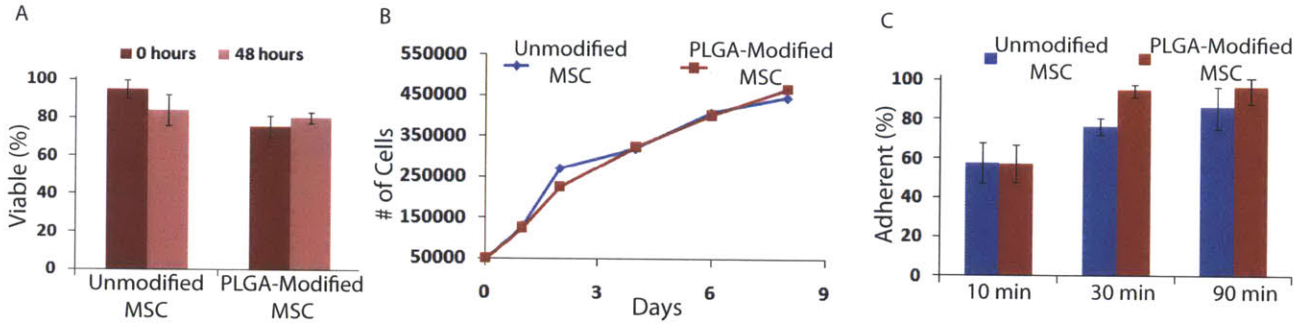


**Figure 4**. Viability, proliferation, and adhesion of modified MSCs. (A) Viability of MSCs engineered with PLGA particles immediately after modification and 48 hr after modification. (B) Proliferation of MSCs engineered with PLGA particles and unmodified MSCs. (C) Adhesion of MSCs engineered with PLGA particles on tissue culture plastic at 10, 30, and 90 min. (Adapted from (*20*))

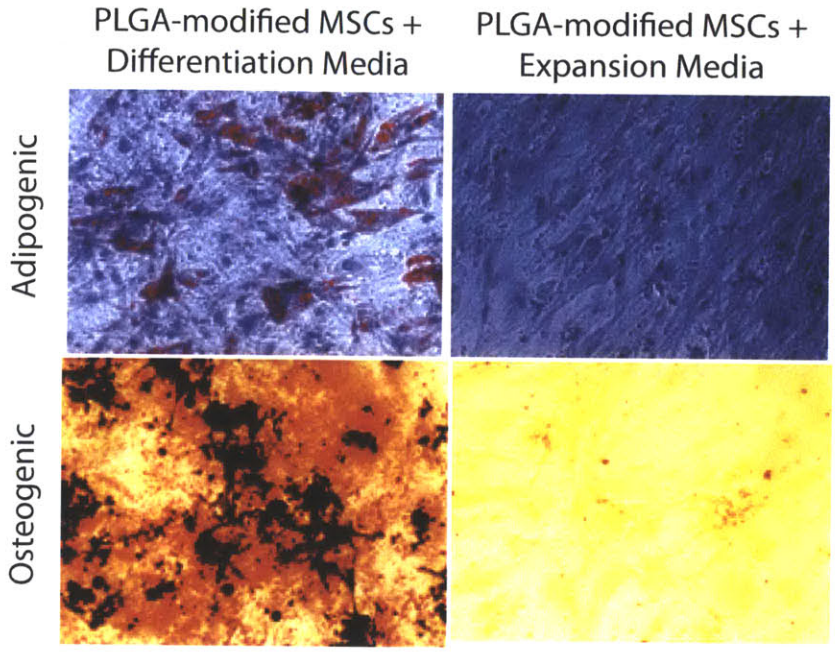


**Figure 5**. Differentiation potential of PLGA modified MSCs. Osteogenesis and adipogenesis 21 days after induction observed by alkaline phosphatase (ALP) and Oil Red O (ORO) staining, respectively. Particle modified MSCs cultured in respective differentiation media showed positive staining for both ORO and ALP. Particle modified MSCs cultured in expansion media, without differentiation factors, showed no ORO or ALP staining. (Adapted from (*20*))

differentiation potential (Fig. 5)

.Following the development of particles that were readily and stably internalized by MSCs, we sought to examine the potential for agents encapsulated within the particles to be released into the intracellular and extracellular milieu using rhodamine dye as a model small molecule (mol. wt. 479). Intracellular accumulation of rhodamine dye was examined over a 10 day period through permeabilization of the cells at different time points following rinsing to remove residual culture media. Dye was released in an initial burst within the first 2 days followed by relatively constant release (Fig. 6A). To examine the potential for rhodamine to be transported into the extracellular miliu, we sampled the media throughout the culture period with a fluorescence spectrophotometer and compared this result to a particle suspension without cells. Remarkably, we detected increasing concentrations of rhodamine over time in the culture media indicating transport from the intracellular to the extracellular milieu. Release of rhodamine from particles without cells showed a characteristic initial burst release with over 40% of encapsulated rhodamine being released within the first day followed by steady sustained release (Fig. 6B). In contrast, rhodamine was released from internalized PLGA depots at a constant rate, with 40% of entrapped rhodamine released by day 5 and 100% by day 10 (Fig. 6B). Importantly the rate of rhodamine delivery was easily tuned by changing the concentration of particles added to the cultures (Fig. 6C). This demonstrates the potential of engineering cells with particles to achieve sustained targeted release of membrane permeable agents to the carrier cell and its microenvironment.

**Controlling particle engineered cells, neighboring cells, and distant cells**

MSCs are multipotent cells capable of self-renewal that can give rise to a number of unique, differentiated mesenchymal cell types including osteoblasts, chondrocytes, and adipocytes. To examine the potential to control MSC phenotype we utilized an osteogenesis assay where differentiation of MSCs to osteoblasts can easily be detected through the characteristic expression of alkaline phosphatase (ALP) (*32*). MSCs differentiate into osteogenic cells in the presence of the glucocorticoid steroid, dexamethasone (DEX) that passively diffuses across the cell membrane (*21*, *22*), but

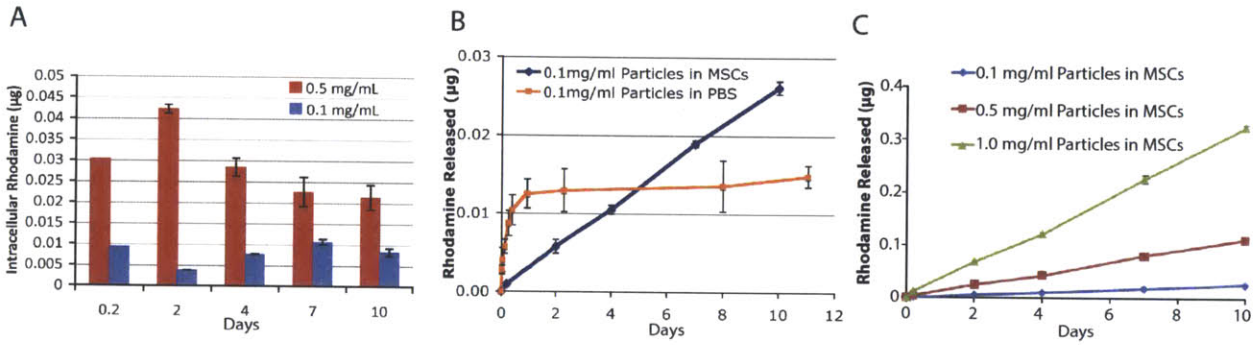


**Figure 6.** Rhodamine intracellular accumulation and extracellular release from MSCs. (A) To quantify the intracellular accumulation of rhodamine over time, MSCs loaded with 0.1 mg/mL or 0.5 mg/mL of rhodamine-PLGA particles were permeabilized with 5 mg/mL of L-lysine at 4 hr, 2 days, 4 days, 7 days, or 10 days, the permeabilized cells were discarded, and the dye concentration in the lysate was assessed with UV-Spectrophotometry. (B) Kinetics of rhodamine dye released into the culture media from MSCs modified particles versus a suspension of PLGA particles without cells. 200 µl of a 0.1mg/mL rhodamine-PLGA particle solution was added to the MSCs leading to internalization of ~19 µg and release was examined in 500 µl of media. To examine release of dye from particles without cells, conditions were normalized to the experimental group with ~19 µg of particles suspended in 500 µl of PBS. C. Extracellular release of a model dye. Sustained and controlled release of dye from MSCs modified with 200 µl of 0.1 mg/mL, 0.5 mg/mL and 1.0 mg/mL rhodamine-PLGA particles into surrounding media at 37 ºC over 10 days. (Adapted from (*20*))

only produce mineralized extracellular matrix in the presence of ascorbic acid (A) and phosphate ions (e.g. from β-glycerol-phosphate (G)) (*32*). Instead of placing DEX into media, we incorporated DEX into PLGA microparticles that were internalized by MSCs (Fig. 7A). Quantification of dexamethasone in media above modified cells demonstrated that DEX was transported from the particle engineered MSCs to the extracellular environment for up to 2 weeks (Fig. 7B). The media was supplemented with A and G and after 21 days, osteogenic differentiation was detected via ALP staining (Fig. 7C). MSCs with blank particles, and MSCs in the presence of A and G alone did not stain positive for ALP (Fig. 7D). Approximately 80% of the MSCs engineered with DEX containing particles in the presence of A and G stained positive for ALP, which was comparable to the ALP staining of MSCs (without particles) in complete osteogenic media. In addition, co-staining cultures with ALP and Von Kossa revealed the formation of bone nodules in DEX-PLGA cultures (Fig. 7E). Since DEX binds to intracellular glucocorticoid receptors (*21*, *22*), these results demonstrate that DEX released from PLGA microparticles induced osteogenic differentiation of particle modified MSCs as previously shown with nanoparticles (*33*, *34*). Thus microparticles that do not readily undergo exocytosis, as nanoparticles do (*19*), can be used to deliver phenotype altering agents such as dexamethasone to intracellularly control the fate of particle modified cells.

Given that DEX can be transported across the MSC membrane into the extracellular environment following internalization of DEX loaded microparticles, we envisioned particle engineered cells could be used to control the phenotype of neighboring cells in a paracrine-like manner. For an *in vitro* model, the previous experiment was repeated, with only half of the MSCs containing DEX-PLGA particles (Fig. 8A). Specifically, MSCs and DEX-PLGA modified MSCs were mixed in a 1:1 ratio and plated in a 6-well plate. Strikingly, following differentiation conditions, the majority of cells within the co-culture with DEX-PLGA particles stained positive for ALP (Fig. 8B). Given that cell adhesion and proliferation properties of the PLGA modified and unmodified cells were similar (Fig. 4), these results are likely not due to differences in adhesion and proliferation between the two populations of cells. This data suggests that DEX released from particle modified MSCs can control the fate of adjacent cells.

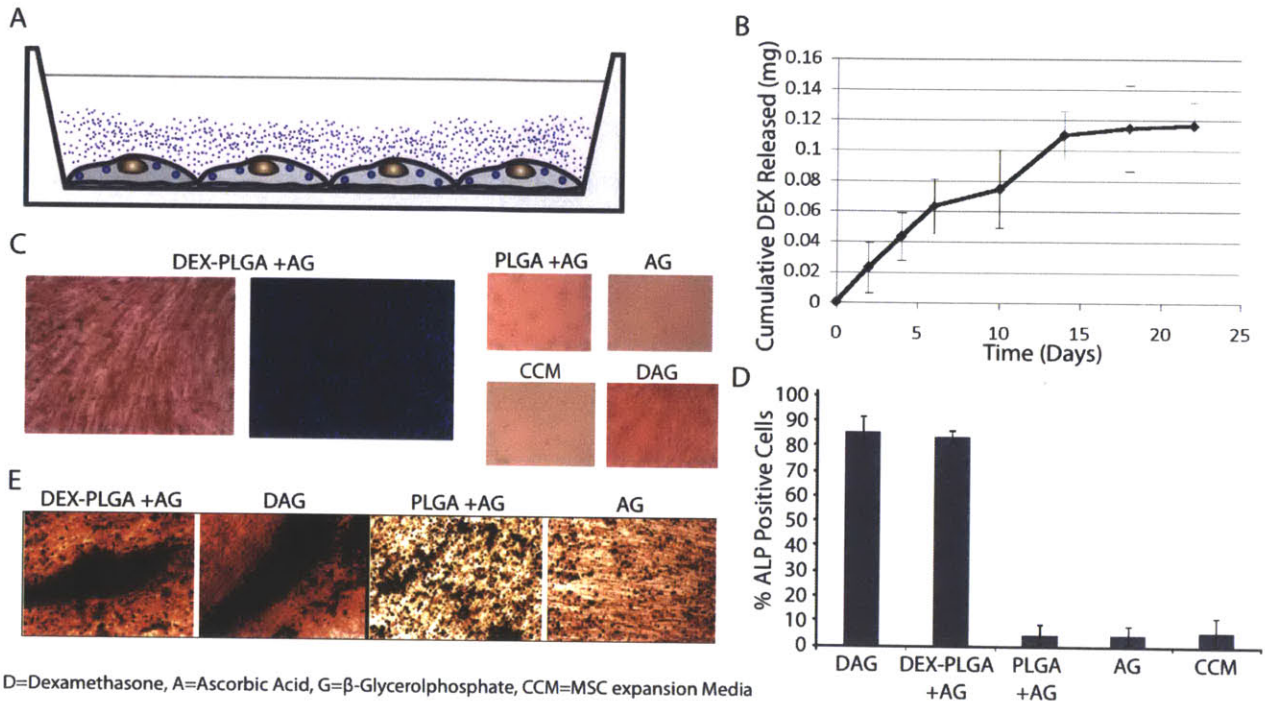


**Figure 7.** Intracrine-like signaling leads to osteogenic differentiation of DEX-PLGA particle modified MSCs. (A) Schematic of DEX release into culture media from adherent MSCs modified with DEX-PLGA particles. (B) Release kinetics of DEX from MSCs incubated with 0.1mg/mL DEX-PLGA particles into media at 37 °C for 21 days. (C) Osteogenic differentiation of DEX-PLGA modified MSCs and controls were assessed via alkaline phosphatase staining (ALP, red), nuclei were counterstained with DAPI (blue). (D) Quantification of ALP staining. (E) Bone nodules were identified via positive dual staining for Von Kossa and ALP in DEX and internalized DEX-PLGA particle containing cultures supplemented with A and G but not in the absence of DEX or DEX-PLGA particles. (Adapted from (*20*))

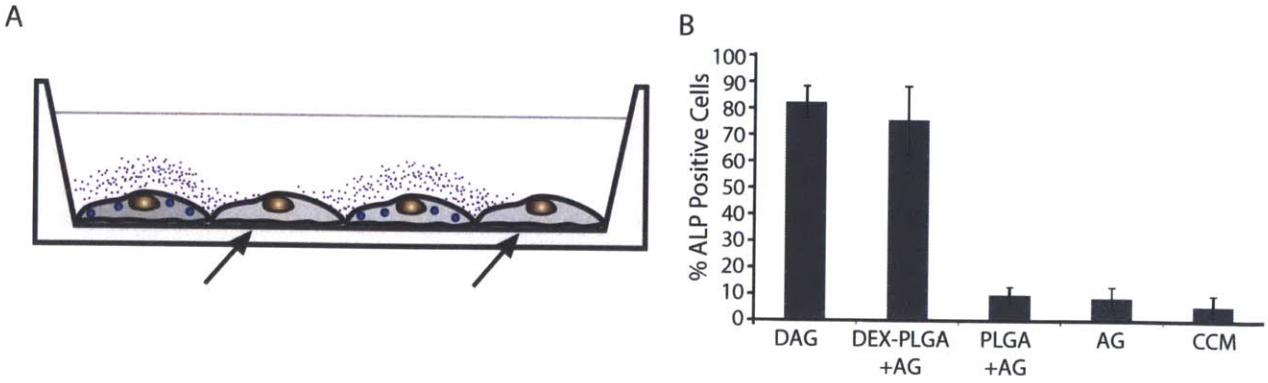


**Figure 8**. Paracrine-like activity of modified MSCs. (A) Schematic illustration of DEX-PLGA modified MSCs controlling the fate of neighboring MSCs without particles (black arrows). (B) Osteogenic differentiation of DEX-PLGA modified MSCs and neighboring MSCs seeded in a 1:1 ratio quantified through ALP staining. D=Dexamethasone, A=Ascorbic Acid, G=β-Glycerolphosphate, CCM=MSC expansion media. (Adapted from (*20*))

Next we examined the potential for extracellular release of DEX from particle-modified cells to promote differentiation of unmodified MSCs in a different culture dish (endocrine-like signaling). On every third day, conditioned media was transferred from particle modified cells (supplemented with G and A) to the unmodified cells and after 21 days stained to detect ALP activity (Fig. 9A). ALP staining of the unmodified cells incubated in conditioned media from DEX-PLGA modified cells was comparable to the DEX-PLGA modified MSCs (Fig. 9B). Importantly, no detectable ALP staining was observed when the media was transferred from MSCs engineered with blank PLGA particles (supplemented with G and A) and from unmodified MSCs (supplemented with G and A) to a separate dish containing unmodified MSCs. To ensure that the released DEX was responsible for induction of osteogenic differentiation and that this was not due to a factor released from the differentiating MSCs, additional experiments were performed. Specifically, media transferred from unmodified MSC cultures following 21 days of osteogenic differentiation (supplemented with DEX, G, and A) resulted in no detectable ALP staining (Fig. 9C). In a separate experiment, lung microvascular fibroblasts with internalized DEX-PLGA particles were used in place of MSCs. Media transferred from the DEX-PLGA modified fibroblast cultures to unmodified MSCs (supplemented with G and A) induced osteogenic differentiation of the MSCs to the same degree as media transferred from DEX-PLGA modified MSCs (Fig. 9D). These two controls demonstrate that the DEX released from the particle modified cells was responsible for inducing osteogenic differentiation of the unmodified MSCs in a different culture dish in an endocrine-like manner.

To determine if engineered endocrine-like signaling could promote differentiation in a more relevant assay, we investigated the ability of adhered DEX-PLGA modified MSCs to impact the fate of cells on a distant transwell membrane in the same culture environment. We incubated MSCs with DEX-PLGA particles on the bottom surface of a transwell dish, and unmodified MSCs on a filter surface that was 2mm above in the presence of A and G (Fig. 9E). Cells were stained to detect ALP activity after 21 days in culture. DEX-PLGA modified MSCs were shown to induce the differentiation of ~80% of the unmodified MSCs on the transwell membrane (Fig. 9F). This demonstrates that agents released from particle-modified cells can impact the fate of distant cells without

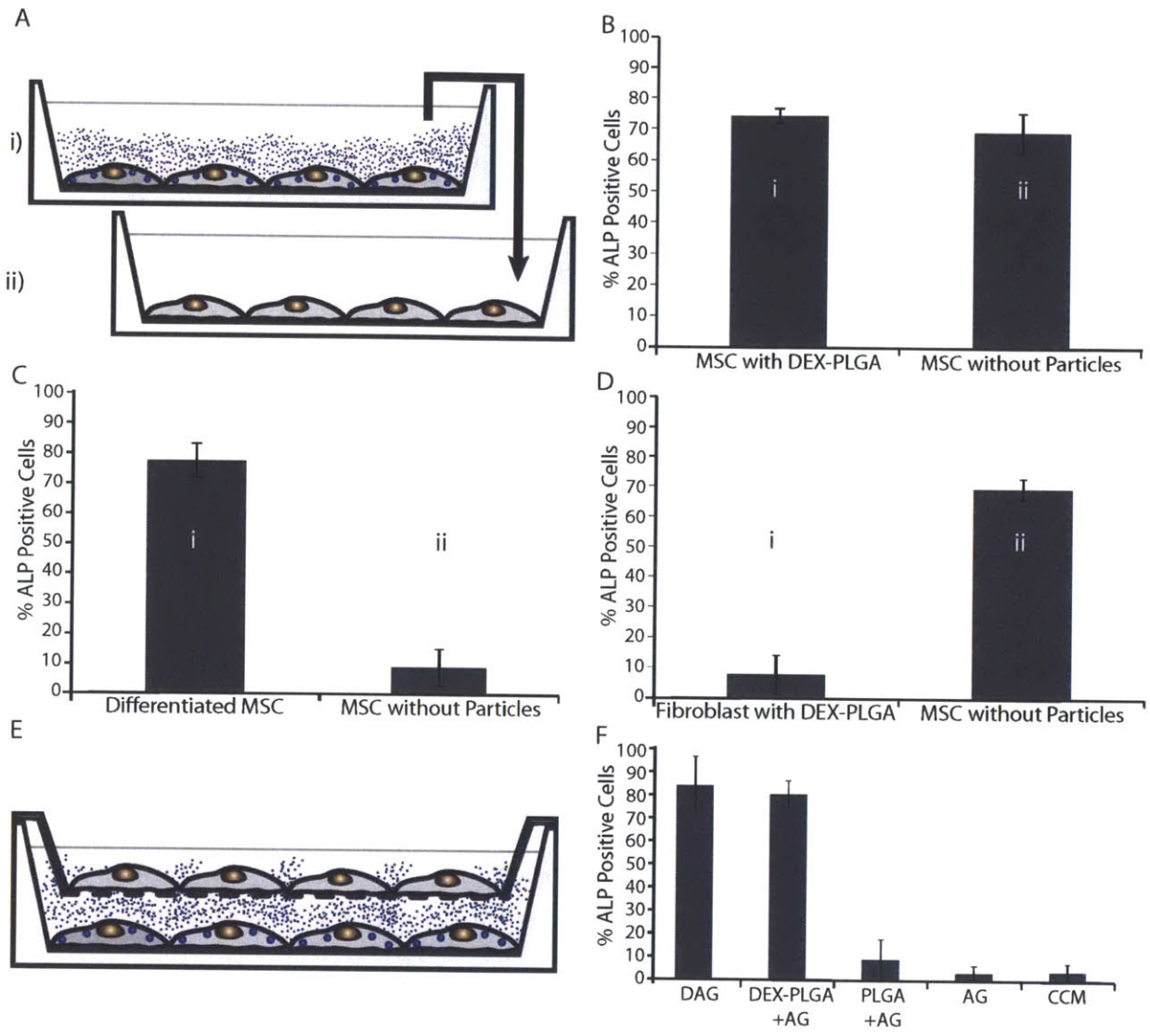


**Figure 9**. Endocrine-like activity of modified MSCs. (A) Schematic illustration of programming cell fate of distant cells (without particles in well 'ii') by transferring conditioned media from well 'i', containing DEX-PLGA modified MSCs, differentiated MSCs, or DEX-PLGA modified fibroblasts to well 'ii'. (B) Osteogenic differentiation of DEX-PLGA modified MSCs and distant cells quantified through ALP staining. (C) Osteogenic differentiation of MSCs treated with conditioned media from differentiated MSCs without DEX-PLGA particles. (D) Osteogenic differentiation of MSCs treated with conditioned media from DEX-PLGA modified fibroblasts. (E) Schematic illustration of DEX-PLGA modified MSCs controlling the fate of MSCs (without particles) separated by a transwell membrane 2 mm above the surface. (F) Osteogenic differentiation of unmodified MSCs atop transwell membrane quantified through ALP staining. (Adapted from (*20*))

cell contact.

**Controlling cell fate after cryopreservation**

To assess the potential for particle modified MSCs to retain their DEX releasing properties following cryopreservation, cells containing DEX-PLGA particles were stored for 10 days at -140° C. Upon thawing and re-plating, particle modified MSCs differentiated into osteogenic cells via intracellular release of DEX, as indicated by positive alkaline phosphatase staining (Fig. 10 A,C) and induced osteogenic differentiation of distant unmodified MSCs, comparable to non-cryopreserved DEX-PLGA modified cells (Fig. 10 B,D) Thus particle engineered MSCs can be cryopreserved without loss of activity.

**Potential for a platform technology**

While small molecules such as DEX and rhodamine can freely cross the membrane of cells such as MSCs, it is well known that many exogenously supplied molecules (i.e. added to the culture media) have limited ability to traverse membranes unless the membranes are permeabilized (*24*). However, we do not anticipate this to be a significant bottleneck to expanding our results to other agents including small molecules, peptides, and proteins given that many cell types including MSCs possess relevant machinery to facilitate transport of agents from the intracellular to the extracellular environment. For example, MSCs and their subpopulations have been shown to express the plasma membrane protein, P-glycoprotein otherwise known as permeability glycoprotein (*35-37*), an ATP-dependent efflux pump responsible for multidrug resistance in tumor cells that is also expressed in hematopoietic stem cells and their progeny (*25*). Interestingly, P-glycoprotein has the ability to transport multiple types of agents across the cell membrane including steroids, lipids, peptides, and drugs. P-glycoprotein can also be modulated to alter drug efflux (*38*). In addition to P-glycoprotein mediated transport of soluble agents, cell-cell communication via soluble cues may occur through gap junctions that permit the movement of small molecules and proteins between cells that are in direct cell contact. This pathway has been exploited for double stranded shRNAs/siRNA delivery (*26*, *39*). MSCs have been shown to

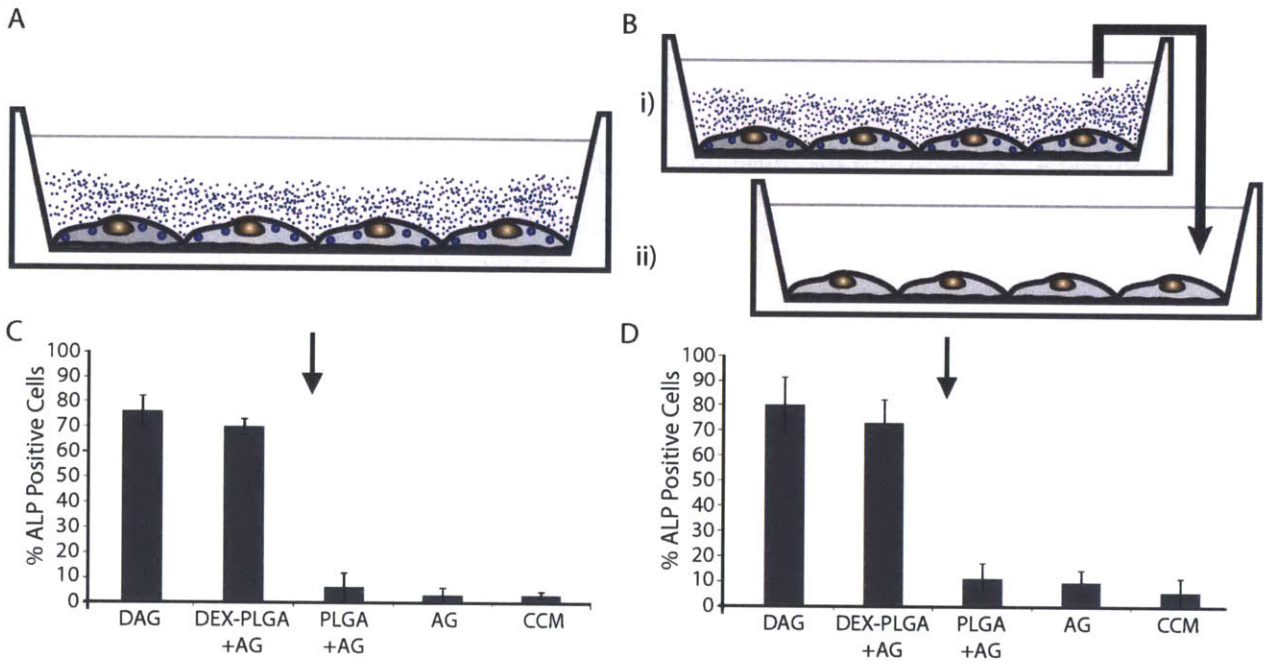


**Figure 10**. Effect of cryopreservation on DEX-PLGA modified MSCs. MSCs modified with DEX-PLGA particles were frozen at -140 °C for 10 days and then thawed to assess their cell programming capability. (A) Schematic of DEX release into culture media from adherent MSCs modified with DEX- PLGA particles. (B) Schematic illustration of controlling the fate of distant cells (without particles) by transferring conditioned media from well 'i', containing DEX-PLGA modified MSCs to well 'ii'. (C) Osteogenic differentiation of DEX-PLGA modified MSCs quantified through ALP staining. (D) Osteogenic differentiation of distant cells grown in conditioned media from DEX-PLGA modified MSCs quantified through ALP staining. D=Dexamethasone, A=Ascorbic Acid, G=β-Glycerolphosphate, CCM=MSC expansion media. (Adapted from (*20*))

express gap junctions and it has been suggested that this could be used as a means to mediate responses of cells that are in direct cell contact with MSCs(*40*, *41*), however in the current study only small molecule delivery was explored. Furthermore, MSCs have been shown to use nanometer scale vesicles called exosomes (*42*, *43*) for transport of multiple intracellular agents to the extracellular environment, as has been shown for other cell types (*44*, *45*). Thus, the collective activity of these mechanisms theoretically permits the delivery and extracellular transport of a large repertoire of therapeutic agents via internalized biodegradable particles. For example, agents could be used to impact cell survival, proliferation, differentiation, extracellular matrix production, cell death, or expression of therapeutic peptides and proteins. We envision this intracellular drug depot will be useful for developing cell-based therapies for tissue regeneration, drug delivery and cancer therapeutics and potentially in combination with cell based targeting strategies (*46-49*). In addition, stable microparticle internalization may enable improved monitoring of cell therapies through the development of enhanced contrast agents.

**Application of platform technology for enhanced MRI imaging**

Monitoring the location, distribution and long-term engraftment of administered cells is critical for demonstrating the success of a cell therapy. Among available imaging-based cell tracking tools, magnetic resonance imaging (MRI) is advantageous due to its non-invasiveness, deep penetration, and high spatial resolution(*50*). While tracking cells in pre-clinical models via internalized MRI contrast agents (iron oxide nanoparticles, IO-NPs) is a widely used method(*51*, *52*), IO-NPs suffer from low iron content per particle, low uptake in non-phagocytotic cell types (e.g., mesenchymal stem cells, MSCs), weak negative contrast, and decreased MRI signal due to cell proliferation and cellular exocytosis(*19*). To examine if our particle-engineered approach could be adapted to enhance MRI tracking of MSCs and provide an advantage over current nanoparticle based approaches, we encapsulated iron oxide nanoparticles (IO:NP, 10 nm) in PLGA microparticles(0.4-1.5 μm).

As with DEX particles, IO:NP PLGA particles were formulated through a single emulsion technique and found to be ~1 μm in size with iron oxide particles clustered

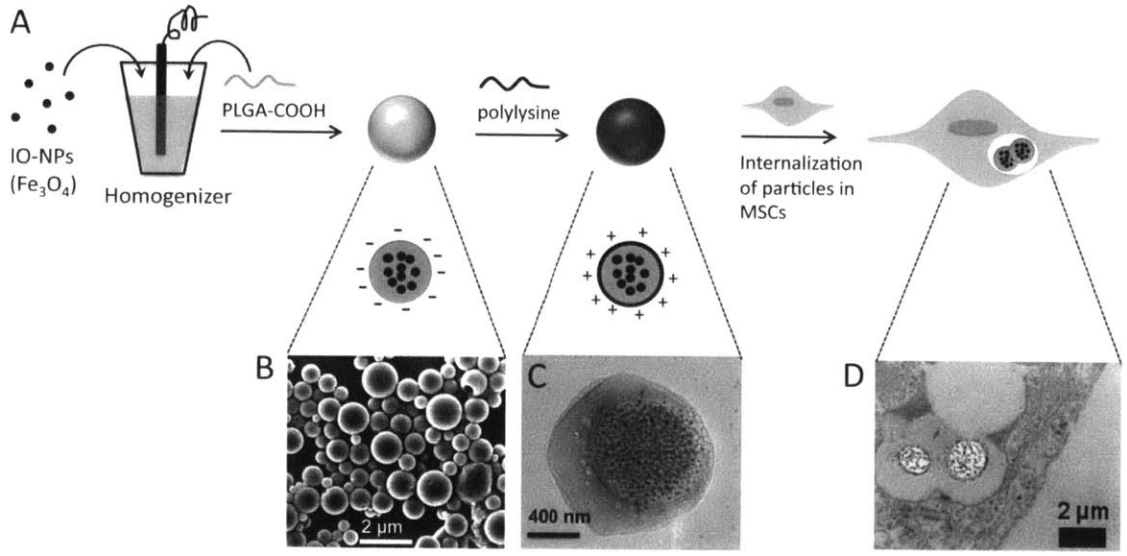


**Figure 11**. IO:PLGA-MPs preparation and internalization by MSCs: (A) Schematic illustration of the preparation of IO:PLGA-MPs with single emulsion method. (B) SEM image of IO:PLGA-MPs. (C) TEM image of a representative IO:PLGA-MP. (D) TEM image of IO:PLGA-MPs internalized in an MSC. (Adapted from (*53*))

in the core of particle (Fig. 11). Interestingly, clustering of iron oxide has previously been shown to result in enhanced T2 signal of nanoparticles(*54*).

MSCs were modified with particles while maintaining a constant Fe concentration (25, 50, 100 or 200 μg/mL) and the amount of Fe loaded into the cells was quantified. MSCs were digested and Fe content was quantified via ICP-AES. The maximum Fe loading/cell was attained at 100μg/mL initial concentration (Fig. 12A). Further increases in the initial Fe concentration did not enhance the final quantity of Fe per cell. Interestingly, maximal Fe loading per cell was 20 and 80 pg Fe/cell for IO-NPs and IO:PLGA-MPs, respectively. A significant 4-fold increase for Fe loading per cell reveals the advantage of using microparticles for internalization of iron oxide.

To assess changes in Fe content over time, following particle internalization and subsequent purification from free particles, MSCs were plated in T25 plates for 28 days (the labeling day was designated as day 1). The culture media was replaced every two days for all samples and at each time point (day 1, 2, 4, 6, 12, and 28) MSCs were collected for quantification of MSC proliferation, Fe concentration, and MRI analysis (by dispersing 200,000 MSCs in 1 mL 3% agarose gel). As shown in Fig. 11B, when MSCs were labeled with IO-NPs, the iron concentration per MSC decreased to ~50% of the initial value by day 4 and the iron concentration per cell approached background by 12 days. However, when MSCs were labeled with IO:PLGA-MPs, within 6 days the concentration had decreased to half of its initial value and after 25 days, the iron concentration per cell remained significantly higher than background. The combination of contrast enhancement due, possibly due to iron oxide clustering, and increased cellular loading in MSCs of IO:PLGA-MPs permitted us to visualize MSCs with MRI for at least 12 days (Fig. 12C). While in the case of IO-NPs labeling there was minimal detectable signal after only 6 days. To further confirm the MRI results and examine the stability of internalized IO:PLGA-MPs, we labeled MSCs with fluorescent IO:PLGA-MPs containing DiI and examined the fluorescent signal by fluorescent confocal microscopy. 18 days after labeling, IO:PLGA-MPs could still be found in 15±5% MSCs (Fig. 12D), which reveals the potential of IO:PLGA-MPs for the long-term tracking of MSCs.

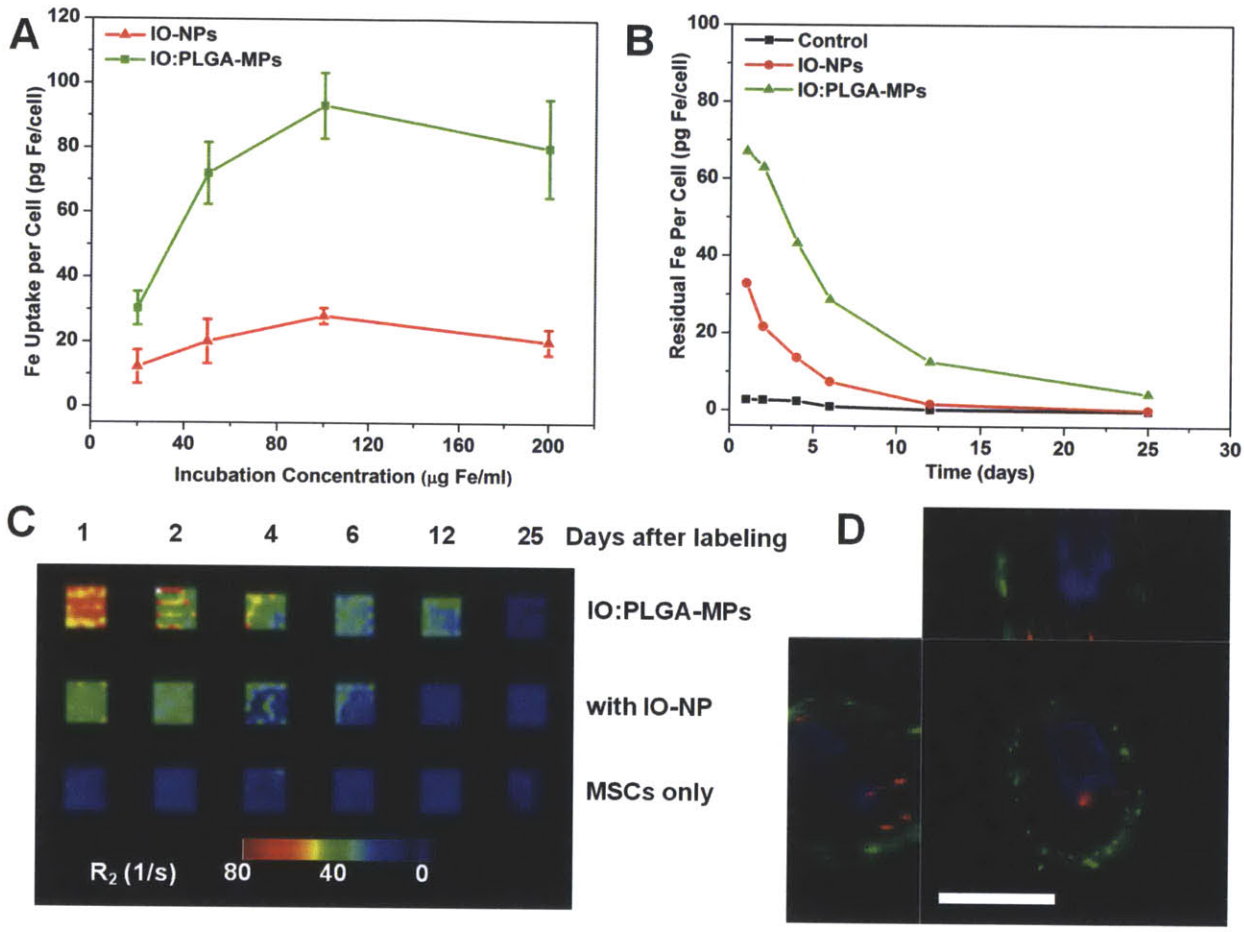


**Figure 12**: Improved retention of IO in MSCs after PLGA encapsulation: (A) Cellular Fe content of MSCs after incubation with magnetic particles as a function of iron concentration. (B) Change in cellular iron content per cell after initial labeling with IO-NPs or IO:PLGA-MPs at the incubation concentration of 50μg Fe/ml. (C) $R_2$-weighted MR images of 200,000 MSCs collected at different time points and suspended in 3% agarose gels (4 × 4 $mm^2$ per square) . (D) Fluorescent confocal image of MSCs 18 days after labeling with IO:PLGA-MPs. The plasma membrane is stained green (DiO), the nucleus is blue (DAPI) and the IO:PLGA-MPs are stained red (DiI). Scale bar is 10μm. (Adapted from (*53*))

## Conclusion

Herein we have developed a strategy to engineer cells with intracellular particles to impart intracellular and extracellular control of cell fate. In our proof of concept studies we have shown that primary human mesenchymal stem cells (MSCs) can efficiently internalize 1-2 micron sized biodegradable particles containing differentiation factors or iron oxide nanoparticles. Drug loaded particles remain localized within the cell for at least 7 days while releasing biologically active agents such as dexamethasone. The release kinetics to the extracellular environment can easily be controlled by tuning the number of internalized particles. Remarkably, differentiation factors released from the particles were shown to promote the differentiation of particle-carrying cells (intracrine-like signaling), neighboring cells (paracrine-like signaling), and the differentiation of distant cells (endocrine-like signaling). In addition to use as an *in vitro* tool to create cell niches in culture where temporal and spatial control of cellular cues is critical, intracellular depots may permit exquisite control over transplanted cells and their microenvironment through impacting cellular phenotype and function. Finally, to demonstrate the utility of this technology as a platform technology we demonstrated the ability to engineer MSCs with iron oxide loaded microparticles, leading to enhanced MRI contrast and prolonged detection of MSCs over existing nanoparticle based approaches. We believe this technology can serve as a platform in which cells can be influenced, tracked, and probed through through incorporation of novel phenotype altering small molecules, modulation of particle formulation to control release kinetics, or conjugation of chemical sensors onto the particle surface opening the door to a wide array of potential applications.

## Materials & Methods

### Mesenchymal stem cell culture and characterization

Primary human MSCs were obtained from the Texas A&M Health Science Center, College of Medicine, Institute for Regenerative Medicine at Scott & White Hospital supported by NIH Grant # P40RR017447. MSCs were derived from healthy consenting donors and thoroughly characterized as previously described (*8-12*, *55*).

MSCs were maintained in α-MEM expansion media (Invitrogen) supplemented with 15% Fetal Bovine Serum (Atlanta Biologicals), 1% (v/v) L-Glutamine (Invitrogen), and 1% penicillin:streptomycin solution (Invitrogen). Cells were cultured to 70-80% confluence before passaging. All experiments were performed using MSCs at passage number 3-6 where cells expressed high levels of MSC markers CD90 and CD29 (>99% cells), and did not express hematopoietic markers CD34 or CD45 (0% of cells) as observed from flow cytometry analysis.

**PLGA Microparticle Fabrication**

Rhodamine 6G dye (Sigma) or the osteogenic differentiation agent, dexamethasone (DEX), were encapsulated in poly (lactic-co-glycolic) acid (PLGA) particles using a single emulsion encapsulation technique. Briefly, 100 mg of 50kDa (0.55-0.75 dL/g inherent viscocity) 50:50 PLGA(carboxylic acid end group) was dissolved in 2 mL dichloromethane. DEX or dye was then added to the PLGA solution and mixed thoroughly. For complete dissolution of DEX, 10% methanol was added to dichloromethane. The PLGA solution was then added to 20 mL of 1% (w/v) polyvinylalcohol (80% hydrolyzed) solution in deionized water and emulsified using a probe sonicator at 30 W for 60 seconds. The solution was then stirred overnight at room temperature on a magnetic stirrer to allow extraction and evaporation of the organic solvent. The remaining solution was centrifuged and rinsed with PBS to isolate particles and lyophilized. Particle size was determined by dynamic light scattering and confirmed by scanning electron microscopy. To determine the encapsulation efficiency, briefly, 10 mg of DEX-PLGA particles were dissolved in anhydrous dimethyl-solfoxide (DMSO) followed by quantification of DEX with a UV-vis spectrophotometer at 251 nm. Blank PLGA particles without any DEX served as control. DEX was reliably encapsulated in DEX-PLGA particles with an efficiency of 71±13.5% (e.g. from an initial 10mg of DEX, ~7.1mg ±1.35 was typically entrapped within the PLGA particles).

**Modifying MSCs with PLGA microparticles.**

To improve particle uptake, PLGA microparticles were incubated with 50 μg/mL poly-L-lysine for 3 hrs before incubation with MSCs. PLGA particle suspensions with

concentrations of 0.1 mg/mL and 0.5 mg/mL in PBS were added to 90% confluent layers of MSCs in a 24 well plate for 10 min after which the PBS was removed and complete media was added. The MSCs were allowed to internalize particles for 24 hrs at 37 °C. To characterize particle internalization and stability of internalized particles, MSCs were loaded with DiO containing PLGA particles and characterized with a Zeiss LSM510 laser scanning confocal microscope equipped with a 63X water dipping objective. After a 24 hr incubation, the cells were fixed with 3.7% formaldehyde at room temperature and stained with 5 μg/mL of propidium iodide (PI) solution or 5 μl/mL DiI Vybrant cell stain solution for 10 min to visualize the cells. The cells were visible through the red fluorescence channel and the particles were visible through the green fluorescence channel. Internalization of particles was examined from 3-D re-constructed Z-stack confocal microscopy images and a particle was considered internalized if it was localized within the plane of the nucleus, yet inside the borders of the cell membrane. The percentage of internalized particles was calculated from the number of particles present inside the cell compared to the total number of particles associated with cells in the field of view for ten random fields. For transmission electron microscopy, particle modified cells were prepared as described above, fixed, and analyzed by the W.M Keck Microscopy Facility at the Whitehead Institute. Specifically, the cells were fixed in 2.5% gluteraldehyde, 3% paraformaldehyde with 5% sucrose in 0.1M sodium cacodylate buffer (pH 7.4), pelleted, and post fixed in 1% OsO4 in veronal-acetate buffer. The cell pellet was stained in block overnight with 0.5% uranyl acetate in veronal-acetate buffer (pH 6.0), then dehydrated and embedded in Spurrs resin. Sections were cut on a Reichert Ultracut E microtome with a Diatome diamond knife at a thickness setting of 50 nm, stained with uranyl acetate, and lead citrate. The sections were examined using a FEI Tecnai spirit at 80KV and photographed with an AMT CCD camera. The viability, adhesion kinetics and proliferation of particle-modified MSCs and unmodified MSCs were examined using our previously reported experimental methodology(*46*). Briefly, the viability of the cells was examined immediately after modification (time 0) and after the cells were incubated within 6-well plates for 48 hrs using a trypan blue exclusion assay. Cell adhesion kinetics were quantified by measuring the number of adherent cells on the tissue culture surface after 10, 30, and 90 min. Proliferation of modified and

unmodified MSCs was quantified by plating cells in T25 flasks at low density and counting the number of cells in the flask for an 8 day period with light microscopy at 10X for ten random fields. Multi-lineage differentiation potential of the particle modified MSCs and unmodified MSCs was examined by incubating cells with osteogenic and adipogenic induction media followed by respective colorimetric staining (*46*). Cells were assayed for osteogenic differentiation and adipogenic differentiation using cell membrane associated alkaline phosphatase activity and Oil Red O staining, respectively.

### *In vitro* release experiment from particle modified MSCs

0.1 mg/mL, 0.5mg/mL, or 1mg/mL PLGA microparticles with entrapped rhodamine dye were incubated with MSCs for 24 hrs at 37 °C. The media was then discarded and the cells were rinsed with PBS and supplied fresh media to create a baseline for the dye release measurements. On days 2, 4, 7, 10 media was collected and the quantity of dye released was measured using a fluorescence spectrophotometer with excitation and emission wavelengths of 540 and 625 nm, respectively. Preliminary characterization of the particle-modification approach showed that 0.1mg/mL particles were efficiently internalized by cells and resulted in adequate cell loading, therefore this concentration was used for the remainder of the experiments. To quantify the amount of dexamethasone released, MSCs were incubated with 0.1 mg/mL DEX-PLGA particles for 24 hrs at 37 °C. On day 2, 4, 6, 10, 14, 18, and 22, 1 mL of media was collected and replenished with fresh media. The released DEX was determined using ultraviolet (UV) spectrophotometer at 251 nm. Cells with no particles and cells with blank particles (no DEX) served as controls.

### Examination of Osteogenic Differentiation

To evaluate osteogenic differentiation, cell membrane associated ALP activity was examined after 21 days by aspirating the culture media and rinsing the cells followed by fixation with 3.7% formaldehyde solution for 10 min at room temperature. After 45 min incubation in 0.06% Red Violet LB salt solution in Tris HCl, DMF and Naphthol AS MX-$PO_4$, the wells were rinsed 3 times with distilled water and visualized

with light microscopy. Osteogenic differentiation was identified by staining for alkaline phosphatase activity. To visualize individual cells, the nuclei of the cells were stained with 100 µL of DAPI solution (1 µg/mL in PBS) after treatment with 100 µL of 0.1% TRITON X solution in PBS. ImageJ® software was used to quantify the percentage of MSCs stained positively for alkaline phosphatase. Some cultures stained for ALP were further examined for the presence of mineralization via Von Kossa staining. Briefly, plates were rinsed 3-4 X in $ddH_2O$, and stained with 2.5% silver nitrate for 30 min. After rinsing 3-4 X in $ddH_2O$, plates were incubated in sodium carbonate formaldehyde for 1-2 min, rinsed, air dried, and examined by light microscopy.

**Differentiation of particle modified cells**

Microparticles containing DEX were incubated with MSCs for 24 hr followed by rinsing to remove free particles and the media was replaced with β-glycerolphosphate (G) and Ascorbic Acid (A) containing media. Cells grown in α-MEM complete media served as a negative control, while cells grown in media supplemented with DEX, G and A served as a positive control for osteogenic differentiation. Additional controls included media containing only G or A and cells containing empty PLGA particles (no DEX). Cultures were maintained for 21 days and then assessed for osteogenic differentiation by ALP staining as described above.

**Differentiation of neighboring and distant cells**

To assess the potential of MSCs modified with DEX-PLGA microparticles to induce osteogenic differentiation of adjacent unmodified MSCs, a model assay was developed. MSCs modified with DEX-PLGA particles were mixed with equal number of unmodified MSCs and plated at a density of 300,000 cells per well in a 6 well plate. The media was supplemented with β-glycerolphosphate (G) and Ascorbic Acid (A). Cells grown in α-MEM complete media served as a negative control, while cells grown in media supplemented with DEX, G and A served as a positive control. Other controls included media containing only G or A and cells containing empty PLGA particles. Cultures were maintained for 21 days and then assessed for osteogenic differentiation as described above. To assess the potential of DEX-PLGA microparticle modified MSCs

to induce osteogenic differentiation of unmodified MSCs at a distant site, two model assays were developed. First, MSCs containing DEX-PLGA microparticles were plated in 6-well culture plates and unmodified MSCs were plated in separate 6-well culture plates. The media added to DEX-PLGA modified MSCs was supplemented with G and A. Media from the particle modified MSCs was transferred to wells containing unmodified MSCs every third day and fresh media with β-glycerolphosphate (G) and Ascorbic Acid (A) was replenished. Cells grown in α-MEM complete media served as a negative control, while cells grown in media supplemented with DEX, G and A served as a positive control. Other controls included media containing only G or A and cells containing empty PLGA particles. Cultures were maintained for 21 days and then assessed for osteogenic differentiation as described above. To rule out the possibility that the observed induction of osteogenesis was mediated by factors secreted by the differentiating DEX-PLGA modified MSCs, the experiment was repeated using lung microvascular fibroblasts (in place of MSCs) modified with DEX-PLGA particles. Towards the same goal, the impact of transferring media from fully differentiated osteogenic cultures of MSCs (without particles) to a separate culture dish containing unmodified cells was assessed. Second, MSCs containing DEX-PLGA microparticles were plated on the bottom well of a transwell plate. Unmodified MSCs were then plated on the membrane of the transwell and the media was supplemented with β-glycerolphosphate (G) and Ascorbic Acid (A). Cells grown in α-MEM complete media (without osteogenic factors) served as a negative control, while cells grown in media supplemented with DEX, G and A served as a positive control. Other controls included media containing only G or A and cells containing PLGA particles without DEX. Cultures were maintained for 21 days and then assessed for osteogenic differentiation as described above.

**Effect of Cryopreservation**

To examine the effect of cryopreservation on DEX release and ability to influence the cellular microenvironment, the DEX-PLGA particles were incubated with MSCs for 24 hr followed by trypsinization with 1X trypsin-EDTA solution. The particle modified cells were frozen in complete cell culture media supplemented with 5% dimethyl

sulfoxide at -140°C. After 10 days the cells were thawed, plated, and the release of DEX was examined in addition to repeating the osteogenic differentiation experiments described above.

## Acknowledgements

This work was supported by National Institute of Health grant HL097172, HL095722 and DE019191 to JMK and by the American Heart Association grant #0970178N to JMK. JAA was supported by National Science Foundation (NSF) Graduate Research Fellowship. We would like to thank Dr. Chenjie Xu of Brigham & Women's Hospital for his assistance with SEM imaging and Nicki Watson of the Whitehead Institute for help with TEM.

## References


1. C. E. Murry, G. Keller, Differentiation of embryonic stem cells to clinically relevant populations: lessons from embryonic development, *Cell* **132**, 661–680 (2008).

2. S. Kumar, S. Ponnazhagan, Bone homing of mesenchymal stem cells by ectopic 4 integrin expression, *The FASEB Journal* **21**, 3917–3927 (2007).

3. H. K. Haider, S. Jiang, N. M. Idris, M. Ashraf, IGF-1-overexpressing mesenchymal stem cells accelerate bone marrow stem cell mobilization via paracrine activation of SDF-1alpha/CXCR4 signaling to promote myocardial repair, *Circ Res* **103**, 1300–1308 (2008).

4. M. Gnecchi *et al.*, Paracrine action accounts for marked protection of ischemic heart by Akt-modified mesenchymal stem cells, *Nat Med* **11**, 367–368 (2005).

5. M. Gnecchi *et al.*, Evidence supporting paracrine hypothesis for Akt-modified mesenchymal stem cell-mediated cardiac protection and functional improvement, *Faseb J* **20**, 661–669 (2006).

6. L. S. Sasportas *et al.*, Assessment of therapeutic efficacy and fate of engineered human mesenchymal stem cells for cancer therapy, *Proc Natl Acad Sci USA* **106**, 4822–4827 (2009).

7. A. A. Mangi *et al.*, Mesenchymal stem cells modified with Akt prevent remodeling and restore performance of infarcted hearts, *Nat Med* **9**, 1195–1201 (2003).

8. M. P. Lutolf, P. M. Gilbert, H. M. Blau, Designing materials to direct stem-cell fate, *Nature* **462**, 433–441 (2009).

9. D. E. Discher, D. J. Mooney, P. W. Zandstra, Growth Factors, Matrices, and Forces Combine and Control Stem Cells, *Science* **324**, 1673–1677 (2009).

10. D. R. Albrecht, G. H. Underhill, T. B. Wassermann, R. L. Sah, S. N. Bhatia, Probing the role of multicellular organization in three-dimensional microenvironments, *Nat Methods* **3**, 369–375 (2006).

11. D. J. Mooney, H. Vandenburgh, Cell delivery mechanisms for tissue repair, *Cell Stem Cell* **2**, 205–213 (2008).

12. T. Dvir, B. P. Timko, D. S. Kohane, R. Langer, Nanotechnological strategies for engineering complex tissues, *Nature Nanotechnology* (2010), doi:10.1038/nnano.2010.246.

13. V. H. Fan *et al.*, Tethered epidermal growth factor provides a survival advantage to mesenchymal stem cells, *Stem Cell* **25**, 1241–1251 (2007).

14. M. Davis, P. Hsieh, A. Grodzinsky, R. T. Lee, Custom design of the cardiac microenvironment with biomaterials, *Circ Res* **97**, 8–15 (2005).

15. Y. Luo, M. S. Shoichet, A photolabile hydrogel for guided three-dimensional cell growth and migration, *Nat Mater* **3**, 249–253 (2004).

16. J. M. Karp, G. S. Leng Teo, Mesenchymal stem cell homing: the devil is in the details, *Cell Stem Cell* **4**, 206–216 (2009).

17. M. T. Stephan, J. J. Moon, S. H. Um, A. Bershteyn, D. J. Irvine, Therapeutic cell engineering with surface-conjugated synthetic nanoparticles, *Nat Med* **16**, 1035–1041 (2010).

18. H. Cheng *et al.*, Nanoparticulate cellular patches for cell-mediated tumoritropic delivery, *ACS nano* **4**, 625–631 (2010).

19. J. Panyam, V. Labhasetwar, Dynamics of endocytosis and exocytosis of poly(D,L-lactide-co-glycolide) nanoparticles in vascular smooth muscle cells, *Pharm Res* **20**, 212–220 (2003).

20. D. Sarkar, J. Ankrum, G. S. L. Teo, C. V. Carman, J. M. Karp, Cellular and extracellular programming of cell fate through engineered intracrine-, paracrine-, and endocrine-like mechanisms, *Biomaterials* **32**, 3053–3061 (2011).

21. E. B. Thompson, M. E. Lippman, Mechanism of action of glucocorticoids, *Metab. Clin. Exp.* **23**, 159–202 (1974).

22. A. E. Grigoriadis, J. N. Heersche, J. E. Aubin, Differentiation of muscle, fat, cartilage, and bone from progenitor cells present in a bone-derived clonal cell population: effect of dexamethasone, *J Cell Biol* **106**, 2139–2151 (1988).

23. A. C. ALLISON, M. R. YOUNG, UPTAKE OF DYES AND DRUGS BY LIVING CELLS IN CULTURE, *Life Sci* **3**, 1407–1414 (1964).

24. S. Hong *et al.*, Interaction of polycationic polymers with supported lipid bilayers and cells: nanoscale hole formation and enhanced membrane permeability, *Bioconjug Chem* **17**, 728–734 (2006).

25. P. M. Chaudhary, I. B. Roninson, Expression and activity of P-glycoprotein, a multidrug efflux pump, in human hematopoietic stem cells, *Cell* **66**, 85–94 (1991).

26. E. J. Wolvetang, M. F. Pera, K. S. Zuckerman, Gap junction mediated transport of shRNA between human embryonic stem cells, *Biochem Biophys Res Commun* **363**, 610–615 (2007).

27. T.-H. Chung *et al.*, The effect of surface charge on the uptake and biological function of mesoporous silica nanoparticles in 3T3-L1 cells and human mesenchymal stem cells, *Biomaterials* **28**, 2959–2966 (2007).

28. H. Gao, W. Shi, L. B. Freund, Mechanics of receptor-mediated endocytosis, *Proc Natl Acad Sci USA* **102**, 9469–9474 (2005).

29. S. K. Sahoo, V. Labhasetwar, Enhanced antiproliferative activity of transferrin-conjugated paclitaxel-loaded nanoparticles is mediated via sustained intracellular drug retention, *Mol Pharm* **2**, 373–383 (2005).

30. H. Jin, D. A. Heller, R. Sharma, M. S. Strano, Size-Dependent Cellular Uptake and Expulsion of Single-Walled Carbon Nanotubes: Single Particle Tracking and a Generic Uptake Model for Nanoparticles, *ACS nano* **3**, 149–158 (2009).

31. B. D. Chithrani, W. C. W. Chan, Elucidating the mechanism of cellular uptake and removal of protein-coated gold nanoparticles of different sizes and shapes, *Nano Lett* **7**, 1542–1550 (2007).

32. C. Maniatopoulos, J. Sodek, A. H. Melcher, Bone formation in vitro by stromal cells obtained from bone marrow of young adult rats, *Cell Tissue Res* **254**, 317–330 (1988).

33. J. K. Vasir, V. Labhasetwar, Biodegradable nanoparticles for cytosolic delivery of therapeutics, *Adv Drug Deliv Rev* **59**, 718–728 (2007).

34. J. M. Oliveira *et al.*, Ex vivo culturing of stromal cells with dexamethasone-loaded carboxymethylchitosan/poly(amidoamine) dendrimer nanoparticles promotes ectopic bone formation, *Bone* **46**, 1424–1435 (2010).

35. N. Y. Frank *et al.*, Regulation of progenitor cell fusion by ABCB5 P-glycoprotein, a novel human ATP-binding cassette transporter, *J Biol Chem* **278**, 47156–47165 (2003).

36. S. G. Kim, C. H. Jeon, H. S. Suh, J.-Y. Choe, I.-H. Shin, P-glycoprotein expression in extracellular matrix formation of chondrogenic differentiation of human adult stem cells, *Cell Biol. Int.* **31**, 1042–1048 (2007).

37. C.-M. Liu, C.-H. Chang, C.-H. Yu, C.-C. Hsu, L. L. H. Huang, Hyaluronan substratum induces multidrug resistance in human mesenchymal stem cells via CD44 signaling, *Cell Tissue Res* **336**, 465–475 (2009).

38. Y. Patil, T. Sadhukha, L. Ma, J. Panyam, Nanoparticle-mediated simultaneous and targeted delivery of paclitaxel and tariquidar overcomes tumor drug resistance, *J Control Release* **136**, 21–29 (2009).

39. V. Valiunas *et al.*, Connexin-specific cell-to-cell transfer of short interfering RNA by gap junctions, *J Physiol (Lond)* **568**, 459–468 (2005).

40. J.-C. Chang, S.-H. Hsu, H.-L. Su, The regulation of the gap junction of human mesenchymal stem cells through the internalization of quantum dots, *Biomaterials* **30**, 1937–1946 (2009).

41. V. Valiunas *et al.*, Human mesenchymal stem cells make cardiac connexins and form functional gap junctions, *J Physiol (Lond)* **555**, 617–626 (2004).

42. R. C. Lai *et al.*, Exosome secreted by MSC reduces myocardial

ischemia/reperfusion injury, *Stem Cell Res* **4**, 214–222 (2010).

43. S. Bruno *et al.*, Mesenchymal Stem Cell-Derived Microvesicles Protect Against Acute Tubular Injury, *J Am Soc Nephrol* **20**, 1053.

44. A. de Gassart, C. Geminard, B. Fevrier, G. Raposo, M. Vidal, Lipid raft-associated protein sorting in exosomes, *Blood* **102**, 4336–4344 (2003).

45. K. Denzer, M. J. Kleijmeer, H. F. Heijnen, W. Stoorvogel, H. J. Geuze, Exosome: from internal vesicle of the multivesicular body to intercellular signaling device, *Journal of cell science* **113 Pt 19**, 3365–3374 (2000).

46. D. Sarkar *et al.*, Chemical engineering of mesenchymal stem cells to induce a cell rolling response, *Bioconjug Chem* **19**, 2105–2109 (2008).

47. D. Sarkar *et al.*, Engineered mesenchymal stem cells with self-assembled vesicles for systemic cell targeting, *Biomaterials* **31**, 5266–5274 (2010).

48. I. Ko *et al.*, Targeting Improves MSC Treatment of Inflammatory Bowel Disease, *Mol Ther* (2010).

49. I. K. Ko, T. J. Kean, J. E. Dennis, Targeting mesenchymal stem cells to activated endothelial cells, *Biomaterials* **30**, 3702–3710 (2009).

50. W. J. Rogers, C. H. Meyer, C. M. Kramer, Technology insight: in vivo cell tracking by use of MRI, *Nat Clin Pract Cardiovasc Med* **3**, 554–562 (2006).

51. M. Srinivas *et al.*, Imaging of cellular therapies, *Adv Drug Deliv Rev* **62**, 1080–1093 (2010).

52. C. Xu *et al.*, Nanoparticle-based monitoring of cell therapy, *Nanotechnology* **22**, 494001 (2011).

53. C. Xu *et al.*, Tracking Mesenchymal Stem Cells with Iron Oxide Nanoparticle Loaded Poly(lactide-co-glycolide) Microparticles, *Nano Lett* **12**, 4131–4139 (2012).

54. S. J. H. Soenen *et al.*, Intracellular nanoparticle coating stability determines nanoparticle diagnostics efficacy and cell functionality, *Small* **6**, 2136–2145 (2010).

55. D. C. Colter, R. Class, C. M. DiGirolamo, D. J. Prockop, Rapid expansion of recycling stem cells in cultures of plastic-adherent cells from human bone marrow, *Proc Natl Acad Sci USA* **97**, 3213–3218 (2000).

## Chapter 3 Preface

The goal of this chapter is to provide a detailed protocol for the synthesis, characterization, and application of drug loaded microparticles to MSCs and other cell types. While Chapter 2 focused on demonstrating the utility of the particle-in-cell platform in a differentiation assay and cell tracking assay, Chapter 3 is meant to enable others to quickly adapt the platform to their own application. In developing this platform a number of challenges arose that required troubleshooting. Examples of positive and negative data and solutions to these challenges are included.

This article is an adaptation of an article that has been submitted to *Nature Protocols*.

**Glossary of Terms**

Emulsion: A mixture of two immiscible liquids by mechanical agitation

Drug Loading: The mass of drug in a particle over the total weight of the particle

Encapsulation Efficiency: The mass of drug encapsulated over the total mass of drug added.

Particle Association: Particles appear to be on the surface or on the interior of cells as measured by microscopy and flow cytometry.

Particle Internalization: Particles are found inside the outer plasma membrane of cells in intracellular compartments or free in the cytosol as determined by confocal microscopy.

**?TROUBLESHOOTING:** Tip to overcome common problems can be found in Table 1.

# Chapter 3: Engineering cells with intracellular depots to control cell phenotype

## Abstract

Cell therapies enable the unprecedented treatment of diseased and damaged tissues by harnessing natural biological processes to replace tissues, destroy tumors, and facilitate tissue regeneration. The greatest challenge facing exogenous cell therapy is the ability to control cell viability, fate, and function following transplantation. Failure to control the phenotype of transplanted cells can be detrimental to patients, leading to poor engraftment following hematopoietic stem cell (HSC) transplantation, reduced insulin production or inadequate glucose sensitivity following pancreatic islet or beta cell transplantation, and insufficient expression of immunomodulatory factors that are essential for the success of mesenchymal stem cell (MSC) based therapies. We have recently developed an approach to control cell phenotype *in vitro* and following transplantation that involves engineering cells with intracellular depots that continuously release phenotype-altering agents that can impact the cell's secretome, viability (persistence), proliferation, and differentiation, regardless of the cell's microenvironment. The same depots can encapsulate contrast agents to permit long-term tracking of transplanted cells, and the depots can be used to deliver drugs or other factors to control the cell's microenvironment (i.e. use the cell as a delivery vehicle). The development, efficient internalization and stabilization of ~1-μm polymeric drug-loaded microparticles within cells is critical for attaining sustained control of cell phenotype. Herein we provide a detailed protocol to generate and characterize agent doped poly(lactic-co-glycolic) acid (PLGA) particles using a single-emulsion evaporation technique (7 hrs), to uniformly engineer cultured cells (15 hrs), to confirm particle internalization, and to troubleshoot the most commonly experienced obstacles.

## Introduction

The success of exogenous cell therapies depends on the fate, function and viability of cells following transplantation. Controlling the phenotype and engraftment of cells following transplantation is critical for the success of cell-based therapies. Unlike the exquisite control that one can exert over cells in a culture dish, once cells are transplanted they are entirely at the mercy of the biological milieu and behave differently depending on their location. The lack of control of transplanted cells leads to variability in cell function and ultimately poor therapeutic outcomes (*1*, *2*). Both allogeneic and autogenic cell-based therapies are prone to significant variability due to heterogeneity within and between cell populations that can be impacted by differences in donors, isolation techniques, and culture mediums. For example, the propensity of embryonic stem cells and iPS cells to differentiate into specific lineages has been shown to vary significantly within and between cell lines (*3*). Variation in the glucose sensitivity of transplanted pancreatic islets can lead to a failure to restore insulin independence (*4*). In addition, MSC differentiation efficiency down osteogenic, chondrogenic, or adipogenic lineages is strongly influenced by the MSC's tissue of origin (*5*). Furthermore, the ability of MSCs to secrete growth factors, chemokines, and cytokines in response to inflammatory stimuli and suppress activated T-cells varies significantly between donors (*2*, *6*). Specifically, MSC secretion of vascular endothelial growth factor (*6*), a primary mediator of MSCs' angiogenic potential, and production of indoleamine 2,3-dioxygenase (*2*), a primary mediator of MSCs' immunomodulatory potential, vary significantly depending on the donor that the MSCs are isolated from. Thus, there is a significant need to develop methods to polarize MSCs toward therapeutic phenotypes to maximize their therapeutic potency regardless of their source. While small-molecule drugs have the ability to influence MSC phenotype *in vitro* (*7-10*); adaptation of pre-conditioning regimens has been substantially limited given that they typically activate signal transduction pathways only for short durations and thus the induced effects do not persist following transplantation.

To maximize potency, establish stable control of cell phenotype, and longitudinally track cell distribution following transplantation, we developed a technique to engineer cells with intracellular agent-loaded microparticles (*11*). Using an osteogenic

differentiation assay we demonstrated the ability of internalized dexamethasone-loaded microparticles to stimulate uniform differentiation of MSCs (*11*). Furthermore, drug released from particle-engineered cells into the microenvironment induced the differentiation of unmodified neighboring and distant cells in a paracrine-like and endocrine-like manner (see Sarkar *et al.* for a detailed report). In addition to establishing control over MSC differentiation, we observed that the efficiency of MSC particle internalization was dependent on the size as well as surface properties of PLGA microparticles. MSCs more efficiently internalized antibody-coated or positively charged particles over negatively charged particles. While multiple cell types efficiently internalize nanoparticles, significant particle leakage through exocytosis has been documented (*12-16*). In addition, nanoparticles typically exhibit lower drug loading and faster release compared to larger microparticles, limiting sustained control of cell phenotype. In contrast to nanoparticles that can be quickly exocytosed or cellular backpacks which are designed to remain on the cell surface (*17*, *18*), we discovered that particles ~1 μm in diameter remained internalized within MSCs for several weeks. To demonstrate the utility of this approach as a platform, we recently adapted it to enable longitudinal tracking of MSCs following transplantation. Tracking the location, engraftment, and distribution of cells following transplantation is critical for evaluating the success of cell-based therapies. While iron oxide nanoparticles have been used to track cells by magnetic resonance imaging (MRI), low iron content per cell and nanoparticle exocytosis prevented detailed and longitudinal monitoring of a cell's location. To overcome these limitations, iron oxide nanoparticles were encapsulated within ~1-μm PLGA microparticles resulting in significantly enhanced iron oxide loading and increased $r_2$ relaxivity of MSCs (*19*). In addition, the enhanced residence time of microparticles within MSCs enabled cells to be detected by MRI for >12 days compared to only 4-6 for nanoparticle-engineered MSCs (see Xu *et al.* for a detailed report)(*19*).

**Nuances and Limitations of the particle engineering platform**

Previously we have shown the flexibility of the platform through cell internalization of particles encapsulated with hydrophobic small molecules, rhodamine 6G and dexamethasone, as well as iron oxide nanoparticles (*11*, *19*). Drug loading and

release kinetics can be tuned for specific applications by modifying the particle synthesis protocol through changing the composition and molecular weight of the polymer. While we anticipate adaptation of the platform to other hydrophobic drugs will be straightforward, encapsulation and delivery of hydrophilic molecules incuding peptides, proteins, DNA, and RNA have yet to be optimized for this platform. Hydrophilic small molecules can be adapted to the platform by modifying particle synthesis. Co-solvents or double-emulsion techniques can be used to enhance the encapsulation of hydrophilic small molecules in microparticles (*20-22*). Thus, iteration of particle formulation strategies should enable adaptation of the particle engineered-MSC platform to hydrophilic drugs. In addition to small molecules, many biological agents including proteins, RNA, and DNA, have been used to control a cell's phenotype including its expression of cell surface receptors, secretome, and differentiation (*23-27*). While techniques to deliver these agents have been established, care must be taken not to damage the structure of the molecules. Secondary and tertiary structures may be damaged during particle synthesis due to exposure to organic solvents and high-intensity agitation or upon sorting to acidic lysosomes following endocytosis. While PLGA nanoparticles have been reported to undergo endolysosomal escape to deliver genes and siRNA (*28-31*), achieving efficient intracellular delivery without inducing cytotoxicity remains a challenge (*32*). In addition, if the goal is to deliver the agent to an extracellular target, as in the case of growth factors that bind to cell surface receptors, the agent must be able to transverse the plasma membrane via diffusion or active transport. Therefore, while this platform can be easily adapted to accommodate a wide variety of agents, a molecule's structure, target, and susceptibility to degradation should be contemplated. With these considerations in mind, the protocol herein will serve as a guide for successfully establishing non-viral transient control over locally or systemically administered cells to develop more effective cell-based therapies (Fig. 1).

# Materials

## REAGENTS

### Particle Preparation

50:50 Poly(DL-lactic-co-glycolic)-COOH (PLGA), i.v. 0.15-0.25 g/dL (Lactel Absorbable Polymers, www.absorbables.com, B6013-1)

50/50 Poly(DL-lactic-co-glycolic)-COOH (PLGA), i.v. 0.55-0.75 g/dL (Lactel Absorbable Polymers, www.absorbables.com, B6013-2)

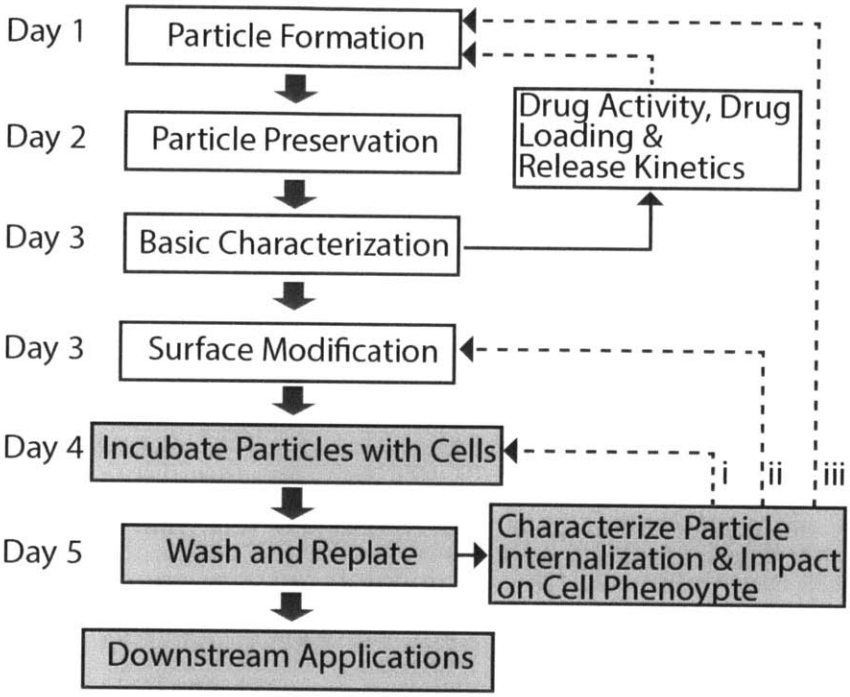


**Figure 1.** Flow Diagram for the Particle Engineering Protocol. Generation and characterization of appropriately sized and charged particles are essential to achieve consistent particle internalization by cells. Drug activity, loading, and release kinetics should be studied to determine the optimal particle characteristics for each application. If drug activity is lost, loading is too low, or release kinetics are inappropriate for the intended application, adjustments to the particle formation protocol should be made and new particles should be generated. Once particles with desired characteristics have been formed, cells can be engineered with particles, characterized, and used in downstream applications. The dotted lines represent iterative loops to follow if poor particle internalization is observed: i. Particles are aggregated, ii. Particles have negative charge, iii. Particles are too large to be internalized. White boxes represent steps involving only particles, while grey boxes represent cells in culture and may require additional lead time to expand cells to the appropriate confluence.

Dichloromethane (DCM) (Sigma Aldrich, www.sigmaaldrich.com, 270997-100ML) CAUTION
Poly(vinyl alcohol) (PVA), $M_w$ 9,000-10,000, 80% hydrolyzed (Sigma Aldrich, www.sigmaaldrich.com, 360627-25G)
Filtered water (MilliQ or Sigma, www.sigmaaldrich.com, W4502-1L)
Glass scintillation vials with polyvinyl-lined caps (VWR, www.vwr.com,, 66010-267)
Rhodamine 6G (Sigma Aldrich, www.sigmaaldrich.com, 252433-250MG)
MW >30,000 Poly-L-lysine hydrochloride (Sigma, www.sigmaaldrich.com, P9404-25MG)
Pasteur pipette (Fisher Scientific, www.fishersci.com, 13-678-4A)
Pasteur pipette rubber bulbs (Sigma Aldrich, www.sigmaaldrich.com, Z111597-12EA)
40-µm cell strainer (Fisher Scientific, www.fishersci.com, 22-363-547)
50-ml Steriflip 0.22µm vacuum filter (Millipore, Millipore.com, SCGP00525)
Transfer pipette (VWR, www.vwr.com, 16001-180)
Aluminum foil (VWR, www.vwr.com, 89068-734)
Disposable capillary cell (zeta potential) (Malvern, www.malvernstore.com, DTS1061)
12 mm square cuvette (DLS) (Malvern, www.malvernstore.com DTS0012)
Methanol (Sigma Aldrich, www.sigmaaldrich.com, 34860-4X4L-R)
Dimethyl sulfoxide (DMSO) (Sigma Aldrich, www.sigmaaldrich.com, 472301-100ML)

**Cell Engineering**

Human mesenchymal stem cells (http://medicine.tamhsc.edu/irm/msc-distribution.html) **CAUTION**
T25 culture flask (VWR, www.vwr.com, 29185-300)
MEM-alpha (Invitrogen, www.invitrogen.com, 12561-072)
Fetal bovine serum (FBS) (Atlanta Biologicals, www.atlantabio.com, S11550)
Penicillin-Streptomycin (P/S) (Invitrogen, www.invitrogen.com, 15140-163)
L-Glutamine (Invitrogen, www.invitrogen.com, 25030-081)
Phosphate-buffered saline without calcium chloride and magnesium chloride (Sigma, www.sigmaalrdich.com, A00475)

**Analysis**

20 kDa-MWCO dialysis tubing (Fisher Scientific, www.fishersci.com, 08-607-068)
Paired standard and weighted dialysis closures (Spectrum Labs, www.spectrumlab.com, 132749)
Fluorodish glass bottom dish (World Precision Instruments, www.wpiinc.com, FD35-100)
Vybrant DiO cell-labeling solution (Invitrogen, www.invitrogen.com, V-22886) **CAUTION**
Hoechst stain (Invitrogen, www.invitrogen.com, H3570)
10% neutral buffered formalin (Sigma, www.sigmaaldrich.com, HT501128) **CAUTION**

## EQUIPMENT

**Particle Preparation**

Scale, Metler Toledo X5105 DualRange
50-ml glass beaker
½-inch magnetic stir bar
Stir plate, Corning PC-420D
Probe sonicator, Misonix Sonicator 3000 with microtip
Tissue homogenizer, Omni International Tissue Master 125 with 7-mm Probe
Clamp stand
Centrifuge, Eppendorf 5430 Centrifuge
Lyophilizer

**Particle Characterization**

Zetasizer, Malvern Instruments, ZEN 3690
Fluorescent microscope, Nikon Eclipse TE2000U
Bench-top flow cytometer, Accuri C6
Confocal microscope, Zeiss 700

## REAGENT SETUP

Poly-L-lysine (PLL) solution: Dissolve 4 mg of PLL into 40 ml of filtered distilled water to make a 0.01% (w/v) PLL solution. Store at 4°C.

## Procedure

### Preparation of Microparticles (7 hours)

1 Dissolve 200 mg of poly(vinyl alcohol) (PVA) in 20 ml of water to make a 1% (w/v) PVA solution. Add stir bar and place on magnetic stir plate for 1 hour to allow for complete dissolution. Note: Concentration of 0.2%-0.5% PVA can also be used.

**CRITICAL STEP** PVA can aggregate and adhere to the bottom of the beaker. The position of the stir bar should be periodically adjusted to free aggregates from the beaker surface and ensure consistent generation of PVA solution.

**?TROUBLESHOOTING**

2 Add 50 mg of PLGA into a 10-ml glass scintillation vial.

3 Add 1 mg of Rhodamine 6G dye (or small molecule of choice) into the vial.

4 In a chemical fume hood, add 2 ml of dichloromethane (DCM) to the glass vial containing PLGA/Rhodamine.

**CAUTION** DCM is an eye and skin irritant and harmful if swallowed. Use proper personal protective equipment (PPE) and always work in a chemical fume hood.

**CRITICAL STEP** DCM will dissolve most plastics, use a glass syringe or glass Pasteur pipette to avoid contamination of the polymer solution.

**CRITICAL STEP** DCM is an organic solvent with a low boiling point. Cap vial to avoid evaporation and loss of volume.

**CRITICAL STEP** The concentration of polymer in the organic solvent is critical to determining the final particle size.

**PAUSE POINT** A 1-2 hour break is acceptable at this point.

5 When the 1% PVA solution is completely dissolved, filter through a 0.2-μm vacuum filter into a clean 50-ml glass beaker.

6 Place the beaker of PVA solution on ice and allow to chill to 4-8°C.

7 When PLGA:Rhodamine solution is completely dissolved, probe sonicate for 10 seconds at 10-12 W to ensure even distribution of the small molecule amongst polymer chains.

**CRITICAL STEP** Wash probe sonicator with acetone and ethanol and dry it completely prior to use to avoid contamination of particles.

**?TROUBLESHOOTING**

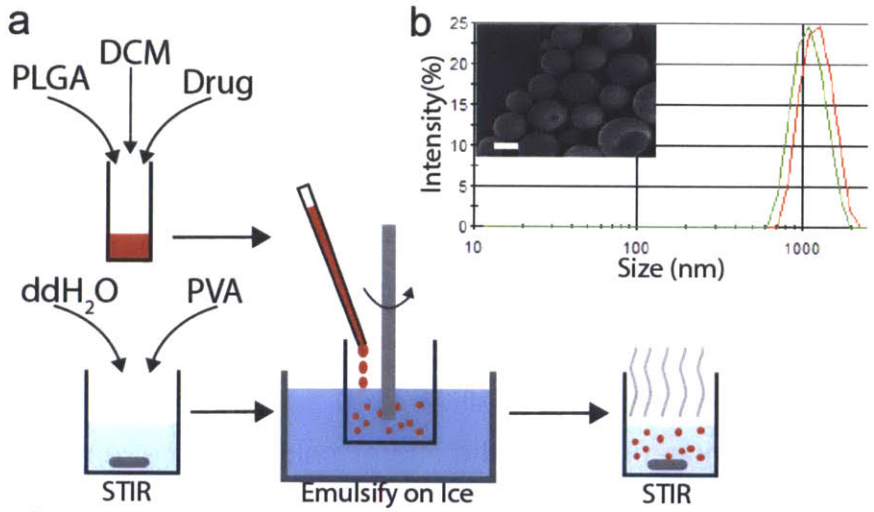


**Figure 2.** Generation of Drug-Loaded Microparticles. (a) Schematic of single emulsion-evaporation technique. Particles are generated by dissolving PLGA and drug into DCM. Drug solution is then added drop-wise to a stabilizing solution of PVA while homogenizing to create an emulsion. Particles are then allowed to solidify in suspension while the solvent evaporates. (b) Representative distribution of particle diameters generated using this method with 0.15-0.25 g/dL i.v. (Green line) or 0.55-0.75 g/dL i.v. (Red line) PLGA. Inset is a representative SEM image of particles. (Scale bar 1 μm)

8 Secure the tissue homogenizer with a clamp stand over an ice bucket.

9 Place beaker of PVA in an ice bucket and position homogenizer probe so that probe is submerged but not in contact with the glass surface (e.g. 0.5 cm).

10 Turn tissue homogenizer on to 35,000 rpm (highest speed on Tissue Master 125).

**CAUTION** Follow manufacturer's safety instructions in product manual.

11 Use a glass Pasteur pipette to add PLGA solution to PVA solution drop-wise while homogenizing.

**CAUTION** Use safety glasses as part of PPE to avoid splash hazard.

**CRITICAL STEP** Solution will foam and undergo a two-fold increase in volume during mixing. Use a 50-ml glass beaker to avoid overflow.

**CRITICAL STEP** When adding PLGA solution to the PVA solution, avoid dripping PLGA onto the homogenizer probe or wall of the beaker.

12 Homogenize for 2 minutes to create single emulsion

**? TROUBLESHOOTING**

13 Turn off homogenizer and remove from beaker.

**CAUTION** Disconnect homogenizer from the energy source before removing.

14 Move particle suspension to a stir plate in a chemical fume hood and add a ½-inch magnetic stir bar.

15 Set stir plate to 300 rpm.

16 Cover with aluminum foil perforated with 10-20 holes to allow for evaporation of organic solvent in a chemical fume hood.

17 Allow 4-5 hours for complete evaporation of the organic solvent.

**CRITICAL STEP** Incomplete evaporation of solvent will result in particle aggregation and loss of microparticles in subsequent steps. To test, take 200 µl of the sample and centrifuge at 1000g for 5 min at room temperature. Particles should easily re-suspend into a single-particle suspension.

**CRITICAL STEP** Excessive evaporation time will lead to breakdown of particles due to hydrolysis and gradual loss of dye or drug loading.

18 Transfer particle suspension to 15-ml centrifuge tubes and centrifuge at 1000g for 5 min at room temperature.

**CRITICAL STEP** Excessive centrifugal forces can cause aggregation of particles that can be difficult to disperse.

**19** Remove supernatant and gently re-suspend in 10 ml of distilled water using a transfer pipette.

**20** Repeat wash process 2 times.

**21** After third wash, re-suspend particles in 1 ml of distilled water.

**22** Filter through 40-µm cell strainer to remove large particulates and aggregates.

**? TROUBLESHOOTING**

**23** Use 1 ml of fresh distilled water to wash cell strainer and collect additional particles.

**24** Transfer particle suspension to 2-ml centrifuge tubes.

**25** Remove 20 µl of particle suspension for characterization.

**26** Freeze particle suspension at -80°C and lyophilize for 24 hours.

**PAUSE POINT** Particles can be frozen overnight.

**Preservation of Microparticles (24 hours)**

**27** Store lyophilized particles in 2-ml centrifuge tubes at -80°C. Seal lids with Parafilm to prevent moisture contamination that can degrade particles.

**PAUSE POINT** Particles can be frozen for at least 6 months.

**Characterization of Microparticles (1.5 hours)**

**28** Add 10 µl of particle suspension to 1 ml of distilled water in a cuvette.

**29** Mix well and insert into Zetasizer to measure hydrodynamic diameter and polydispersity index of the PLGA microparticles through dynamic light scattering (DLS).

**? TROUBLESHOOTING**

**30** Transfer 20 µl of diluted particle suspension to a clean glass slide.

**31** Using a fluorescent microscope at 40X magnification, visualize particles to confirm particle size and polydispersity. SEM can also be performed to confirm the size distribution and assess the surface morphology.

**CRITICAL STEP** Presence of large particles or debris can cause errors in DLS measurements.

**?TROUBLESHOOTING**

**32** Dilute 2 µl of concentrated particle suspension in 1 ml of distilled water.

**33** Add diluted particle suspension into a disposable capillary cell and measure zeta-potential with a Zetasizer. PLGA-COOH should generate particles with a zeta-potential of ~ -40 mV.

**CRITICAL STEP** Excessive particle concentration and high ion concentrations (e.g. cell media) can cause the electrodes on the capillary cell to burn resulting in inaccurate measurements.

**? TROUBLESHOOTING**

**Microparticle Surface Charge Modification (3 hours)**

**34** Measure 5 mg of lyophilized particles into a 1.5 ml centrifuge tube.

**35** Quick spin to minimize loss of particles.

**36** Add 1 ml of 0.01% PLL solution and gently re-suspend particles.

**37** Shake at 37°C for 2 hours to allow for adsorption of PLL onto the surface of particles.

**38** Add 10 µl of PLL-modified particle suspension and dilute in 1 ml distilled water.

**39** Measure zeta-potential as in step 33.

**? TROUBLESHOOTING**

**PAUSE POINT:** PLL-modified particles can be frozen at -20 °C for 6 months.

**Engineering Cells with Microparticles (14-18 hours)**

**40** Grow MSCs to 70-80% confluence in T25 flask.

**CRITICAL STEP** Incubating cells with particles at lower confluence will result in excessive amount of free particles in solution and particles adhered to the flask surface.

**41** Prepare particle-laden media by diluting 0.3 mg of PLL-modified particles in 1 ml of MEM-alpha with 1% FBS, 1% P/S, and 1% L-glutamine.

**42** Probe-sonicate at 1-3 W, pulsed for 10 seconds to ensure particles are uniformly dispersed in solution.

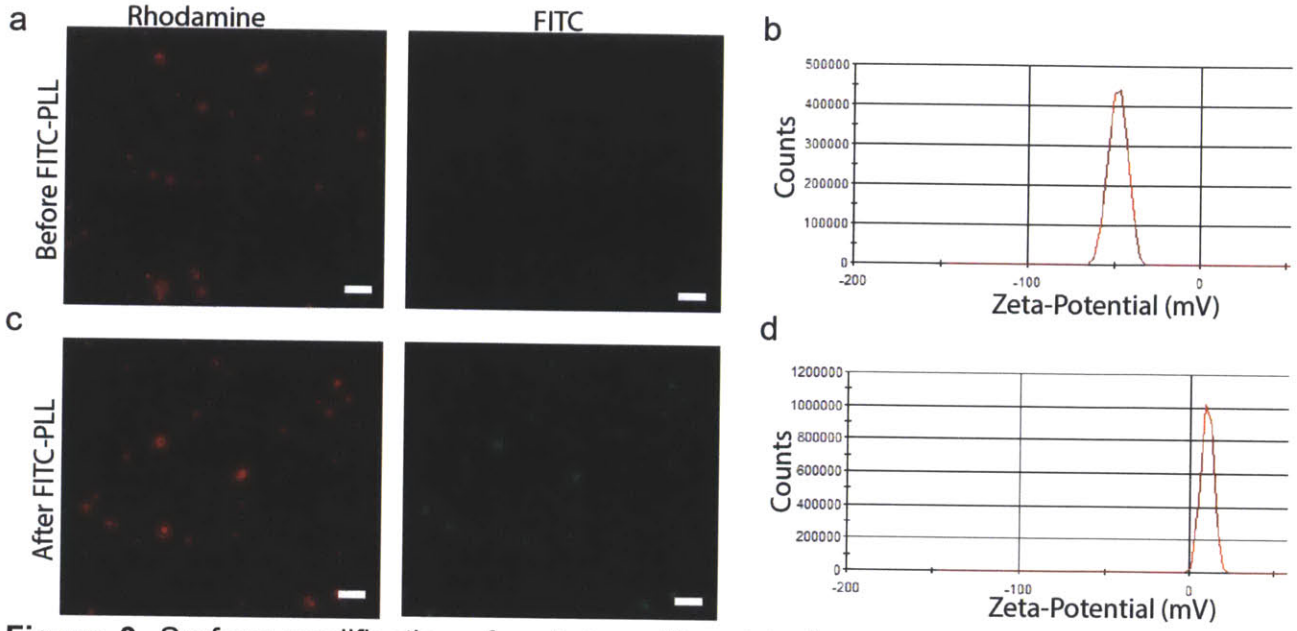


**Figure 3.** Surface modification of particles with polylysine to enhance particle uptake. Rhodamine-PLGA particles were imaged (a) before and (b) after surface modification with positively charged FITC-poly-L-lysine (FITC-PLL). (Scale bar 5 μm). The FITC-PLL coating results in a shift in zeta-potential from (c) -48 mV before coating to (d) +10 mV after coating.

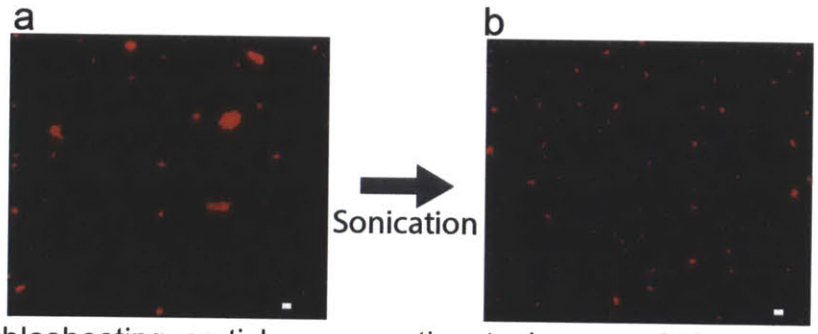


**Figure 4.** Troubleshooting particle aggregation to improve MSC uptake of particles. Particle aggregation can be caused by numerous factors including high particle concentration during preservation, presence of excessive residual PVA, or weak zeta-potential. Aggregation effectively reduces the concentration of particles in the media that MSCs are capable of internalizing (leading to reduced internalization). Shown are representative images of a 0.1 mg/ml particle suspension in media (a) before and (b) after sonication. If particle aggregation is suspected, use a fluorescence microscope to confirm (if fluorescent dye was loaded in particles), and disassociate particle aggregates through use of a sonication probe or water-bath sonication. (Scale bars 10 μm)

**43** Add suspended particles to 2 ml of 1% FBS-supplemented MEM-alpha media to create 3 ml of 0.1 mg/ml particle suspension.

**44** Wash MSCs with PBS-/- three times.

**45** Add particle-laden media to MSCs and incubate overnight (e.g. >12 hrs).

**CRITICAL STEP** Shorter incubation times will result in particle association with the cell membrane; however internalization of particles may not be complete.

**46** Aspirate spent media and wash flask three times with PBS-/- at room temperature to remove free particles.

**? TROUBLESHOOTING**

**47** Add 10% FBS media or split and proceed with downstream analysis or experiments.

**48** See 'Quantification of Drug Loading and Release' and 'Analysis of MSC Microparticle Uptake.' for instructions on further characterization of particles and particle loaded cells.

## Quantification of Drug Loading and Release

The concentration of drug and duration of MSC exposure to small molecules is critical to control the phenotype. For example, protocols to induce differentiation of MSCs *in vitro* typically rely on multiple days of continuous activation of signal transduction pathways by select agents included within the media. With the particle engineering approach, the drug loading and release kinetics can be altered by modifying the particle synthesis protocol through changing the specific composition and molecular weight of the polymer, the concentration of drug, or through using co-solvents to aid in dissolution of the small molecule in the polymer solution. Quantification of drug loading, encapsulation efficiency, and release kinetics should be iterated until a formulation with desirable characteristics is generated. Drug loading is the mass fraction of a particle that is composed of drug and calculated by Equation 1. Meanwhile, encapsulation efficiency describes the fraction of drug incorporated into particles compared to the total amount of drug that was added during particle synthesis and is calculated by Equation 2.

**Quantification of drug loading and encapsulation efficiency**: Weigh 2 mg of particles into each of three 1.5-ml centrifuge tubes. Collect dry particles into the bottom of the tube by quickly spinning in a benchtop centrifuge. Two methods can be used to solubilize drug contained in the particles i) dissolving the particle (polymer and drug) in a solvent such as DMSO or ii) swelling the particle to allow release of the drug into solution. To dissolve particles, add 0.5 ml of DMSO to particles and allow particles to completely dissolve. The DMSO solution can then be analyzed directly by spectrophotometry. Releasing drug by the swelling method maintains the PLGA as a solid and can easily be separated from the drug in solution, however this method should only be used if the encapsulated drug has high solubility in methanol. Add 0.5 ml methanol to swell particles and release small molecules into solution. Particles will clump together and release will be rapid. To ensure complete release, incubate on a shaker at 37°C for 1 hour. Centrifuge solutions at 2000g for 5 min at room temperature to pellet debris and collect supernatant into labeled tubes. Samples can be analyzed by high-performance liquid chromatography according to the absorbance spectrum of the small molecule. Prepare standard solutions of the small molecule in methanol (alternative solvents may be required dependent on the solubility of the small molecule) for calibration. Include a control generated from blank particles (i.e. without the small molecule). Drug loading and encapsulation efficiency can be determined by Equations 1 and 2 respectively, where $C_R$ is the drug concentration of the release media, $V_R$ is the volume of release media, $m_{mp}$ is the mass of microparticles, and $m_D$ and $m_{PLGA}$ are respectively the mass of drug and mass of PLGA initially added during particle synthesis.

$$Drug\ Loading: \%DL = \frac{C_R V_R}{m_{mp}} \times 100 \qquad (1)$$

$$Encapsulation\ Efficiency: \%EE = \frac{\frac{C_R V_R}{m_{mp}}}{\frac{m_D}{m_D + m_{PLGA}}} \times 100 \qquad (2)$$

**Release kinetics**: Release of small molecules from microparticles *in vitro* can be determined using dialysis as previously described(*33*, *34*). While release kinetics of drug from particles internalized within cells is influenced by the intracellular environment (e.g. presence of enzymes or altered pH), the simplified dialysis system is an important

tool that can provide insight into the release kinetics and should highlight relevant trends as well as pitfalls including excessive burst release and incomplete release. Verify that the maximum drug concentration in the release media remains an order of magnitude below the solubility limit in the release media; elevated bulk concentrations reduce the rate of dissolution of drug from the particle(*35*). Prepare a 10 mg/ml particle suspension in PBS. Pipette 200 µl of solution into a 2-inch section of 20 kDa-MWCO dialysis tubing clamped with a weighted closure. Carefully close the second end of the dialysis tubing with an un-weighted closure. Load two additional tubings for replicates (for n=3). Place loaded tubings within 50-ml centrifuge tubes. Add 40 ml of PBS-/- to each tube and cap securely. Place tubes in a rack on an orbital shaker at 37°C. At each time point, collect 1 ml from the outer fluid and store in a labeled centrifuge tube. Replace with an equal volume of fresh PBS-/-. Samples can be frozen at -80°C until analysis. Samples may need to be diluted with methanol or another solvent prior to analysis to reach a detectable drug concentration within the linear range of the calibration curve. Cumulative release can be determined from Equation 3 where $CR_t$ is cumulative drug release at sample time *'t'*, $C_t$ is drug concentration of sample at time *'t'*, $V_R$ is volume of release media, $C_i$ is drug concentration at sample time *'i'* and $V_r$ is volume removed at each sample time.

$$Cumulative\ release\ at\ time\ 't': CR_t = C_t V_R + \sum_{i=0}^{t-1} C_i V_r \qquad (3)$$

Release media can also be used to assess the bioactivity of the released agent to ensure the agent was not damaged during encapsulation. The intracellular concentration of drug at specific time points can be determined by washing MSCs that contain internalized particles with PBS, followed by a PBS solution containing 0.1% (v/v) Triton X 100 to lyse the cell membranes. Drug within the solution can then be analyzed to determine the intracellular drug concentration.

## Analysis of MSC Microparticle Uptake

After engineering of MSCs with microparticles, it is critical to analyze the cells to ensure efficient internalization. Poor uptake of particles will result in non-uniform

exposure of cells to the encapsulated agent and reduce the concentration and duration in which the particles are able to control cell phenotype. Described here are techniques to assess the uniformity of microparticle uptake within the cell population, presence of free microparticles, and subcellular location of microparticles.

**Quantifying the uniformity and degree of microparticle association with cells:** Following step 46, MSCs can be analyzed by flow cytometry to determine the degree and uniformity of cell uptake of dye-loaded microparticles. Harvest cells by washing three times with 2 ml PBS-/- and incubating for 3-4 min with trypsin or Accutase cell detachment solution. Centrifuge detached cells in a 15-ml conical tube at 300g for 5 min at room temperature to pellet cells. Re-suspend pellet in 1 ml of fresh culture media and analyze with a flow cytometer. Unmodified (native) MSCs and free microparticles serve as useful controls to determine cell gating and to set the threshold for background fluorescence. Fluorescence intensity of microparticle-engineered MSC will rise with increased microparticle loading. Side scatter has also been observed to increase due to the increased granularity of the microparticle-loaded cells. Following analysis via flow cytometry, samples can be plated on glass slides and visualized with a fluorescent microscope to assess the relative number of free microparticles vs. cell-associated microparticles. While flow cytometry and fluorescence microscopy are useful aids in determining ideal microparticle formulations and incubation conditions that maximize association of microparticles with cells, they cannot easily distinguish between membrane-bound and intracellular microparticles.

**? TROUBLESHOOTING**

**Confirming microparticle internalization:** To assess internalization of microparticles within cells, MSCs can easily be analyzed by confocal microscopy. Engineer MSCs with dye-loaded microparticles as described above in steps 40-47. Coat a glass-bottom dish or chamber slide with 100 µl of 20 µg/ml fibronectin for 1 hour to aid in rapid cell attachment. Meanwhile, harvest MSCs and re-suspend in media supplemented with 5 µl/ml Vybrant DiO membrane dye and 1 µg/ml Hoechst nuclear dye. Incubate on ice for 15 min. Aspirate fibronectin from dish or slide, and add 100 µl of cell suspension as a

droplet on the fibronectin-coated spot. Carefully transport to 37°C incubator and incubate for 5 min. Use microscope to examine cell attachment: the majority of cells

should be attached but not spread on the culture surface. Aspirate liquid and replace with 1 ml of 10% neutral buffered formalin. Fix cells for 5 min, wash 4 times with PBS-/- and analyze by confocal microscopy.

**CRITICAL** Extended incubation after plating will lead to cell spreading making it difficult to determine if microparticles are intracellular or membrane associated.

**? TROUBLESHOOTING**

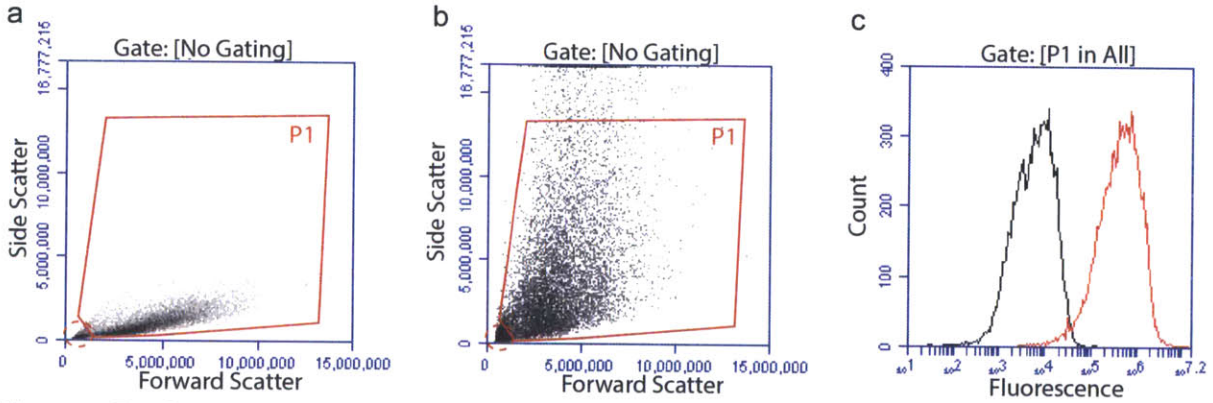


**Figure 5**. Gating fluorescent particle-engineered MSCs in flow cytometry. Forward scatter but not side scatter is preserved between (a) unmodified (native) and (b) particle-engineered MSCs. Increased particle internalization increases side scatter. To adequately measure the fluorescence of particle-engineered cells and not free particles or debris, gate (Red box labeled P1) using a range of side scatter larger than the typical range for cells. Free particles and cell debris will cluster in the bottom left corner of the forward/side scatter plot (Dashed red circle). Apoptotic cells may be excluded using appropriately labeled Annexin V. (c) Fluorescent particle-engineered cells (Red line) should display significantly higher fluorescence than unmodified (native) cells (Black line).

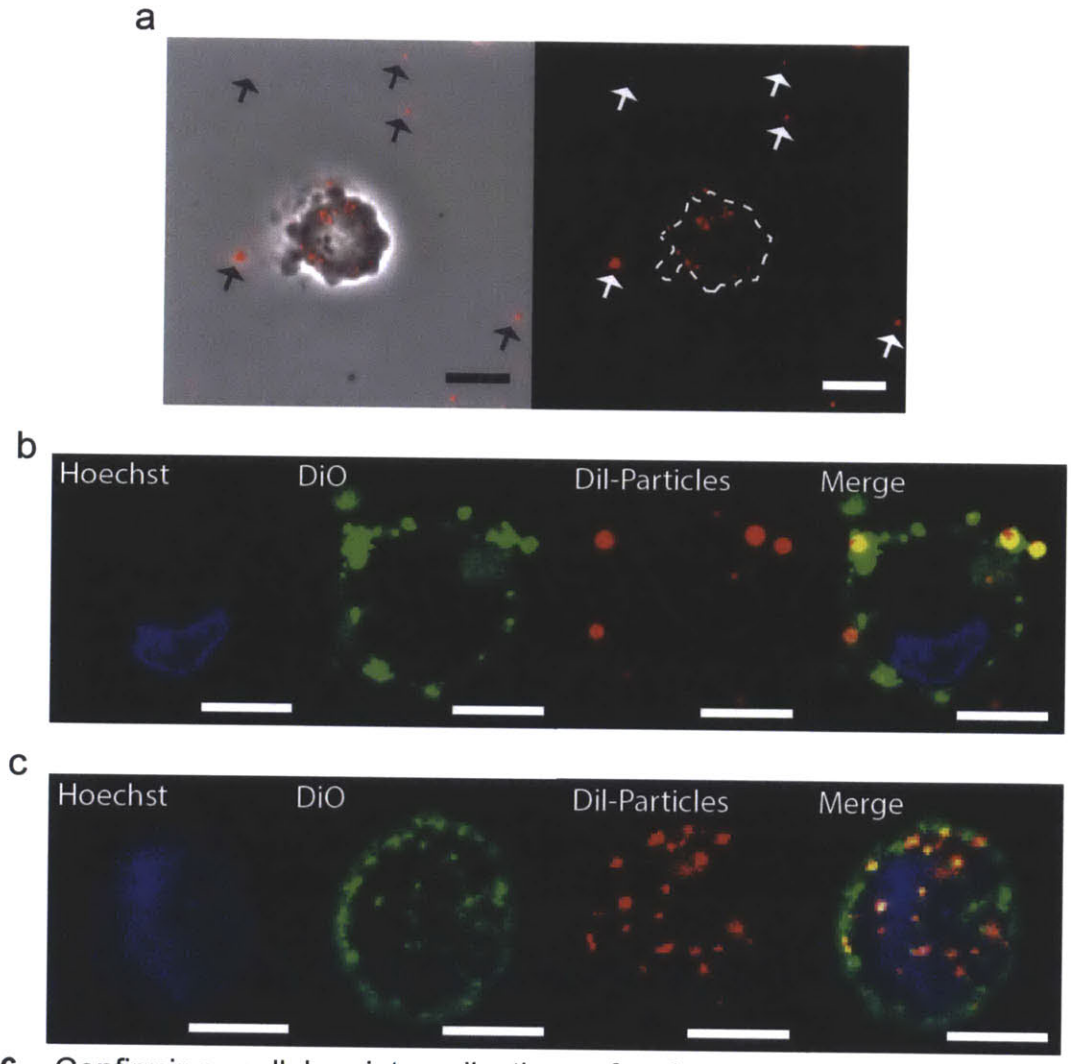


**Figure 6.** Confirming cellular internalization of microparticles. (a) An inverted fluorescence microscope can be used to examine the association of cells and particles, and the presence of free particles (arrows) but cannot be used to conclusively determine if particles have been internalized. The cell perimeter is outlined in the red fluorescence channel to distinguish particles that could possibly be internalized from those that are on the periphery. Representative confocal microscopy images of MSCs with particle internalization at (b) low and (c) high efficiencies. Images represent a slice through the cell at the plane of the nuclei showing the presence of (b) mostly outer membrane associated particles and (c) numerous intracellular particles. (Scale bars 10 μm)

# Troubleshooting

**TABLE 1: Troubleshooting table.**

| Step | Problem | Possible Reason | Solution |
|---|---|---|---|
| 1 | PVA not dissolving | PVA stuck to beaker | Use ultrasonic water bath to detach PVA clumps from beaker |
| 7 | PLGA not dissolving | Large polymer pellets or high molecular weight PLGA take more time to dissolve | Use ultrasonic water bath to facilitate dissolution of polymer pellets |
| 12 | Solutions not mixing, two layers visible | Surface area of beaker is too large | Use a beaker with a smaller diameter to reduce surface area |
| | | Homogenizer is not adequately submerged | Lower homogenizer so tip is submerged in PVA solution |
| | Emulsion overflows | PVA solutions have a tendency to foam. | Reduce PVA concentration to 0.25-0.5% |
| | | Beaker is too short | Use taller beaker |
| 21 | Particle clumping | Solvent evaporation was not complete | Leave suspension on stir plate for an additional 2 hours with adequate ventilation |
| | | Centrifugal forces too high | Reduce centrifuge speed and increase time to pellet particles |
| | | Particles have neutral charge due to excessive PVA coating | Wash with larger volume of distilled water before initial spin or reduce PVA concentration to 0.25-0.5% |
| 29 | Repeat readings yield different results | Presence of large particles or debris that are settling | Filter suspension with cell strainer prior to measurement or allow large particles to settle out for 2 min and then carefully collect particles in suspension into a new tube |
| 31 | Presence of large particles | PLGA concentration or agitation speed were not adequate | Filter the particle suspension with 5-μm Supor Membrane using a 20-mL syringe |
| 33 | Zeta-potential is near zero | Ion concentration is too high causing electrodes to burn | Dilute particle suspension and use a new capillary cell |
| | | Excessive PVA residue on particle surface | Reduce PVA concentration to 0.25-0.5% or add additional wash step prior to measurement |
| 39 | No change in zeta-potential after PLL modification | Inadequate adsorption of PLL onto the particle surface | Prepare fresh batch of PLL and make sure particles remain in suspension during modification |

| Step | Problem | Possible Reason | Solution |
|---|---|---|---|
| 46 | Excessive number of free particles remain after washing | Concentration of particle-laden media was too high | Reduce concentration of particle-laden media |
| | | Particles added when cells were at low confluence | Re-plate cells, allow cells to attach for 20 min, then wash with PBS to remove free particles |
| | | | Separate cells from free particles using Ficoll Density Gradient Separation |
| | | | Wash cells with trypsin for 1 min to remove particles, then replace with normal full serum media |
| Particle Uptake | Poor or inconsistent particle loading in cells | Particles are too large | Reduce polymer concentration or increase agitation speed to generate smaller particles, and carefully verify size distribution |
| | | | Reduce the size of the beaker used during emulsification so solution is more evenly and vigorously mixed |
| | | Particles are clumping | Probe-sonicate to break up clumps and confirm with microscopy before adding to cells |
| | | | Excipients such as polyethylene glycol, sorbitol, or mannose can be added prior to lyophilization at non-toxic concentrations |
| | | | Reduce particle concentration |
| | | Particle suspension not evenly distributed over cells, flask tilted | Gently tilt flask front-to-back and side-to-side in incubator to evenly coat cells; DO NOT SWIRL |
| | | Low particle fluorescence due to low dye loading | Check and increase dye loading |
| | | Poor cell health | Check viability and morphology of MSCs before particle incubation and use fresh media |
| | | | Check toxicity of drug and reduce drug loading accordingly |
| | | | Reduce particle concentration |
| | | | Reduce duration of particle incubation in 1% FBS |
| | | | Check for microbial contamination |

## Anticipated Results

This protocol establishes a robust technique for controlled delivery of small molecules or other cargo intracellularly to an exogenous population of cells through the generation of drug-loaded microparticles (Fig. 1, 2), followed by surface modification of microparticles (Fig. 1, 3), and functionalization of cells with microparticles (Fig. 1, 6). Particles can be loaded with a wide variety of agents known to influence cell phenotype and to control cells following transplantation (Fig. 7). This technique has previously been employed to induce MSC osteogenic differentiation(*11*) and enable longitudinal MRI tracking(*19*).

We anticipate this protocol can be adapted to deliver a wide range of molecules to a many cell types to influence cell phenotype, control cell microenvironment, and/or track cells following local or systemic administration. For example, here we show that in addition to MSCs, MIN6 beta cells, and macrophages are easily functionalized with internalized ~1-μm microparticles using this protocol (Fig. 8). The particle-engineered cell platform is highly tunable and can be adapted to a variety of applications such as promoting and accelerating engraftment of HSCs, enhancing glucose sensitivity of transplanted beta cells, and maximizing the immunomodulatory function of MSCs (Fig. 7). This protocol has been optimized to reproducibly produce particle-modified MSCs and to provide tips to troubleshoot commonly experienced problems throughout the process (Table 1) such as particle aggregation (Fig. 4) and cell gating for flow cytometry (Fig. 5). We envision this platform being useful to continually deliver agents to cells *in vitro* and *in vivo* to influence cell phenotype including differentiation, direct reprogramming, survival, secretome, immunogenicity, and proliferation. By controlling drug loading, molecular weight and composition of the microparticles, release kinetics can be tuned to continuously release drugs over days to weeks and potentially even months. We anticipate the platform could also be adapted to accommodate the use of a particles made from other materials such as alginate, which may be desirable for encapsulating hydrophilic or sensitive molecules such as peptides or proteins. In addition, molecules can be transported to the extracellular environment passively via diffusion or actively through exosomes or drug efflux pumps (Fig. 7). This can be used to influence the cell's microenvironment as we have previously demonstrated with

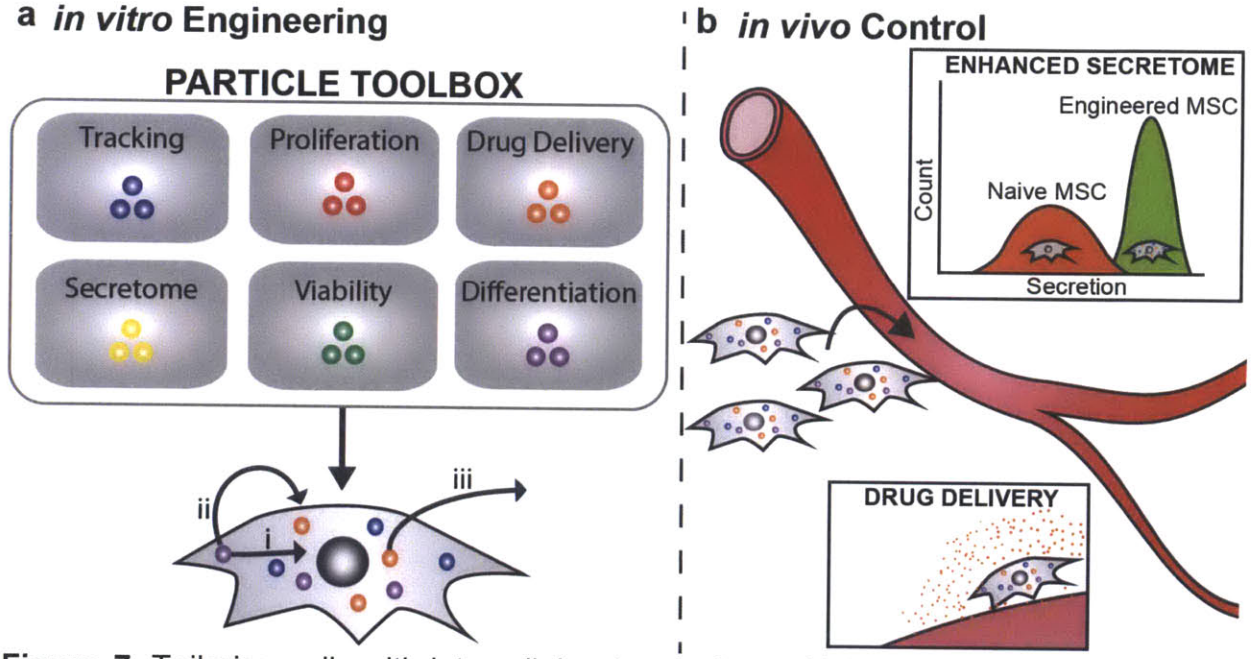


**Figure 7**. Tailoring cells with intracellular depots for multiple applications. (a) A diverse toolbox of particles can be generated and used to engineer cells to track their location, to locally deliver drugs, or to control cell phenotype including proliferation, viability, differentiation, and secretome by targeting i) intracellular targets, ii) membrane bound targets (in an autocrine-like manner), and iii) extracellular receptors (in a paracrine-like manner). (b) Engineered cells can be transplanted locally or systemically. For example. drugs released from intracellular particles can be used to control the phenotype of the particle-modified cell by enhancing (b-top) the MSC' secretome. Alternatively the platform can be used to (b-bottom) locally deliver drugs to tissues where cells reside (where the cell is used as a delivery vehicle).

dexamethasone(*11*). Furthermore, particle-engineered MSCs maintain their phenotype after cryopreservation, enabling off-the-shelf control of MSC phenotype(*11*). Finally, we have shown particle formulations containing dexamethasone, rhodamine, or iron oxide remain stable within MSCs for >18 days making this a useful platform for prolonged exposure to small molecules(*11*) and simultaneous longitudinal tracking of a cell's location(*19*).

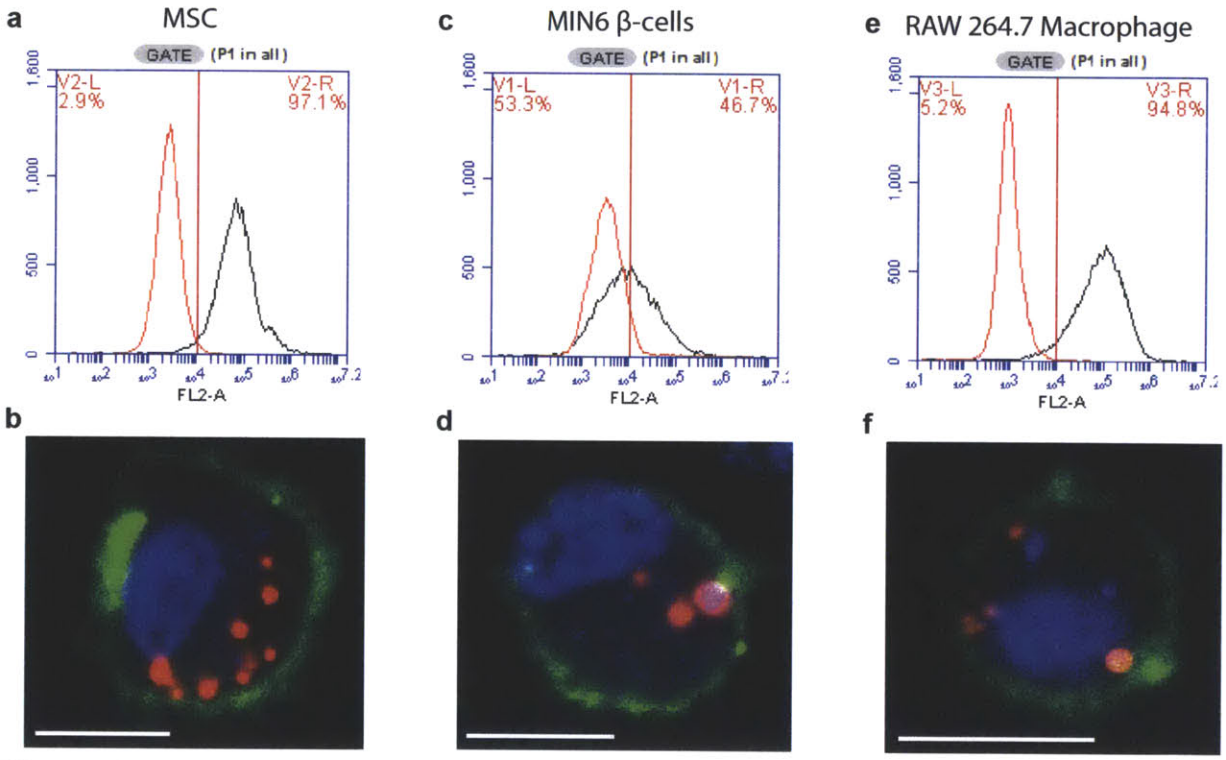


**Figure 8**. Potential for universal applicability of the particle engineered cell platform. The particle engineering protocol was applied to (a,b human bone marrow MSCs, (c,d) MIN6 beta-cells, and (e,f) RAW 264.7 macrophages. One day following particle engineering, cells were harvested and analyzed by flow cytometry. All cells showed increased fluorescence (black lines) compared to unmodified controls (red lines). The percentage of cells with particles are stated in the upper right corner of each graph. To confirm particle internalization, confocal imaging was performed as described above. Images represent a slice through (b) an MSC, (d) a MIN6 cell, and (f) a RAW 264.7 macrophage at the plane of the nuclei showing internalization of particles. (Scale bars 10 μm, Green: membrane, Red: particles, Blue: nuclei)

**References**

1. L. von Bahr *et al.*, Long-term complications, immunologic effects, and role of passage for outcome in mesenchymal stromal cell therapy, *Biol. Blood Marrow Transplant.* **18**, 557–564 (2012).

2. M. François, R. Romieu-Mourez, M. Li, J. Galipeau, Human MSC suppression correlates with cytokine induction of indoleamine 2,3-dioxygenase and bystander M2 macrophage differentiation, *Mol Ther* **20**, 187–195 (2012).

3. P. Cahan, G. Q. Daley, Origins and implications of pluripotent stem cell variability and heterogeneity, *Nature Reviews Molecular Cell Biology* (2013).

4. D. Fomina-Yadlin *et al.*, Small-molecule inducers of insulin expression in pancreatic alpha-cells, *Proceedings of the National Academy of Sciences* **107**, 15099–15104 (2010).

5. L. Da Silva Meirelles, P. Chagastelles, Mesenchymal stem cells reside in virtually all post-natal organs and tissues, *Journal of cell science* (2006).

6. V. Zhukareva, M. Obrocka, J. D. Houle, I. Fischer, B. Neuhuber, Secretion profile of human bone marrow stromal cells: donor variability and response to inflammatory stimuli, *Cytokine* **50**, 317–321 (2010).

7. W. Wu, Z. Ye, Y. Zhou, W.-S. Tan, AICAR, a small chemical molecule, primes osteogenic differentiation of adult mesenchymal stem cells, *Int J Artif Organs* **34**, 1128–1136 (2011).

8. Y. Suzuki, H. W. Kim, M. Ashraf, H. K. Haider, Diazoxide potentiates mesenchymal stem cell survival via NF-kappaB-dependent miR-146a expression by targeting Fas, *Am J Physiol Heart Circ Physiol* **299**, H1077–82 (2010).

9. Q. Dong, Y. Yang, L. Song, H. Qian, Z. Xu, Atorvastatin prevents mesenchymal stem cells from hypoxia and serum-free injury through activating amp-activated protein kinase, *Int J Cardiol* **153**, 311–316 (2011).

10. D. M. Brey *et al.*, High-throughput screening of a small molecule library for promoters and inhibitors of mesenchymal stem cell osteogenic differentiation, *Biotechnol Bioeng* **108**, 163–174 (2011).

11. D. Sarkar, J. Ankrum, G. S. L. Teo, C. V. Carman, J. M. Karp, Cellular and extracellular programming of cell fate through engineered intracrine-, paracrine-, and endocrine-like mechanisms, *Biomaterials* **32**, 3053–3061 (2011).

12. I. I. Slowing *et al.*, Exocytosis of Mesoporous Silica Nanoparticles from Mammalian Cells: From Asymmetric Cell-to-Cell Transfer to Protein Harvesting, *Small* **7**, 1526–1532 (2011).

13. X. Jiang *et al.*, Endo- and exocytosis of zwitterionic quantum dot nanoparticles by

live HeLa cells, *ACS nano* **4**, 6787–6797 (2010).

14. J. Panyam, V. Labhasetwar, Dynamics of endocytosis and exocytosis of poly(D,L-lactide-co-glycolide) nanoparticles in vascular smooth muscle cells, *Pharm Res* **20**, 212–220 (2003).

15. H. Jin, D. A. Heller, R. Sharma, M. S. Strano, Size-Dependent Cellular Uptake and Expulsion of Single-Walled Carbon Nanotubes: Single Particle Tracking and a Generic Uptake Model for Nanoparticles, *ACS nano* **3**, 149–158 (2009).

16. B. D. Chithrani, W. C. W. Chan, Elucidating the mechanism of cellular uptake and removal of protein-coated gold nanoparticles of different sizes and shapes, *Nano Lett* **7**, 1542–1550 (2007).

17. A. Swiston, J. Gilbert, D. Irvine, R. Cohen, M. Rubner, Freely Suspended Cellular "Backpacks" Lead to Cell Aggregate Self-Assembly, *Biomacromolecules*, 4920–4925 (2010).

18. M. T. Stephan, J. J. Moon, S. H. Um, A. Bershteyn, D. J. Irvine, Therapeutic cell engineering with surface-conjugated synthetic nanoparticles, *Nat Med* **16**, 1035–1041 (2010).

19. C. Xu *et al.*, Tracking Mesenchymal Stem Cells with Iron Oxide Nanoparticle Loaded Poly(lactide-co-glycolide) Microparticles, *Nano Lett* **12**, 4131–4139 (2012).

20. E. Cohen-Sela, M. Chorny, N. Koroukhov, H. D. Danenberg, G. Golomb, A new double emulsion solvent diffusion technique for encapsulating hydrophilic molecules in PLGA nanoparticles, *J Control Release* **133**, 90–95 (2009).

21. R. Karnik *et al.*, Microfluidic platform for controlled synthesis of polymeric nanoparticles, *Nano Lett* **8**, 2906–2912 (2008).

22. T. T. Thomas, D. S. Kohane, A. Wang, R. Langer, Microparticulate formulations for the controlled release of interleukin-2, *J Pharm Sci* **93**, 1100–1109 (2004).

23. M. Sawada, P. Hayes, S. Matsuyama, Cytoprotective membrane-permeable peptides designed from the Bax-binding domain of Ku70, *Nat Cell Biol* **5**, 352–357 (2003).

24. M. Ieda *et al.*, Direct Reprogramming of Fibroblasts into Functional Cardiomyocytes by Defined Factors, *Cell* **142**, 375–386 (2010).

25. C. E. Murry, G. Keller, Differentiation of embryonic stem cells to clinically relevant populations: lessons from embryonic development, *Cell* **132**, 661–680 (2008).

26. S. Brenner *et al.*, CXCR4-transgene expression significantly improves marrow engraftment of cultured hematopoietic stem cells, *Stem Cell* **22**, 1128–1133 (2004).

27. H. K. Haider, S. Jiang, N. M. Idris, M. Ashraf, IGF-1-overexpressing mesenchymal stem cells accelerate bone marrow stem cell mobilization via paracrine activation of SDF-1alpha/CXCR4 signaling to promote myocardial repair, *Circ Res* **103**, 1300–1308 (2008).

28. J. Panyam, V. Labhasetwar, Biodegradable nanoparticles for drug and gene delivery to cells and tissue, *Adv Drug Deliv Rev* **55**, 329–347 (2003).

29. J. Panyam, W.-Z. ZHOU, S. PRABHA, S. K. Sahoo, V. Labhasetwar, Rapid endo-lysosomal escape of poly(dl-lactide-co-glycolide) nanoparticles: implications for drug and gene delivery, (2002).

30. Y. Patil, T. Sadhukha, L. Ma, J. Panyam, Nanoparticle-mediated simultaneous and targeted delivery of paclitaxel and tariquidar overcomes tumor drug resistance, *J Control Release* **136**, 21–29 (2009).

31. S. Acharya, S. K. Sahoo, PLGA nanoparticles containing various anticancer agents and tumour delivery by EPR effect, *Adv Drug Deliv Rev* **63**, 170–183 (2011).

32. B. P. Timko *et al.*, Advances in drug delivery, *Annual Review of Materials Research* **41**, 1–20 (2011).

33. J. W. Kostanski, P. P. DeLuca, A novel in vitro release technique for peptide containing biodegradable microspheres, *AAPS PharmSciTech* **1**, E4 (2000).

34. S. S. D'Souza, P. P. DeLuca, Methods to Assess in Vitro Drug Release from Injectable Polymeric Particulate Systems - Springer, *Pharm Res* (2006).

35. A. Dokoumetzidis, P. Macheras, A century of dissolution research: From Noyes and Whitney to the Biopharmaceutics Classification System, *Int J Pharm* **321**, 1–11 (2006).

# Chapter 4 Preface

This chapter is intended to introduce readers to an emerging challenge in MSC therapy and motivate the need for the application discussed in Chapter 5. As described in Chapter 1, MSCs have classically been proclaimed to be 'immune privileged' allowing for cells to be taken from a donor and injected into an unrelated patient without the need for immunological matching. However, recent evidence has shown that MSC interactions with immune cells are more nuanced and MSCs are not 'immune privileged' as classically thought. In this chapter, I provide an up-to-date survey of MSCs clinical use and provide a historical perspective looking back at the origin of the 'Universal Donor' hypothesis and recent reports that challenge its validity. We provide a vision for the future of MSC based therapies and the need for strategies to minimize MSC immunogenicity and maximize MSC immunomodulatory potency, a challenge I address with a particle-in-cell approach in Chapter 5.

This article is an adaptation of a manuscript under review at *Nature Biotechnology*

**Glossary of Terms**

Antigen: Small fragment of protein that can elicit a response from the immune system

MHC: Major histocompatibility complex proteins are expressed on the surface of cells, MHC-I displays self-antigens to immune cells and MHC-II displays antigens from the environment.

Immune privileged: A property of a cell or location that prevents a cell that would normally be rejected from being eliminated by the immune system.

# Chapter 4: Mesenchymal stem cells are immune evasive, but not immune privileged: A historical perspective


## Abstract

The diverse immunomodulatory properties of mesenchymal stem cells (MSCs) present a significant opportunity for the treatment of a multitude of inflammatory conditions. MSCs have long been reported to be hypoimmunogenic or 'immune privileged', enabling transplantation across MHC barriers and the creation of off-the-shelf culture-expanded MSC therapies. However, recent studies suggest that MSCs do not persist long-term *in vivo* and may not be immune privileged as initially considered leading to immune rejection and the generation of anti-donor antibodies. MSC's appear to mask their immunogenicity, at least initially, via their immunosuppressive properties. The impact of rejection on the efficacy of allogeneic MSC therapies has yet to be determined. Also, no definitive clinical advantage of autogeneic MSCs over unmatched allogeneic MSCs has been demonstrated to date, although comparisons are currently under investigation. While MSCs may function through a brief 'hit and run' mechanism, it is hypothesized that evasion from host immune detection and prolonged MSC persistence may improve clinical outcomes and prevent patient sensitization towards donor antigens. Herein we review the current state of MSC clinical trials and then provide a historical perspective by revisiting the original discoveries of MSCs immunosuppressive potential and the development of the 'Universal Donor' promise. We also provide an overview of the allogeneic MSC rejection literature, and discuss emerging strategies for overcoming barriers to MSC persistence to guide the future of MSC based therapeutics.


## Landscape of MSC Therapy

Mesenchymal stem cells (MSCs), also referred to as multi-potent mesenchymal stromal cells, were originally identified by Friedenstein over four decades ago by their multi-lineage differentiation potential(*1-3*). However, the current primary therapeutic interest is based on their ability to modulate inflammatory processes. MSCs produce

exosomes and a multitude of cytokines and growth factors that reduce immune responses through inhibiting B- and T-cell proliferation, monocyte maturation, and promoting induction of $T_{regs}$ and M2 macrophages(*4-6*). Positive data from pre-clinical models and elucidation of the immunomodulatory properties of MSCs has prompted a significant rise in the number of clinical trials that harness MSCs for the treatment of multiple diseases including myocardial infarction, stroke, graft versus host disease (GvHD), lupus, arthritis, Crohn's disease, acute lung injury, chronic obstructive pulmonary disease (COPD), cirrhosis, multiple sclerosis, amyotrophic lateral sclerosis (ALS), and diabetes(*7*).

Today, numerous cell preparations from academic and corporate institutions are being investigated in nearly 300 clinical trials ( >80% of which are Phase I or II, Figure 1a, 125 have reached their scheduled completion, and 28 have been reported to be placebo controlled). Clinical trials examining the safety and efficacy of MSCs have used both allogeneic (165) and autogeneic (125) cells (Figure 1b). MSCs are typically manipulated via culture expansion as *in situ* they exist in limited quantities, thus they require clinical trials to gain FDA approval and have only recently begun to reach market approval. In contrast, minimally manipulated (e.g. non-culture expanded) MSCs have been used clinically for bone regeneration during the past decade. Cellect by DePuy, an intraoperative technique to concentrate auto-MSCs for bone regeneration entered the market in 2003(*8*) (the product has since been discontinued following a change in FDA regulatory requirements), and Osteocel by Osiris Therapeutics Inc. (now Osteocel Plus by NuVasive), a cryopreserved immuno-depleted bone allograft retaining native adherent allo-MSCs has been available since 2005(*9*). Clinical trials to explore MSC therapy have been driven predominately by companies with proprietary allogeneic MSC (allo-MSC) preparations such as Osiris' Prochymal™, Mesoblast's Revascor®, Athersys' MultiStem®, Stemedica's Stemdyne-MSC™, Allocure's AC607, Cellerix's Cx601, Stempeutic's Stempeucel™, and Orthofix's Trinity Evolution™. Many of these preparations derive their product from a small number of donors through extensive culture expansion to generate therapeutic doses to treat entire cohorts of patients. In addition, smaller clinician sponsored trials have also been conducted in medical centers and academic institutions, often under hospital exemption in Europe, although these

studies typically utilize much lower passage MSCs(*10*). Importantly, allo-MSC therapy has consistently been shown to be safe, enabling future trials to be conducted with improved trial design and refined MSC-based therapies(*7*, *11*).

Several recent industry sponsored Phase II clinical trials and clinician sponsored trials have generated positive results. Tigenix's Cx611 culture expanded adipose-derived allo-MSCs reduced joint swelling by 20% or more in 1/5 of patients at a 6-month follow-up, while placebo treated patients showed no improvement(*12*). Additionally, Mesoblast reported improved heart muscle function and reduced major adverse cardiac events by 78% compared to placebo in congestive heart failure patients at an 18-month follow-up in a placebo controlled Phase II trial(*13*). In late 2011 Athersys reported 13.5% and 10.9% increase in ejection fraction in acute myocardial infarction patients receiving 50 and 100 million cells, respectively, via intracoronary adventitial injections compared to historical controls (phase I trial)(*14*). Osiris reported reduced stress-induced arrhythmias and hypertrophy compared to placebo in an ongoing Phase II trial of Prochymal™ for acute myocardial infarction, although data on the primary endpoints has yet to be reported(*15*). In 2011, FBC-Pharmicell's auto-MSC preparation, Hearticellgram-AMI®, gained approval in South Korea, becoming the first culture-expanded MSC therapy to receive regulatory approval(*16*). To date one allogeneic culture-expanded MSC product has received regulatory approval, Osiris' Prochymal™, approved in Canada in May of 2012 and shortly after in New Zealand for the treatment of steroid-refractory GvHD in children(*17*). Prochymal™ is now available for adults and children in 8 other countries including the United States for steroid refractory grade III and IV GvHD under an Expanded Access Program. Clinician driven studies without placebo controls have also generated positive data with unmatched-allogeneic and haplo-identical MSCs for the prevention and treatment of acute GvHD(*18*, *19*). Prophylactic treatment with MSCs at the time of bone marrow transplantation reduced the incidence of grade III or IV GvHD, 0% vs 26% compared to historical data(*19*). In another study, 30/55 patients with severe GvHD showed a complete response to MSC therapy (resolution of all symptoms) and had significantly improved survival, 52% vs 16%, compared to patients that showed little or no improvement following MSC therapy(*18*).

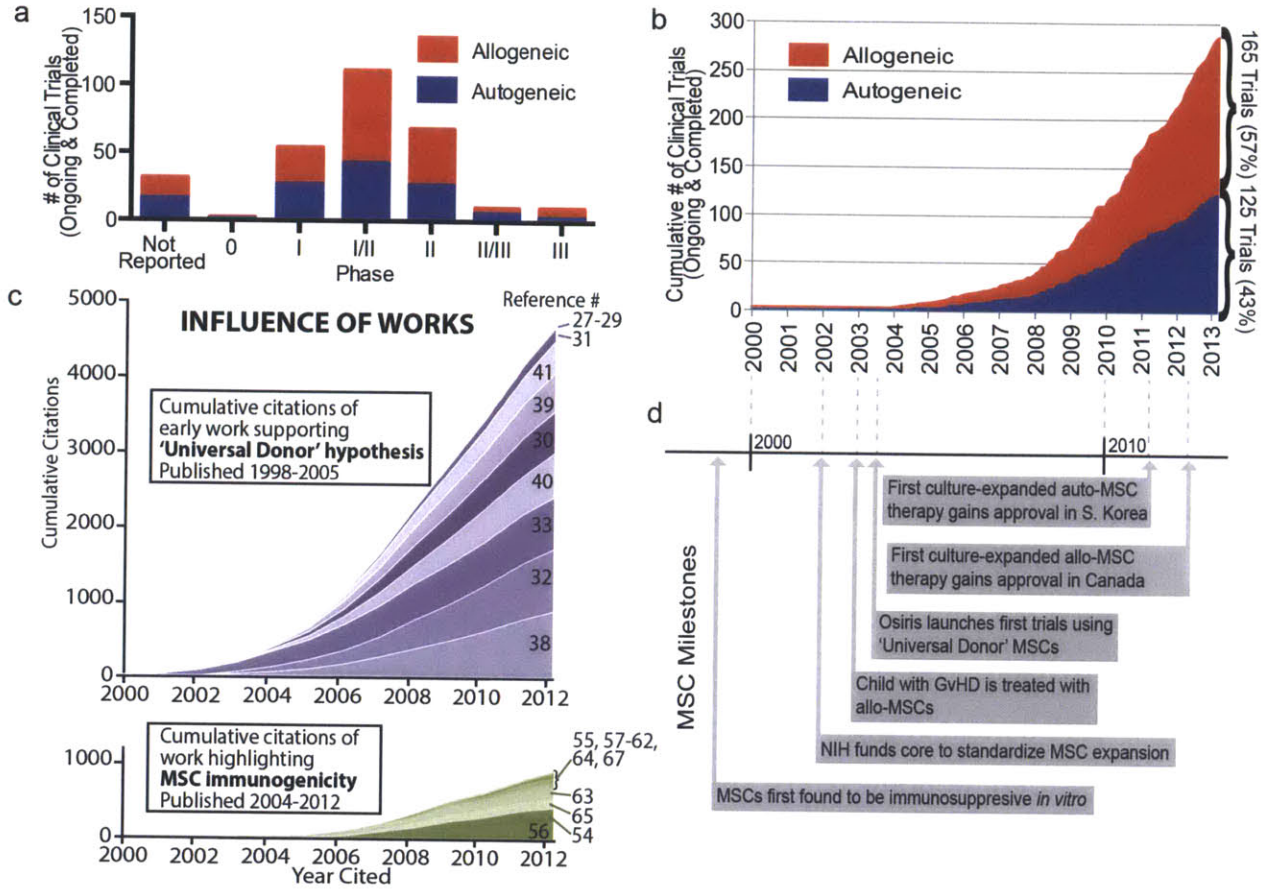


**Figure 1** The rise of MSC therapy. (a) The number of clinical trials in each phase using (Red) allogeneic or (Blue) autogeneic MSCs as reported by clinicaltrials.gov. (b) The cumulative total number of clinical trials that utilize allogeneic or autogeneic MSCs are plotted according to the year they were initiated. (c) Cumulative citations from (Purple) early publications that support the 'Universal Donor' hypothesis and from (Green) work that highlights MSC immunogenicity are plotted from 2000-2012. Shades represent contributions of individual papers (references denoted on right). This graph represents the overall influence each paper continues to exert on the field staring from (bottom) the most influential to the (top) least influential. (d) Timeline of significant milestones that have marked the progress of MSC therapy. Data was collected for (a) and (b) from ClinicalTrials.gov registry on 25 Feb, 2013. Searches for 'Mesenchymal Stem Cells', 'Mesenchymal Stromal Cells', 'Multipotent stromal cells', 'bone marrow stromal cells', 'Stem cells for Spinal Fusion', 'Prochymal', and 'connective tissue progenitor' returned 293 unique MSC trials. 5 trials did not indicate the source (auto vs allo) of the MSCs, and two reported using both allogeneic and autogeneic MSCs. Citation data for (c) was collected from Web of Knowledge (Searched April 24, 2013).

While case studies(*20*, *21*) and clinical studies of small groups of patients(*10*, *18*) have suggested MSCs have significant clinical utility, demonstration of MSC therapeutic effect in large placebo-controlled trials has remained elusive, thus limiting the clinical application of MSCs. Several placebo controlled studies have yielded disappointing results, showing only marginal improvement or failing to show efficacy over placebo, including Osiris Prochymal™ trials targeting steroid-resistant GvHD, first-line GvHD, COPD, and type 1 diabetes. Of note, MSC products in general have not been optimized to maximize therapeutic potential and it is believed that certain allo-MSC products may be over-passaged leading to reduced potency. Furthermore, cell therapy trials often suffer from a large placebo effect making it difficult to show efficacy. Importantly, retrospective sub-population analysis of the steroid-resistant GvHD trial earned Prochymal™ its first approval in Canada.

While allo-MSC therapy faces several challenges, auto-MSC therapy is not without drawbacks. Auto-MSC therapy generally requires several weeks after cell harvest to expand MSCs *ex vivo* to generate a therapeutic dose. Furthermore, significant variation in MSCs' secretome and immunomodulatory potency has been observed between donors. Thus, auto-MSC therapy may not be suitable for the treatment of acute conditions and variability between patient-derived MSCs is likely to lead to highly variable outcomes. While both auto-MSCs and unmatched allo-MSCs are being explored in clinical trials, direct comparisons are scarce. In the recent POSEIDON trial, the safety and efficacy of auto- and allo-MSCs were compared after administration into the remodeled cardiac scar of patients with chronic cardiac ischemia. Unfortunately, clinical improvement was limited at 30 days in both allogeneic and autogeneic groups. Auto-MSCs were associated with marginal improvements in a 6 min walk test and Minnesota Living with Heart Failure Questionnaire while allo-MSCs were associated with fewer, but not statistically significant, arrhythmias. Administration of either auto- or allo-MSCs resulted in a small improvement in ejection fraction (~2%). Without a strong positive effect, a placebo group, or analysis of donor cell persistence, it is difficult to use this trial to effectively compare the efficacy of allo- vs auto- MSCs. Although both were shown to be safe, comparisons of auto- and allo- MSCs are warranted in future studies(*22*). Furthermore, in contrast to auto-MSC therapy, allo-MSC therapy has the

luxury of harvesting MSCs from healthy donors and selecting lots based on potency assays(*23*).

It is critical to consider that most patients receiving allo-MSC transplantations undergo minimal to no MHC matching prior to treatment, as MSCs are classically thought of as immune privileged. As such, allogeneic preparations are treated as a "one-size-fits-all" off-the-shelf cell-based therapy. However, MSCs have been shown to have variable expression of immunogenic and immunosuppressive factors that make their interaction with immune cells nuanced and context dependent. To understand the origin of the "immune privileged" promise, we must revisit the early discoveries of the immunomodulatory potential of MSCs, and the clinical trials that swiftly followed. Herein we aim to provide a historical review of the origin of MSC's immune privileged status and review old and new evidence that challenges the 'Universal Donor' hypothesis (Box 1). For a recent in-depth immunological analysis of allogeneic MSC rejection see Griffin et. al(*24*).

## The Rise of Mismatched MSC Therapy

From 1998 to 2000, researchers at Osiris Therapeutics presented a series of abstracts at American Hematological Society meetings that suggested MSCs interaction with hematopoietic cells extended beyond supporting hematopoiesis(*25*, *26*) to serving a key role as immune regulators(*27-29*). Specifically, they reported hMSCs suppressed activated T-cell proliferation(*29*, *30*) and mixed lymphocyte reactions (MLR) in a genetically-unrestricted manner(*28*, *31*). As even third party MHC-mismatched hMSCs were capable of suppressing an ongoing MLR, Klyushnenkova *et. al.* proposed the concept of generating a large supply of culture expanded allo-MSCs from a 'Universal Donor', that could then be used to treat all patients(*28*, *31*). While these early reports illuminated the therapeutic potential of allo-MSCs, the mechanisms mediating their immunosuppressive properties were not understood. Additional work by Osiris and others supported and extended these findings within *in vivo* models.

In 2002, Bartholomew *et. al.* showed that the addition of baboon MSCs to cultures of stimulated allogeneic peripheral blood leukocytes (PBL) resulted in

**Box 1. Take Home Messages**

1. MSCs were declared immune privileged without a complete understanding of their context-dependent immunosuppressive and immunogenic potential. As such, MSCs are often cited as immune privileged to justify their allogeneic use.

2. Confusion over whether MSCs are immunogenic draw largely from early *in vitro* studies that declared MSCs as non-immunogenic, and from the lack of infusion related reactions in clinical trials. In hindsight it appears MSCs' immunosuppressive nature, which distinguishes them from fibroblasts, masks their immunogenicity.

3. Animal studies suggest that MSC persistence depends on MHC expression, route of administration, and destination of the cells (e.g. within tumors mismatched allo-MSC persist). Importantly, allo-rejection does not impact the efficacy of MSC therapy in all cases as a brief 'hit and run' mechanism may be sufficient to achieve a therapeutic effect.

4. Clinical trials and animal studies have revealed allogeneic MSCs elicit an anti-donor antibody response. Preclinical studies show that this leads to rapid rejection of repeat MSC doses and prevents MSC recipients from accepting subsequent tissue/blood transplants, although this has yet to be demonstrated clinically.

5. While preclinical evidence shows both extended MSC persistence (through obviating transplantation shock) and immune evasion enhances treatment efficacy, advantages of using autologous over allogeneic MSCs have yet to be demonstrated in clinical trials.

6. Approaches to enhance immune evasion through modification of MSCs or the host exhibit significant potential to improve MSC persistence enabling MSCs to function beyond a 'hit and run' mechanism, and should be considered for next generation MSC based therapy.

7. Standard MSC phenotype analysis should include examination of immunomodulation and immunogenicity (MHC receptor expression) at baseline and after activation (e.g. TNF-α and/or IFN-γ stimulation) to simulate MSC exposure to inflammatory signals post-transplantation.

suppression of PBL proliferation in an MSC-dose dependent manner(*32*). Furthermore, the addition of MSCs to an ongoing MLR resulted in suppression of the proliferative response regardless of the MSC donor (auto-, allo-, and third-party MSCs). Although, suppression was partially reversed by the addition of IL-2, suggesting MSCs did not induce allogeneic anergy(*32*). To test the immunosuppressive potential of MSCs *in vivo*, skin grafts from MHC-mismatched baboons were performed immediately prior to intravenous injection of donor-matched or third-party MSCs. Administration of donor or third party MSCs extended the survival of the skin graft from 7 days (control without MSCs) to 11.3 and 11.8 days, respectively(*32*). In parallel, Liechty *et. al.* reported the finding that human MSCs could persist as long as 13 months after intraperitoneal injection into pre-immune and immune competent fetal-sheep (a model in which xenogenic or allogeneic HSC are rejected)(*33*). Others have subsequently reported that donor-derived MSCs promote tolerance of other transplanted tissues, including pancreatic islets(*34*) and heart allografts(*35*), however specific tolerance towards unmatched MSCs or repeat doses of MSCs has not been convincingly demonstrated.

MSC mediated immune suppression has been shown to be dependent on a myriad of factors including cell dose, proximity to immune cells, and requisite stimulation by inflammatory cytokines(*36*, *37*). Extensive *in vitro* work during the past decade has shown that MSC immunomodulatory potential is MHC unrestricted, and significant efforts have begun to elucidate the mechanism of MSC-immunomodulation. Specifically, not only do allo-MSCs fail to elicit a response in MLRs, but third party MSCs suppress ongoing MLRs as effectively as auto-MSCs in a dose-dependent manner(*30*, *38-40*). In addition, allo-MSCs inhibit T-cell proliferation induced by the potent mitogens, PHA, Con A, and SpA(*38*, *39*). Interestingly, MSC T-cell suppression is also transient, as T-cells respond to allo-antigen upon removal from MSC co-cultures(*40*).

Over a decade ago MSCs were postulated to act as immune regulators either through cell contact dependent signaling or secretion of cytokines and growth factors, leading to a series of studies to elucidate the mechanism of MSC:immune cell interactions(*38*, *39*). Culture expanded hMSCs typically express low levels of MHC I, are MHC II negative, and do not express the co-stimulatory molecules B7-1, B7-2, or CD40, suggesting cell contact may not be the primary mechanism of

immunomodulatory action(*30*, *39*, *41*). This was verified by the initial studies examining the mechanism of MSC T-cell suppression, that showed immune-suppression was not dependent on cell contact, but was augmented by close proximity. Specifically while hMSC mediated suppression of T-cells was apparent in both mixed co-cultures (direct cell-cell contact) and transwell assays, immune-suppression was maximized in mixed co-culture conditions(*38*). Tse *et. al.* examined the effect of soluble factors through a series of inhibitor studies. Inhibition of either PGE2 or indoleamine-2,3-dioxygenase (IDO) each resulted in only a partial reduction of hMSCs suppressive effects(*30*). These and other studies suggest that MSC suppressive potential cannot be pinned to a single factor, but rather a cocktail of soluble factors, many of which are inducible by inflammatory environments(*6*, *36*). Inflammation responsive immune-suppression is supported by data showing enhanced T-cell suppression when MSCs are preconditioned with IFN-γ for 48 hours(*41*), and by data showing a limited effect observed in transwell(*38*, *40*) and conditioned media(*40*) experiments in which MSC exposure to IFN-γ is minimized or eliminated. Furthermore, recent studies have shown MSCs can be polarized to pro- and anti-inflammatory phenotypes by preconditioning with cytokines, including IFN-γ and TNF-α(*5*, *42*), and signaling through toll-like receptors(*37*, *43*, *44*). See reviews by Ren *et al*(*45*), Ranganath *et al.*(*36*), and Prockop(*6*) for a thorough discussion of MSC's therapeutic secretome and its' immunosuppressive potential.

## First Clinical Trials

With MSCs immunomodulatory potential established in MLRs and early pre-clinical models, MSCs were rapidly transitioned to the clinic. In 2004, Le Blanc et. al. were among the first to clinically administer allo-MSCs(*21*). Third party haploidentical MSCs were harvested from the mother of a 9-year-old boy suffering from treatment resistant grade IV GvHD. The boy received MSCs 73 and 170 days after bone marrow transplantation, with rapid recovery after each MSC infusion, and survival beyond 1 year. In contrast, the 24 patients at the same treatment facility with acute grade IV GvHD not receiving MSC therapy died an average of 2 months following bone marrow transplantation. This landmark case study provided an early glimpse of MSCs'

therapeutic potential. Just 8 months after the publication of Le Blanc's Lancet article, Osiris Therapeutics began recruiting patients for the first large scale clinical trials of allo-MSCs for the treatment of acute GvHD and acute myocardial infarction (ClinicalTrials.gov).

While the mechanisms mediating MSC immune-modulation and apparent immune privileged status were beginning to be examined, MSC use in clinical trials soared (Figure 1b). By 2010, over 100 clinical trials were underway worldwide, with over half utilizing allo-MSCs(*7*). Unfortunately, while safety endpoints were consistently met, MSCs failed to show efficacy over placebo in the first randomized double blind placebo controlled phase III clinical trials(*46*, *47*). These setbacks have raised several questions regarding limitations of current approaches and how MSC therapy can be improved to realize its potential(*48*).

## MSC Persistence is Limited

A limitation of MSC therapy is that MSCs do not persist following infusion. Using bioluminescence imaging, intravital microscopy, donor DNA analysis, and donor RNA analysis, the persistence of human (in SCID mouse), mouse (in syngeneic mouse), and rat (in allogeneic rat) MSCs was shown to be limited with the majority of cells dying within 48 hours following systemic infusion(*49-51*). This trend has recently been confirmed through analysis of tissues at autopsy of patients who received allo-MSC infusions within a year prior to their death(*52*). Tissues from 18 patients who received MHC-mismatched or haplo-identical MSCs were analyzed; no ectopic tissue was observed, and only one patient showed significant levels of donor DNA in multiple tissues. However, the donor positive patient was not representative of the average patient, as he was severely immune compromised, septic, and received the MSC infusion just 7 days prior to his death(*52*). While allo- and auto-MSCs alike may fail to persist following systemic infusion simply due to stresses encountered during transplantation (nutrient/growth factor deprivation due to transport limitations of nutrients and oxygen(*53*), shear stress, lack of attachment), it is likely that a more active immunological process is also responsible for the limited persistence of allo-MSCs.

## Allo-MSCs are Not Immune Privileged

Preclinical and clinical observations have led multiple groups to question the 'immune privileged' status of MSCs, and subsequently, the use of a 'Universal Donor' for MSC therapy. While the majority of *in vitro* studies have highlighted the immunosuppressive properties of MSCs, several studies have provided evidence that mismatched MSCs are immunogenic. While culture expanded MSCs express low levels of MHC I and are negative for MHC II, exposure to IFN-γ or differentiation into mature cell types has been shown to significantly increase expression of both MHC classes(*41*).

In 2005 one of the earliest reports of MSC allo-rejection was published. Eliopolous *et. al.* examined the persistence of mMSC transfected with erythropoietin (EPO-MSC) in syngeneic and allogeneic unmatched hosts(*54*). EPO-MSCs were seeded on a collagen scaffold and injected subcutaneously in syngeneic (C57/Bl6) or allogeneic (Balb/c) hosts. As a surrogate for MSC survival, the rise in hematocrit (HCT) in response to EPO production was measured for over 140 days. Mice receiving syngeneic EPO-MSC exhibited a sustained increase in HCT while those receiving allogeneic EPO-MSC exhibited a spike in HCT followed by a return to baseline. Analysis of collagen scaffolds removed 15 days post-implantation revealed significant infiltration by CD8+ T-cells and NK cells only in the allogeneic EPO-MSC treated animals. In addition, administration of a second dose of allogeneic EPO-MSC resulted in a second but diminished spike in HCT suggesting the initial challenge may have sensitized the animals to allo-antigen(*54*).

While allo-MSCs are not as immunogenic as unmatched fibroblasts or hematopoietic stem cells which elicit rapid rejection in immunocompetent hosts, MSCs are not 'immune privileged' and elicit a humoral and cellular immune response *in vivo,* as Eliopoulos *et. al.* first reported nearly a decade ago. Zangi *et. al.* injected luciferase expressing mMSCs or fibroblasts in syngeneic and allogeneic hosts and compared their persistence(*55*). The majority of syngeneic mMSCs and fibroblasts were detectable for the duration of the experiment (40 days), while in the allogeneic setting fibroblasts died

by a day 10 and mMSCs by day 20. In addition, mice showed enhanced sensitivity to allogeneic fibroblasts if the mice had previously been treated with allo-MSCs from the same donor, rejecting fibroblasts at day 2 compared to day 14 in naïve mice. In addition, allo-MSC treated mice had elevated levels of CD4+, CD122+ CD44+, and $CD62L^{low}$ T-cells indicating the formation of T-cell memory(*55*). Others have since reported that infusion of allo-MSCs can induce immune memory. Mice inoculated with unmatched allo-MSCs exhibit rapid rejection of donor derived splenocytes within 24 hours of the second transplant, suggesting the initial mMSC injection sensitized the host to donor antigens and induced a memory T-cell response(*56*). In another model, mice receiving intraperitoneal injections of allo-MSCs produced elevated titers of allo-reactive antibodies and rejected subsequent allogeneic skin grafts(*57*). Similarly, evidence of immune detection and lack of long-term engraftment of allo-MSCs has been observed in a variety of other species, including rat(*58*, *59*), baboon(*60*), rhesus macaquea(*61*), and pig(*62*). In addition to generation of allo-reactive antibodies, intracranial injection of allo-MSCs resulted in an increase in CD4+ and CD8+ T-cells in mice(*58*) and CD8+, CD16+, and CD8+/CD16+ T-cells in rhesus macaques(*61*). Allo-MSCs have been shown to be susceptible to antibody-dependent complement mediated cytotoxicity in pigs(*62*) and rats(*59*). Allo-MSC also appear to elicit a response from innate immunity. Human MSCs were shown to promote macrophage and neutrophil infiltration at the injection site in rats and mice(*63*, *64*). Furthermore, hMSC engage complement on their surface(*65*), although the effect of complement on MSC function is currently debated and complement mediated lysis of MSCs is likely allo-antibody dependent(*66*, *67*).

## MSC Immunosuppression Masks Immunogenicity

While MSCs cannot be generally considered as immune privileged, they appear to delay their own allo-rejection. The timing and severity of MSC rejection appears to be strongly context dependent and is dictated by a balance between MSC's expression of immunogenic factors and the potency of immunosuppressive factors (Figure 2). Indeed it appears the immunosuppressive properties of MSCs may mask their immunogenicity within *in vitro* assays (such as MLR or T-cell suppression assays), where the concentration of MSCs is high enough to strongly influence the microenvironment within

the cell culture well. Similarly, unmatched allo- and xeno-MSCs have been reported to preferentially persist within *in vivo* environments that are immune suppressed such as tumors while failing to persist in other tissues within the same animal(*51*, *68*). This suggests that local immune suppression is required to mask MSC immunogenicity(*68*). Detailed *in vivo* studies on MSC immunogenicity are needed using human MSCs or non-human primate MSCs that more closely mirror human biology as murine and human MSCs exhibit differences in expression of immunomodulatory factors(*69*). Specifically, hMSC immune modulation is often mediated through IDO, while mMSCs secrete virtually no IDO but high levels of iNOS(*69*).

Importantly, it has yet to be shown clinically that MSC persistence or immune tolerance is required or would lead to enhanced treatment efficacy. Many believe the observed therapeutic effect of MSCs is due to a 'hit and run' mechanism through the production of exosomes or secretion of trophic factors during the initial days following injection(*6*, *52*) while others believe that the main therapeutic response may be achieved through a yet-to-be-defined reprogramming of the immune system mediated through apoptotic bodies(*70*). Conventional wisdom suggests that MSC therapy could be significantly advanced, at minimum by increasing duration of secretome expression through extending their persistence following transplantation(*36*).

Interestingly, while no adverse events have been linked to administration of allo-MSCs, an anti-donor response has been observed. Both the POSEIDEN trial and a recent phase II Mesoblast trial reported generation of anti-donor antibodies in 13% of allo-MSC treated patients. The impact of antibody production on the efficacy of MSC therapy is still under investigation. However, the therapy still appears safe as Osiris and others frequently administer repeat doses without complications(*11*). Depending on the therapeutic mechanism of MSCs, such a response may not negatively impact the therapy, however, sensitization to donor antigens could have long-term consequences. Patient sensitization to donor antigens could facilitate rapid rejection of subsequent MSC infusions as seen in animal models discussed above and could disqualify patients from future cell, tissue, and organ transplants. To become a sustainable model of therapy, strategies to overcome allogeneic rejection and allo-antibody production should be established.

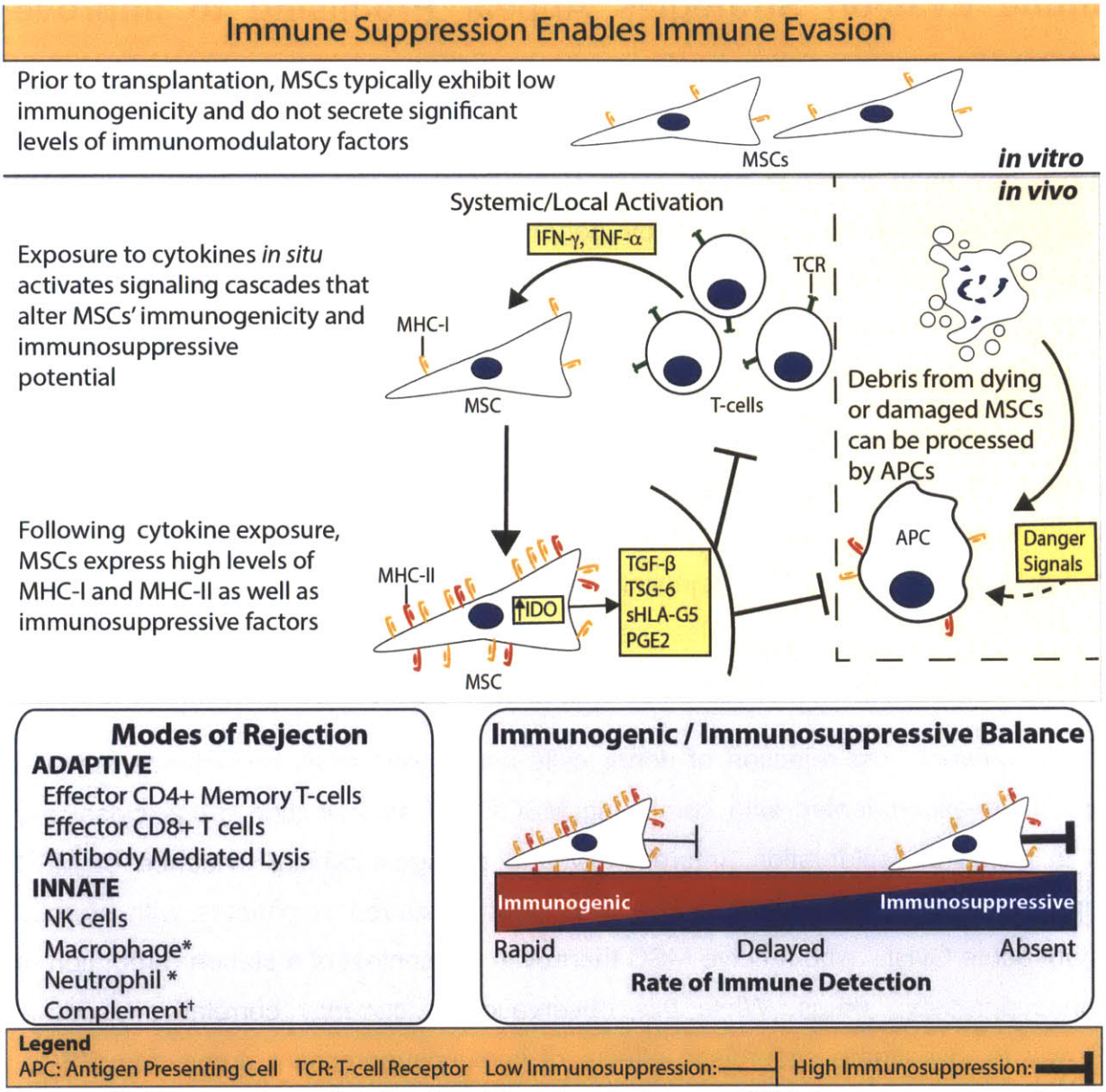


**Figure 2** Proposed model for the interplay between MSC immunosuppression and immunogenicity. MSCs immunosuppressive potential and immunogenicity are both induced by elevated levels of systemic or local inflammatory cytokines (secreted by T-cells and other cell types). High immunosuppressive potential permits MSCs to suppress inflammation and delay or evade allo-rejection through suppression of T-cell activation and inhibition of APC maturation. However, MSCs that fail to tip the balance towards immunosuppression, are prone to immune detection and destruction through multiple modes of rejection(*24*). (*shown in xenogenic models(*63*, *64*), †described within *in vitro* assays(*65*))

## Immune Evasion Strategies Appear Promising to Improve MSC Persistence

Overcoming MHC-barriers is a significant challenge in transplant biology. Recent progress has been made in solid organ transplantation through induction of mixed hematopoietic chimerism facilitated by donor HSC transplantation(*71*). In addition, allogeneic cell products like Viacyte's PEC-01™ harnesses immune-isolation membrane based devices (Encaptra®) and tissue engineered products like Organogenesis' Apligraf® and Shire's SRM003(Formerly VASCUGEL®) temporarily avoid rejection by encasing differentiated allogenic cells in collagen or gelatin gels. Unfortunately without induced tolerance or physical barriers the majority of allogeneic tissues and cells, MSCs included, remain susceptible to rejection. Work is currently underway to enhance MSC persistence by overcoming allo-rejection, which in turn may enhance the therapeutic effect of MSCs. These strategies can be divided into two primary categories: modification of the host, and modification of MSCs.

To prevent host rejection of donor cells and extend MSC persistence, several groups have experimented with combining MSCs and anti-rejection drugs classically used in organ transplantation. Interestingly, the strongest clinical evidence of MSC therapeutic effect, as described above, has been observed in patients with steroid-resistant acute GvHD, who receive MSC therapy in the context of a standard regimen of immunosuppressant drugs. While this observation is currently correlative, work is underway to investigate synergistic effects of immunosuppressant drugs and MSCs. Adding cyclosporine A to co-cultures of MSCs in an *in vitro* MLR assay resulted in significantly enhanced suppression of cell lysis over cyclosporine A or MSCs alone(*72*). However, Buron *et. al.* found that mycophenolate acid consistently synergized with MSCs to suppress MLRs, although the effect was mild. In contrast, dexamethasone, rapamycin, cyclosporine A, and tacrolimus synergized or antagonized MSC MLR suppression depending on the dose of the drug and the responder:MSC ratio(*73*). Unfortunately, the mechanism by which immunosuppressive drugs augmented or interfered with the immunosuppressive properties of MSCs were not evaluated, and detailed mechanistic studies are needed. In one of the few studies of

immunosuppressive drug interactions with MSCs *in vivo*, Ge *et. al.* investigated the effect of low dose rapamycin and MSCs in a cardiac allograft model(*74*). Combining a 14-day course of low dose rapamycin with unmatched allo-MSC therapy resulted in long-term persistence of GFP-labeled allo-MSCs and tolerance (100 day) of a heart graft of MSC donor origin(*74*). The mice did not accept 3$^{rd}$ party allografts, indicating generation of specific tolerance toward the MSC donor antigens. Mice receiving rapamycin and MSC therapy showed elevated levels of tolerogenic dendritic and T-cells and no signs of allo-antibodies(*74*). More research is needed to characterize the impact of immunosuppressive drugs on MSC phenotype and *in vivo* persistence. Nevertheless, specific combinations of immunosuppressive drugs, including rapamycin, may have synergistic effects with MSCs through protecting MSC's from host rejection. We have also recently shown that steroid conditioning of MSCs can augment their anti-inflammatory properties (unpublished). Furthermore, short-course immunosuppression, which has shown promise in preventing GvHD(*75*) and prolonging liver allograft survival(*76*, *77*), may be sufficient to extend MSC persistence and augment their therapeutic effect. In addition to the administration of small molecules to prevent allo-rejection, the host immune response could also be modulated by antibody-mediated depletion of specific cells, such as NK or cytotoxic lymphocytes. However, such strategies could increase the risk of infection in vulnerable patient populations.

Rather than modify the host to prevent allo-MSC rejection, or use physical matrix or membrane-based barriers that are not amendable to systemic infusion, MSCs can be directly modified to reduce their immunogenicity (Figure 3). For example, de la Garza-Rodea *et al.* looked to viruses for inspiration in evading immune detection. To permanently suppress MHC-I surface expression, hMSCs were transfected with viral immunoevasins from Bovine Herpes Virus Type 1, Epstein-Barr Virus and Human Cytomegalovirus (HCMV)(*78*). Of these, only the US11 protein from HCMV was found to strongly suppress hMSC expression of MHC-I. US11-MSCs locally injected into the ear of immunocompetent mice persisted similarly to hMSC in immunodeficient mice (~50% detectable at 14 days), However immune evasion was achieved only after NK cell depletion, as the lack of MHC-I expression made hMSCs susceptible to NK cell lysis(*78*). Similarly, Soland *et. al.* infected hMSCs with immunoevasins from HCMV(*79*).

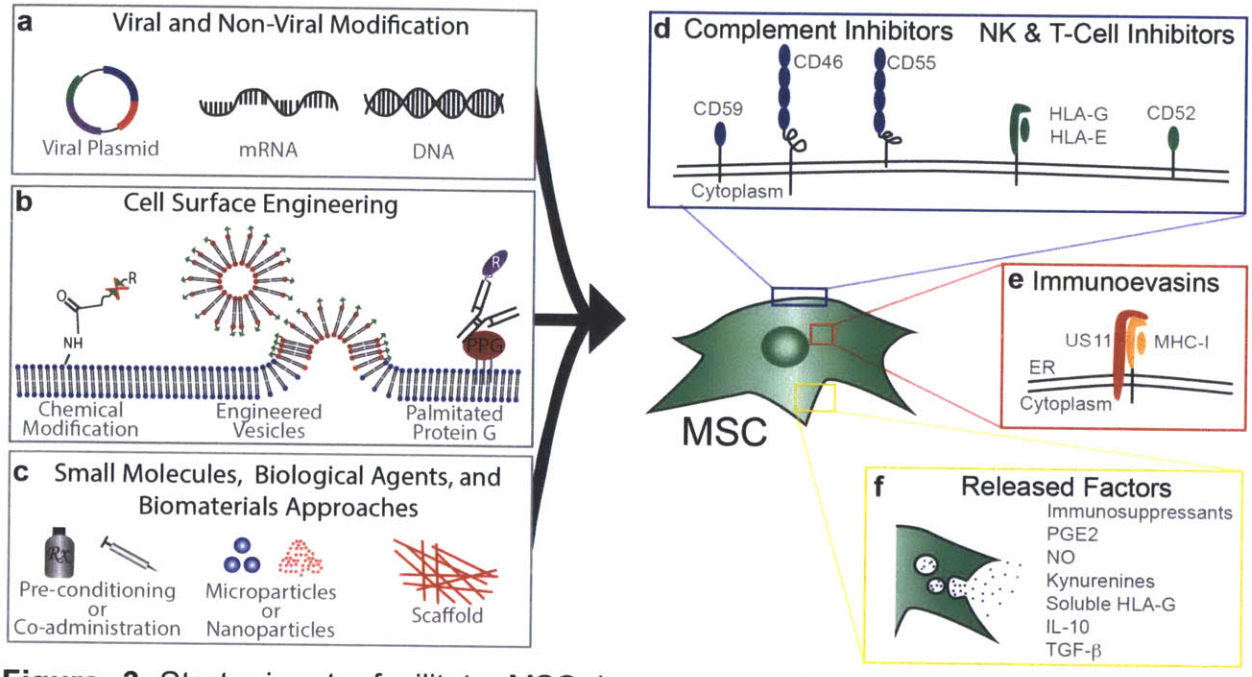


**Figure 3** Strategies to facilitate MSC immune evasion. While co-administration of immunosuppressive drugs with MSCs and transfection with immunoevassins have been harnessed, multiple engineering strategies can likely be applied to achieve immunoevasion including (a) viral and non-viral modification, (b) cell surface engineering, and (c) small molecule, biological agent, and biomaterials approaches. The response time can potentially be extended by use of (c) agent-doped cell internalized degradable microparticles(*80*) or nanoparticles or seeding cells on agent-doped scaffolds prior to implantation. (d) Surface expression of decoy or inhibitory receptors can also be directly engineered onto the cell surface through several techniques including (b) chemical modification including covalent conjugation chemistry(*81*, *82*), engineered vesicles(*83*), or through insertion of antibody fusion proteins into the cell membrane via palmitated protein G (PPG)(*84*). Increased persistence can also be achieved through reducing immunogenicity through the use of (e) immunoevasins or (f) sustained release of immunosuppressive factors.

hMSCs were genetically engineered to express HCMV proteins, US2, US3, US6, or US11. Expression of two of the viral proteins, US6 and US11, resulted in significant suppression of MHC-I surface expression, thereby avoiding recognition of the hMSCs by cytotoxic lymphocytes. Interestingly, in contrast to de la Garza-Rodea's report, expression of US11 also resulted in protection from NK cell lysis in co-cultures with NK-92MI cells. However, the mechanism of NK cell evasion was not fully elucidated. Virally modified hMSCs injected into the liver of pre-immune fetal sheep were less susceptible to NK toxicity and had a 1.8 fold increase in engraftment (% of cells found in the liver of donor origin) compared to unmodified hMSCs(*79*). While these viral strategies appear to address an aspect of MSC rejection, they have yet to be demonstrated as a viable strategy to prevent immune memory induction in a fully immune competent host, or to enhance the therapeutic effect of MSCs in disease models. In addition to forced expression of viral immunoevasins (Fig. 3a,e), MSCs could be engineered to overexpress inhibitory molecules that suppress complement activation (CD46, CD55, CD59) and inhibit NK activation (HLA-E, HLA-G) (Fig. 3a,d). MSCs could also be decorated with immune evasive moieties through chemical cell surface modification approaches(*82-84*) (Fig. 3b,d). Alternatively, MSCs could be preconditioned or loaded(*80*) with small molecule drugs or biologicals that increase the expression of surface receptors or the production of immunosuppressive factors (e.g. PGE2, IDO, HLA-G, IL-10), increasing their immunomodulatory potency and possibly inducing tolerance (Fig. 3c,f).

## A Revised Vision for Allogeneic MSC Therapy

While a comprehensive understanding of MSC allo-rejection is still under development and questions remain, it is clear that MSCs are not immune privileged, at least not to the extent that has been classically proclaimed, but could be considered 'immune evasive'. Despite substantial data on MSC allo-rejection, unmatched allo-MSCs have continued to be referred to as immune privileged and their use in clinical trials has continued to escalate (Figure 1). In addition, the community appears reluctant to abandon the immune-privileged paradigm, evidenced by the number of citations for articles that support the 'Universal Donor' hypothesis compared to the number of

citations for articles that highlight MSC immunogenicity (Figure 1C). It is clear that immunogenicity needs to be recognized as a characteristic of MSCs and its impact on MSC therapy needs to be examined.

MSC production of potent immunomodulatory exosomes and secreted factors has shown significant promise in pre-clinical models and in select clinical trials as discussed. Furthermore, efficient expansion of MSCs enables them to overcome the fundamental limitation of solid organ and hematopoietic stem cell transplantation; supply. Unmatched MSCs may be an appropriate option where a 'hit and run' mechanism of action mediated through transient secreted factors(*50*), exosomes(*85*), or mitochondrial transfer(*86*, *87*) is sufficient to provide therapeutic benefit. In addition, apoptotic bodies generated from dying cells have been shown to be able to modulate inflammatory reactions(*70*), however this mechanism of action has yet to be credited for MSCs therapeutic effects. Moreover, the hypothesis that extended persistence will translate to sustained therapeutic effect and improved clinical outcomes has yet to be tested clinically. Nevertheless, for the millions of patients suffering from chronic conditions, who have placed their hope in stem cell-based therapies, the approach for allo-MSC therapy needs revision. Patients must be prevented from becoming immunized, which could blunt or inhibit the activity of future MSC therapies. In addition to the immune evasion strategies discussed above, banking MSCs from a diverse donor population or harnessing patient specific MSCs through iPS cells(*88*) are alternative solutions to avoid patient sensitization. Due to the ease of MSC expansion, a banking system, much like that for blood, is not difficult to imagine. MSCs from a representative subset of the population could be harvested, typed, and expanded for clinical use. With time, healthy donors would populate the cell bank with sufficient variety of MHC antigens. Evidence suggests this should improve outcomes(*74*) as well as enable serial injection of MSCs without rejection or co-administration of immunosuppressive drugs. Work is already underway via a recently awarded $10 million NIH grant to compare efficacy of MHC matched and mismatched MSCs in a non-human primate model of pancreatic islet transplantation(*89*).

As MSC persistence correlates with the relative expression of immunogenic and immunosuppressive factors (Figure 2), development of next generation MSC therapies

should focus on shifting this balance. Specifically, MSC potency assays must be established based on MSCs expression of immunogenic/immunosuppressive factors at baseline and after TNF-α and IFN-γ stimulation (simulates MSC exposure to inflammatory signals post-transplantation), and standardized to ensure patients receive functional and comparable doses(*23*). The ISCT minimal criteria that is often used in research cannot predict immunomodulatory function or immunogenicity of a batch of MSCs and significant variability in immunomodulatory potency between donors, tissue sources and culture conditions has been documented(*5*, *90-92*). For MSCs to reach their potential in the next decade, new strategies to maximize MSC potency are needed. In addition to finding optimal sources of MSC, the therapeutic potential of MSC can likely be enhanced through increasing their persistence and controlling the MSC secretome by polarizing them to an anti-inflammatory phenotype prior to delivery(*36*, *37*). It will also be critical to prevent patients from becoming sensitized to allo-antigens which would lead to rapid rejection of subsequent MSC doses and reduce the efficacy of MSC therapy.

## Acknowledgements

This work was supported by National Institutes of Health grant HL095722 to JMK and by a Prostate Cancer Foundation Challenge Award to J.M.K. JAA was supported by the Hugh Hampton Young Memorial Fellowship.

## References


1. A. J. Friedenstein, I. I. Piatetzky-Shapiro, K. V. Petrakova, Osteogenesis in transplants of bone marrow cells, *J Embryol Exp Morphol* **16**, 381–390 (1966).

2. A. Friedenstein, J. Gorskaja, N. Kulagina, Fibroblast precursors in normal and irradiated mouse hematopoietic organs, *Exp Hematol* (1976).

3. A. J. Friedenstein, R. K. Chailakhyan, U. V. Gerasimov, Bone marrow osteogenic stem cells: in vitro cultivation and transplantation in diffusion chambers, *Cell Tissue Kinet* **20**, 263–272 (1987).

4. A. J. Nauta, W. E. Fibbe, Immunomodulatory properties of mesenchymal stromal cells, *Blood* **110**, 3499–3506 (2007).

5. M. François, R. Romieu-Mourez, M. Li, J. Galipeau, Human MSC suppression correlates with cytokine induction of indoleamine 2,3-dioxygenase and bystander M2 macrophage differentiation, *Mol Ther* **20**, 187–195 (2012).

6. D. J. Prockop, Two Negative Feedback Loops Place Mesenchymal Stem/Stromal Cells (MSCs) at the Center of Early Regulators of Inflammation, *Stem Cell* (2013), doi:10.1002/stem.1400.

7. J. Ankrum, J. Karp, Mesenchymal stem cell therapy: Two steps forward, one step back, *Trends Mol Med* **16**, 203–209 (2010).

8. D. AcroMed, Ed., New Minimally Invasive Technique for Bone Grafts May Reduce Pain Associated with Back Surgery*investor.jnj.com* (2003) (available at http://www.investor.jnj.com/common/mobile/iphone/releasedetail.cfm?ReleaseID=113119&CompanyID=JNJ&mobileid=).

9. Osteocel® Information - ACE Surgical Supply*acesurgical.com* (available at http://www.acesurgical.com/osteocel_info.html).

10. L. von Bahr *et al.*, Long-term complications, immunologic effects, and role of passage for outcome in mesenchymal stromal cell therapy, *Biol. Blood Marrow Transplant.* **18**, 557–564 (2012).

11. M. M. Lalu *et al.*, A. P. Beltrami, Ed. Safety of Cell Therapy with Mesenchymal Stromal Cells (SafeCell): A Systematic Review and Meta-Analysis of Clinical Trials, *PLoS ONE* **7**, e47559 (2012).

12. TiGenix reports positive Phase IIa study results in refractory rheumatoid arthritis with allogeneic stem cell product Cx611*tigenix.com* (2013) (available at http://www.tigenix.com/public/uploads/pdf/en/f517459e904cc86.32694073_TiGenix%20Cx611%20Phase%20IIa%20results%20Final.pdf).

13. Positive Results from Phase 2 Trial of Mesoblast's Adult Stem Cell Therapy at the

American Heart Association Annual Meeting*prnewswire.com* (2011) (available at http://www.prnewswire.com/news-releases-test/positive-results-from-phase-2-trial-of-mesoblasts-adult-stem-cell-therapy-presented-at-the-american-heart-association-annual-meeting-133835958.html).

14. M. S. Penn *et al.*, Adventitial delivery of an allogeneic bone marrow-derived adherent stem cell in acute myocardial infarction: phase I clinical study, *Circ Res* **110**, 304–311 (2012).

15. Prochymal Significantly Reduces Hypertrophy, Arrhythmia and Progression to Heart Failure in Patients Suffering a Heart Attack*investor.osiris.com* (2012) (available at http://investor.osiris.com/releasedetail.cfm?releaseid=688302).

16. H. Yang, South Korea's stem cell approval, *Nat Biotechnol* **29**, 857–857 (2011).

17. D. Cyranoski, Canada approves stem cell product, *Nat Biotechnol* **30**, 571–571 (2012).

18. K. Le Blanc *et al.*, Mesenchymal stem cells for treatment of steroid-resistant, severe, acute graft-versus-host disease: a phase II study, *Lancet* **371**, 1579–1586 (2008).

19. M. E. Bernardo *et al.*, Co-infusion of ex vivo-expanded, parental MSCs prevents life-threatening acute GVHD, but does not reduce the risk of graft failure in pediatric patients undergoing allogeneic umbilical cord blood transplantation, *Bone Marrow Transplant* **46**, 200–207 (2011).

20. N. H. Riordan *et al.*, Non-expanded adipose stromal vascular fraction cell therapy for multiple sclerosis, *J Transl Med* **7**, 29 (2009).

21. K. Le Blanc *et al.*, Treatment of severe acute graft-versus-host disease with third party haploidentical mesenchymal stem cells, *Lancet* **363**, 1439–1441 (2004).

22. J. M. Hare *et al.*, Comparison of Allogeneic vs Autologous Bone Marrow–Derived Mesenchymal Stem Cells Delivered by Transendocardial Injection in Patients With Ischemic CardiomyopathyThe POSEIDON Randomized TrialMesenchymal Stem Cells and Ischemic Cardiomyopathy, *JAMA* **308**, 2369–2379 (2012).

23. C. A. Bravery *et al.*, Potency assay development for cellular therapy products: an ISCT review of the requirements and experiences in the industry, *Cytotherapy* **15**, 9–19 (2013).

24. M. D. Griffin *et al.*, Anti-donor immune responses elicited by allogeneic mesenchymal stem cells: what have we learned so far? *Immunol. Cell Biol.* **91**, 40–51 (2013).

25. S. E. Haynesworth, M. A. Baber, A. I. Caplan, Cytokine expression by human marrow-derived mesenchymal progenitor cells in vitro: effects of dexamethasone and IL-1 alpha, *J Cell Physiol* **166**, 585–592 (1996).

26. S. M. Devine, R. Hoffman, Role of mesenchymal stem cells in hematopoietic stem cell transplantation, *Curr. Opin. Hematol.* **7**, 358–363 (2000).

27. H. Lazarus, P. Curtin, S. Devine, P. McCarthy, K. Holland, Role of mesenchymal stem cells (MSC) in allogeneic transplantation: early phase I clinical results, *Blood* **96**, 392a (2000).

28. E. Klyushnenkova, J. D. Mosca, K. R. McIntosh, M. A. Thiede, Human mesenchymal stem cells suppress allogeneic T cell responses in vitro: implications for allogeneic transplantation, *Blood* **92**, 2652 (1998).

29. W. T. Tse, W. Beyer, J. D. Pendleton, A. D'Andrea, Bone marrow derived mesenchymal stem cells suppress T cell activation without inducing allogeneic anergy, *Blood* **96**, 1034a (2000).

30. W. T. Tse, J. D. Pendleton, W. M. Beyer, M. C. Egalka, E. C. Guinan, Suppression of allogeneic T-cell proliferation by human marrow stromal cells: implications in transplantation, *Transplantation* **75**, 389–397 (2003).

31. E. Klyushnenkova *et al.*, T cell responses to allogeneic human mesenchymal stem cells: immunogenicity, tolerance, and suppression, *J Biomed Sci* **12**, 47–57 (2005).

32. A. Bartholomew *et al.*, Mesenchymal stem cells suppress lymphocyte proliferation in vitro and prolong skin graft survival in vivo, *Exp Hematol* **30**, 42–48 (2002).

33. K. W. Liechty *et al.*, Human mesenchymal stem cells engraft and demonstrate site-specific differentiation after in utero transplantation in sheep, *Nat Med* **6**, 1282–1286 (2000).

34. T. Ito *et al.*, Mesenchymal stem cell and islet co-transplantation promotes graft revascularization and function, *Transplantation* **89**, 1438–1445 (2010).

35. F. Casiraghi *et al.*, Pretransplant infusion of mesenchymal stem cells prolongs the survival of a semiallogeneic heart transplant through the generation of regulatory T cells, *J Immunol* **181**, 3933–3946 (2008).

36. S. H. Ranganath, O. Levy, M. S. Inamdar, J. M. Karp, Harnessing the Mesenchymal Stem Cell Secretome for the Treatment of Cardiovascular Disease, *Stem Cell* **10**, 244–258 (2012).

37. R. S. Waterman, S. L. Tomchuck, S. L. Henkle, A. M. Betancourt, D. Unutmaz, Ed. A New Mesenchymal Stem Cell (MSC) Paradigm: Polarization into a Pro-Inflammatory MSC1 or an Immunosuppressive MSC2 Phenotype, *PLoS ONE* **5**, e10088 (2010).

38. M. Di Nicola *et al.*, Human bone marrow stromal cells suppress T-lymphocyte proliferation induced by cellular or nonspecific mitogenic stimuli, *Blood* **99**, 3838–3843 (2002).

39. K. Le Blanc, L. Tammik, B. Sundberg, S. E. Haynesworth, O. Ringden, Mesenchymal stem cells inhibit and stimulate mixed lymphocyte cultures and mitogenic responses independently of the major histocompatibility complex, *Scand. J. Immunol.* **57**, 11–20 (2003).

40. M. Krampera *et al.*, Bone marrow mesenchymal stem cells inhibit the response of naive and memory antigen-specific T cells to their cognate peptide, *Blood* **101**, 3722–3729 (2003).

41. K. Le Blanc, C. Tammik, K. Rosendahl, E. Zetterberg, O. Ringdén, HLA expression and immunologic properties of differentiated and undifferentiated mesenchymal stem cells, *Exp Hematol* **31**, 890–896 (2003).

42. H. Hemeda *et al.*, Interferon-γ and Tumor Necrosis Factor-α Differentially Affect Cytokine Expression and Migration Properties of Mesenchymal Stem Cells, *Stem Cells Dev* **19**, 693–706 (2010).

43. M. Mastri *et al.*, Activation of Toll-like receptor 3 (TLR3) amplifies mesenchymal stem cell trophic factors and enhances therapeutic potency, *AJP: Cell Physiology* (2012), doi:10.1152/ajpcell.00191.2012.

44. O. Delarosa, W. Dalemans, E. Lombardo, Toll-like receptors as modulators of mesenchymal stem cells, *Front Immunol* **3**, 182 (2012).

45. Y. Shi *et al.*, How mesenchymal stem cells interact with tissue immune responses, *Trends in Immunology* **33**, 136–143 (2012).

46. C. R. Mills, Osiris Therapeutics Announces Preliminary Results for PRochymal Phase III GvHD Trials*Osiris Press Release* (2009) (available at http://files.shareholder.com/downloads/OSIR/2468414599x0x317779/7677da46-286a-47c4-865d-36c148119a1a/OSIR_News_2009_9_8_General.pdf).

47. C. R. Mills, Osiris Therapeutics Reports Interim Data for COPD Stem Cell Study*Osiris Press Release* (2009) (available at http://files.shareholder.com/downloads/OSIR/2468414599x0x302507/36275c0d-85b9-4726-a51a-708830588b08/OSIR_News_2009_6_23_General.pdf).

48. J. Galipeau, The mesenchymal stromal cells dilemma—does a negative phase III trial of random donor mesenchymal stromal cells in steroid-resistant graft-versus-host disease represent a death knell or a bump in the road? *Cytotherapy* **15**, 2–8 (2013).

49. C. Toma, W. R. Wagner, S. Bowry, A. Schwartz, F. Villanueva, Fate Of Culture-Expanded Mesenchymal Stem Cells in The Microvasculature: In Vivo Observations of Cell Kinetics, *Circ Res* **104**, 398–402 (2009).

50. R. H. Lee *et al.*, Intravenous hMSCs Improve Myocardial Infarction in Mice because Cells Embolized in Lung Are Activated to Secrete the Anti-inflammatory Protein TSG-6, *Cell Stem Cell* **5**, 54–63 (2009).

51. S. Kidd *et al.*, Direct evidence of mesenchymal stem cell tropism for tumor and wounding microenvironments using in vivo bioluminescent imaging, *Stem Cell* **27**, 2614–2623 (2009).

52. L. von Bahr *et al.*, Analysis of tissues following mesenchymal stromal cell therapy in humans indicates limited long-term engraftment and no ectopic tissue formation, *Stem Cell* **30**, 1575–1578 (2012).

53. G. F. Muschler, C. Nakamoto, L. G. Griffith, Engineering principles of clinical cell-based tissue engineering, *J Bone Joint Surg Am* **86-A**, 1541–1558 (2004).

54. N. Eliopoulos, J. Stagg, L. Lejeune, S. Pommey, J. Galipeau, Allogeneic marrow stromal cells are immune rejected by MHC class I- and class II-mismatched recipient mice, *Blood* **106**, 4057–4065 (2005).

55. L. Zangi *et al.*, Direct imaging of immune rejection and memory induction by allogeneic mesenchymal stromal cells, *Stem Cell* **27**, 2865–2874 (2009).

56. A. J. Nauta *et al.*, Donor-derived mesenchymal stem cells are immunogenic in an allogeneic host and stimulate donor graft rejection in a nonmyeloablative setting, *Blood* **108**, 2114–2120 (2006).

57. A. T. Badillo, K. J. Beggs, E. H. Javazon, J. C. Tebbets, A. W. Flake, Murine bone marrow stromal progenitor cells elicit an in vivo cellular and humoral alloimmune response, *Biol. Blood Marrow Transplant.* **13**, 412–422 (2007).

58. D. M. Camp, D. A. Loeffler, D. M. Farrah, J. N. Borneman, P. A. LeWitt, Cellular immune response to intrastriatally implanted allogeneic bone marrow stromal cells in a rat model of Parkinson's disease, *J Neuroinflammation* **6**, 17 (2009).

59. S. Schu *et al.*, Immunogenicity of allogeneic mesenchymal stem cells, *J Cell Mol Med* **16**, 2094–2103 (2012).

60. K. J. Beggs *et al.*, Immunologic consequences of multiple, high-dose administration of allogeneic mesenchymal stem cells to baboons, *Cell transplantation* **15**, 711–721 (2006).

61. I. A. Isakova, J. Dufour, C. Lanclos, J. Bruhn, D. G. Phinney, Cell-dose-dependent increases in circulating levels of immune effector cells in rhesus macaques following intracranial injection of allogeneic MSCs, *Exp Hematol* **38**, 957–967.e1 (2010).

62. A. J. Poncelet, J. Vercruysse, A. Saliez, P. Gianello, Although pig allogeneic mesenchymal stem cells are not immunogenic in vitro, intracardiac injection elicits an immune response in vivo, *Transplantation* **83**, 783–790 (2007).

63. K. H. Grinnemo *et al.*, Xenoreactivity and engraftment of human mesenchymal stem cells transplanted into infarcted rat myocardium, *J. Thorac. Cardiovasc. Surg.* **127**, 1293–1300 (2004).

64. Z. Xia *et al.*, Macrophagic response to human mesenchymal stem cell and poly(epsilon-caprolactone) implantation in nonobese diabetic/severe combined immunodeficient mice, *J Biomed Mater Res A* **71**, 538–548 (2004).

65. G. Moll *et al.*, Mesenchymal stromal cells engage complement and complement receptor bearing innate effector cells to modulate immune responses, *PLoS ONE* **6**, e21703 (2011).

66. Y. Li, F. Lin, Mesenchymal stem cells are injured by complement after their contact with serum, *Blood* **120**, 3436–3443 (2012).

67. K. Le Blanc, D. Mougiakakos, Multipotent mesenchymal stromal cells and the innate immune system, *Nat Rev Immunol* **12**, 383–396 (2012).

68. J. L. Dembinski *et al.*, Tumor stroma engraftment of gene-modified mesenchymal stem cells as anti-tumor therapy against ovarian cancer, *Cytotherapy* **15**, 20–32.e2 (2013).

69. G. Ren *et al.*, Species Variation in the Mechanisms of Mesenchymal Stem Cell-Mediated Immunosuppression, *Stem Cell* **27**, 1954–1962 (2009).

70. R. E. Voll *et al.*, Immunosuppressive effects of apoptotic cells, *Nature* **390**, 350–351 (1997).

71. D. A. Leonard, C. L. Cetrulo Jr, D. A. McGrouther, D. H. Sachs, Induction of Tolerance of Vascularized Composite Allografts, *Transplantation* **95**, 1 (2012).

72. R. Maccario *et al.*, Human mesenchymal stem cells and cyclosporin a exert a synergistic suppressive effect on in vitro activation of alloantigen-specific cytotoxic lymphocytes, *Biol. Blood Marrow Transplant.* **11**, 1031–1032 (2005).

73. F. Buron *et al.*, Human mesenchymal stem cells and immunosuppressive drug interactions in allogeneic responses: an in vitro study using human cells, *Transplant Proc* **41**, 3347–3352 (2009).

74. W. Ge *et al.*, Infusion of mesenchymal stem cells and rapamycin synergize to attenuate alloimmune responses and promote cardiac allograft tolerance, *Am J Transplant* **9**, 1760–1772 (2009).

75. L. Luznik *et al.*, High-dose cyclophosphamide as single-agent, short-course prophylaxis of graft-versus-host disease, *Blood* **115**, 3224–3230 (2010).

76. W. H. Huang, Y. Yan, B. De Boer, G. A. Bishop, A. K. House, A short course of cyclosporine immunosuppression inhibits rejection but not tolerance of rat liver allografts, *Transplantation* **75**, 368–374 (2003).

77. W. H. Huang *et al.*, A short course of mycophenolate immunosuppression inhibits rejection, but not tolerance, of rat liver allografts in association with inhibition of

interleukin-4 and alloantibody responses, *Transplantation* **76**, 1159–1165 (2003).

78. A. S. de la Garza-Rodea *et al.*, Exploitation of herpesvirus immune evasion strategies to modify the immunogenicity of human mesenchymal stem cell transplants, *PLoS ONE* **6**, e14493 (2011).

79. M. A. Soland *et al.*, Modulation of Human Mesenchymal Stem Cell Immunogenicity through Forced Expression of Human Cytomegalovirus US Proteins, *PLoS ONE* **7**, e36163 (2012).

80. D. Sarkar, J. Ankrum, G. S. L. Teo, C. V. Carman, J. M. Karp, Cellular and extracellular programming of cell fate through engineered intracrine-, paracrine-, and endocrine-like mechanisms, *Biomaterials* **32**, 3053–3061 (2011).

81. E. Saxon, C. R. Bertozzi, Cell surface engineering by a modified Staudinger reaction, *Science* **287**, 2007–2010 (2000).

82. D. Sarkar *et al.*, Chemical engineering of mesenchymal stem cells to induce a cell rolling response, *Bioconjug Chem* **19**, 2105–2109 (2008).

83. D. Sarkar *et al.*, Engineered mesenchymal stem cells with self-assembled vesicles for systemic cell targeting, *Biomaterials* **31**, 5266–5274 (2010).

84. I. K. Ko, T. J. Kean, J. E. Dennis, Targeting mesenchymal stem cells to activated endothelial cells, *Biomaterials* **30**, 3702–3710 (2009).

85. C. Lee *et al.*, Exosomes mediate the cytoprotective action of mesenchymal stromal cells on hypoxia-induced pulmonary hypertension, *Circulation* **126**, 2601–2611 (2012).

86. D. J. Prockop, Mitochondria to the rescue, *Nat Med* **18**, 653–654 (2012).

87. M. N. Islam *et al.*, Mitochondrial transfer from bone-marrow–derived stromal cells to pulmonary alveoli protects against acute lung injury, *Nat Med* **18**, 759–765 (2012).

88. Y. Jung, G. Bauer, J. A. Nolta, Concise Review: Induced Pluripotent Stem Cell Derived Mesenchymal Stem Cells: Progress Toward Safe Clinical Products, *Stem Cell* **30**, 42–47 (2012).

89. With $10 Million Grant, Norma Sue Kenyon, Ph.D., Aims to Develop Co-Transplant Criteria | Miller School of Medicine | University of Miami*med.miami.edu* (available at http://med.miami.edu/news/with-10-million-grant-norma-sue-kenyon-ph.d.-aims-to-develop-co-transplant-).

90. V. Zhukareva, M. Obrocka, J. D. Houle, I. Fischer, B. Neuhuber, Secretion profile of human bone marrow stromal cells: donor variability and response to inflammatory stimuli, *Cytokine* **50**, 317–321 (2010).

91. M. Strioga, S. Viswanathan, A. Darinskas, O. Slaby, J. Michalek, Same or not the

same? Comparison of adipose tissue-derived versus bone marrow-derived mesenchymal stem and stromal cells, *Stem Cells Dev* **21**, 2724–2752 (2012).

92. S. M. Melief, J. J. Zwaginga, W. E. Fibbe, H. Roelofs, Adipose Tissue-Derived Multipotent Stromal Cells Have a Higher Immunomodulatory Capacity Than Their Bone Marrow-Derived Counterparts, *Stem Cells Translational Medicine* (2013), doi:10.5966/sctm.2012-0184.

## Chapter 5 Preface

In this chapter the particle-in-cell platform is put to use to minimize MSC immunogenicity and maximize MSC's immunomodulatory potency. As described in Chapters 1 and 4, MSC therapy depends on the ability of MSCs to modulate inflammatory processes through the expression of immunomodulatory factors. In this chapter, a small molecule is identified that significantly enhanced MSC's therapeutic potential, without negatively impacting other aspects of cell phenotype including viability, proliferation, and morphology, and metabolic activity. As the enhancement is most prominent when the drug is continuously present, the particle-in cell approach is then used to enable sustained control of MSCs' therapeutic phenotype.

This article is an adaptation of a manuscript submitted to *Nature Biotechnology*.

**Glossary of Terms**

Indoleamine-2,3-dioxygenase: Intracellular enzyme responsible for degrading tryptophan

Budesonide: Synthetic glucocorticoid steroid.

Peripheral Blood Mononuclear Cells: Immune cell population (Predominately CD4+ and CD8+ T cells) isolated from blood after depleting neutrophils and red blood cells.

1-methyl-tryptophan: Competitive inhibitor of IDO, prevents degredation of tryptophan

RU486: Competitive inhibitor of the glucocorticoid receptor, prevents docking of glucocorticoid steroids

siRNA: short double stranded RNA sequence used to destroy mRNA in a cell, thereby knocking down expression of the gene.

# Chapter 5: Enhanced mesenchymal stem cell immunomodulatory potency through sustained intracellular delivery of small molecules


## Abstract

Mesenchymal stem cells are being explored to treat numerous inflammatory conditions, however, clinical studies have yielded mixed results. Recent data suggests that this is due to highly variable and inadequate MSC potency. We report a discovery that glucocorticoid steroids significantly augment MSC expression and activity of indoleamine-2,3-dioxygenase, a primary mediator of MSC immunomodulatory function. This effect is dependent on signaling through the glucocorticoid receptor and mediated through up-regulation of FOXO3, which acts as an enhancer. Treatment of MSCs with the glucocorticoid steroid budesonide, results in a significant up-regulation of IDO 24 hours following IFN-γ stimulation and the enhancement is most notable when cells are continuously exposed to budesonide compared to a simple pre-treatment regimen. To translate this finding to a platform that could be used *in vivo* without requiring systemic glucocorticoid immunosuppression, we engineered MSCs with intracellular PLGA microparticles loaded with budesonide. MSCs efficiently internalized budesonide microparticles and exhibited enhanced expression and activity of IDO over budesonide preconditioned and naïve MSCs, resulting in a 2-fold enhancement in MSC suppression of stimulated PBMC co-cultures. In addition to suppressing PBMC proliferation, budesonide modified MSCs (BUD-MSCs) also suppressed PBMC secretion of IFN-γ. Addition of the IDO inhibitor 1-methyl-tryptophan abolished the suppressive properties of the BUD-MSCs, implicating IDO as the primary mediator of BUD-MSC's enhanced immunosuppressive effects.

## Introduction

The potential of mesenchymal stem cells (MSCs) to ameliorate inflammation arising from numerous diseases has been established in preclinical animal models leading to hundreds of MSC clinical trials (*1*). While MSCs appear to be beneficial in several disease models, treatment of patients has led to highly variable outcomes. For example, subsets of patients with graft versus host disease (GvHD) have responded remarkably well to MSC therapy with at least temporary resolution of symptoms (*2*, *3*), while for others their prognosis is unaltered (*4*, *5*). Factors limiting MSC therapy include variable immunomodulatory potency (*6-8*), dependence on *in vivo* activation by host inflammatory mediators to achieve MSC immunomodulation (*7-9*), and limited MSC persistence (*10*, *11*). Recent work has shown significant variability in MSCs' cytokine-induced secretome (*8*), *in vitro* immunomodulatory potential (*6*, *7*), and treatment efficacy dependent on donor (*6*, *7*), the MSCs tissue of origin (*6*, *12*), and cell preparations from different passages (*2*). Furthermore, limited persistence shortens the therapeutic window in which MSCs modulate inflammatory responses via secretion of growth factors and cytokines, release of exosomes, or activity of immunomodulatory enzymes such as iNOS and IDO. Thus, techniques to augment the potency of MSCs are needed for a therapeutic effect to be exerted within a short therapeutic window. We hypothesize that engineering MSCs to maximize and sustain immunosuppressive potential will enable the generation of enhanced cell-based therapies and eliminate the need to contemplate which tissue or donor MSCs are derived from.

One of the primary factors mediating MSC immune suppression is the tryptophan depleting enzyme indoleamine-2,3-dioxygenase (IDO). Inhibiting IDO with 1-methyl-DL-tryptophan (1-MT) in human MSCs abrogates MSCs' immunosuppressive potential in peripheral blood mononuclear cell (PBMC) co-cultures (*7*, *13*). In contrast to secreted factors implicated in MSC immune suppression such as PGE2 (*14*) or TSG-6 (*10*), IDO is an intracellular enzyme. Specifically, IDO is the first and rate-limiting enzyme involved in degradation of tryptophan down the kynurenine pathway and is predominately expressed in antigen presenting cells (APCs) in response to type I interfons (*15*). Additionally, human MSCs have been shown to have IDO dependent antimicrobial affects against staphylococcus aureus, staphylococcus epidermis, and toxoplasma

gondii (*16*). As in APCs, expression of IDO in MSCs occurs in response to inflammation, induced by exposure to interferon-γ (IFN-γ). Both the depletion of tryptophan and the generation of kynurenine byproducts have potent suppressive effects on immune cells (*15*, *17*). IDO has been implicated in promoting both physiological and pathological tolerance. IDO expressed by cells in the placenta is responsible for fetal tolerance, and inhibition of IDO by the inhibitor 1-methyl-tryptophan (1-MT) results in allograft rejection of the fetus (*18*). More recently, IDO has been found to be overexpressed in solid tumors, promoting tolerance towards tumor antigens (*19*) and tryptophan depletion has been shown to suppress T-cell proliferation through activation of general control non-depressing 2 (GCN2) kinase (*20*). In addition to tryptophan depletion, IDO generates tryptophan catabolites that inhibit the proliferation of activated T-cells (*21*) and induce naïve T-cells to become FoxP3+ T-regulatory cells (*22*). Due to the role of IDO as a negative regulator of inflammation and inducer of tolerance, the level and regulation of its expression is of great interest for maternal-fetal tolerance, tumor immunity, allergy, autoimmune disease, transplant tolerance, and MSC therapy. Unfortunately, the level of MSC IDO expression varies significantly between donors and between MSC tissue sources leading to variability in MSC's ability to suppress activated T-cells (*6*, *7*).

As elevated IDO activity correlates with enhanced suppression of T-cell activation and proliferation, augmenting MSC IDO levels should increase their immunomodulatory potency. Interestingly, IDO expression in macrophages and dendritic cells has been shown to be augmented by exposure to glucocorticoid steroids mediated in part through cell-cell contact signaling through GITR and GITRL interactions (*23*, *24*). Similarly, augmented IDO expression following glucocorticoid steroid treatment has also been observed in astrocytes, although the mechanism of steroid enhanced IDO activity is not known (*25*). While MSCs are frequently administered to patients with GvHD who are already receiving glucocorticoid steroids (*3*, *26*), the impact of glucocorticoid steroids on MSCs broadly, and IDO activity specifically has not been investigated.

Herein we report that glucocorticoid steroids significantly boost MSC's IDO activity and immunosuppressive phenotype and we introduce a cell engineering strategy to sustain therapeutic potency. Specifically, we observe that budesonide treated MSCs

show similar metabolic activity, viability, and morphology to untreated MSCs, yet exhibit a favorable shift between their expression of immunogenic and immunosuppressive factors. In addition to enhancing IFN-γ-induced IDO expression and activity, budesonide treatment also significantly reduced MSC expression of MHC molecules. We found that combined exposure to both budesonide and inflammatory cues resulted in the highest levels of IDO expression, as IDO is only expressed in response to inflammatory signaling. Additionally, the response was broadly applicable to glucocorticoids as dexamethasone produced a similar IDO response, and blocking the glucocorticoid receptor inhibited the enhanced IDO expression. To engineer cells with enhanced and sustained immunosuppressive potency that can be activated upon entering an inflammatory environment without requiring systemic administration of immunosuppressant drugs, we utilized a particle engineering approach. Budesonide loaded microparticles were efficiently internalized by MSCs and resulted in significant enhancement of MSC IDO expression and activity, similar to soluble budesonide. *In vitro* co-culture assays with PBMCs revealed the engineered MSCs could be activated *in situ* in response to IFN-γ produced by PBMCs. Engineered MSC suppression of PBMCs was enhanced further by pre-activating MSCs with IFN-γ to increase expression of IDO prior to the initiation of the PBMC co-cultures. Addition of the IDO inhibitor 1-methyl-tryptophan completely abolished the suppressive properties of the engineered MSCs, implicating IDO as a key immunosuppressive factor. We believe this engineering strategy could be used to augment MSC potency, resulting in enhanced cell-based therapies.

# Results

### Impact of budesonide on MSC phenotype

Glucocorticoid steroids are commonly prescribed anti-inflammatory drugs that have diverse effects on immune cells, however their effect on MSC immunogenicity and immunomodulatory potential has not been thoroughly examined. Glucocorticoid steroids exert their effects through binding cytoplasmic glucocorticoid receptors and translocating to the nucleus where they bind glucocorticoid responsive elements (GREs), resulting in promotion or suppression of gene expression (*27*). As such,

glucocorticoid steroids, such as budesonide, have variable effects on cells of different origins, including growth inhibition (*28*), suppression of MHC expression (*27*, *29*), and induction of IDO (*25*).

To examine if budesonide alters MSC potency without negatively impacting MSC phenotype, MSCs were exposed to 0.001-100 μM budesonide for 24-72 hours. Metabolic activity, as assessed by XTT, was not significantly affected by budesonide treatment for 24, 48, or 72 hours over the dosage range tested (Fig. 1a). Flow cytometry analysis revealed no significant changes in MSC viability as evidenced by dual negative staining for Annexin-V and propidium iodide after 72 hours of budesonide exposure (Fig. 1b). Phase contrast imaging of treated cells did not show any appreciable impact of budesonide on the morphology of MSCs after 48 hours of budesonide exposure (Fig. 1c). In addition, MSCs treated with budesonide for 48 hours showed no evidence of increased cell death when evaluated for double stranded DNA breaks by TUNEL staining (Fig 1d). Collectively these data show MSC metabolic activity, morphology, proliferation, and viability were preserved over a wide range of budesonide concentrations.

Next we analyzed the effect of budesonide on MSC expression of MHC I and MHC II molecules. MSCs' naturally low expression of MHC I, lack of MHC II, and failure to elicit hyperacute rejection upon infusion has been used to justify the use of unmatched allogeneic MSCs in animal models and clinical trials. However, upon exposure to an inflammatory environment, expression of both MHC molecules increases (*30*). Interestingly, glucocorticoids have been shown to reduce expression of MHC molecules in many cell types (*27*, *29*). Expression of class I and class II MHC molecules, HLA-ABC and HLA-DR respectively, were examined to investigate budesonide's impact on MSC's immunophenotype before and after IFN-γ stimulation. MSCs were exposed to vehicle or budesonide for 24 hours after which media was changed to include IFN-γ and the cells were cultured for an additional 48 hours prior to antibody staining and flow cytometry analysis. Cells in the 'drug preconditioning' group were exposed to budesonide only during the first 24 hours while cells in the 'drug sustained' group were exposed to budesonide for the duration of the experiment (Fig. 2a). Figure 2b shows that MSC expression of HLA-ABC was reduced by over 50%

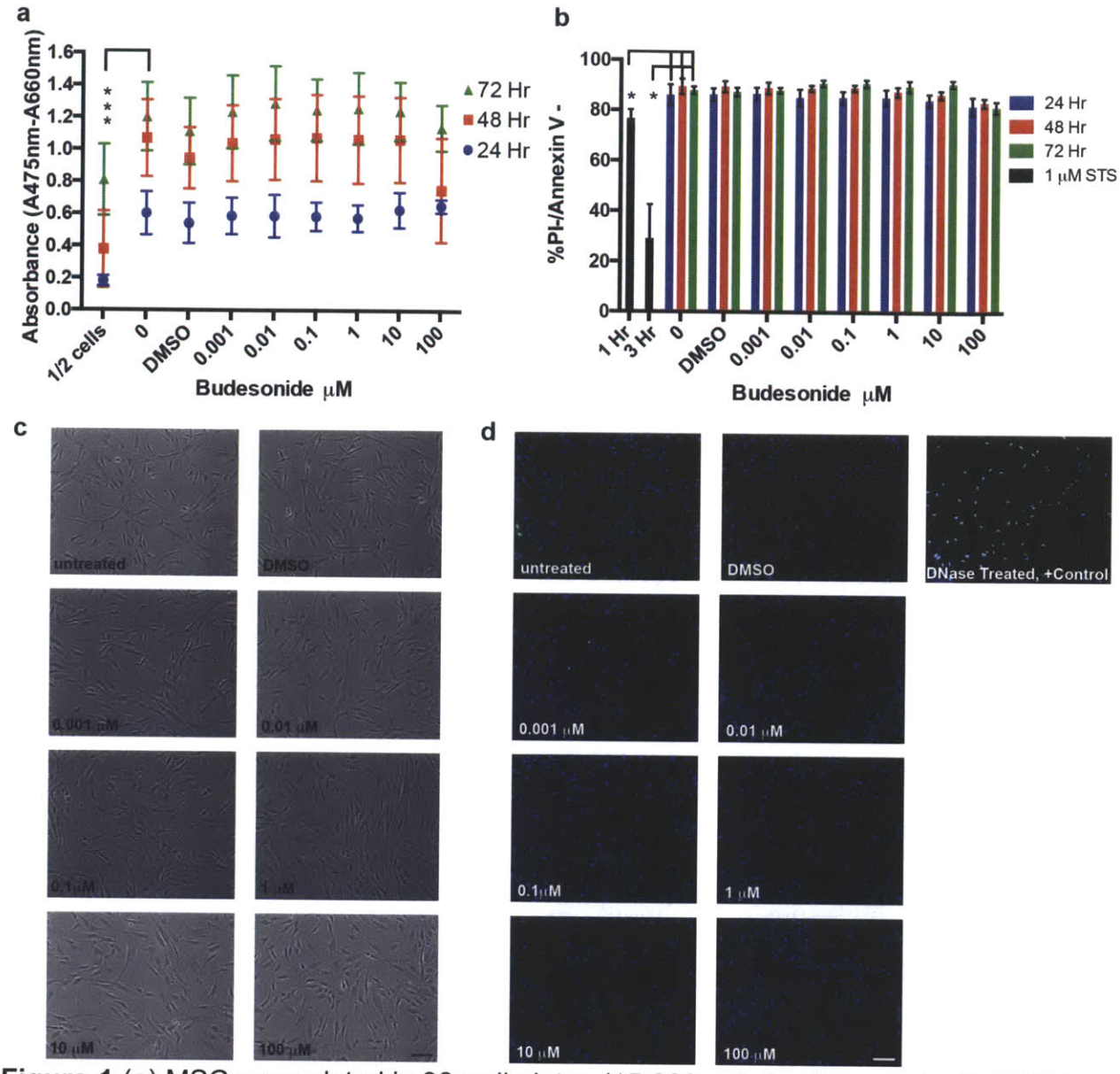


**Figure 1** (a) MSC were plated in 96 well plates (15,000 cells/well) treated with DMSO or 0.001-100uM budesonide and their metabolic activity was assessed by XTT at 24, 48, and 72 hours. ½ cell condition (7,500 cells/well) used as control to show a reduction in XTT signal when fewer cells are present. (b) MSCs were plated in 24 well plates (30,000 cells/well) treated with DMSO or 0.001-100uM budesonide. At 24, 48, and 72 hours after plating, cells were harvested, and viability was measured by staining with Annexin V and propidium iodide. Staurosporine (STS) treatment for 1 and 3 hour was used as a positive control for cell death. (c) Representative phase contrast images of MSCs treated with budesonide for 48 hours show no change in morphology, density, or adherence. (d) TUNEL staining for double stranded DNA breaks after 48 hour budesonide exposure shows no increase in apoptosis. Stain control cells were treated with DNase to induce DNA breaks to serve as a positive control for TUNEL stain. (DAPI, Blue; TUNEL, Green). (Bars are mean±SEM, 2-way ANOVA with Fishers LSD test, n=3, *$p<0.05$) Scale bar 100μm.

for all doses of budesonide in both the precondition and drug sustained groups ($p<0.001$). Following exposure to 100 μM budesonide, stimulation with IFN-γ reduced HLA-ABC expression by only ~15% (not significant (NS), Fig. 2b, c). Budesonide treatment did not result in any increase of HLA-DR expression in unstimulated conditions or decrease in HLA-DR in stimulated conditions except for the 100 μM treated group. Preconditioning with 100 μM budesonide reduced IFN-γ induced HLA-DR expression by 11% (NS) while sustained exposure resulted in a 40% reduction ($p<0.001$, Fig. 2.d,e).

MSC's immunosuppressive potential was evaluated following exposure to budesonide through assessment of IDO protein content and activity. Following treatment of MSCs with 1 μM budesonide for 24 hours, MSCs were additionally exposed to 100 ng/ml IFN-γ for 48 hours (Fig. 3a). MSCs were collected, lysed, and IDO protein content was analyzed by western blot. Budesonide treatment alone did not result in any increase in IDO protein content over untreated MSCs (Fig. 3b). IFN-γ stimulation resulted in increased IDO content in both untreated and budesonide treated MSCs, with budesonide treated cells containing significantly more IDO than untreated controls. To determine the extent to which budesonide could enhance MSC IDO expression, IDO content of MSCs from multiple donors and passages was analyzed with and without budesonide treatment. Enhancement in IDO expression following budesonide exposure was observed in MSCs from multiple donors, regardless of the baseline level of IDO expression (no budesonide treatment) for each donor (Fig. 3c). In addition, high passage, P8 and P10, MSCs treated with budesonide expressed IDO at levels greater or similar to untreated P5 MSCs (Fig. 3d). Interestingly, IDO expression was most significantly enhanced when budesonide was continuously present versus simply pretreated (Fig. 3e,f). To demonstrate the ability to enhance the immunomodulatory potency of MSCs with poor immunosuppressive potential, donor #7083, which had the lowest baseline IFN-γ inducible IDO expression (no budesonide treatment) of the three donors, was used for all subsequent experiments. As the immunomodulatory function of IDO is dependent on its activity as an enzyme, an enzymatic activity assay was performed. Specifically, MSCs were grown according to the protocol depicted in Fig. 3a, collected, lysed to isolate IDO from the cytoplasm, and

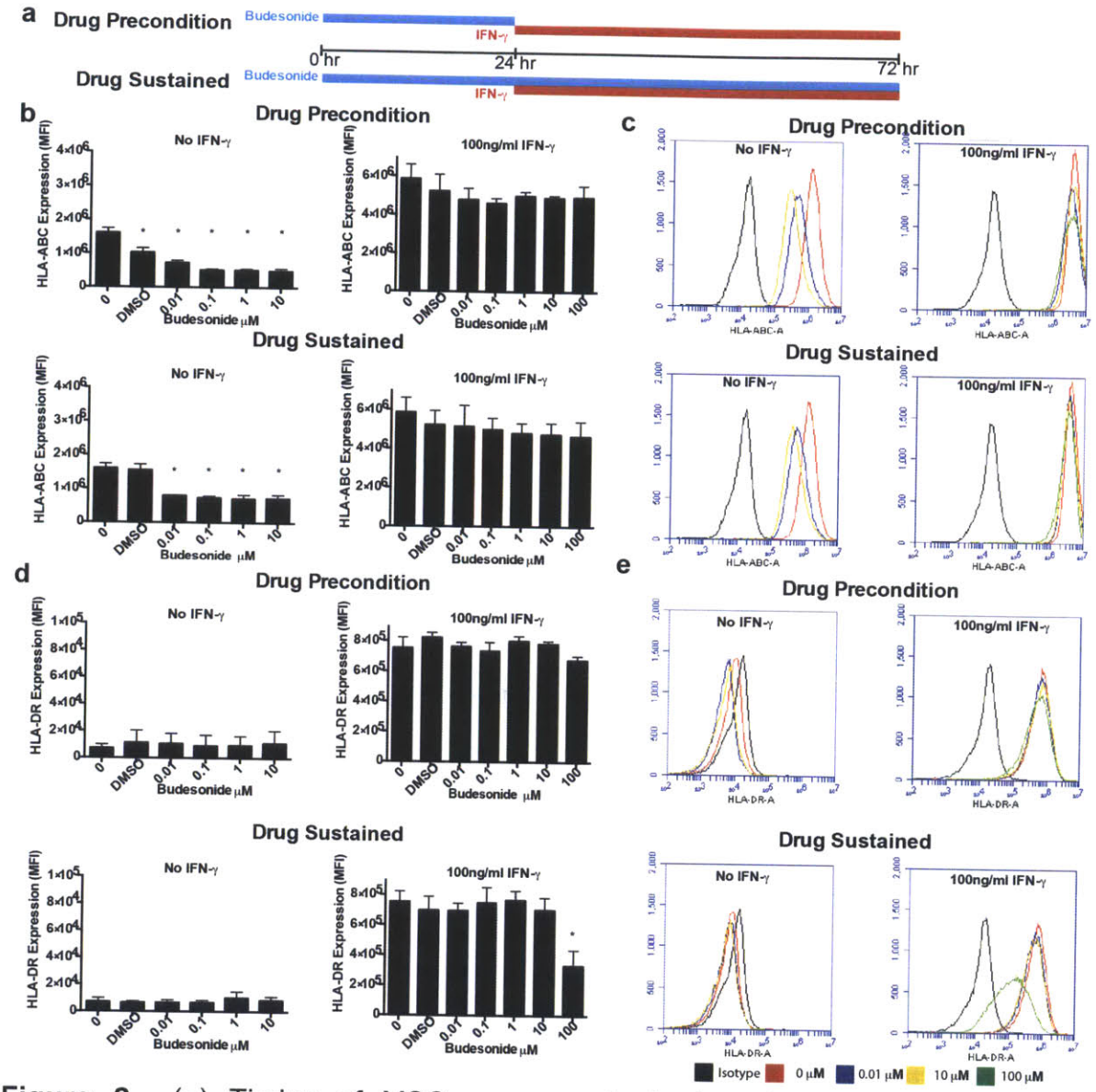


**Figure 2** (a) Timing of MSC exposure to budesonide and IFN-γ in the Drug Precondition and Drug Sustained groups. Flow cytometric analysis of (b,c) HLA-ABC and (d,e) HLA-DR surface expression of MSCs. MSC were plated in 25 $cm^2$ flasks (100,000 MSC/flask) with media containing vehicle or budesonide and were either stimulated with IFN-γ or left unstimulated. MSC were then cultured an additional 48 hours without budesonide (Drug Precondition) or with budesonide (Drug Sustained). (b,d) show mean fluorescence intensity (MFI) for each condition. (Bars are mean±SEM, One-way ANOVA with Bonferroni correction for multiple comparisons, n=3, *p<0.001 compared to untreated control). (c,e) show representative flow cytometry plots including isotype controls.

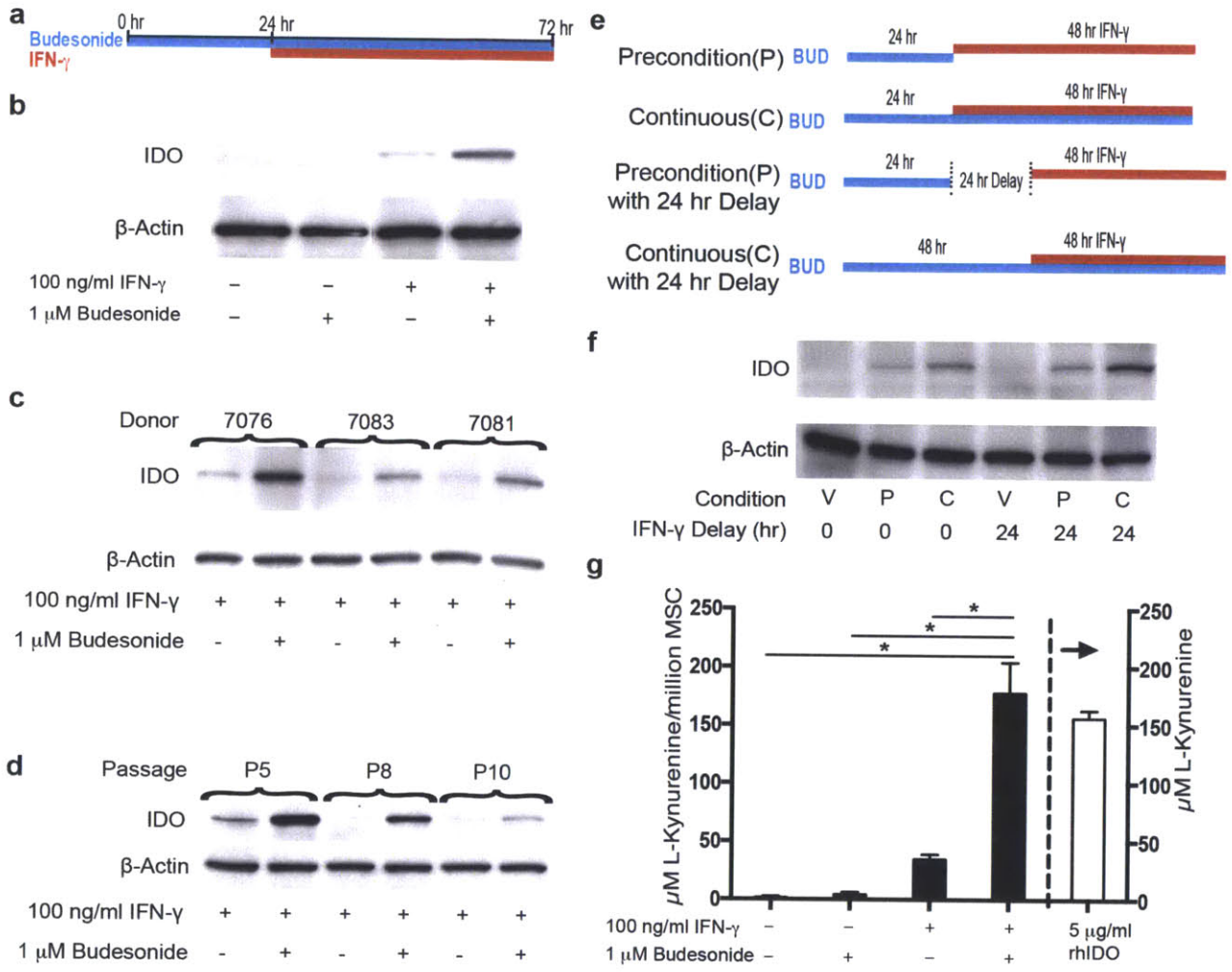


**Figure 3.** IDO expression is maximized following IFN-γ and budesonide exposure. (a) Timing of MSC exposure to budesonide and IFN-γ. (b) Western blot of IDO protein content measured from MSC exposed to 1 μM budesonide and 100 ng/ml IFN-γ. β-actin shown as loading control. (c) Western blot of IDO protein content measured from MSCs harvested from three independent donors exposed to 1 μM budesonide and 100 ng/ml IFN-γ. β-actin shown as loading control. (d) P5, P8, and P10 MSCs were treated with vehicle or budesonide for 24 hours and then additionally with 100 ng/ml IFN-γ for 48 hours. Cell lysate was collected and analyzed for IDO content by western blot. (e) Impact of IFN-γ and budesonide on the enzymatic activity of IDO harvested from MSC (donor 7083) lysate measured by production of kynurenine. 5μg/ml rhIDO was used as an internal control for the assay(right axis). (Bars are mean±SEM One-way ANOVA with Tukey correction for multiple comparisons, n=3, *p<0.001). (f) Timing of MSC exposure to budesonide and IFN-γ. A 0 or 24 hour delay was introduced between preconditioning and IFN-γ exposure in the preconditioning group. (g) Western blot of IDO protein content measured from MSCs exposed to (V) DMSO vehicle, or (P) preconditioned, or (C) continuously exposed to 1 μM budesonide. A 0 or 24 hour delay was introduced between the 24 hour budesonide preconditioning and exposure to IFN-γ. β-actin shown as loading control.

the quantity of L-kynurenine produced was measured by a colorimetric assay. Exposure to budesonide had a dramatic effect on MSC's IDO activity. While IDO expression naturally increases upon stimulation with IFN-γ, additional conditioning by budesonide resulted in an over 4-fold increase in IDO activity (Fig. 3g).

**Mechanism of IDO augmentation**

To begin to elucidate the mechanism of budesonide-mediated enhancement of MSC IDO expression, we examined the timing and activation of intracellular pathways likely to be involved. Elevated IDO levels were first detected by western blot 24 hours after IFN-γ exposure (Fig. 4 a,b), consistent with previous reports that show IFN-γ stimulates new transcription of IDO mRNA in MSCs (*6*). Furthermore, the effect does not appear to be mediated through increased sensitivity to IFN-γ, as the timing and degree of Stat-1 phosphorylation between untreated (Fig. 4a) and budesonide treated (Fig. 4b) MSCs were nearly identical. Next we examined if budesonide was exerting its effect on IDO expression through the glucocorticoid receptor. Blocking the glucocorticoid receptor with 2 μM of RU486 reversed budesonide's enhancing effect on IDO expression back to baseline levels (Fig. 4c). This data suggests budesonide mediated enhancement of IDO is dependent on the glucocorticoid receptor. Consistent with this observation is the finding that treatment with either budesonide or dexamethasone, both glucocorticoid steroids, results in similar enhancement in IDO expression (Fig. 4d). Interestingly, the promoter region for the IDO gene does not contain any known GREs. Thus, steroid enhancement of IDO is likely mediated through up-regulation of a glucocorticoid responsive intermediary that enhances the transcription of IDO. Therefore we looked for transcription factors known to bind the IDO promoter that are also sensitive to glucocorticoid steroids. IDO has previously been reported to be promoted by FOXO3 (*17*), a transcription factor which has recently been shown to be a target of the glucocorticoid receptor (*31*). To determine FOXO3's role in budesonide-mediated enhancement of MSC IDO, we performed siRNA knockdown experiments. MSCs were transfected with FOXO3 siRNA or scramble siRNA as a control and then treated with budesonide for 24 hours, after which cells were treated with IFN-γ. FOXO3 expression was measured 6 hours after IFN-γ addition (preliminary

experiments revealed peak FOXO3 content at this time point) and IDO was measured 30 hours after IFN-γ addition. Transfection of MSCs with FOXO3 siRNA resulted in nearly complete inhibition of FOXO3 (Fig. 4e) and reverted budesonide treated MSC IDO expression (Fig. 4f) and activity (Fig. 4g) back to the level of untreated MSCs. Collectively this data suggests budesonide's effect on MSC IDO expression is mediated by glucocorticoid induced expression of FOXO3 which then acts as a genomic enhancer to augment the expression of IDO.

**Establishing prolonged control of MSCs**

We next sought to examine if we could prolong enhanced MSC IDO activity without the need for continuous exposure to soluble budesonide. Glucocorticoid steroids are commonly used clinically and potentially could be co-administered with MSCs, however, their lack of specificity causes them to have numerous off-target effects that can be detrimental to the overall health of a patient (*32-34*). Thus, developing a method to control MSC phenotype without requiring co-administration of systemic glucocorticoid steroids thereby minimizing systemic exposure is desirable. To achieve prolonged control of MSC IDO activity we drew from our prior experience loading MSCs with drug loaded poly(lactic-co-glycolic acid) (PLGA) microparticles. Previously we have shown that 1 μm particles can be efficiently internalized into MSCs and remain stable for at least 7-days during which time, small molecule drugs can be released to influence the phenotype of cells (*35*, *36*).

Budesonide microparticles ~1 μm in diameter with low polydispersity were formulated to control MSC IDO activity (Fig. 5a,b). Surface modification of the particles with poly-L-Lysine resulted in a zeta potential of +10 mV (Fig. 5b), which we have previously shown enhances particle uptake (*35*). Budesonide was extracted from the particles and the drug loading (7.05%, Fig. 5b) and encapsulation efficiency (51.2%, Fig. 5b) were determined by HPLC. 10 kDa molecular weight PLGA was used to formulate the particles to ensure rapid release of the drug during the first week following MSC particle modification. Release kinetic experiments were performed, revealing a burst release of 20% of total drug in the first 12 hours followed by a continuous release, with ~80% of total drug released by day 10 (Fig. 5c). MSC internalization of particles

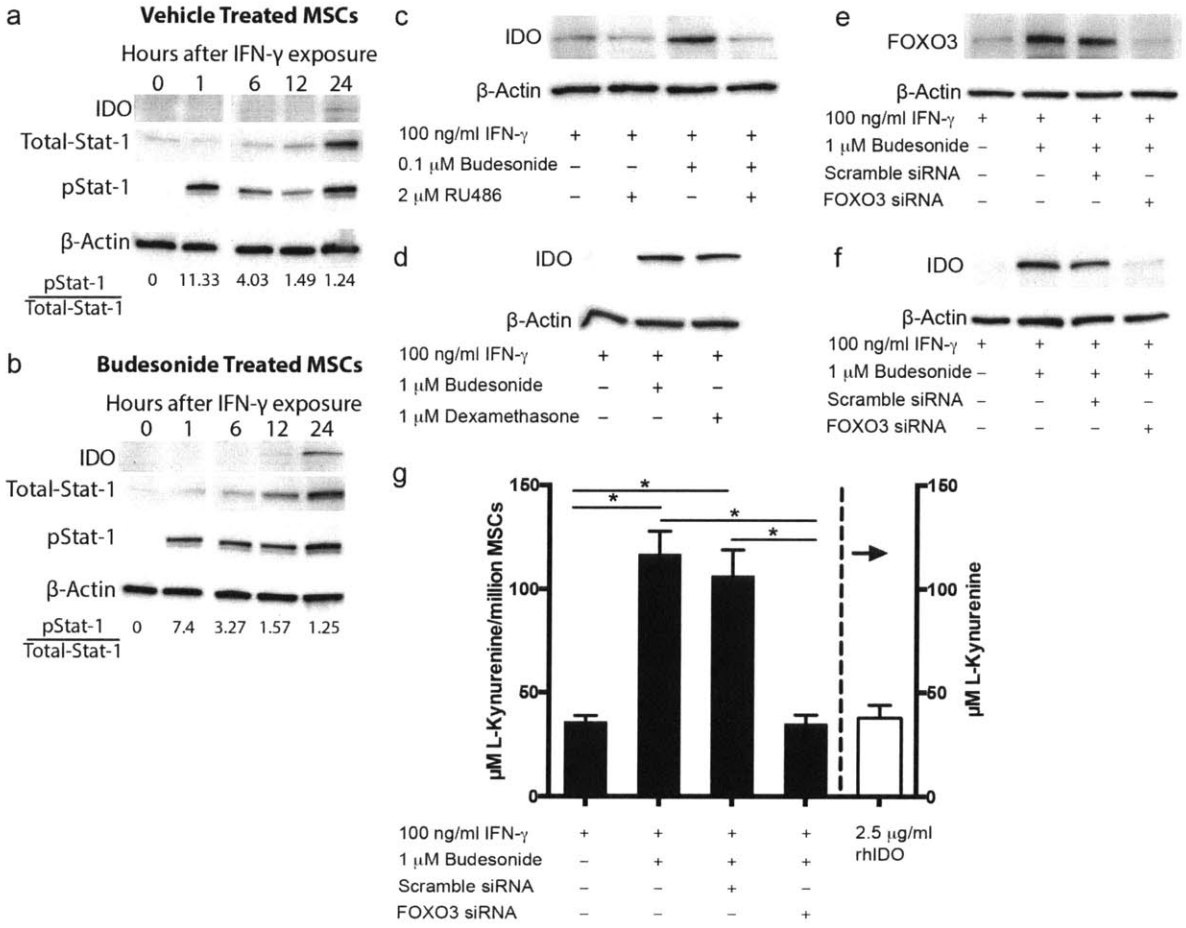


**Figure 4**. Budesonide enhancement of IDO occurs through glucocorticoid receptor mediated upregulation of FOXO3 and not increased sensitivity to IFN-γ. MSCs were treated with (a) vehicle only or (b) 1 μM budesonide for 24 hours and then additionally exposed to 100 ng/ml IFN-γ (continuous exposure to vehicle or budesonide). Lysates of (a) untreated (vehicle only) MSCs and (b) 1 μM budesonide treated MSCs were collected at 0, 1, 6, 12, and 24 hours after IFN-γ exposure. To determine the timing of IDO up-regulation IDO protein content was measured at each time point. To determine if budesonide enhanced MSC sensitivity to IFN-γ, the degree of Stat-1 phosphorylation was measured as stat-1 phosphorylation is classically induced by IFN-γ stimulation. Ratio of pStat-1 to total Stat-1 is shown for each time point. (c) Inhibition of the glucocorticoid receptor with RU486 reverts IDO levels back to baseline levels in budesonide treated MSCs. (d) Western blot of IDO protein content measured from IFN-γ stimulated MSC exposed to DMSO vehicle, budesonide, or dexamethasone. To test the dependence of enhanced IDO expression on FOXO3, siRNA knockdown was performed. MSCs were transfected with FOXO3 siRNA or scrambled siRNA for 5 hours and then treated with budesonide for 24 hours followed by IFN-γ treatment. Cell lysates were collected 6 and 30 hours following addition of IFN-γ and analyzed for (e) FOXO3 and (f) IDO respectively. (g) Activity of IDO harvested from lysates of vehicle, budesonide, budesonide/FOXO3 siRNA, and budesonide/scrambled siRNA treated MSCs 48 hours after IFN-γ stimulation. (Bars are mean±SEM, One-way ANOVA with Tukey correction for multiple comparisons, n=3, *$p<0.01$).

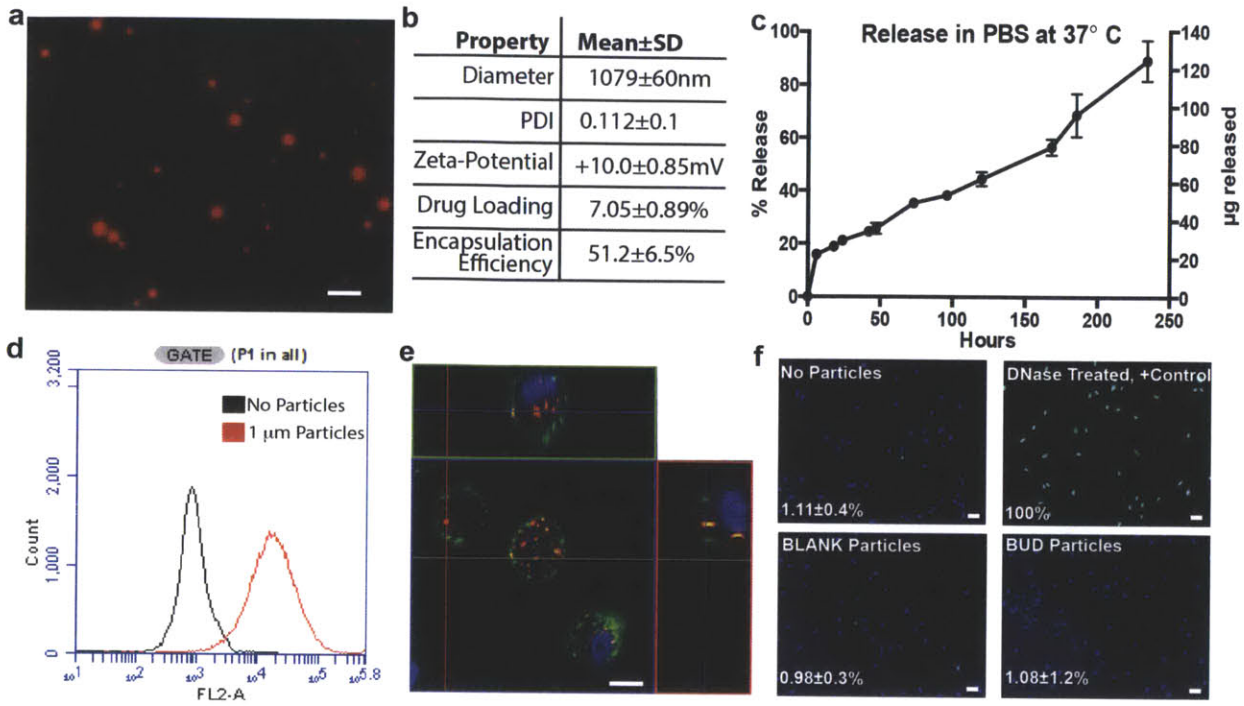


**Figure 5.** Sustained control of MSC phenotype. (a) Fluorescent image of DiI labeled Budesonide PLGA microparticles(Scale bar 5 µm). (b) Physicochemical properties of budesonide PLGA microparticles. (c) Release kinetics of budesonide from 2mg of PLGA microparticles into PBS at 37°C. (d) MSC association with 1 µm, PLL coated particles was assessed by flow cytometry (Representative plot). (e) Representative confocal image of an MSC modified with 1 µm diameter PLGA particles (red) revealing particles are predominately intracellular rather than membrane associated (membrane stained Green, nuclei shown in Blue, scale bar 10 µm). (f) Particle modified MSC viability examined by TUNEL staining. TUNEL stain shown in green with nuclei counterstained with Hoechst (Blue). (bottom) Percent apoptotic cells (mean±SD ,TUNEL+/Hoechst+ nuclei, n=3) shown in each image (Scale bar 50 µm).

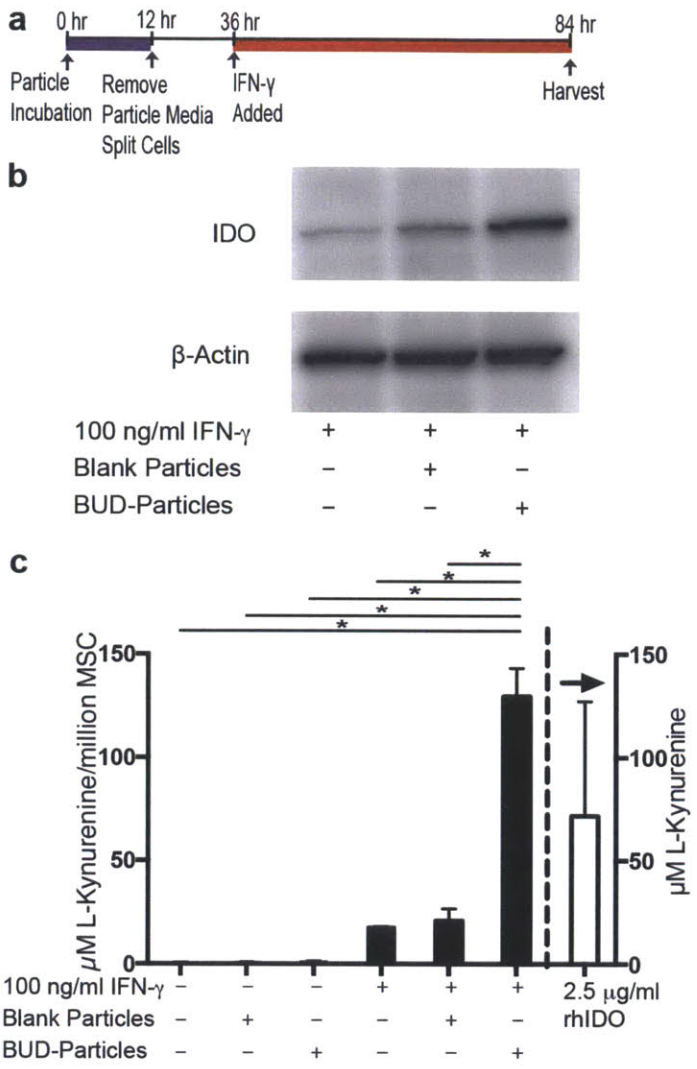


**Figure 6.** Budesonide particles enhance MSC's therapetutic potential. (a) Timing of MSC particle modification and exposure to IFN-γ. MSCs were modified with particles overnight, harvested and split into new flasks and then exposed to IFN-γ for 48 hours. (b) Western blot of IDO protein content measured from unmodified, Blank-Particle modified, or BUD-Particle modified MSCs exposed to 100ng/ml IFN-γ. β-actin shown as loading control. (c) Impact of BUD-Particle modification on MSC IDO activity with and without stimulation with 100ng/ml IFN-γ. IDO activity measured by the production of L-kynurenine from generated from MSC lysate incubated with tryptophan. 5μg/ml rhIDO was used as an internal control for the assay(right axis). (Bars are mean±SEM, One-way ANOVA with Tukey correction for multiple comparisons, n=3, *p<0.001).

was optimized as previously described (*35*) by modulating the size and zeta-potential of the particles. MSC association with 1 μm PLGA particles coated with poly-L-Lysine was confirmed by flow cytometry showing nearly all MSCs associated with particles (Fig. 5d). Confocal imaging revealed PLGA particles were not merely associating with the outer plasma membrane, but internalized (Fig. 5e). MSC's were engineered with BUD-Particles without impacting cell viability (Fig. 5f).

To test if the intracellular release of budesonide from PLGA particles would work similarly to soluble budesonide, we examined the expression and activity of IDO within cell lysates. MSCs were modified with either BUD-PLGA or Blank-PLGA particles overnight, allowed to rest 24 hours, and then stimulated with IFN-γ for 48 hours, after which cells were harvested for analysis (Fig. 6a). As with soluble budesonide, BUD-PLGA particle modification significantly increased the content of IDO in MSC lysate (Fig. 6b). BUD-PLGA modified MSCs exhibited a 5X augmentation in IDO enzymatic activity over Blank-PLGA modified and unmodified MSCs (Fig. 6c), an effect similar to what was observed with soluble budesonide (Fig. 3g). In addition, when compared head to head, BUD-PLGA particle modified MSCs expressed higher levels of IDO than MSCs simply pretreated with soluble budesonide before IFN-γ activation (Fig. 7a).

**Enhanced suppression of inflammation *in vitro***

To test our hypothesis that enhanced IDO activity would lead to enhanced immunosuppression, MSCs were co-cultured with CD3/CD28 Dynabead activated PBMCs. BUD-Particle modified MSCs showed significantly enhanced suppression over budesonide preconditioned MSCs, which showed no advantage over naïve MSCs (Fig. 7b). To determine the degree of BUD-Particle modified MSC enhancement over naïve MSCs, ratiometric MSC:PBMC co-cultures were established by fixing the number of PBMCs in each well and varying the number of MSCs plated to achieve MSC:PBMC ratios of 1:4, 1:8, or 1:16. Unmodified, Blank-Particle modified, and BUD-Particle modified MSCs each suppressed PBMC proliferation in a cell-dose dependent manner. However, BUD-Particle MSCs showed enhanced suppression of PBMCs at all ratios tested as evidenced by reduced proliferation (Fig. 8c,d) and decreased IFN-γ production

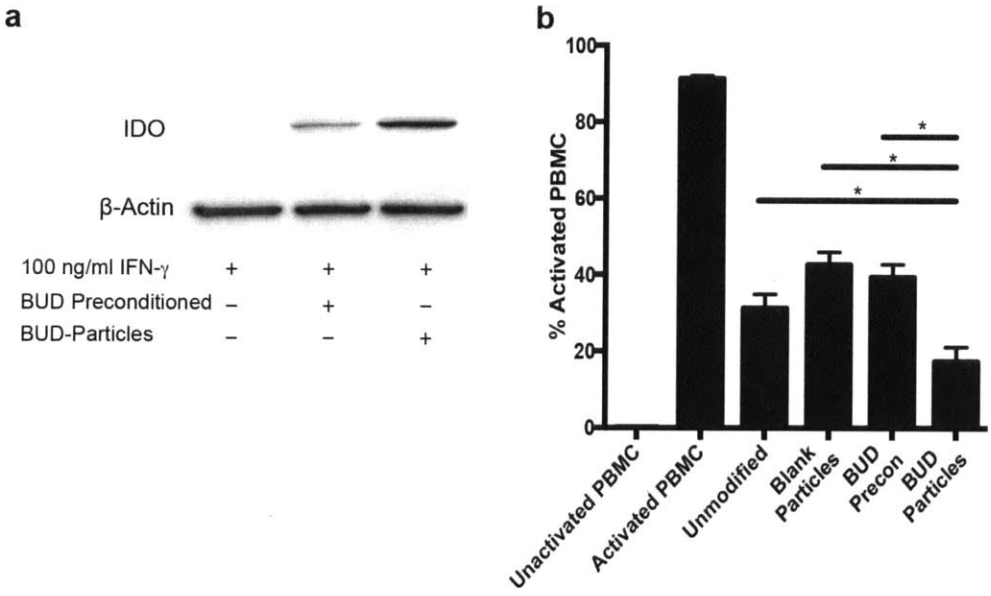


**Figure 7.** (a) IDO content following 48 hours of IFN-γ stimulation in untreated, budesonide preconditioned, and budesonide-particle modified MSCs. β-actin shown as loading control. (b) Bud-particle engineered MSCs exhibit enhanced suppression over budesonide preconditioned MSCs. Quantification of MSC suppression of PBMCs after 5 day MSC:PBMC co-cultures. Data represents average of three experiments conducted with independent PBMC donors. Un-stimulated control for each donor used to set threshold for PBMC activation. (Bars are mean±SEM, Ordinary One-way ANOVA with Tukey correction for multiple comparisons, n=3, *$p<0.05$)

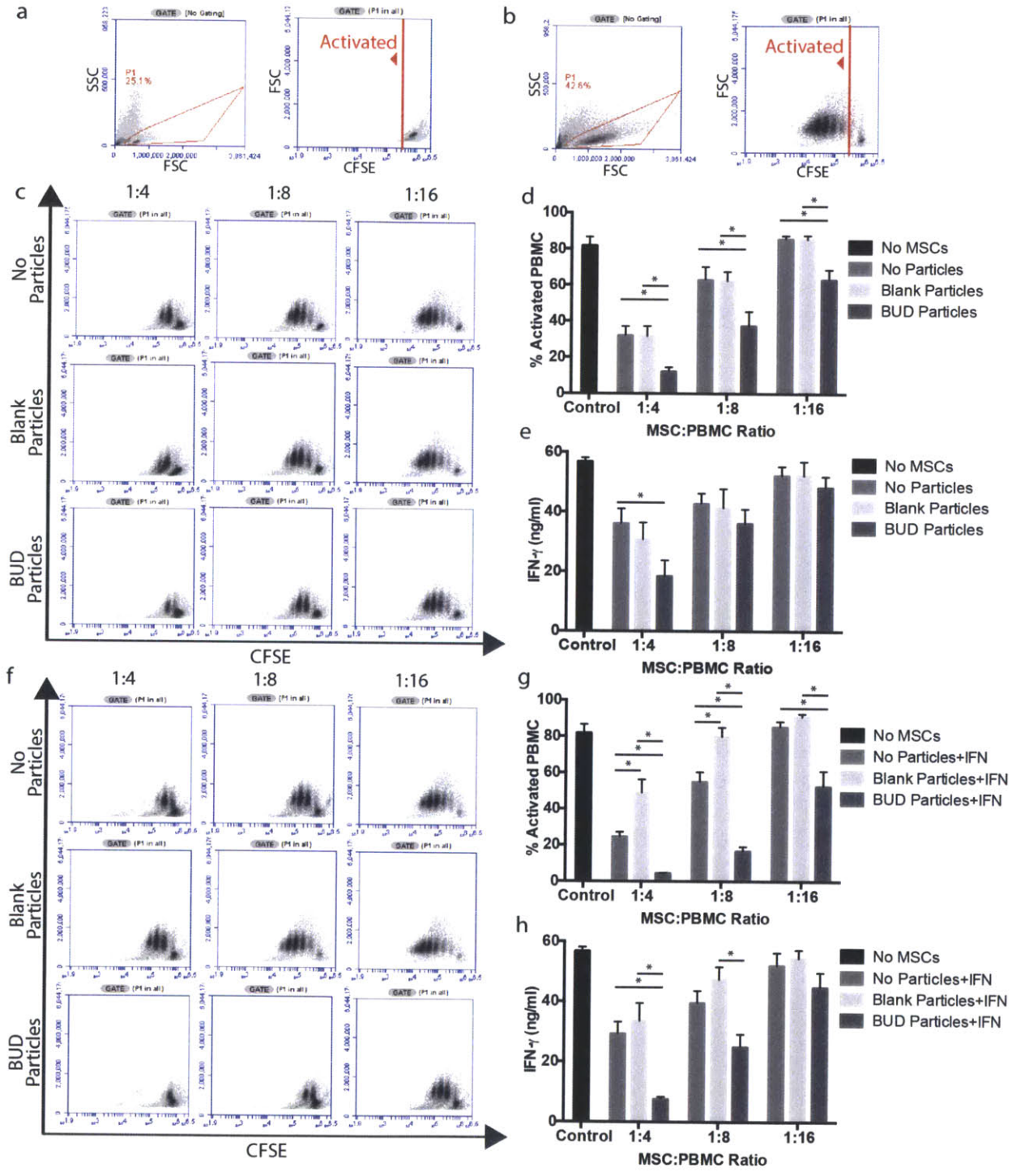
a
b
c
d
e
f
g
h
Activated
SSC
FSC
CFSE
P1
25.1%
42.6%
1:4
1:8
1:16
No Particles
Blank Particles
BUD Particles
% Activated PBMC
IFN-γ (ng/ml)
MSC:PBMC Ratio
Control
No MSCs
No Particles
Blank Particles
BUD Particles
No Particles+IFN
Blank Particles+IFN
BUD Particles+IFN

**Figure 8.** Engineered MSCs exhibit enhanced suppression. Gating and representative flow cytometry plot of (a) unstimulated and (b) CD3+/CD28+ Dynabead stimulated CFSE stained PBMCs (CFSE vs. Forward Scatter). (c) Representative CFSE vs forward scatter flow cytometry plots of PBMCs harvested from 5 day MSC:PBMC co-cultures. MSC:PBMC ratio and type of MSC particle modification are listed on each column and row respectively. As PBMCs are activated and divide, CFSE is diluted 1:2, resulting in discrete daughter generations that shift to the left with each cell division. (d) Quantification of MSC suppression of PBMCs harvested from three independent donors. Un-stimulated control for each donor used to set threshold for PBMC activation. (e) IFN-γ concentration measured from supernatant of MSC:PBMC co-cultures as marker of PBMC activation. (f) Representative CFSE vs. forward scatter flow cytometry plots of PBMCs harvested from 5 day MSC:PBMC co-cultures containing MSCs preconditioned with IFN-γ to stimulate IDO activity. MSC:PBMC ratio and type of MSC particle modification are listed on each column and row respectively. (g) Quantification of MSC suppression of PBMCs harvested from three independent donors. Un-stimulated control for each donor used to set threshold for PBMC activation. (h) IFN-γ concentration measured from supernatant of preconditioned MSC:PBMC co-cultures as marker of PBMC activation. Un-stimulated PBMC controls showed no detectable secretion of IFN-γ. (Bars are mean±SEM, Two-way ANOVA with Tukey correction for multiple comparisons, n=3, *$p<0.05$).

(Fig. 8e). Impressively, BUD-Particle MSC co-cultures at 1:8 and 1:16 ratios were as effective at suppressing PBMC proliferation and IFN-γ secretion as native MSCs at 1:4 and 1:8 ratios, respectively. In other words, twice as many unmodified MSCs are required to achieve an equivalent *in vitro* suppressive effect as BUD-Particle MSCs.

As IDO activity is dependent on IFN-γ stimulation, we hypothesized the effect could be further accentuated by pre-activation of MSCs. Thus, the MSC:PBMC co-cultures were repeated with MSCs preconditioned with IFN-γ for 48 hours to stimulate IDO expression prior to plating in the co-cultures. Pre-activation of MSC IDO expression resulted in similar trends in unmodified MSCs, inferior suppression by Blank-Particle MSCs, and further enhanced BUD-Particle MSCs ability to suppress PBMC proliferation (Fig. 8f,g) and IFN-γ secretion (Fig. 8h) compared to co-cultures with unactivated MSCs.

Next we sought to examine the mechanism responsible for the enhanced suppression. Soluble budesonide released from the MSCs did not appear to be responsible, as PBMCs treated with 1 μM and 10 μM budesonide (no MSCs) were activated to the same degree as untreated PBMCs (Fig. 9a). In order to determine if the enhanced suppressive effect of BUD-Particle modified MSCs can be attributed to IDO or that of other soluble factors, we used a widely used inhibitor of IDO, 1-methyl-DL-tryptophan (1-MT) to inhibit IDO activity. MSC:PBMC co-cultures were repeated at a MSC:PBMC ratio of 1:8 with or without the addition of 1 mM 1-MT. Inhibition of IDO with 1-MT completely abolished BUD-Particle MSCs inhibitory effect suggesting IDO is significantly responsible for the enhanced immunomodulatory potency of BUD-Particle MSCs (Fig. 9b).

## Discussion

Herein we have elucidated the effect of budesonide on MSCs immunogenicity and immunosuppressive properties. Budesonide treatment resulted in an over 4-fold increase in IFN-γ stimulated MSC IDO activity. Unlike other cell types such as fibroblasts (*28*) and lymphocytes (*37*), MSC viability, metabolic activity, and morphology, were not significantly impacted by exposure to a wide range of budesonide concentrations. In addition to enhancement of MSC IDO activity, we also observed a

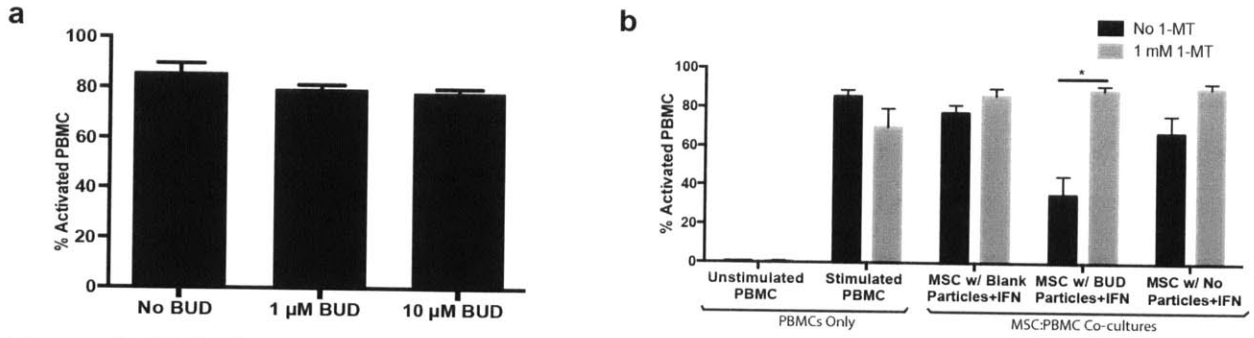


**Figure 9.** PBMC suppression is due to IDO and not soluble budesonide. (a) Budesonide alone does not suppress CD3/CD28 stimulated activation of PBMCs. Quantification of budesonide mediated suppression or PBMC harvested from three independent donors. Un-stimulated control for each donor used to set threshold for PBMC activation. (Bars are mean±SEM) (b) Inhibition of IDO abolishes MSC suppression of PBMCs. Quantification of MSC suppression of PBMCs harvested from three independent donors with and without addition of the IDO inhibitor 1-MT. Co-cultures performed with MSCs preconditioned with IFN-γ to stimulate IDO activity at an MSC:PBMC ratio of 1:8. Un-stimulated control for each donor used to set threshold for PBMC activation. (Bars are mean±SEM, Two-way ANOVA with Tukey correction for multiple comparisons, n=3, *$p<0.05$).

reduction in MSC expression of HLA-ABC at all doses in unstimulated conditions and a reduction in HLA-DR expression at high doses in IFN-γ stimulated conditions. The reduced expression of MHC molecules further minimizes the hypo-immunogenic phenotype of native MSC, however, following IFN-γ stimulation the level of HLA-ABC and HLA-DR expression remains high, and is thus unlikely to significantly alter MSC rejection in allogeneic transplant settings. In fact, previous attempts to shield MSCs from allo-rejection through reduction of HLA-ABC expression required near complete blockade of HLA-ABC presentation in both unstimulated and IFN-γ stimulated conditions by viral immunoevasins (*38*, *39*). Overall, budesonide treatment maintained MSCs proliferative capabilities while reducing MSC's immunophenotype and greatly enhancing MSC's immunomodulatory potency through increased IDO activity. To our knowledge, this is the first report of small molecule enhancement of IDO activity in MSCs and the approach represents a significant opportunity to augment MSC-based therapies.

Enhanced expression of IDO was shown to be dependent on both the glucocorticoid receptor and FOXO3, as inhibition of either abrogated the effect. In addition to the current report of FOXO3 enhancement of MSC immunosuppression, enhanced FOXO3 expression has also recently been reported to be a marker of tolerogenic dendritic cells (*40*, *41*). FOXO3 expressing dendritic cells produce reduced levels of IL-6 (*40*) and elevated levels of IDO (*41*). Inhibition of FOXO3 in tumor associated dendritic cells results in decreased levels of IDO and enhanced anti-tumor immune responses (*41*, *42*). While these studies have examined the FOXO3-IDO pathway in the context of pathology, we believe there is great potential to leverage the tolerogenic effects to treat graft versus host disease, autoimmune conditions such as Crohn's and multiple sclerosis, and prevent rejection of transplanted tissues.

As the enhanced therapeutic phenotype of MSCs was most prominent in cultures continuously exposed to budesonide, we employed an engineering strategy to continuously control MSCs. MSCs were engineered with budesonide loaded PLGA particles that continuously release budesonide, resulting in a 5-fold enhancement in IFN-γ stimulated MSC IDO activity. BUD-Particle MSCs were shown to exhibit enhanced immunosuppressive potency in PBMC co-culture assays in an IDO

dependent manor. Inhibition of IDO with 1-MT led to abrogation of MSCs' suppressive potential, implicating IDO as a primary mechanism of budesonide mediated MSC enhancement. BUD-Particle engineered MSCs were twice as potent in suppressing PBMC proliferation and IFN-γ secretion, as determined from ratiometric co-culture experiments. Enhancing the potency of a single MSC enables fewer MSCs to be administered to achieve the same therapeutic effect and enables a single cell to exert a significant impact on its microenvironment. In addition, this technique can be used to augment the potency of MSCs harvested from different donors and tissues, eliminating the need to select MSCs from only donors or tissues that have high native immunosuppressive potential. Furthermore, as enhanced IDO activity has been shown to lead to tolerance in the setting of pregnancy (*18*), solid organ transplant (*43*), and tumor evasion (*19*), BUD-PLGA MSCs may be able to extend their therapeutic window by promoting tolerance and evading immune clearance.

In the current study we have demonstrated the utility of BUD-Particle MSCs in *in vitro* co-cultures. However, the potential benefits of an MSC therapeutic with enhanced IDO expression could be far reaching. This strategy may be used to augment therapeutic potency of MSC therapies by suppressing active inflammation and inducing tolerance in the setting of GvHD, Crohn's disease, and transplant biology. In addition, modified MSCs with enhanced IDO activity could also be applied to prevent bio-fouling of orthopedic implants and other medical devices due to IDO's antimicrobial properties (*16*).

We have previously shown intracellular PLGA particles can be used to influence MSC differentiation (*35*) and track MSCs by MRI (*36*), and now we show that this platform can be adapted to augment and control MSC's therapeutic potency. Further studies are needed to demonstrate the ability of BUD-Particle MSCs to induce immune tolerance *in vivo* and the long-term function and safety of the engineered therapy must be evaluated.

## Methods

### Culture of MSCs

Primary human MSCs were obtained from Texas A&M Health Science Center, College of Medicine, Institute for Regenerative Medicine at Scott & White Hospital which has a grant from NCRR of the NIH, Grant #P40RR017447 (Donors 7076, 7081, and 7083). MSCs were maintained in cell-start (Invitrogen) coated flasks with StemPro MSC SFM culture media (Invitrogen) supplemented with 1% (v/v) L-Glutamine (Invitrogen), and 1% penicillin:streptomycin (Invitrogen). Cells were plated at a density of 6,000 cells/cm$^2$ and were passaged when flasks reached 70-80% confluence. All experiments were performed with passage 3-6 MSCs (Population doubling level between 4-8 from initial plating) unless indicated otherwise.

### Metabolic activity, viability, and morphology assays

Metabolic activity of MSCs was assessed by XTT (ATCC) following 24, 48, or 72 hour exposure to budesonide. Briefly, 15,000 MSCs were plated in each well of a 96 well plate in 100 µl of culture media containing DMSO vehicle and 0.001, 0.01, 0.1, 1, 10, or 100 µM budesonide. Cultures were maintained for 24, 48, or 72 hours in a humidified culture chamber. Culture media with no cells and wells with half the starting cell density were used as internal controls for each experiment. All conditions were explored in 5 wells for each experiment. To measure metabolic activity, 50 µl of activated XTT reagent was prepared and added to each well per manufacturer's instructions. The plate was incubated for 3 hours and read at 450 nm and 630 nm for reference. To determine the morphology and viability of budesonide treated MSCs, 30,000 cells were plated into each well of a 24 well plate with vehicle or 0.001-100 µM budesonide supplemented culture media. Cells were grown for 24, 48, or 72 hours. Before harvest, 4 random fields of each well were imaged at 10X using an inverted phase contrast microscope to capture cell morphology and differences in cell proliferation. To determine viability, cells were then harvested with Accutase, washed, and re-suspended in 100 µl stain solution containing 5 µl/ml FITC-Annexin-V and 1 µl propidium iodide (Invitrogen) and stained on ice for 15 min. Cells were washed with 400 µl PBS, centrifuged, re-suspended in fresh PBS and analyzed by an Accuri C6 flow cytometer. MSCs treated with staurosporine to

induce cell death were used as a positive control for each experiment. TUNEL staining of budesonide treated and particle modified MSCs was performed per manufacture's instructions using a *in situ* cell death detection kit-fluorescein (Roche) to label double strand DNA breaks indicative of apoptosis and counterstaining nuclei with Hoescht (Invitrogen). Fixed, DNase treated MSCs (300 U/ml DNase, 1 mg/ml BSA, in 50 mM TrisHCL for 10 min at room temperature) were used as a positive control for double strand DNA breaks. ImageJ (NIH) was used to quantify the number of dual stained nuclei, all conditions were performed in triplicate.

**Flow Cytometry**

Expression of MHC molecules on MSCs following 24 hour preconditioning or continuous exposure to various doses of budesonide was determined using an Accuri C6 flow cytometer. For each condition, MSCs were grown in T25 flasks, harvested with Accutase, washed, and split for staining with either Alexa Fluor 488 anti-human HLA-ABC and Alexa Fluor 647 anti-human HLA-DR or isotype controls. Cells were re-suspended in antibody solution in PBS+1% BSA and stained on ice for 15 min. Cells were washed with 400 µl PBS+1%BSA, centrifuged, and analyzed by flow cytometry. Mean fluorescence intensity (MFI) was determined using CFlow software.

**IDO Activity Assay**

MSC cultures were grown to 80% confluence in T75 flasks. Cells were washed with PBS, harvested with Accutase cell dissociation reagent (Invitrogen), centrifuged, counted, and resuspended in 300 µl of ice cold PBS(without $Ca^{2+}$/$Mg^{2+}$ ions) with 0.1% (w/v) Triton X-100. Cell suspensions were lysed through triplicate freeze thaw cycles, and briefly pulse sonicated using a probe sonicator with power output of 3W. Lysates were centrifuged at 25000 rcf at 4°C for 30 minutes. 250 ul of sample supernatant, recombinant human IDO (rhIDO), or L-kynurenine standard were mixed in a 1:1 ratio with 250 µl of IDO buffer (40 mM ascorbic acid, 20 µM methylene blue, 200 µg/ml catalase, 800 µM L-tryptophan, in 50 mM MES buffer, pH 6.5). Samples were incubated at 37°C for 45 min, followed by addition of 100 µl of tricholoracetic acid (30%, w/v) and incubated at 52°C for 30 min. Samples were centrifuged at 2500 rcf for 10 min to

remove proteins, and 100 µl of the resultant supernatant for each sample was added to a 96 well plate (all samples and standards measured in duplicate). 100 µl of Ehrlich's reagent (0.8% p-dimethylaminobenzaldehyde in glacial acetic acid) was added to each well to induce a color change. Samples were incubated at room temperature for 10 min and then read on a microplate reader at 490 nm. rhIDO was used as a positive control in each assay and an internal L-kynurenine standard (8-5000 µM) was included to determine kynurenine production of IDO from MSC lysate.

**siRNA Transfection**

T25 flasks were seeded with 166,000 MSCs and incubated overnight at 37° C. siRNA transfection was performed as follows. 10 ul of Lipofectamine RNAiMAX transfection reagent (Invitrogen) per sample was diluted into 0.5 ml of Opti-MEM media (Invitrogen), and gently mixed. 20 µl of SignalSilence FOXO3 siRNA (Cell Signaling Technology, #6302S) or scramble control siRNA (Cell Signaling Technology, #6201S ) per sample was diluted into 0.5 ml of Opti-MEM media and gently mixed. Both solutions were incubated at room temperature for five minutes. The solutions were then gently mixed and incubated for twenty minutes at room temperature in the dark. During this time, the cells were washed with PBS-/-. Following incubation, the PBS was removed, and 1 ml of siRNA complex was added to each flask. The media of each flask was brought to 1.5 ml by adding 0.5 ml OPTIMEM media and the cells were incubated at 37° C in the dark for 5 hours after which the media was replaced with full media.

**Western Blots**

MSC cell lysates were prepared by washing T25 plates with ice cold PBS three times to remove media followed by addition of 200 µl ice cold RIPA buffer (10 µl/ml PMSF solution, 10 µl/ml sodium orthovanadate, and 10 µl/ml protease inhibitor cocktail). Cells were lifted using a cell scraper, collected in Eppendorf tubes, and incubated on ice for 5 min. Lysate was then clarified by centrifugation at 8000 rcf at 4°C for 10 min. The supernatant containing soluble protein was transferred to clean tubes and total protein concentration was determined by microBCA (Thermo Scientific). Western blots were performed using BioRad's Mini Protean Tetra Cell apparatus for the electrophoresis and

transfer. Briefly, 10-20 µg of protein, mixed 1:1 with Laemmli Buffer were loaded into each well of 10% Tris-HCl gels with Tris running buffer for SDS-PAGE. Proteins were then transferred to a Polyvinyl difluoride membrane using the transfer apparatus according to the BioRad protocol. Following transfer, the membrane was incubated with 5% BSA in TBST buffer overnight, washed with TBST and incubated with primary antibodies (rabbit anti-IDO (12006S), rabbit anti-stat-1 (9172P), rabbit anti-pstat-1 (7649P), rabbit anti-FOXO3 (2497P), rabbit anti-β-actin (4970S), Cell Signaling). Horseradish peroxidase conjugated anti-rabbit antibody (Cell Signaling, 7074S) was used as a secondary and protein bands were visualized following incubation with Amersham ECL Prime Detection Reagent (GE Healthcare) according to the manufacturer's instructions. Beta actin staining was performed to determine relative protein expressions and a Precision Plus Protein Dual Color Standard (Bio-Rad) was used to determine the molecular weight of the bands. Western blot images were analyzed and processed using ImageJ (NIH).

**Budesonide Particle Formulation**

PLGA particles were formulated using an oil-in-water single emulsion technique. 10 kDa molecular weight 50:50 poly(lactic-co-glycolic acid) with a carboxylic acid end group (inherent viscosity 0.15-0.25 dL/g) was obtained from Lactel Absorbable polymers. 50 mg of PLGA, 8 mg of budesonide, and 10 µl of DiI, were dissolved in 2 ml of dichloromethane in a glass vial. After dissolving, PLGA:Drug solution was probe sonicated for 30 seconds to thoroughly mix the drug within the polymer. The solution was then added drop wise to 20 ml of filtered 1% (w/v) polyvinyl alcohol (80% hydrolyzed, Sigma) on ice while homogenizing at 33,000 rpm using a Tissue Master 125 homogenizer (Omni International). After 2 min homogenization, particles suspensions were gently stirred in a chemical hood for 4 hours to allow for evaporation of solvent. Suspensions were then centrifuged, and washed with distilled water 3 times before lyopholization and characterization. Blank particles were formed in parallel by omitting the addition of budesonide in the above procedure. The zeta-potential of particles was modified through adsorption of poly-l-lysine (PLL). Briefly, 6 mg/ml particle suspensions were prepared in 100 µg/ml PLL solution in distilled water and gently

agitated for 2 hours. Particles were then frozen for subsequent use. The hydrodynamic diameter, polydispersity, and zeta potential of particles was measured in distilled water using a Malvern Zetaziser ZS90. Averages from three separate samples are reported. In addition, 40X fluorescence microscopy images were acquired to confirm the size and polydispersity of the particle suspensions.

**Budesonide Particle Loading and Release Kinetics**

High pressure liquid chromatography (HPLC) was used to determine the drug loading, encapsulation efficiency, and release kinetics of the budesonide microparticles. To determine drug loading, 2-3 mg of particles were weighed into Eppendorf tubes, quickly spun into a pellet, and swollen by addition of 500 µl methanol. Samples were agitated at 37°C for 2 hours to allow for complete release of budesonide from the particles. Samples were centrifuged to pellet PLGA, and supernatant was collected, filtered, and analyzed by an Agilent 1100 series HPLC. An Agilent Zorbax Eclipse XDB-C18 column (4 x 250 mm, 5 µm) was used with a mobile phase composed of 70:30 acetonitrile:0.1% acetic acid, 25 µl injection volume, and 1 ml/min flow rate. Budesonide was detected by peak absorbance at 248 nm and quantified by comparison to internal standard curves. Drug loading was calculated as the dry mass of drug per mg of PLGA particles. Encapsulation efficiency was calculated as the ratio of encapsulated drug to total drug added to formulate particles. All samples were prepared in triplicate. Release kinetics were determined by suspending 2 mg of particles in 200 µl of PBS placed in a 2 inch section of 6-8,000 molecular weight cut off dialysis bag (Spectra Labs). Dialysis bags were submerged in 40 ml of PBS to simulate infinite sync conditions and agitated at 37°C. At each time point, 1 ml of PBS was collected and replaced with fresh PBS. Samples were frozen until HPLC analysis using the method as described above. All samples were prepared in triplicate.

**Particle Modification of MSCs**

MSCs were cultured to 80% confluence prior to particle modification. PLL coated budesonide or blank particles were thawed, briefly sonicated to break up particle clumps, and suspended in 1% supplement StemPro culture media to make 10 ml of 0.1

mg/ml particle media for each T75 flask. Flasks were modified at the end of the day and incubated with particle media overnight. Following particle modification, MSCs were washed three times with PBS, provided with fresh full supplement culture media and allowed to rest for 24 hours before subsequent experimentation. To confirm particle internalization, confocal microscopy was performed as previously described (*35*).

**PBMC Isolation from whole blood**

Fresh whole blood from 3 donors was obtained from Research Blood Components for each experiment (Watertown, MA). Upon delivery, blood was diluted 1:1 with sterile PBS-/- supplemented with 2% fetal bovine serum, layered on top of Ficoll-Paque Premium (GE Healthcare), and centrifuged at 400 rcf with the brake off. The buffy coat was collected and washed with PBS:FBS solution. PBMCs were counted and either used immediately or frozen in freezing media (RPMI supplemented with 10% DMSO, 40% FBS, 1% Penicillin/Streptomycin, 1% L-Glut).

**MSC:PBMC Co-cultures**

The ratio of MSCs to PBMCs was established by adding 260,000 PBMCs and 65,000, 32,500, or 16,250 MSCs to each well of a 24-well plate. MSCs were particle modified and allowed to rest a day before the co-culture experiments. Unmodified, blank-particle modified, or bud-particle modified MSCs were plated in 24 well plates and allowed to adhere. PBMCs labeled with a CellTrace CFSE Cell Proliferation Kit (Invitrogen) according to the manufacturer's instructions. 260,000 PBMCs were then added to each well. To stimulate PBMCs proliferation, 260,000 CD3+/CD28+ Dynabeads (StemCell Technologies) were also added to each well. Total culture volume of each well was standardized to 0.5 ml of RPMI supplemented with 10% FBS, 1% (v/v) L-Glutamine 1% penicillin:streptomycin. PBMCs stimulated with Dynabeads but without MSCs were used as an activated control and un-stimulated PBMCs grown without MSCs were used as an un-activated control for each donor. Co-cultures were maintained for 5 days after which the media from the wells (containing PBMCs) was collected and centrifuged to pellet the PBMCs. The conditioned media was then collected for subsequent analysis. PBMC pellets were re-suspended in PBS-/- containing 1% FBS and PBMC proliferation was

assessed by flow cytometery. Un-stimulated PBMC controls were used to set the threshold for PBMC activation for each donor. To inhibit IDO activity, the MSC:PBMC co-cultures were repeated with or without the addition 1 mM of the enzymatic inhibitor 1-methyl-DL-tryptophan (1-MT, Sigma) prepared in RPMI media. Data was analyzed using Accuri's CFlow software. IFN-γ content of co-culture supernatant was determined using an ELISA MAX Deluxe Human IFN-γ kit (Biolegend) by comparing to internal standards according to manufacturer's instructions.

**Statistical Analysis**

All statistics were performed using Prism 6 (GraphPad). Two-way ANOVA's were performed on data sets with two independent variables (dose and time or MSC group and MSC:PBMC ratios) and one-way ANOVA was performed on data sets with a single independent variable (effect of budesonide conditioning on MSC IDO activity). Fisher's LSD test without correction for multiple comparisons was used when assessing effect of budesonide doses on MSC metabolic activity and viability as the test has a higher Type I error and would therefore highlight any potential negative impact of budesonide on MSCs that would require further evaluation. Bonferroni correction for multiple comparisons, which is a more conservative test than the Fisher's LSD method, was used for the MHC expression data as all comparisons were made with respect to the untreated control. For all other statistics, the mean of all groups were compared to all other groups and thus, Tukey correction for multiple comparisons was used to minimize Type I error.

## Acknowledgements

This work was supported by National Institutes of Health grant HL095722 to JMK and by a Prostate Cancer Foundation Challenge Award to J.M.K. J.A.A. was supported by the Hugh Hampton Young Memorial Fellowship.

## References


1. J. Ankrum, J. Karp, Mesenchymal stem cell therapy: Two steps forward, one step back, *Trends Mol Med* **16**, 203–209 (2010).

2. L. von Bahr *et al.*, Long-term complications, immunologic effects, and role of passage for outcome in mesenchymal stromal cell therapy, *Biol. Blood Marrow Transplant.* **18**, 557–564 (2012).

3. K. Le Blanc *et al.*, Mesenchymal stem cells for treatment of steroid-resistant, severe, acute graft-versus-host disease: a phase II study, *Lancet* **371**, 1579–1586 (2008).

4. C. R. Mills, Osiris Therapeutics Announces Preliminary Results for PRochymal Phase III GvHD Trials*Osiris Press Release* (2009) (available at http://files.shareholder.com/downloads/OSIR/2468414599x0x317779/7677da46-286a-47c4-865d-36c148119a1a/OSIR_News_2009_9_8_General.pdf).

5. J. Galipeau, The mesenchymal stromal cells dilemma—does a negative phase III trial of random donor mesenchymal stromal cells in steroid-resistant graft-versus-host disease represent a death knell or a bump in the road? *Cytotherapy* **15**, 2–8 (2013).

6. S. M. Melief, J. J. Zwaginga, W. E. Fibbe, H. Roelofs, Adipose Tissue-Derived Multipotent Stromal Cells Have a Higher Immunomodulatory Capacity Than Their Bone Marrow-Derived Counterparts, *Stem Cells Translational Medicine* (2013), doi:10.5966/sctm.2012-0184.

7. M. François, R. Romieu-Mourez, M. Li, J. Galipeau, Human MSC suppression correlates with cytokine induction of indoleamine 2,3-dioxygenase and bystander M2 macrophage differentiation, *Mol Ther* **20**, 187–195 (2012).

8. V. Zhukareva, M. Obrocka, J. D. Houle, I. Fischer, B. Neuhuber, Secretion profile of human bone marrow stromal cells: donor variability and response to inflammatory stimuli, *Cytokine* **50**, 317–321 (2010).

9. D. J. Prockop, Two Negative Feedback Loops Place Mesenchymal Stem/Stromal Cells (MSCs) at the Center of Early Regulators of Inflammation, *Stem Cell* (2013), doi:10.1002/stem.1400.

10. R. H. Lee *et al.*, Intravenous hMSCs Improve Myocardial Infarction in Mice because Cells Embolized in Lung Are Activated to Secrete the Anti-inflammatory Protein TSG-6, *Cell Stem Cell* **5**, 54–63 (2009).

11. S. Kidd *et al.*, Direct evidence of mesenchymal stem cell tropism for tumor and wounding microenvironments using in vivo bioluminescent imaging, *Stem Cell* **27**, 2614–2623 (2009).

12. M. Strioga, S. Viswanathan, A. Darinskas, O. Slaby, J. Michalek, Same or not the same? Comparison of adipose tissue-derived versus bone marrow-derived

mesenchymal stem and stromal cells, *Stem Cells Dev* **21**, 2724–2752 (2012).

13. G. Ren *et al.*, Species Variation in the Mechanisms of Mesenchymal Stem Cell-Mediated Immunosuppression, *Stem Cell* **27**, 1954–1962 (2009).

14. A. J. Nauta, W. E. Fibbe, Immunomodulatory properties of mesenchymal stromal cells, *Blood* **110**, 3499–3506 (2007).

15. D. Bubnoff, T. Bieber, The indoleamine 2,3-dioxygenase (IDO) pathway controls allergy, *Allergy* **67**, 718–725 (2012).

16. R. Meisel *et al.*, Human but not murine multipotent mesenchymal stromal cells exhibit broad-spectrum antimicrobial effector function mediated by indoleamine 2,3-dioxygenase, *Leukemia* **25**, 648–654 (2011).

17. D. H. Munn, A. L. Mellor, Indoleamine 2,3 dioxygenase and metabolic control of immune responses, *Trends in Immunology* **34**, 137–143 (2013).

18. D. H. Munn *et al.*, Prevention of allogeneic fetal rejection by tryptophan catabolism, *Science* **281**, 1191–1193 (1998).

19. G. C. Prendergast, R. Metz, A. J. Muller, Towards a genetic definition of cancer-associated inflammation: role of the IDO pathway, *Am. J. Pathol.* **176**, 2082–2087 (2010).

20. D. H. Munn *et al.*, GCN2 kinase in T cells mediates proliferative arrest and anergy induction in response to indoleamine 2,3-dioxygenase, *Immunity* **22**, 633–642 (2005).

21. P. Terness *et al.*, Inhibition of allogeneic T cell proliferation by indoleamine 2,3-dioxygenase-expressing dendritic cells: mediation of suppression by tryptophan metabolites, *J. Exp. Med.* **196**, 447–457 (2002).

22. F. Fallarino *et al.*, IDO mediates TLR9-driven protection from experimental autoimmune diabetes, *J Immunol* **183**, 6303–6312 (2009).

23. U. Grohmann *et al.*, Reverse signaling through GITR ligand enables dexamethasone to activate IDO in allergy, *Nat Med* **13**, 579–586 (2007).

24. P. Puccetti, U. Grohmann, IDO and regulatory T cells: a role for reverse signalling and non-canonical NF-kappaB activation, *Nat Rev Immunol* **7**, 817–823 (2007).

25. J. Türck, C. Oberdörfer, T. Vogel, C. R. Mackenzie, W. Däubener, Enhancement of antimicrobial effects by glucocorticoids, *Med. Microbiol. Immunol.* **194**, 47–53 (2005).

26. P. Kebriaei *et al.*, Adult human mesenchymal stem cells added to corticosteroid therapy for the treatment of acute graft-versus-host disease, *Biol. Blood Marrow Transplant.* **15**, 804–811 (2009).

27. J. Webster, J. Cidlowski, Mechanisms of Glucocorticoid-receptor-mediated Repression of Gene Expression, *Trends Endocrinol. Metab.* **10**, 396–402 (1999).

28. S. Hammer *et al.*, Glucocorticoids mediate differential anti-apoptotic effects in human fibroblasts and keratinocytes via sphingosine-1-phosphate formation, *J. Cell. Biochem.* **91**, 840–851 (2004).

29. J. R. Spurzem, O. Sacco, G. A. Rossi, J. D. Beckmann, S. I. Rennard, Regulation of major histocompatibility complex class II gene expression on bovine bronchial epithelial cells, *J. Lab. Clin. Med.* **120**, 94–102 (1992).

30. K. Le Blanc, C. Tammik, K. Rosendahl, E. Zetterberg, O. Ringdén, HLA expression and immunologic properties of differentiated and undifferentiated mesenchymal stem cells, *Exp Hematol* **31**, 890–896 (2003).

31. N. Lützner, H. Kalbacher, A. Krones-Herzig, F. Rösl, FOXO3 Is a Glucocorticoid Receptor Target and Regulates LKB1 and Its Own Expression Based on Cellular AMP Levels via a Positive Autoregulatory Loop, *PLoS ONE* **7**, e42166 (2012).

32. J. H. Toogood, Side effects of inhaled corticosteroids, *J. Allergy Clin. Immunol.* **102**, 705–713 (1998).

33. A. L. Buchman, Side Effects of Corticosteroid Therapy, *Journal of Clinical Gastroenterology* **33**, 289 (2001).

34. R. El Fakih, G. A. Obi, A. Scholoff, G. Carrum, R. T. Kamble, Systemic effects of oral budesonide in hematopoietic transplant: implications of drug interaction with azoles, *Bone Marrow Transplant* **47**, 1370–1371 (2012).

35. D. Sarkar, J. Ankrum, G. S. L. Teo, C. V. Carman, J. M. Karp, Cellular and extracellular programming of cell fate through engineered intracrine-, paracrine-, and endocrine-like mechanisms, *Biomaterials* **32**, 3053–3061 (2011).

36. C. Xu *et al.*, Tracking Mesenchymal Stem Cells with Iron Oxide Nanoparticle Loaded Poly(lactide-co-glycolide) Microparticles, *Nano Lett* **12**, 4131–4139 (2012).

37. C. W. Distelhorst, Recent insights into the mechanism of glucocorticosteroid-induced apoptosis, *Cell Death Differ* **9**, 6–19 (2002).

38. A. S. de la Garza-Rodea *et al.*, Exploitation of herpesvirus immune evasion strategies to modify the immunogenicity of human mesenchymal stem cell transplants, *PLoS ONE* **6**, e14493 (2011).

39. M. A. Soland *et al.*, Modulation of Human Mesenchymal Stem Cell Immunogenicity through Forced Expression of Human Cytomegalovirus US Proteins, *PLoS ONE* **7**, e36163 (2012).

40. A. S. Dejean *et al.*, Transcription factor Foxo3 controls the magnitude of T cell

immune responses by modulating the function of dendritic cells, *Nature Immunology* **10**, 504–513 (2009).

41. S. K. Watkins, A. A. Hurwitz, FOXO3: A master switch for regulating tolerance and immunity in dendritic cells, *oncoimmunology* **1**, 252–254 (2012).

42. S. K. Watkins *et al.*, FOXO3 programs tumor-associated DCs to become tolerogenic in human and murine prostate cancer, *J. Clin. Invest.* **121**, 1361–1372 (2011).

43. H. Liu, L. Liu, B. S. Fletcher, G. A. Visner, Sleeping Beauty-based gene therapy with indoleamine 2,3-dioxygenase inhibits lung allograft fibrosis, *The FASEB Journal* **20**, 2384–2386 (2006).

# Appendix I Preface

This appendix complements Chapter 2 by providing a stand-alone version of our work to track MSCs with intracellular iron oxide microparticles. In addition to controlling cells phenotype, in this Appendix we demonstrate intracellular microparticles can be used to track the location of MSCs. As both controlling cell phenotype and tracking cells location are critical to developing improved cell based therapies, this work demonstates the platform potential of the particle-in-cell technology for engineered cell-based therapies. This appendix also extends the analysis of the effect of internalize micoparticles on the phenotype of MSCs found in Chapter 2 to include *in vitro* migration, *in vivo* homing, and *in vivo* transmigration.

This appendix is an adaptation of a peer-reviewed article published on July 12 ,2012 in *Nano Letters*. Reprinted with permission, copyright 2013, American Chemical Society.

Xu C, Miranda-Nieves D, Ankrum J, Matthiesen ME, Phillips JA, Roes I, Wojtkiewicz GR, Juneja V, Kultima JR, Zhao W, Vemula PK, Lin CP, Nahrendorf M, and Karp JM. (2012). Tracking Mesenchymal Stem Cells with Iron Oxide Nanoparticle Loaded Poly(lactide-co-glycolide) Microparticles. Nano Lett , 12(8), 4131–9.

**Glossary of Terms**

Relaxivity: Property of MR imaging that enables increased contrast.

Particle Dilution: Reduced number of particles per cell due to cell division.

Homing: Preferential collection of cells in specific tissues following systemic infusion

Transmigration: Passage of a cell out of a blood vessel and into the tissue beneath the vessel wall.

# Appendix I: Tracking Mesenchymal Stem Cells with Iron Oxide Nanoparticle Loaded Poly(lactide-co-glycolide) Microparticles

## Abstract

Monitoring the location, distribution and long-term engraftment of administered cells is critical for demonstrating the success of a cell therapy. Among available imaging-based cell tracking tools, magnetic resonance imaging (MRI) is advantageous due to its non-invasiveness, deep penetration, and high spatial resolution. While tracking cells in pre-clinical models via internalized MRI contrast agents (iron oxide nanoparticles, IO-NPs) is a widely used method, IO-NPs suffer from low iron content per particle, low uptake in non-phagocytotic cell types (e.g., mesenchymal stem cells, MSCs), weak negative contrast, and decreased MRI signal due to cell proliferation and cellular exocytosis. Herein, we demonstrate that internalization of IO-NP (10 nm) loaded biodegradable poly(lactide-co-glycolide) microparticles (IO:PLGA-MPs, 0.4-3μm) in MSCs enhances MR parameters such as the $r_2$ relaxivity (5-fold), residence time inside the cells (3-fold) and $R_2$ signal (2-fold) compared to IO-NPs alone. Intriguingly, *in vitro* and *in vivo* experiments demonstrate that internalization of IO:PLGA-MPs in MSCs did not compromise inherent cell properties such as viability, proliferation, migration and their ability to home to sites of inflammation.

## Introduction

Mesenchymal stem cells (or multipotent stromal cells, MSCs) hold great promise for the treatment of multiple diseases and disorders including graft versus host disease(*1*, *2*), type I diabetes(*3*, *4*), and myocardial infarction(*5*, *6*). To develop effective MSC therapies, it is essential in both experimental models and clinical trials to monitor and understand the location, distribution and long-term engraftment of administrated cells, preferably in a noninvasive manner. This will facilitate evaluation of treatment efficacy; reveal optimal transplantation conditions including cell dosage, delivery route, timing of injections; and ultimately improve patient treatment(*7*, *8*).

Recently, imaging techniques including optical imaging, radionuclide imaging and magnetic resonance imaging (MRI), have been used for tracking transplanted MSCs(*8*, *9*). However, they suffer from limitations. For example, optical imaging is limited by the penetration ability of light, and radionuclide imaging suffers from the poor spatial resolution and rapid decay of radioisotopes(*10*). In comparison, MRI is an attractive tool for longitudinal MSC monitoring of specific tissue locations in humans because of its non-invasiveness, deep penetration, high spatial resolution (~100 μm) and the relatively longer retention of MRI contrast agents in cells(*11*, *12*).

Currently, the most widely used labeling agents for MRI tracking are iron oxide ($Fe_3O_4$) nanoparticles (IO-NPs) with core size ranging from 4 nm to 20 nm(*13*). Despite their favorable biocompatibility, IO-NPs suffer from time-dependent decrease in MRI signal due to cell proliferation and exocytosis of IO-NPs(*14-16*). When a cell proliferates, particles (either NPs or MPs) are distributed evenly or unevenly between two daughter cells. After a few cycles, only a fraction of cells contain particles and become undetectable. However, if the signal from a single particle was strong enough to be detected by MRI (e.g., polystyrene-based microparticles(*10*)), those cells containing one or more particles should be detectable. Furthermore, exocytosis dilutes particle concentration(*17*). Interestingly, the exocytosis process is dependent on particle size(*18*); with larger particles exocytosed at a slower rate. Previously we have shown that MSCs can efficiently internalize ~1 micron sized biodegradable poly(lactide-co-glycolide) microparticles (PLGA MPs) that are loaded with differentiation factors, and the particles remain localized within the cell for several days(*19*). Combining these two ideas, we hypothesized that a micron-sized particle with stronger MRI signal and reduced exocytosis could address the dilution limitation of IO-NPs and enable improved longitudinal tracking of MSCs.

Herein, we demonstrate that confinement of IO-NPs in micron-sized PLGA particles (IO:PLGA-MPs) both enhances molar relaxivity of the Fe and localization (through concentrating Fe in discreet locations) that increases the signal to noise ratio, and leads to longer detectable time of labeled MSCs compared to IO-NPs. Furthermore, the effects of IO:PLGA-MPs on MSC viability, proliferation, migration, and cell homing ability have been investigated using a series of *in vitro* and *in vivo* models.

## Results and Discussion

### Design of IO-NP encapsulated PLGA MPs for cell labeling

To evaluate the effect of size on particle retention time in cells, we labeled MSCs with either fluorescent polystyrene NPs (50 nm) or polystyrene MPs (1 μm) (Bangs Labs). Subsequently, fluorescent intensity of the labeled MSCs was monitored over two weeks using flow cytometry (Fig. 1). When MSCs were labeled with NPs, fluorescent-positive MSCs constituted 80% and 10% at day-1 and day-7, respectively. On the contrary, at day-1 and day-7, 100% and 70% of the microparticle labeled MSCs demonstrated positive fluorescent signals. After 14 days, only microparticle-labeled cells showed fluorescence (>30% of the cells). This suggests that micron-sized particles are retained within cells for the long term, which should permit prolonged cell tracking. Thus, we further explored encapsulation of IO-NPs in biocompatible and biodegradable PLGA MPs that can be internalized by cells as a potential strategy to improve cell labeling with MRI contrast agents.

### Fabrication and characterization of IO:PLGA-MPs

A schematic of the IO:PLGA-MPs fabrication method is described in Fig. 2A. Oleic acid stabilized IO-NPs (10 nm core size and 25 nm hydrodynamic diameter, Fig. 2B) were encapsulated in PLGA (inherent viscosity: 0.55-0.75 dL/g with carboxyl end-groups) using a single emulsion method(*14*). Scanning and transmission electron microscope images (SEM and TEM, respectively) show that IO:PLGA-MPs were spherical in shape an average size ~0.8μm (Fig. 2B,C), and IO-NPs were encapsulated within the core of PLGA-MPs (TEM, Fig. 2D). The amount of Fe loading was quantified using Inductively Coupled Plasma Atomic Emission Spectroscopy (ICP-AES) after the dissolution of IO:PLGA-MPs in 70% nitric acid. The IO:PLGA-MPs had Fe loading of 15.65±1.2 wt% ($Fe_3O_4$ weight percentage of 21.61±1.7%). IO-NPs functionalized with carboxy groups were utilized as a control for all experiments. Magnetic properties of IO:PLGA-MPs were studied by a vibration sample magnetometer (VSM) (Fig. 3A). The saturation magnetization (*Ms*) values of IO-NPs and IO:PLGA- MPs were found to be

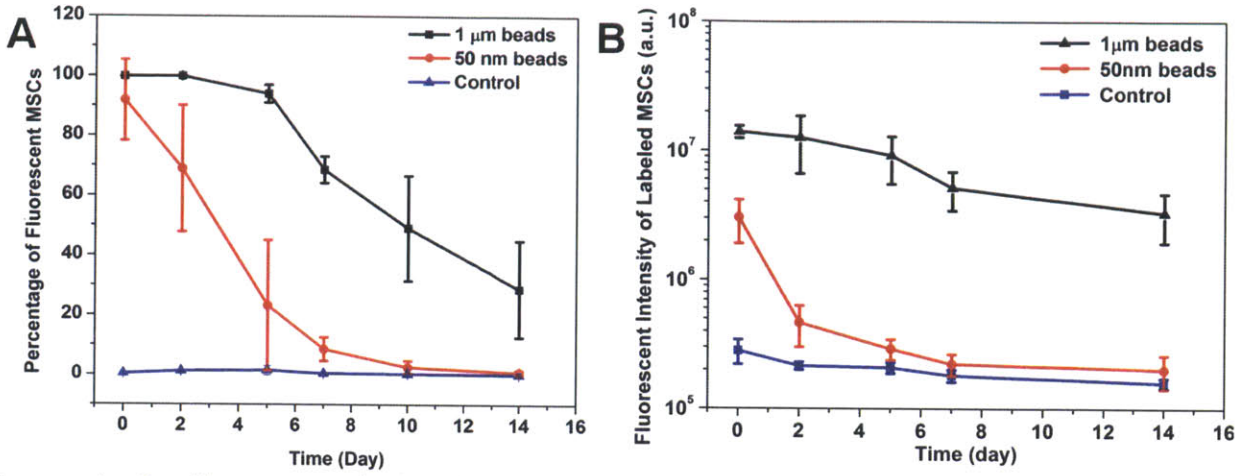


**Figure 1**: Continuous analysis of MSCs labeled with 50 nm polystyrene NPs or 1 μm polystyrene MPs with flow cytometry. (A) Percentage of fluorescent MSCs; (B) Fluorescent intensity of the fluorescent MSCs. (Adapted from (*20*))

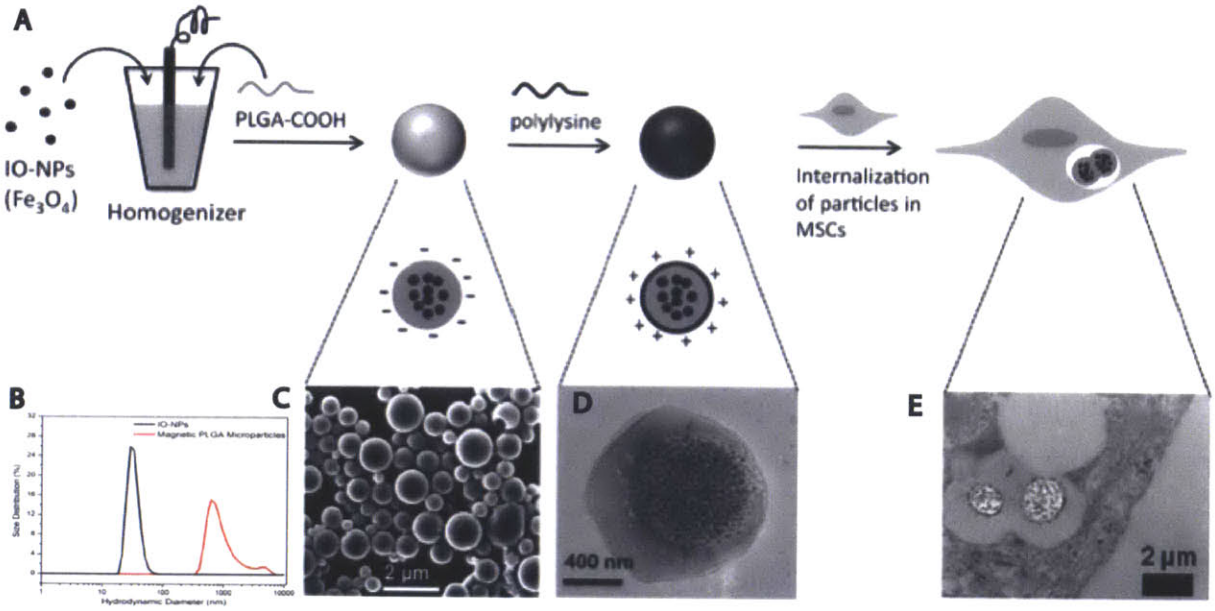


**Figure 2**. IO:PLGA-MPs preparation and internalization by MSCs: (A) Schematic illustration of the preparation of IO:PLGA-MPs with single emulsion method. (B) Hydrodynamic diameter of IO-NPs and IO:PLGA-MPs measured by dynamic light scattering (C) SEM image of IO:PLGA-MPs. (D) TEM image of a representative IO:PLGA-MP. (E) TEM image of IO:PLGA-MPs internalized in a MSC. (Adapted from (*20*))

~40 emu/gram of iron, which is consistent with previous reports(*21*). The hysteresis curve of IO:PLGA-MPs matches well with that of IO-NPs, which indicates that encapsulation did not change the inherent superparamagnetic property of IO-NPs. The magnetic properties were further examined with $T_2$ relaxation rate ($1/T_2$) as a function of iron concentration by a benchtop magnetic resonance relaxometer (Fig. 3B). The magnetic relaxivity ($r_2$) values were derived from the slope of the linear fit, which revealed that the encapsulation of IO-NPs in PLGA matrix significantly increased $r_2$ from 61.16 to 316.6 $mM^{-1} \cdot s^{-1}$ (~5-fold) compared to IO-NPs, which was the result of IO-NP aggregation inside PLGA and thus their enhanced ability to decrease the transverse relaxation time of protons in surrounding water (*14*, *22*, *23*). The increased magnetic relaxivity enhances the hypointense signal. As shown in Fig. 3C, when dispersed in a 3% agarose hydrogel suspension, IO:PLGA-MPs provided higher negative contrast (higher $1/T_2$ or $R_2$ value) than IO-NPs, as suggested by the pseudocolor in Fig. 3C. The average $R_2$ signal from IO:PLGA-MPs was approximately twice that of the signal generated from IO-NPs.

To examine the potential for enhanced contrast of IO:PLGA-MPs *in vivo*, suspensions of both IO-NPs and IO:PLGA-MPs in agarose gels (without cells) were injected subcutaneously into the back of a healthy mouse (Fig. 4A). 60 minutes after injection, the mouse was subjected to whole body multi-slice multi-echo $T_2$ weighted MRI. The collected images were reconstructed into a 3D $1/T_2$ ($R_2$) volumetric image (Fig. 4B) through Amira-Visage Imaging software. Pseudocolor was applied to reveal the contrast enhancement of particles. As shown in Fig. 4B, IO:PLGA-MPs generated a stronger negative contrast than IO-NPs using two Fe concentrations (20 μg Fe/ml (0.36mM) and 40 μg Fe/ml (0.71mM)). Under both conditions, the average $R_2$ signal from IO:PLGA-MPs was approximately twice that of the signal generated from IO-NPs.

**Labeling MSCs with IO:PLGA-MPs**

Given that positively charged particles typically show enhanced internalization into the cells compared to negatively charged particles(*24*), the negatively charged IO-NPs and MP, as measured by zeta potential (-30±10mV and -2.7±1.0mV in PBS accordingly), were coated with poly-L-lysine coating leading to a surface charge of

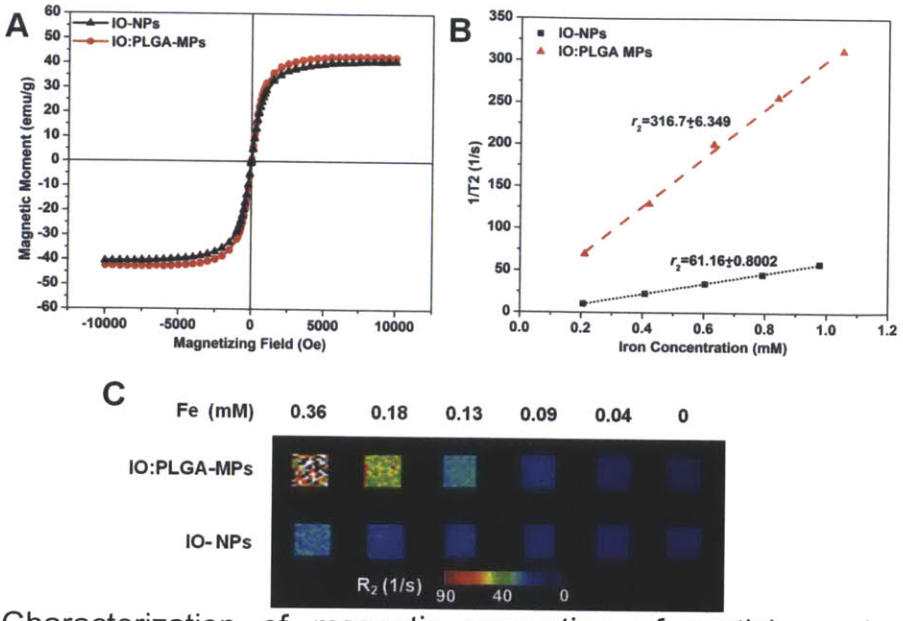


**Figure 3**: Characterization of magnetic properties of particles prior to cellular internalization: (**A**) Hysteresis loop and (**B**) $1/T_2$ versus iron concentration for IO-NPs and IO:PLGA-MPs measured at 300 K. Relaxivity values $r_2$ were obtained from the slope of the linear fit of the experimental data. (**C**) $R_2$-weighted MRI images of 3% agarose gels containing IO-NPs and IO:PLGA-MPs at iron concentrations of 0, 0.04, 0.09, 0.13, 0.18, and 0.36mM. Pseudocolor was applied to reveal the $R_2$ value (unit: Hz or 1/s), as indicated by the scale bar. (Adapted from (*20*))

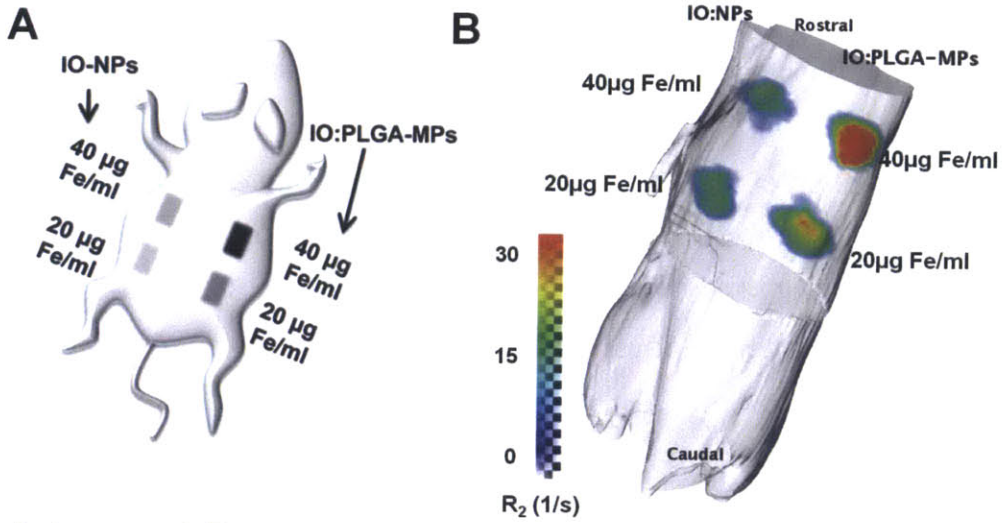


**Figure 4**: Improved $R_2$ contrast enhancement *in vivo* after PLGA encapsulation: **A**) Schematic illustration of the subcutaneous injection of 45 µL 3% agarose suspension of either IO-NPs (left) or IO:PLGA-MPs (right) or at the iron concentration of 20 µg Fe/ml (0.36mM) and 40 µg Fe/ml (0.71mM) on the back of the mouse. **B**) 3D reconstruction of a mouse with the $R_2$ map collected with a 4.7 T Bruker Pharmascan scanner and calculated within the Osirix environment. Scale bar indicates the value of $R_2$ (unit: 1/s or Hz). (Adapted from (*20*))

10±5.2 mV and 15.1±6.2 mV in PBS. To remove potential signal from free particles, typically, IO:PLGA-MPs were incubated with MSCs for 12 hours at physiological conditions, and then cells were detached by trypsinization and purified from free particles with Ficoll-Paque.(*25*)

Particles were applied to cells while maintaining a constant Fe concentration (25, 50, 100 or 200 μg/mL) and the amount of Fe loaded into the cells was quantified. This was achieved by digesting the cells and quantifying the Fe content via ICP-AES. The maximum Fe loading/cell was attained at 100 μg/mL initial concentration (Fig. 5A). Further increases in the initial Fe concentration did not enhance the final quantity of Fe per cell. Interestingly, maximal Fe loading per cell was 20 and 80 pg Fe/cell for IO-NPs and IO:PLGA-MPs, respectively. A significant 4-fold increase for Fe loading per cell reveals the advantage of using MPs for internalization of iron oxide. Given that no statistically significant difference was found in Fe loading between 50-100 μg/mL, to minimize use of reagents further internalization experiments were performed using 50 μg/mL of Fe.

To assess changes in Fe content over time, following particle internalization and subsequent purification from free particles, MSCs were plated in T25 plates for 28 days (the labeling day was designated as day 1). The culture media was replaced every two days for all samples and at each time point (day 1, 2, 4, 6, 12, and 28) MSCs were collected for quantification of MSC the proliferation, Fe concentration, and MRI analysis (by dispersing 200,000 MSCs in 1 mL 3% agarose gel). As shown in Fig. 5B, when MSCs were labeled with IO-NPs, the iron concentration per MSC decreased to about half of the initial value after 4 days. The iron concentration per cell was close to background after 12 days, however, when MSCs were labeled with IO:PLGA-MPs, within 6 days the concentration had decreased to half of its initial value and after 25 days, the iron concentration per cell was still significantly higher than background. The combination of contrast enhancement, and increased cellular loading in MSCs of IO:PLGA-MPs permitted us to visualize MSCs with MRI for at least 12 days (Fig. 5C), while in the case of IO-NPs labeling there was minimal detectable signal after day 6. To further confirm the MRI results and examine the stability of the internalized IO:PLGA-MPs, we labeled MSCs with fluorescent IO:PLGA-MPs containing lipophilic

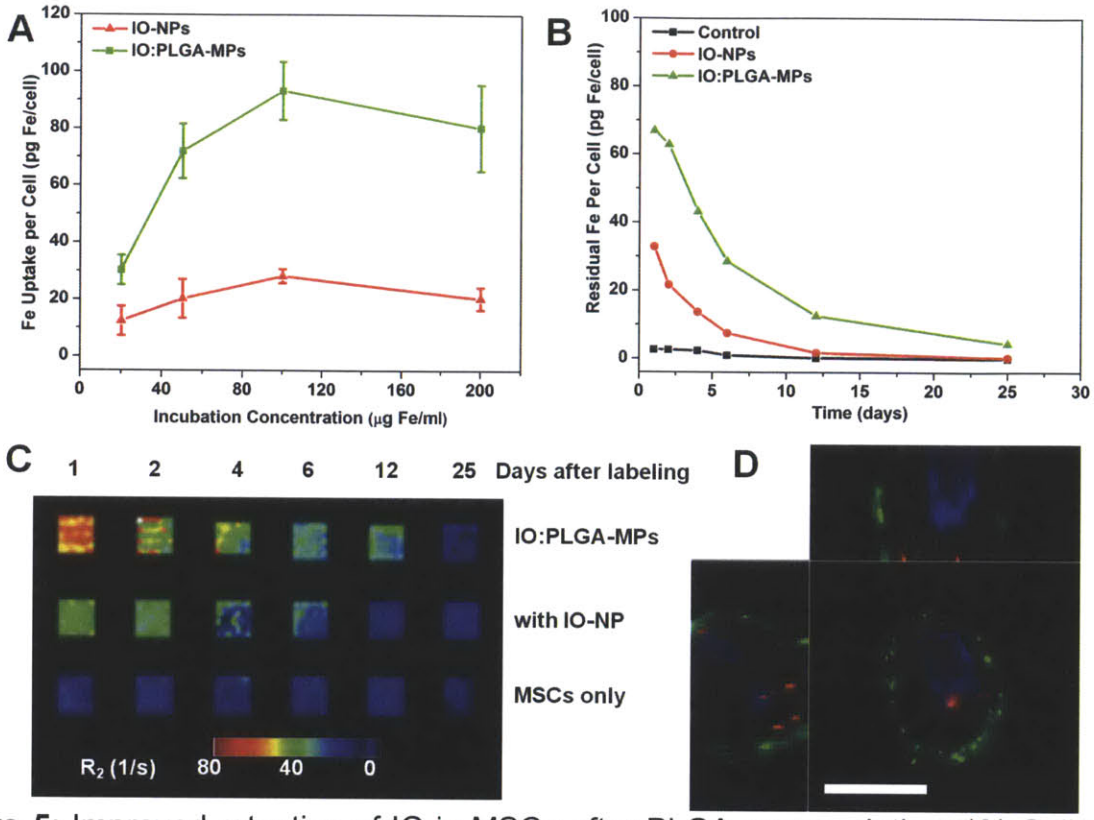


**Figure 5**: Improved retention of IO in MSCs after PLGA encapsulation: (**A**) Cellular Fe content of MSCs after incubation with magnetic particles as a function of iron concentration. (**B**) Change in cellular iron content per cell after initial labeling with IO-NPs or IO:PLGA-MPs at the incubation concentration of 50μg Fe/ml. (**C**) $R_2$-weighted MR images of 200,000 MSCs collected at different time points and suspended in 3% agarose gels (4 × 4 $mm^2$ per square) . (D) Fluorescent confocal image of MSCs 18 days after labeling with IO:PLGA-MPs. The plasma membrane is stained green (DiO), the nucleus is blue (DAPI) and the IO:PLGA-MPs are stained red (DiI). Scale bar 10μm. (Adapted from (*20*))

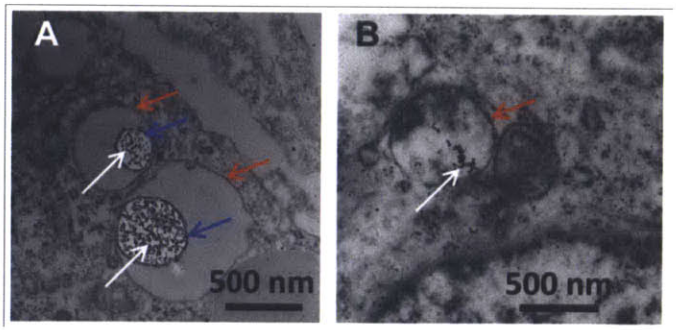


**Figure 6.** TEM images of MSCs after 12 hours labeling with (**A**) IO:PLGA-MPs and (**B**) IO-NPs. White arrow: location of IO-NPs, Blue arrow: PLGA-MPs, Red arrow: membrane of intracellular compartment. (Adapted from (*20*))

carbocyanine dye (i.e. DiI), and examined the fluorescent signal with fluorescent confocal microscopy. 18 days after labeling, we still observed the presence of IO:PLGA-MPs in 15±5% MSCs (Fig. 5D), which revealed the potential of IO:PLGA-MPs for long-term tracking of MSCs.

The location of internalized IO:PLGA-MPs and IO-NPs in MSCs after 12 hours labeling was characterized using TEM. In both cases, particles were present in intracellular compartments (Fig. 6). However, enhanced local density of IO-NPs was observed when they were encapsulated within PLGA-MPs (Fig. 6A) whereas in the absence of PLGA-MPs, lower density of IO-NPs was observed in a scattered manner (Fig. 6B). This result suggests that the advantage of IO-NPs encapsulation in PLGA-MPs may be enhanced contrast due to particle clustering(*26*).

**IO:PLGA-MPs impact on MSCs**

To investigate the potential negative impact on MSC phenotype, the viability, proliferation and migration ability of MSC were examined following IO:PLGA-MPs internalization using a series of *in vitro* and *in vivo* experiments. As shown in Fig. 7A, there was no noticeable influence on cell viability for both types of magnetic particles compared to native cells 24 hours following particle internalization. To assess the potential impact on cell proliferation, MSCs were labeled with two types of magnetic particles and studied for 12 days (Fig. 7B), during which confluence was reached typically at day 9. Compared with the control, MSCs labeled with both types of magnetic particles showed similar rates of proliferation. The number of MSCs tripled in 5 days.

The migration of MSCs *in vitro* was examined with a transwell assay. MSCs with or without internalized particles in media with 1% FBS were seeded on the insert, which was placed in chambers receiving complete media (with 10% FBS). MSCs with or without internalized particles showed similar adhesion on the insert 1hr following cell seeding (Fig. 8). Sixteen hours later, the migrated MSCs (bottom of filter) were stained and counted. Similar to Huang's report(*27*), MSC modified with IO-NPs showed a statistically significantly increased level of migration rate (~3x) (Fig. 7C,D&F). The mechanism mediating this increase is not well understood. The encapsulation of IO-NPs inside PLGA limited this effect. MSCs labeled with IO:PLGA-MPs showed similar

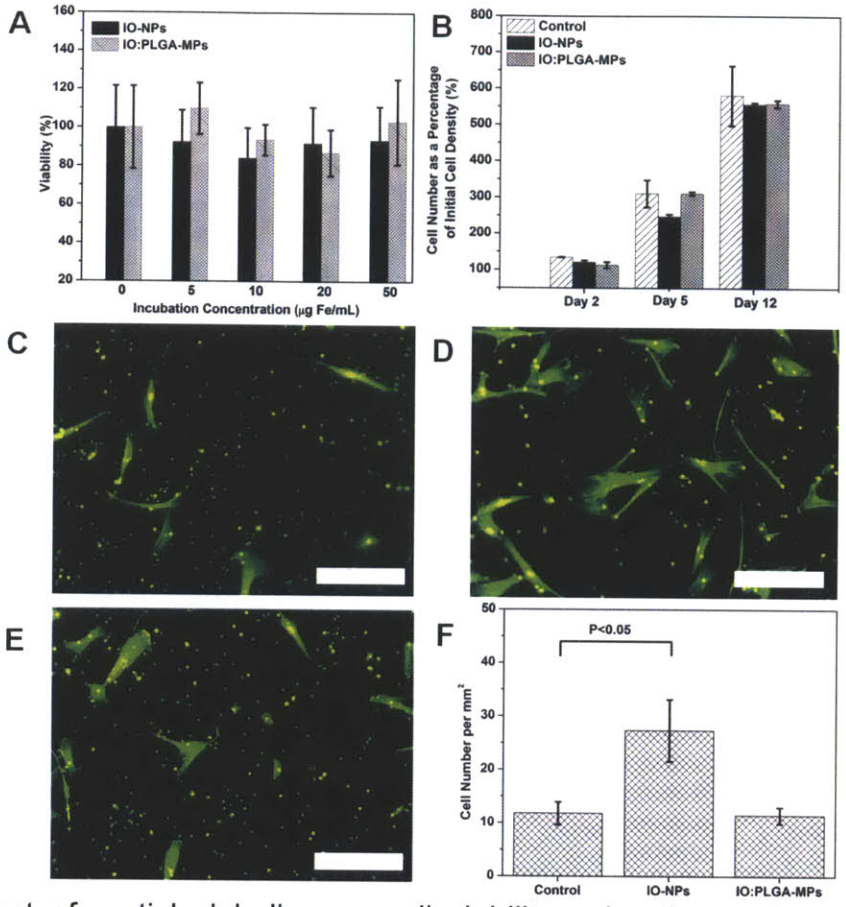


**Figure 7:** Impact of particle labeling on cell viability, migration and proliferation. (**A**) Viability of iron-labeled MSCs as a function of iron concentration during the incubation. (**B**) Proliferation of MSCs labeled with magnetic particles. (**C-E**) Representative images of migrated MSCs through FluoroBlok™ 8.0 μm colored PET membrane (images acquired of Phalloidin-FITC stained cells shown as green from underside of membranes). (**C**) Unmodified control MSCs, (**D**) MSCs labeled with IO-NPs, (**C**) MSCs labeled with IO:PLGA-MPs. (**F**) Quantification of migrated MSCs (each experiment was repeated 3 times). Scale bar is 200 μm. (Adapted from (*20*))

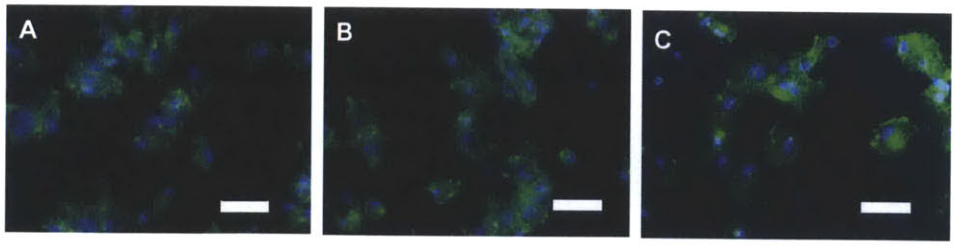


**Figure 8**: MSCs on FluoroBlok™ 8.0 μm colored PET membrane 1 hour after seeding (images acquired of Phalloidin-FITC/DAPI double-stained cells from upside of membranes) (**A**) unlabeled MSCs, (**B**) IO-NPs labeled MSCs, (**C**) IO:PLGA-MPs labeled MSCs. Scale bar is 100 μm. (Adapted from (*20*))

migration through the 8 μm membrane as the unlabeled MSCs (Fig. 7C, E&F).

**Homing of labeled MSCs in an inflamed ear model**

The *in vitro* migration assay (Fig. 7C-F) revealed that internalization of IO:PLGA-MPs does not impact MSC migration. Given that homing of systemically administered MSCs can be influenced by factors not accounted for in our *in vitro* assay including shear stress, immune system interference and endothelial barriers(*28*), we investigated the influence of internalized IO:PLGA-MPs on MSCs ability to home *in vivo* to a distant site of inflammation in an mouse model.

Previously, we examined the homing of systemically infused MSCs to a site of inflammation *in vivo* with dynamic real-time intravital confocal microscopy, using injection of lipo-polysaccharide (LPS) into the ear of a mouse(*29*). To facilitate cell imaging, unlabeled MSCs and MSCs labeled with IO:PLGA-MPs (>97% labeling efficiency) were treated with cell tracker dyes (DiD, Molecular Probes) and infused via tail vein. After 24 hours, the ears were imaged with intravital confocal microscopy. As we have previously shown, unmodified MSCs preferentially migrate to inflamed sites (Fig. 9A&B). Similarly, IO:PLGA-MPs labeled MSCs exhibited a similar response (Fig. 9C&D). The number of cells at the site of inflammation was comparable between the IO:PLGA-MPs labeled and unlabeled MSCs. Approximately 20-fold more cells per unit volume were found in the inflamed ear (Fig. 9E) compared to non-inflamed (saline) ear. In both cases, ~1/3 MSCs had transmigrated outside the blood vessel into the ear tissue, indicating that particle labeling did not impact transendothelial migration. Collectively, these results reveal that labeling of MSCs with IO:PLGA-MPs does not negatively impact MSC phenotype.

## Conclusion

Herein, we demonstrated that MSC internalization of IO-NP (10 nm) loaded biodegradable MPs (0.8 μm) can enhance MR parameters such as the relaxivity (5-fold), residence time inside the cells (3-fold) and $R_2$ signal (2-fold) compared to free IO-NPs. Intriguingly, *in vitro* and *in vivo* experiments demonstrated that MSC internalization of IO:PLGA-MPs did not compromise inherent cell properties such as viability,

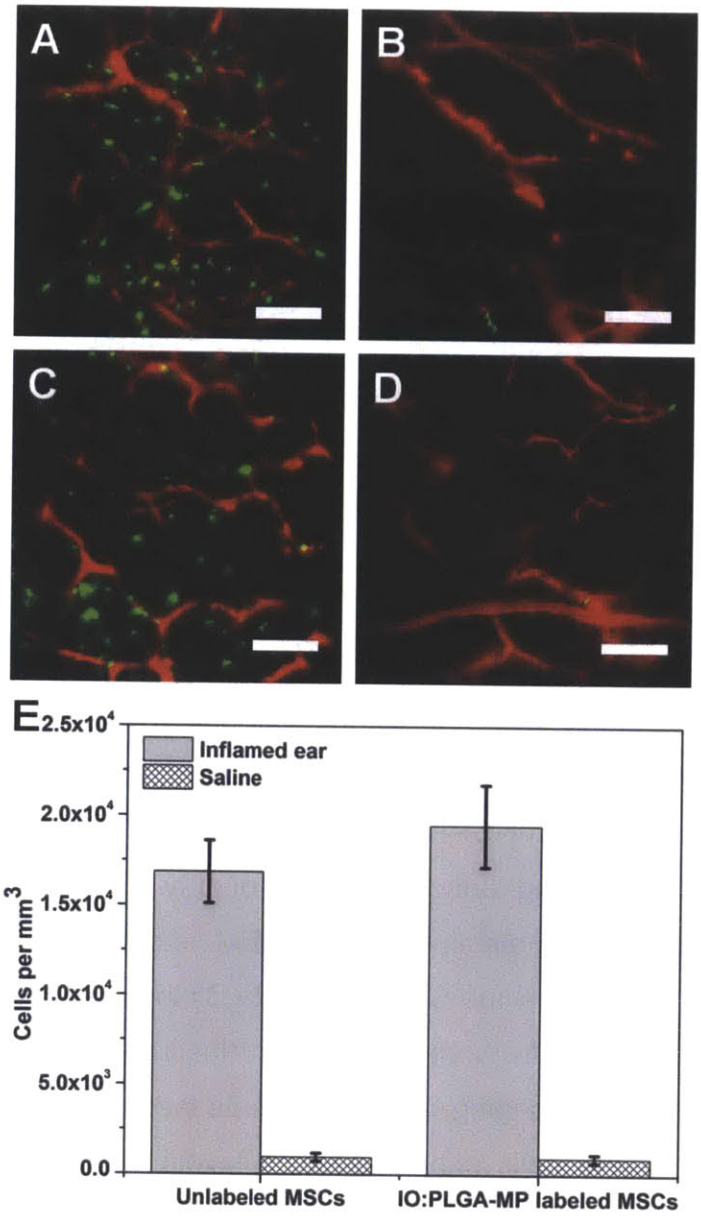


**Figure 9:** (**A-B**) Representative images of homed unlabeled MSCs and (**C-D**) MSCs prelabeled with IO:PLGA-MPs in the (**A,C**) LPS ears and (**B,D**) saline ears. Green signal indicates MSCs and red signal is from the blood vessels perfused with FITC-Dextran, Bar = 100 μm. (**E**) Quantification of the MSCs in LPS and saline ears (each experiment was repeated 3 times). (Adapted from (*20*))

proliferation, migration and their ability to systemically home to sites of inflammation.Thus, labeling cells with IO:PLGA-MPs may offer a potential opportunity for longitudinal tracking of MSC or other cell types without compromising cell phenotype including cell migration/homing ability.

## Materials and Methods

### Materials

All chemicals and solvents were of analytical grade from Sigma-Aldrich and were used without further purification unless otherwise mentioned. IO-NPs coated with oleic acid and water-soluble IO-NPs functionalized with carboxy groups were purchased from Ocean Nanotech (AR).

### Mesenchymal stem cell culture and characterization

Primary human MSCs were obtained from the Texas A&M Health Science Center, College of Medicine, Institute for Regenerative Medicine at Scott & White Hospital, which has a grant from NCRR of the NIH, Grant #P40RR017447. MSCs were derived from healthy consenting donors and thoroughly characterized as previously described.(*30*) MSCs were maintained in α-MEM expansion media (Invitrogen) supplemented with 15% Fetal Bovine Serum (Atlanta Biologicals), 1% (v/v) L-Glutamine (Invitrogen), and 1% penicillin:streptomycin solution (Invitrogen). Cells were cultured to 70-80% confluence before passaging. All experiments were performed using MSCs at passage number 3-6, where cells expressed high levels of MSC markers CD90 and CD29 (>99% cells), yet did not express hematopoietic markers CD34 or CD45 as observed from flow cytometry analysis. Before cell experiments, MSCs were detached with Trypsin 0.05% - EDTA 0.53mM (Gibco) and filtered with 40 μm Nylon Mesh (Fisher Scientific)..

### Animal welfare

BALB/C mouse (Charles River Laboratories, Wilmington, MA) were used for the *in vivo* studies. All studies were in accordance with US National Institutes of Health guidelines for care and use of animals under approval of the Institutional Animal Care

and Use Committees of Massachusetts General Hospital (Protocol number 2010N000064). All injections were performed under anesthesia, and all efforts were made to minimize suffering. Animals were humanely sacrificed after experiments.

**Fabrication of IO:PLGA-MPs**

Particles were prepared by following the procedures developed by Nkansah et al(*14*) with some minor modifications. Briefly, 10 mg $Fe_3O_4$ NPs (10 nm, Ocean Nanotech, AR) coated with oleic acid were mixed with 100 mg PLGA (acid terminated, 50:50, I.V.: 0.55-0.75 dL/g, Durect® Absorbables Durect Corporation) in 2 mL chloroform. The organic phase was then added to 20 mL of a 3% (w/v) aqueous solution of poly(vinyl alcohol) (MW: 90k, 80% hydrolyzed). To make the micronsized particles, a homogenizer (Tissue Master 125, Omni International) was used to disperse the organic phase into the aqueous phase (24,000 rpm for 2 min) in a 50 mL beaker. The homogenized mixture was then stirred overnight in a chemical fume hood at room temperature to allow for evaporation of chloroform. Finally, particles were isolated by centrifugation at 7,500 rpm for 5 minutes, washed thrice with distilled water, frozen at -80°C and lyophilized for 2 days.

**Characterization of IO:PLGA-MPs**

TEM: The IO:PLGA-MPs were subject to dehydration using graded ethanol (20%, 40%, 60%, 80%, 100%) and embedded in Epon 812 resin. Resin blocks were sectioned using a microtome and imaged with JEOL 200CX (80kV).

SEM: The IO:PLGA-MPs were deposited on silica wafers and coated with 10 nm gold. Then the PLGA-particle morphology was visualized via SEM (JEOL 6320 at 5kV).
Iron quantification: Iron content of particles was determined using ICP (HORIBA JOBINYVON, model: Activa) after digestion in 70 % nitric acid.

Hydrodynamic diameter quantification: The hydrodynamic diameter and polydispersity of particles were collected by Malvern Zetasizer Nano ZS90 in water by averaging 3 runs.

Hysteresis loop measurement: Samples were examined with a magnetometer (DMS Model 880 VSM vintage) at 37 °C. The measurements were normalized for the grams of iron in each sample, verified through ICP.

Relaxivity measurement *($r_2$)* with benchtop relaxmeter: The Fe concentration of samples was quantified with ICP first. Then five solutions with different Fe concentrations were prepared and placed in NMR tubes. T2 was measured in the Minispec Mq-20 (Bruker Optik GmbH, Germany). $r_2$ was derived by extracting the slope from the plot of 1/T2 versus Fe concentration (mM).

Sample preparation for MRI: The particles were diluted to different concentrations (0, 5, 10, 15, 20, and 40 µg Fe/mL) in PBS and mixed with equivalent volume of 6% agarose-gel solution to obtain a final agarose concentration of 3%. Subsequently, the mixture was pipetted into a 3% agarose-gel-made plate. Pipetting was gently performed to avoid air bubbles. After 12 hours, MRI samples were imaged using a 4.7 T Bruker Pharmascan scanner at 37°C.

*In-vivo* MRI of IO:PLGA-MP: A BALB/C mouse (Charles River Laboratories, Wilmington, MA) was used for the *in vivo* studies. Mice were anesthetized using ketamine/xylazine first. Then 45µL 3% agarose gels containing either IO-NPs or IO:PLGA-MPs with 20 and 40 µg Fe/ml were subcutaneously injected on the back of the mouse. After one hour the mice were euthanized and multi-slice multi-echo T2 (TR = 2800 ms, 4 averages, 128x128x16 matrix size, 0.432 mm x 0.312 mm x 1 mm voxel size) scanning was performed with effective echo times of 8.68, 17.36, 26.04, 34.72, 43.40, 52.08, 60.76, 69.44, 78.12, 86.80, 95.48, 104.16, 112.84, 121.52, 130.20, and 138.88 ms on the mouse with a 4.7 T Bruker Pharmascan scanner along with a RARE T2 sequence (TR= 2000 ms, effective TE = 36.0, 256x256x16 matrix size, 0.216 mm x 0.156 mm x 1 mm voxel size) ms, 8 averages). Amira (Visage Imaging) was used for the 3D reconstructions, which utilized the T2 maps calculated within the Osirix environment.

**MSCs labeling with IO:PLGA-MPs**

Particles were incubated with Poly-L-lysine (0.01%) for 40 minutes at room temperature in PBS. Then, the complex was added to cells in α-MEM expansion media

supplemented with 1% FBS, 1% (v/v) L-Glutamine, and 1% penicillin:streptomycin solution for 12 hours. Cells were then permitted to recover in fresh media (15% FBS). For experimentation, labeled cells were washed twice with PBS, trypsinized, centrifuged with Ficoll-Paque (GE Healthcare), re-dispersed and counted in PBS.

Labeling efficiency of MSCs with IO:PLGA-MPs: to facilitate the identification of particles internalized within MSCs, we incorporated the fluorescent dye, DiI during the preparation of IO:PLGA-MPs. Then MSCs were labeled with the fluorescent IO:PLGA-MPs and analyzed with flow cytometry.

Fe quantification in MSCs: For a typical sample, 0.1 mL of cell suspension was digested overnight using 0.3 mL concentrated nitric acid (~70%) and 0.1 mL hydrogen peroxide (30%). Samples were then diluted to a volume of 10 mL with deionized water, yielding a final nitric acid concentration of 2%. Iron concentration was determined with ICP.

MRI sample preparation: Agar wells were prepared using a 3% agar solution heated in a water bath until fully dissolved and poured into a PDMS mold. MSCs suspension samples were mixed with agar powder to a concentration of 3% and heated. Once the agar was fully dissolved, samples were transferred into an agar well and allowed to set. MRI samples were imaged using a Bruker 4.7 T MRI scanner.

TEM: MSCs were labeled with IO-NPs or IO:PLGA-MPs (50 μg Fe/mL) for 12 hours, and then washed twice with PBS. MSCs were fixed in phosphate-buffered Karnofsky's solution followed by staining with 2% osmium tetroxide at 4°C overnight, and dehydration using graded ethanol and embedded in Epon 812 resin. Resin blocks were sectioned using a microtome, doubly stained with uranyl acetate and lead hydroxide, and imaged with JEOL 200CX (80kV).

**Influence of magnetic particle labeling on MSC properties**

Viability study: 200,000 MSCs were seeded in T25 flasks 24 hours before the experiment. Poly-L-lysine coated IO-NPs or IO:PLGA-MPs dispersed in serum free media were added to the plates and incubated for 24 hours at 37°C. Unmodified MSCs were treated with serum free media in the same way. Then, the cells were permitted to

recover in fresh media (15% FBS) for 30 minutes before being collected with 1X trypsin. Finally, the collected cells were counted. Each condition was performed in triplicate.
Proliferation assessment: 2 million MSCs were labeled with magnetic particles (IO-NPs or IO:PLGA-MPs) as described above and sub-cultured in T25 flasks. At each time point (day 1, 3, 6, 9, 12), MSCs in three flasks were trypsinized and counted.

Transwell migration assay: In a 24- well transwell plate (FluoroBlok™ 8.0 µm colored PET membrane, BD), complete medium with 10% FBS was added into the (bottom) wells. 30,000 MSCs labeled with particles and purified with Ficoll-Paque were seeded into the insert in media containing 1% FBS. After 16 hours of incubation at 5% $CO_2$ and 37°C, inserts were washed twice with PBS, fixed in 4% paraformadehyde for 15 minutes, stained in 0.5% Phalloidin-FITC (Sigmal-Aldrich) for 10 minutes, and counted.

### *In-vivo* MSC homing

Cell preparation: 18 hours prior to injection, MSCs were labeled with IO:PLGA-MPs as described above. 2 hours before injection, serum-free medium was replaced with 15% FBS containing MEM-α for 30 min. Then cells were trypsinized, centrifuged, and re-suspended at $2x10^6$ cells/mL in PBS. DiD stock (Invitrogen Inc.) was diluted to 20 µM in PBS. Equivalent volumes of cells and DiD solution were mixed together and incubated for 20 minutes at room temperature in the dark. Then, the labeled MSCs were centrifuged and washed twice with PBS. Finally, MSCs were passed through a 40µm cell strainer, and re-suspended at $10^7$ cell/mL in PBS.

Animals: BALB/C mice (Charles River Laboratories, Wilmington, MA) were anesthetized using ketamine/xylazine and the hair around the base of both ears was trimmed with scissors. To assess the potential for IO:PLGA-MP loaded MSCs to preferentially home to a site of inflammation, we utilized a model where 24 hours prior to cell infusion, inflammation was induced through injection of 30µg of E. coli lipopolysaccharide (LPS, Sigma, St. Louis, MO) in 30 µL of saline into the base of the left ear, whereas the right ear received 30µL 0.9% of saline as a control. $1 \times 10^6$ MSCs suspended in 100 µL PBS (pH 7.4) were injected retro-orbitally 24 hours post LPS injection. For delineation of vasculature during imaging, ~100 µL of 2 mg/mL FITC-

dextran (2 x $10^6$ kDa; Sigma, St. Louis, MO) was injected retro-orbitally just prior to imaging.

Dynamic real-time intravital confocal microscopy. Homing of unmodified and modified MSCs to the skin was imaged noninvasively (in real time) using a custom-built video-rate laser-scanning confocal microscope designed specifically for live animal imaging(*31*). To image the vasculature and surrounding tissue, we positioned the mouse's ear on a coverslip (with index matching gels) and obtained high-resolution images with cellular details through the intact mouse skin at depths of up to 250 μm. The laser beams were focused onto the sample (mouse ear skin) using a 60X, 1.2NA water immersion objective lens (Olympus, Center Valley, PA). DiD-labeled MSCs were excited with a 635 nm continuous-wave (CW) laser (Coherent, Inc., Santa Clara, CA) and detected through a 695 nm ± 27.5 nm band pass filter (Omega Optical, Brattleboro, VT). FITC-dextran was excited with a 491 nm CW laser (Cobalt, Stockholm, Sweden) and detected through a 520 ± 20 nm bandpass filter (Semrock, Inc., Rochester, NY). For static images, 15 frames were averaged from the live video mode to improve the signal to noise ratio. The total number of "homed" cells from each MSC population within the mouse ear was quantified from the z-stacks acquired. For publication purposes, the contrast and brightness of the images were changed using ImageJ software.

## Acknowledgement

This work was supported by the Harvard Stem Cell Institute, and the National Institute of Health grants HL095722 and HL097172 to JMK. D.M.N is supported by MIT-UROP program and the John Reed Fund. J.A.A. is supported by the Hugh Hampton Young Memorial Fund and the National Science Foundation. M.N. was supported by funds from the National Heart, Lung, and Blood Institute, National Institutes of Health, Department of Health and Human Services, under Contract No. HHSN268201000044C. We thank Dr. Nikolay Sergeyev (MGH) in "Center for Systems Biology Mouse Imaging Program" for helping us perform the relaxivity measurement with the benchtop relaxometer.

## Competing Financial Interests

J.M.K. is a co-owner of Megacell Therapeutics, a company that has an option to license IP generated by J.M.K. J.M.K. may benefit financially if the IP is licensed and further validated. The interests of J.M.K. were reviewed and are subject to a management plan overseen by the Brigham & Women's Hospital and Partners HealthCare in accordance with their conflict of interest policies. The remaining authors declare no competing financial interests.

## References


1. J. A. Pérez-Simon *et al.*, Mesenchymal stem cells expanded in vitro with human serum for the treatment of acute and chronic graft-versus-host disease: results of a phase I/II clinical trial, *Haematologica* **96**, 1072–1076 (2011).

2. Y. Tian, Y. B. Deng, Y. J. Huang, Y. Wang, Bone marrow-derived mesenchymal stem cells decrease acute graft-versus-host disease after allogeneic hematopoietic stem cells transplantation, *Immunol. Invest.* **37**, 29–42 (2008).

3. P. Fiorina *et al.*, Immunomodulatory function of bone marrow-derived mesenchymal stem cells in experimental autoimmune type 1 diabetes, *J Immunol* **183**, 993–1004 (2009).

4. F. E. Ezquer *et al.*, Systemic administration of multipotent mesenchymal stromal cells reverts hyperglycemia and prevents nephropathy in type 1 diabetic mice, *Biol. Blood Marrow Transplant.* **14**, 631–640 (2008).

5. S. Aggarwal, M. F. Pittenger, Human mesenchymal stem cells modulate allogeneic immune cell responses, *Blood* **105**, 1815–1822 (2005).

6. I. M. Barbash *et al.*, Systemic delivery of bone marrow-derived mesenchymal stem cells to the infarcted myocardium: feasibility, cell migration, and body distribution, *Circulation* **108**, 863–868 (2003).

7. Z. Lee, J. E. Dennis, S. L. Gerson, Imaging stem cell implant for cellular-based therapies, *Exp. Biol. Med. (Maywood)* **233**, 930–940 (2008).

8. M. Srinivas *et al.*, Imaging of cellular therapies, *Adv Drug Deliv Rev* **62**, 1080–1093 (2010).

9. C. Xu *et al.*, Nanoparticle-based monitoring of cell therapy, *Nanotechnology* **22**, 494001 (2011).

10. D. J. Stuckey *et al.*, Iron particles for noninvasive monitoring of bone marrow stromal cell engraftment into, and isolation of viable engrafted donor cells from, the heart, *Stem Cell* **24**, 1968–1975 (2006).

11. D. L. Kraitchman, Imaging of stem cells using MRI, *Basic research in cardiology* (2008).

12. W. J. Rogers, C. H. Meyer, C. M. Kramer, Technology insight: in vivo cell tracking by use of MRI, *Nat Clin Pract Cardiovasc Med* **3**, 554–562 (2006).

13. H. B. Na, I. C. Song, T. Hyeon, Inorganic nanoparticles for MRI contrast agents, *Adv. Mater.* (2009).

14. M. K. Nkansah, D. Thakral, E. M. Shapiro, Magnetic poly(lactide-co-glycolide) and cellulose particles for MRI-based cell tracking, *Magn Reson Med* **65**, 1776–1785 (2011).

15. R. Guzman *et al.*, Long-term monitoring of transplanted human neural stem cells in developmental and pathological contexts with MRI, *Proc Natl Acad Sci USA* **104**, 10211–10216 (2007).

16. E. S. M. Lee *et al.*, Microgel iron oxide nanoparticles for tracking human fetal mesenchymal stem cells through magnetic resonance imaging, *Stem Cell* **27**, 1921–1931 (2009).

17. J. Panyam, V. Labhasetwar, Dynamics of endocytosis and exocytosis of poly(D,L-lactide-co-glycolide) nanoparticles in vascular smooth muscle cells, *Pharm Res* **20**, 212–220 (2003).

18. B. D. Chithrani, W. C. W. Chan, Elucidating the mechanism of cellular uptake and removal of protein-coated gold nanoparticles of different sizes and shapes, *Nano Lett* **7**, 1542–1550 (2007).

19. D. Sarkar, J. Ankrum, G. S. L. Teo, C. V. Carman, J. M. Karp, Cellular and extracellular programming of cell fate through engineered intracrine-, paracrine-, and endocrine-like mechanisms, *Biomaterials* **32**, 3053–3061 (2011).

20. C. Xu *et al.*, Tracking Mesenchymal Stem Cells with Iron Oxide Nanoparticle Loaded Poly(lactide-co-glycolide) Microparticles, *Nano Lett* **12**, 4131–4139 (2012).

21. Y. X. Wang, S. M. Hussain, G. P. Krestin, Superparamagnetic iron oxide contrast agents: physicochemical characteristics and applications in MR imaging, *Eur Radiol* **11**, 2319–2331 (2001).

22. F.-Y. Cheng *et al.*, Stabilizer-free poly(lactide-co-glycolide) nanoparticles for multimodal biomedical probes, *Biomaterials* **29**, 2104–2112 (2008).

23. K. A. Brown *et al.*, Scaling of transverse nuclear magnetic relaxation due to magnetic nanoparticle aggregation, *J Magn Magn Mater* **322**, 3122–3126 (2010).

24. V. Mailänder, K. Landfester, Interaction of nanoparticles with cells, *Biomacromolecules* (2009).

25. N. Lee *et al.*, Magnetosome-like ferrimagnetic iron oxide nanocubes for highly sensitive MRI of single cells and transplanted pancreatic islets, *Proceedings of the National Academy of Sciences* **108**, 2662–2667 (2011).

26. S. J. H. Soenen *et al.*, Intracellular nanoparticle coating stability determines nanoparticle diagnostics efficacy and cell functionality, *Small* **6**, 2136–2145 (2010).

27. T.-H. Chung *et al.*, Iron oxide nanoparticle-induced epidermal growth factor receptor expression in human stem cells for tumor therapy, *ACS nano* **5**, 9807–9816 (2011).

28. G. Chamberlain, H. Smith, G. E. Rainger, J. Middleton, Mesenchymal stem cells exhibit firm adhesion, crawling, spreading and transmigration across aortic endothelial

cells: effects of chemokines and shear, *PLoS ONE* **6**, e25663 (2011).

29. D. Sarkar *et al.*, Engineered cell homing, *Blood* **118**, e184–91 (2011).

30. D. C. Colter, R. Class, C. M. DiGirolamo, D. J. Prockop, Rapid expansion of recycling stem cells in cultures of plastic-adherent cells from human bone marrow, *Proc Natl Acad Sci USA* **97**, 3213–3218 (2000).

31. I. Veilleux, J. A. Spencer, D. P. Biss, D. Cote, C. P. Lin, In vivo cell tracking with video rate multimodality laser scanning microscopy, *IEEE Journal Select Topics in Quantum Electronics* **14**, 10–18 (2008).

# Appendix II Preface

In this Appendix I discuss an additional project I was heavily involved in throughout the duration of my PhD involving biomimicry of the North American porcupine quill to develop novel medical devices. While the primary focus of this thesis is on the development of improved cell-based therapies, I have also always had an interest in medical devices. While these topics may seem divergent, as a biomedical engineer I find them quite similar. Both involve first acquiring a deep understanding of a natural system (MSCs or porcupine quills) and then using that newly acquired knowledge and the tools of engineering to solve important problems in medicine.

This appendix is an adaptation of a peer-reviewed article published on December 26, 2012 in *Proceedings of the National Academy of Sciences*. Reprinted with Permission.

Cho WK, Ankrum J, Guo D, Chester SA, Yang SY, Kashyap A, Campbell GA, Wood RJ, Rijal RK, Karnik R, Langer R, Karp JM. (2012). Microstructured barbs on the North American porcupine quill enable easy tissue penetration and difficult removal. Proceedings of the National Academy of Sciences, 109(52), 21289–94.

**Glossary of Terms**

Quill: Modified hair of porcupine used for self defense and display

Barb: 100 micron sized backward facing scale found at the tip of quills

Stress Concentration: Zone of high stress caused by local geometry that is prone to fracture before the bulk medium.

Puncture: Initial breaking of a surface barrier

Penetration: Movement into a medium following puncture.

# Appendix I: Microstructured Barbs on the North American Porcupine Quill Enable Easy Tissue Penetration and Difficult Removal

## Abstract

North American porcupines are well known for their specialized hairs, or quills that feature microscopic backwards-facing deployable barbs that are used in self-defense. Herein we show that the natural quill's geometry enables easy penetration and high tissue adhesion where the barbs specifically contribute to adhesion and unexpectedly, dramatically reduce the force required to penetrate tissue. Reduced penetration force is achieved by topography that appears to create stress concentrations along regions of the quill where the cross sectional diameter grows rapidly, facilitating cutting of the tissue. Barbs located near the first geometrical transition zone exhibit the most substantial impact on minimizing the force required for penetration. Barbs at the tip of the quill independently exhibit the greatest impact on tissue adhesion force and the cooperation between barbs in the 0-2 mm and 2-4 mm regions appears critical to enhance tissue adhesion force. The dual functions of barbs were reproduced with replica molded synthetic polyurethane quills. These findings should serve as the basis for the development of bio-inspired devices such as tissue adhesives or needles, trocars, and vascular tunnelers where minimizing the penetration force is important to prevent collateral damage.

## Introduction

The North American porcupine has ~30,000 quills on the dorsal surface(*1*) that are released when a predator contacts the porcupine. In contrast to other mammals such as the African porcupine, hedgehog, and echidna that have smooth spines, each quill tip contains microscopic backward facing barbs (*1-4*). It has been well documented that it is difficult to remove porcupine quills once the quills are lodged within tissue (typically through both skin and muscle)(*1*, *3*). However, the forces involved in

penetration and pull-out have yet to be described and a comprehensive mechanism remains elusive.

## Results and Discussion

North American porcupine quills (Fig. 1A) have two distinct regions. The conical black tip contains a layer of microscopic backward facing barbs on its surface (Fig. 1B), while the cylindrical white base contains smooth scale-like structures (Fig. 1C). As shown in Fig. 1D, barbs overlap slightly and have dimensions ranging from 100-120 mm in length, with a maximum width of 35-45 mm. There is 1-5 mm space between the tip of each barb and the shaft of the quill. The size of the barbs becomes larger farther from the apex of the tip (Fig. 1E). Since the length of the barbed region varies (Fig. 2), we standardized tests by only using quills with a barbed region of 4 mm.

Fig. 1F shows the results of penetration-retraction tests including a barbless control quill whose barbs were carefully removed by gentle sanding to avoid altering the diameter of quill (Fig 3). The force required for penetration into tissue was defined as the *penetration force* and the maximum force required to remove the quill with respect to baseline was defined as *pull-out force*. Surprisingly, Fig. 1F shows that the quill with barbs required 54% less penetration force compared to the barbless quill. Regarding pull-out force, quills with and without barbs required 0.44±0.06 N and 0.11±0.02 N, respectively, and the barbed quill required less work of penetration and higher work of removal (Fig. 1G). Also, the barbed quill requires significantly less force and work to penetrate into tissue, compared to an 18 gauge hypodermic needle, which has a diameter of 1.161±0.114 mm, similar to the diameter of a porcupine quill (1.262±0.003 mm) (Figs. 1G).

As an additional control for the presence of barbs, we performed penetration-retraction tests using the naturally barbless African porcupine quills (Fig. 1F). The work of penetration and work of removal were 2.13±0.04 mJ and 0.22±0.06 mJ, respectively (Figs. 1F and G). The profile of the force versus extension plot for the African quill exhibited a similar profile to the barbless North American quill. Thus, barbs appear essential for both reducing penetration force and generating tissue adhesion.

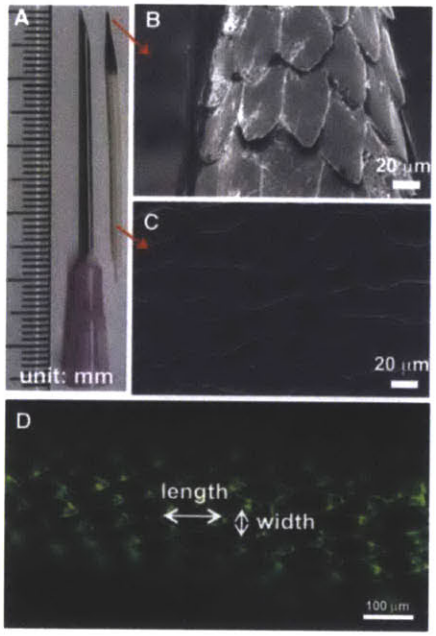



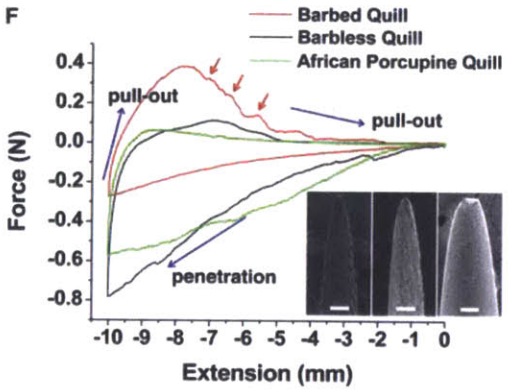


G

| | Penetration Force (N) | Pull-out Force (N) | Work of Penetration (mJ) | Work of Removal (mJ) |
|---|---|---|---|---|
| Barbed Quill | 0.33 ± 0.08 | 0.44 ± 0.06 | 1.08 ± 0.37 | 1.73 ± 0.41 |
| Barbless Quill | 0.71 ± 0.09* | 0.11 ± 0.02* | 2.41 ± 0.28* | 0.28 ± 0.03* |
| 18 Gauge Needle | 0.59 ± 0.11* | 0.04 ± 0.006*† | 2.75 ± 0.70* | 0.10 ± 0.02* |
| African Porcupine Quill | 0.65 ± 0.03* | 0.06 ± 0.01* | 2.13 ± 0.04* | 0.22 ± 0.06* |

**Figure 1.** Geometrical features of the North American porcupine quill and analysis of the penetration and removal forces with muscle tissue. (*A*) North American porcupine quill. (*B, C*) FE-SEM images showing the microstructure of the quill tip and base, respectively. (*D*) Fluorescence image enables visual delineation of the geometry of single barbs. (*E*) FE-SEM image showing the microstructure of the tip of the porcupine quill. (*F*) Representative force versus extension plots show puncture, penetration, and removal of barbed, barbless, and African porcupine quills from muscle tissue (see Fig. 12 for experimental set-up). Inset shows micron-level topography of the three quills. Scale bars represent 100 mm. Red arrows indicate resistance as the barbed quill is removed from the tissue (not observed for others). (*G*) Summary of experimental values obtained from penetration/removal of barbed quill, barbless quill, 18 gauge needle, and African porcupine quill (Mean ± standard deviation, n=5). Each mean is compared to every other mean using one-way ANOVA with Tukey's Honestly Significant Difference post-hoc analysis to correct multiple comparisons at 95% confidence interval by using GraphPad Prism 6 (*$p$<0.05, compared to barbed quill and $^{\dagger}p$<0.05, compared to barbless quill). (Adapted from (*5*))

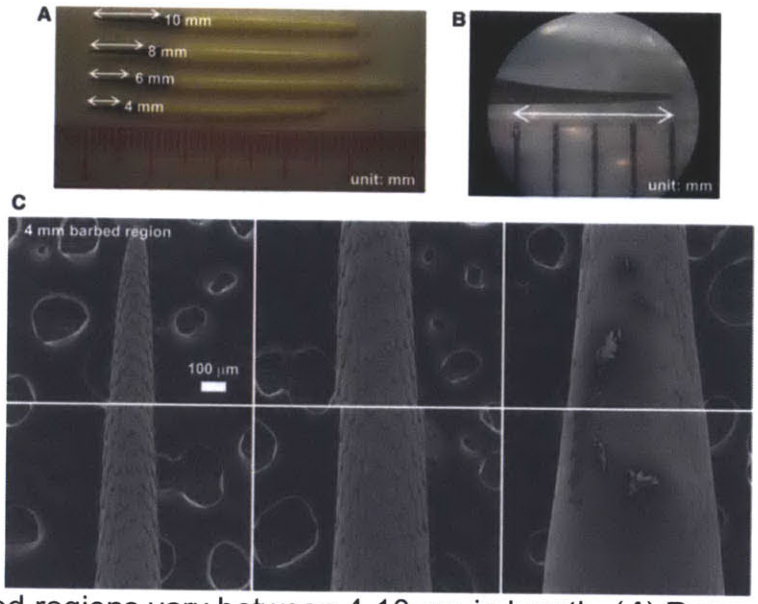


**Figure 2.** Barbed regions vary between 4-10mm in length. (*A*) Representative quills with different lengths of barbed regions where the length is typically in the range of 3-5 mm. (*B*) Optical microscopic image confirms the length of a quill with a 4 mm barbed region. (*C*) Sequential FE-SEM images of a single quill show the transition from functional barbs to a smooth surface containing barbs that have yet to emerge (i.e. those that cannot yet engage tissue). (Adapted from (*5*))

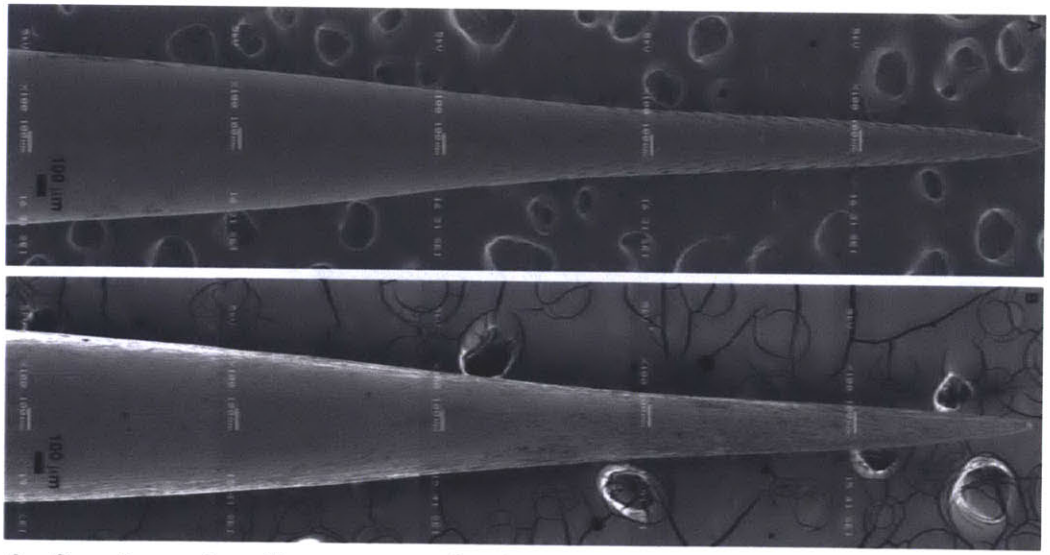

**Figure 3.** Sanding of quills removes barbs but does not substantially alter the quill morphology or size. FE-SEM images show (*A*) the barbed quill with 4 mm-barbed region and (*B*) the barbless quill after removal of the barbs by sanding. Gentle sanding didn't significantly change the diameter of quill. Specifically, while sanding of barbs led to a 3~7% reduction in diameter for the first 0-2 mm from the apex of tip, sanding of other regions showed ~1% reduction. (Adapted from (*5*))

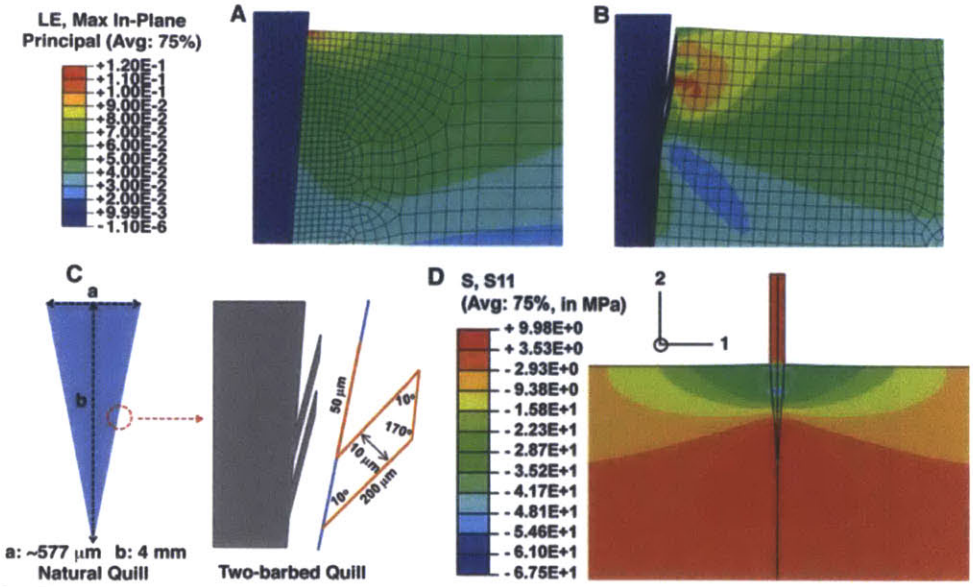


**Figure 4.** Finite element analysis shows that the tissue is primarily stretched and deformed near the barbs. (*A-B*) Strain field distribution in skin tissue when a barbless quill or two-barbed is penetrated into tissue, respectively. The Young's modulus of both quills was set at 3.25 GPa for finite element analysis. LE refers to for Logarithmic (L) strain (ε) and represents true strain. 75% refers to the averaging threshold of the extrapolated results to achieve a smooth colored contour map. (*C*) Geometry of two-barbed quill with the dimensions of a single barb and the distance between two barbs indicated. The simplified geometry is based on the middle point of 4 mm barbed region of natural quill. (*D*) Finite element modeling of the quill penetration into skin tissue shows compressive stresses (in MPa) from the tissue acting on the quill at a distance from the quill tip. This is the stress state following a 10 mm-penetration into the skin tissue. S means stress and S11 refers to the stress vector on the plane normal to "1" in the "1" direction. 75% refers to the averaging threshold of the extrapolated results to achieve a smooth colored contour map. (Adapted from (*5*))

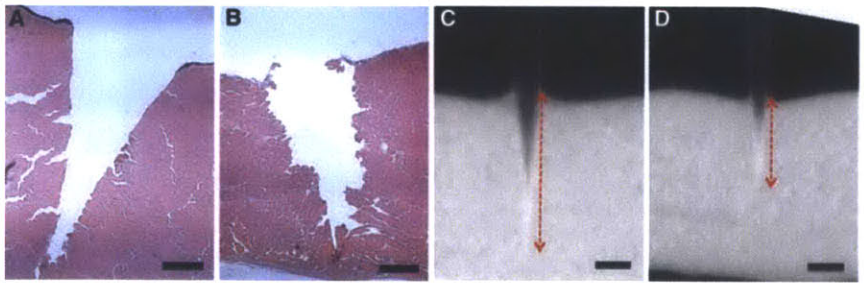


E

| | Penetrating Depth (mm) |
|---|---|
| Barbed Quill | 4.19 ± 0.39 |
| Barbless Quill | 2.50 ± 0.33 |

**Figure 5.** Barbs reduce tissue damage and facilitate penetration into tissue. (*A, B*) Representative histological images of tissue samples that were penetrated with barbed and barbless quills, respectively, showing significantly less damage induced by the barbed quills (n=5). The scale bar represents 200 mm. (*C, D*) Micro-computed tomography (Micro-CT) images present the penetrated (*C*) barbed and (*D*) barbless quills within tissue. Both quills were penetrated into tissue with an applied force of 0.2 N. The red dashed arrows indicate the penetrating depth of quill. The scale bar represents 1 mm. (*E*) Mean penetrating depth of barbed and barbless quills observed in micro-CT images (n=3). (Adapted from (*5*))

During the penetration process, tissue initially deforms under the advancing quill tip until a critical load leads to tissue puncture (*6*, *7*). At the critical load, the quill tip initiates a crack that expands the hole circumferentially through stretching and tearing tissue fibers, permitting the quill to penetrate into tissue. The rupture of the tissue surface occurs via a planar mode I crack ahead of the tip, and the crack faces are wedged open by the advancing quill similar to what has been described for needles (*8*, *9*). The work of penetration is the energy absorbed by the tissue during the penetration process and includes the energy required to deform and tear the tissue upon penetration (*10*). The barbed quill requires less work of penetration (Fig. 1G) while minimizing tissue damage. Stress concentrations generated by the barbs during penetration likely stretches or tears tissue fibers locally at the interface of the quill.

To visualize the effect of barbs on penetration, we examined the strain distribution in tissue using finite element analysis (FEA) for a barbless quill and a simplified two-barbed quill (Figs. 4A and B). Values for the geometry and material properties of the quill and tissue for FEA were experimentally derived (Fig. 4C). The analysis revealed that tissue is primarily stretched and deformed by high stress concentrations near the barbs. The local stress concentrations likely reduce the need to deform the entire circumference of tissue surrounding the quill, consequently reducing the penetration force. The concept of stress concentration has been used to design blades and knives, albeit at a much larger scale than what is utilized by porcupine quills. Compared to straight blades, serrated blades require less work to cut tissue by localizing strain at points on the tips of the teeth of the blade. The strain concentration causes the tissue to fail with a lower input force (*11*). Consequently, serrated blades provide cleaner cuts with minimal deformation of the tissue (*11*).

While porcupine quill barbs are relatively small compared to the jagged edge of a serrated knife, we observed a cleaner interface between tissue and barbed quills compared to barbless quills upon histological analysis of the tract left by quills after penetration (Figs. 5A and B). This result suggests that the tissue absorbs less energy and is damaged less during penetration by a barbed quill. Furthermore, when 0.2N was applied to barbed and barbless quills, the barbed quills advanced significantly deeper

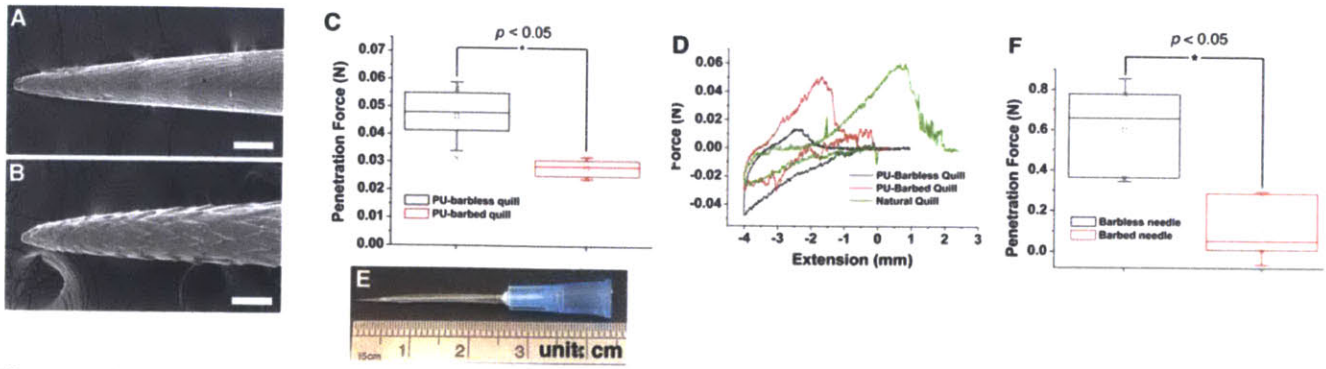


**Figure 6.** The reduced penetration force of the natural porcupine quill can be replicated in synthetic polyurethane quills. (*A, B*) FE-SEM images show the barbless and barbed synthetic PU quills. The scale bar represents 100 mm. (*C*) The forces required to penetrate the PU quills into muscle tissue to 4 mm-depth (Experimental details in Fig. 12B). The mean values are shown with standard deviation (n=5, student *t*-test at the level of 95% significance). The box plot whiskers are set to ± 1.2 standard deviations. (*D*) Representative force versus extension plots from the penetration-retraction tests of the natural quill and replica molded PU quills performed in muscle tissue. (*E*) Fabricated quill-mimetic needle. (*F*) The forces required to penetrate the fabricated barbed/barbless needles into a model of human skin. The data shows the mean penetration force with standard deviation (n=3, each needle was used at least 4 times, student *t*-test at the level of 95% significance). The two "X"s in box plots of (C) and (F) indicate 1st and 99th percentiles. (Adapted from (*5*))

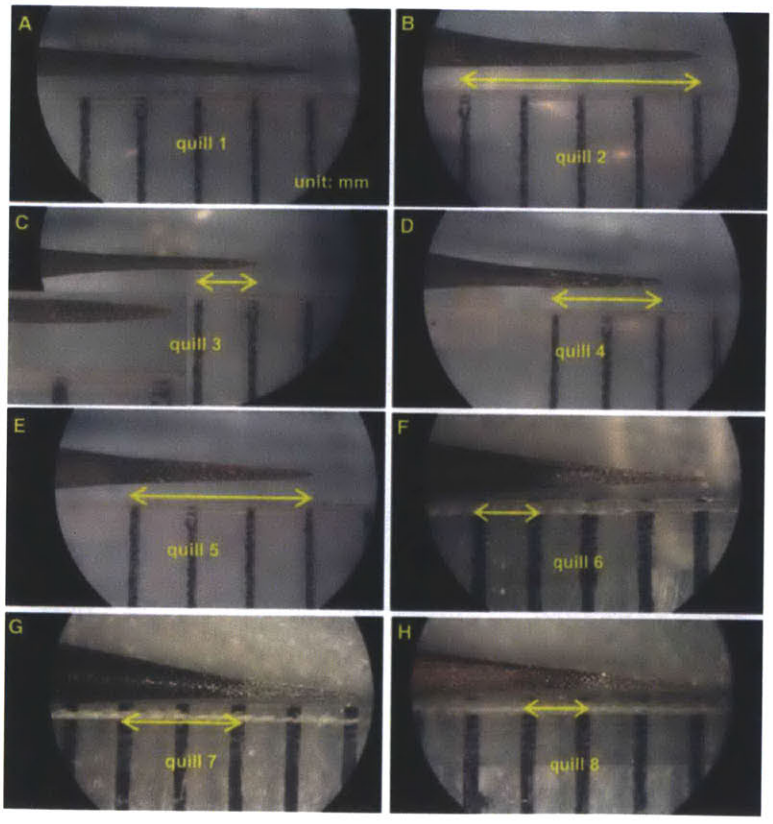


**Figure 7.** Selective ablation of barbs is achieved by gentle sanding. (*A-H*) Representative optical micrographic images confirm the barbed region for eight quills that have been sanded to obtain barbed regions of specific length. Inset in (C) shows the enlarged images for 1 mm barbed region. (Adapted from (*5*))

into muscle (4.19±0.39 mm) than barbless quills (2.50±0.33 mm) (Figs. 5C-E) as measured by micro-computed tomography (micro-CT).

To investigate the role of barb deflection in the reduction of penetration force, we reproduced quills with non-deployable barbs using replica molding that reproduces the surface topography of the quill. We fabricated both barbless and barbed (non-deployable) polyurethane (PU) quills by replica molding (Figs. 6A and B). While the penetration force for insertion of barbless PU quills to a depth of 4 mm was 0.046 ± 0.010 N, the barbed PU quill required 35% less force, 0.030 ± 0.006 N (Fig. 6C). Additionally, the penetration force of natural barbed quills with muscle tissue was 0.043 ± 0.013 N (Fig. 6D), which was not significantly different from that of the PU barbed quill. Although the barbs of the PU quill cannot bend, the PU quill includes the same topography (i.e. barbs) creating stress concentrations during penetration into the tissue. Therefore, the experimental results with the fabricated PU quills support that stress concentration at barbs helps to reduce the penetration force of the natural porcupine quill. As barbs and muscle tissue fibers are on the same length scale (~50-100 mm), (*12*) the stress concentrations at barbs can potentially stretch tissue fibers locally. To apply this phenomenon to the development of a medical needle to achieve reduced penetration force (see SI text), we fabricated a prototypic hypodermic needle with microscopic barbs. The PU-barbed needle showed 80% less penetration force compared to the PU barbless needle (Figs. 6E and F).

Upon penetration of a quill into tissue, tensile and compressive 'zones' arise in the surrounding tissue. The quill has three geometrical transition zones as shown in Fig. 8A. FEA shows that tissue compression occurs tangential to the quill from the first transition zone, which is ~3 mm from the apex of tip with a maximum at the second transition zone (Fig. 4D). This suggests that barbs closest to the first transition zone may experience the greatest interaction with tissue. To understand the interaction and contribution of each region of the barbed tip, we isolated individual regions of quill tips via sanding (Fig. 7, Fig 8B). Compared to the barbless quill, the penetration force does not decrease if only the first 1 or 2 mm of barbed region at the tip of the quill is included (quills 3 and 4). However, when barbs in the 2-3 mm region are included, the penetration force significantly decreases. Quill 6, which has barbs only in the 2-4 mm

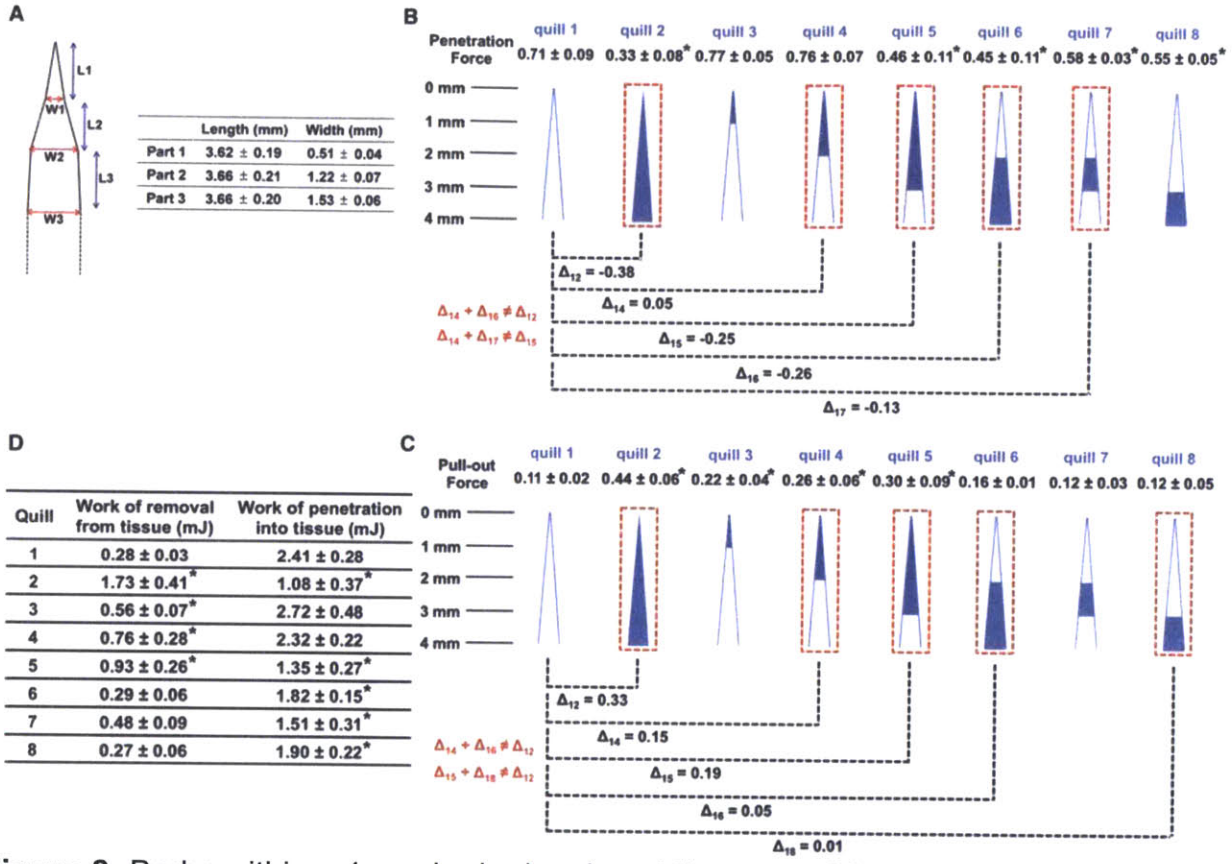


**Figure 8.** Barbs within a 4 mm barbed region at the apex of the quill work independently to minimize penetration force and cooperatively to maximize pull-out from tissue. (*A*) Dimensional analysis of the porcupine quill through length scale measurements of natural quills (mean ± standard deviation, n=5). In terms of curvature, there are three transition points. L and W indicate length and width, respectively. (*B, C*) Penetration and pull-out forces were obtained with the prepared quills via sanding to isolate the contribution of barbs within different regions (see Fig. 7) (mean ± standard deviation, n=5). The penetrating depth for all experiments was 10 mm (see Figure 12A for the experimental set-up). Cartoons depict quills prepared with specific lengths of barbs obtained through ablation with sand paper. The blue color indicates the barbed region and the white color indicates the barbless region. The penetration and pull-out forces of the prepared quills are compared to those of the barbless quill (quill 1). The difference in force is defined as $\Delta_{ij}$ ($\Delta_{ij}$ = penetration (or pull-out) force of *quill j*–penetration (or pull-out) force of *quill i*)). (*D*) Summarized work of penetration and work of removal obtained through penetration-retraction tests with muscle tissue (mean ± standard deviation, n=5). All are compared to quill 1 (*$p$<0.05, one-way ANOVA Fisher's Least Significant Difference post-hoc analysis at 95% confidence interval by using GraphPad Prism 6). (Adapted from (*5*))

region, resulted in a significant reduction of penetration force, ~0.26 N. Additionally, the 2-3 mm (quill 7) and 3-4 mm (quill 8) barbed regions independently reduce the penetration force compared to the barbless quill (quill 1). Therefore it appears the 2-4 mm barbed region close to the first transition zone is most critical for reducing the penetration force.

The presence of barbs contributes 0.33 N of pull-out force (comparing quills with a 4 mm barbed region to barbless quills ($\Delta_{12}$ = 0.33)). The 1-3 mm barbed region had less impact on pull-out force compared to the 1 mm region at the tip (Comparing quill 3 with 5). Comparing the pull-out forces between quill 5 and 2 ($\Delta_{52}$ = 0.14) suggests that the 1 mm region near the transition zone (at the base) is likely critical. However, the presence of barbs solely in the 2-4 mm region (quill 6) or in the 2-3 mm region (quill 7) did not substantially increase pull-out force compared to the barbless quill. Furthermore, barbs in the 3-4 mm region alone did not increase the pull-out force. This data suggests that barbs in different regions likely work cooperatively. Cooperativity is further supported by the lack of additive effects ($\Delta_{14}+\Delta_{16}\neq\Delta_{12}$ and $\Delta_{15}+\Delta_{18}\neq\Delta_{12}$). Taken together, the first 1 mm barbed region of tip independently makes the greatest impact on pull-out force, and the cooperation between 0-2 mm and 2-4 mm regions increases the force. Cooperativity may be a function of barb overlap where increased compressive force from tissue on barbs near the transition zone impacts barbs closer to the tip. Or barbs near the tip may experience different stresses due to the cutting of tissue by the more proximal barbs. Figure 8D shows the summary of work of removal for all quill preparations. Together these data suggest that the quill achieves adhesion by a mechanism that is more complex than simply hooking tissue fibers.

To examine how barbs generate mechanical adhesion, we investigated quill removal from both fibrous tissue and a non-fibrous control (Fig. 9). Tissue fibers interlock under the barbs, suggesting barbs may be deployed or bent during removal from tissue. We postulated that such deployment of the barbs could increase tissue adhesion by projecting barbs radially away from the quill (thus increasing the apparent quill diameter) to significantly increase frictional resistance and promote further mechanical interlocking with tissue. The ability of deployment or bending of barbs to contribute to tissue adhesion was further tested with porcine skin, which has similar

mechanical properties to human skin (*13*, *14*). The deployment or bending of barbs was observed following penetration-retraction tests with significant residual tissue adhered to the quill (Figs. 10A-D). The pull-out force for porcine skin was 2.36 ± 0.83 N (Fig. 10E) while the work of removal was 2.34 ± 0.68 mJ. Interestingly, we observed a direct correlation between the pull-out force and the number of bent barbs following removal of the quill from skin (Figs. 10F-I) and significantly greater work is required to remove a natural quill from muscle tissue compared to a PU barbed quill (Fig. 6D). Natural quill with deployable barbs requires 0.144 ± 0.048 mJ for removal, compared to 0.053 ± 0.023 mJ for non-deployable PU-barbed quill. The PU-barbed quill produces the maximum force after 2 mm of pull-out and then disengages the tissue completely at 4 mm of pull-out. However, natural quill drags tissue for a relatively long displacement generating peak-adhesion after it has been pulled beyond 4 mm. The natural quill is able to stretch tissue maximally during removal by using the bending of barbs, which increases engagement with tissue fibers. The non-deployable barbs of the PU quill, however, pull tissue and cut as the quill is removed.

Reproducing the strong tissue adhesion property of the porcupine quill would be useful for the development of mechanically interlocking tissue adhesives. As a proof of concept, we fabricated a prototypic quill-mimetic patch that has a hexagonal array of 7 replica molded PU quills (Fig. 11A). While the barbless PU quill patch showed minimal pull-out resistance (0.063 ± 0.033 N), the barbed PU quill patch achieved significantly greater tissue adhesion (0.219 ± 0.059 N, Fig. 11B). The work of removal for the barbed quill patch was >30x that of the barbless quill patch (Fig. 11B). As observed in figure 11C, the barbed quill array achieved significant interlocking with tissue whereas the barbless quill array achieved minimal interaction with tissue and thus could be easily removed. Although current barbed array systems have shown tissue adhesion, all of them feature initially deployed barbs that require high penetration force and cause tissue damage during penetration (*15*, *16*). The quill-mimetic patch is unique in that it can both easily penetrate tissue and achieve high tissue adhesion.

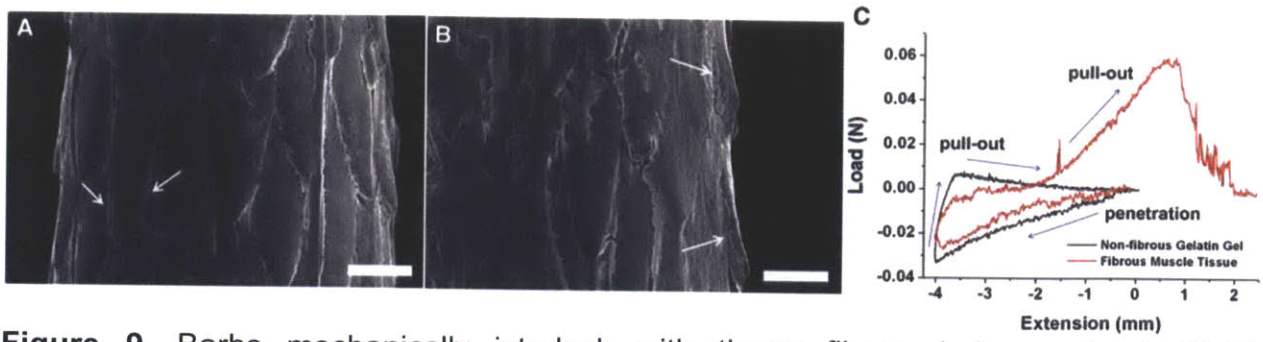


**Figure 9.** Barbs mechanically interlock with tissue fibers during pull-out. (*A-B*) characteristic FE-SEM images following removal of a barbed quill following a 4 mm penetration depth into tissue (For the FE-SEM image of the quill prior to penetration into tissue, see Fig. 1B). Residual tissue was present along the length of the barbs and under the barbs as indicated with white arrows. Scale bar represents 50 mm. (*C*) Representative force-extension curves show penetration and pull-out forces that were obtained with fibrous muscle tissue and a density matched non-fibrous model tissue fabricated from gelatin gel (n=5). (Adapted from (*5*))

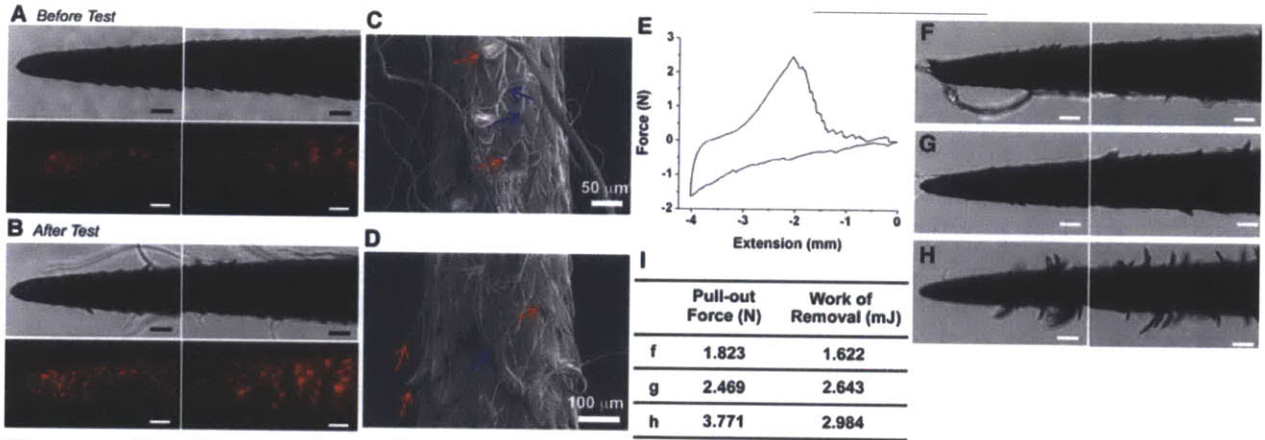


**Figure 10.** Generation of mechanical adhesion by microstructured barbs. (*A*, *B*) Representative optical and fluorescent images of porcupine quills before and after removal from porcine skin. Fluorescence images are useful to delineate the boundaries of individual barbs and are obtained by merging several images taken at different focal planes along the Z-axis. The scale bar represents 100 mm. (*C, D*) FE-SEM micrographs following removal of quills from porcine skin. Residual tissue is indicated by blue arrows. Red arrows in figures indicate bending of barbs during pull-out. (*E*) A representative force versus extension plot for a penetrating depth of 4 mm where puncture typically occurs following tissue compression of 1-2 mm (n=5). (*F-H*) Images of quills following removal from porcine skin are useful to examine the heterogeneity of tissue interactions and to establish the relationship between the bending of barbs and relative level of tissue adhesion summarized in the table (*I*). The scale bar in each image represents 100 mm. See Figure 12A for the experimental set-up for the tests with porcine skin. (Adapted from (*5*))

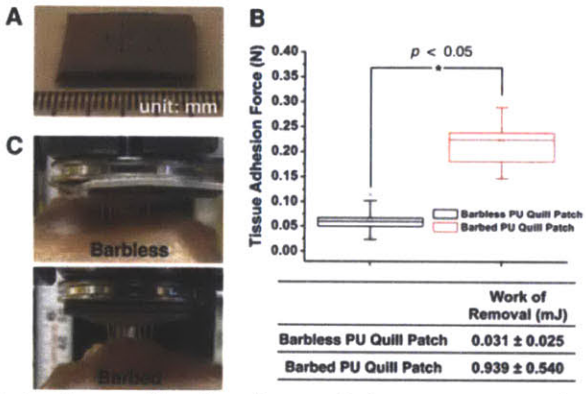


**Figure 11.** A prototypic quill-mimetic patch as a mechanically interlocking tissue adhesive. (*A*) The digital photograph shows the fabricated quill-mimetic patch, which consists of 7 PU barbless or barbed quills. (*B*) The tissue adhesion forces obtained from barbless and barbed PU quill patches (n=5, student *t*-test at the level of 95% significance). The box plot whiskers are set to ± 1.2 standard deviations. The two "X"s in box plot indicate 1st and 99th percentiles. (*C*) Shows the quill-mimetic patches interacting with muscle tissue during the retraction process from muscle tissue. (Adapted from (*5*))

## Conclusions

Herein we report how the North American porcupine quill displays a unique geometry that serves two polar opposite functions. Barbs on quills enable easy penetration into tissue and strong tissue adhesion during removal through the presence of backwards facing deployable barbs. Similar to how biomimicry of cockleburs inspired the development of Velcro® hook-and-loop fastener (*17*) and gecko is inspiring the development of tape-based tissue adhesives (*18*, *19*), these findings should serve as the basis for the bio-inspired development of new devices including needles for easy penetration with compliant substrates such as tissue or microneedles where effective insertion without deformation (buckling) is required (*20*). Mimicking the porcupine quill should be useful for biomedical applications including local anesthesia, abscess drainage, vascular tunneling, and trocar placement in addition to the development of mechanically interlocking tissue adhesives.

## Materials and Methods

### Materials

North American (specifically, Pacific Northwest) porcupine quills and African porcupine quills were purchased from Minute Bear Trading, USA. Fluorescein (sodium salt, dye content ~70%, Aldrich), rhodamine B (dye content ~90%, Sigma-Aldrich), ethanol (ACS reagent, ≥ 99.5%, 200 proof, Sigma-Aldrich), formalin solution (neutral buffered, 10%, Sigma), Sylgard® 184 silicone elastomer kit (Dow Corning, Corp., USA), UV-curable polyurethane acrylate (Minuta Tech., Korea), Irgacure 2959 (Ciba Specialty Chemicals Corporation), 18 gauge, 19 gauge, and 25 gauge needles (Becton Dickinson Company), artificial human skin (SynDaver™ Labs), muscle tissue of domesticated fowl (Shaw's, Inc.), gelatin powder (DifcoTM, BD), sand paper (3M wetordry sandpaper 413Q 400 and Norton MultiSandTM, 60), cyanoacrylate glue (Loctite 495, Loctite Corp.), industrial razor blades (surgical carbon steel, single edged No. 9, VWR), polyether ether ketone (PEEK) hex nuts (Small Parts), silicone rubber film with backing adhesive (McMaster-Carr), pin mount stubs (25.4 mm in diameter, 9.5 mm in height, and 3.2 mm in pin diameter, Ted Pella, Inc.), 5 min and 60 min epoxy glues (ITW

Performance Polymers) were used as received. The fresh porcine skin was purchased from a local butcher shop.

**Penetration-retraction Tests with Muscle Tissue and Gelatin Gel.**

Penetration-retraction tests were performed with the mechanical tester (Model 5540, Instron Corporation). Only quills with a barbed region of 4 mm in length were selected for testing, as measured with a millimeter ruler and a dissecting optical microscope (SZ-6 PLUS, Cambridge Instruments). The muscle tissue was cut into specimens with 3-4 cm width, 2-3 cm length, and 4-5 mm thickness using a razor blade. The tissue specimens were mounted within the lower grips at the base of the mechanical tester. During fixation, care was taken not to excessively compress the tissue. After the specimen was fixed between the grips, the exposed excess tissue over the grips was cut with a blade, generating a flat tissue surface (Fig. 12A). The explanted muscle tissue was static, aside from when it was compressed during penetration followed by elastic relaxation as insertion force was removed. The quill was fixed between the upper grips and the tip adjusted to contact the tissue surface. The quill was penetrated into the muscle tissue to the desired depth, typically 10 mm, at a rate of 1 mm/sec and was pulled out at a rate of 0.033 mm/sec to study how the barbs function during removal from tissue. For the duration of all experiments, the tissue was kept moist with phosphate buffered saline. Each quill was used for a single measurement. For details of experiment with gelatin gel as a non-fibrous tissue control, please see SI text.

**Preparation of the Stained Quills for Visualization during Adhesive Measurements**

Porcupine quills were immersed into 0.01% aqueous fluorescein or rhodamine B solution. After 1h, quills were removed from the staining solution and washed thoroughly with water. The stained quills were dried overnight before use.

**Penetration-retraction Tests with Porcine Skin**

Fresh porcine skin was cut into specimens with 3-4 cm width and 3 cm length using a razor blade. For adhesive measurements, porcupine quills were inserted into porcine skin, vertically aligned within the lower grips, with a penetrating depth of 4 mm.

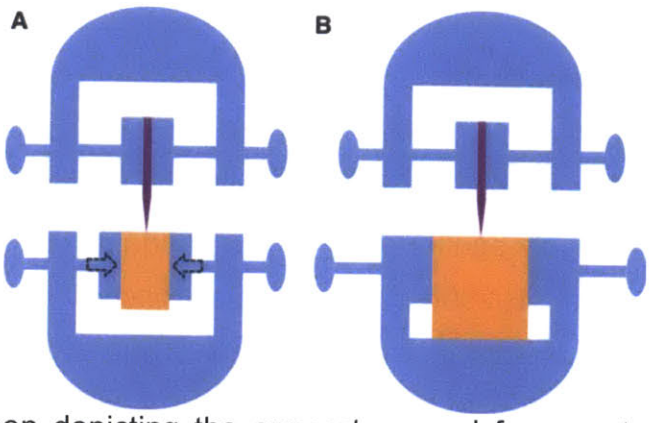


**Figure 12.** Cartoon depicting the apparatus used for *penetration-retraction* tests. (*A*) set-up for the test with muscle tissue, which was under compression. (*B*) set-up for the test with muscle tissue without compression. The muscle tissue in (B) was cut to fit exactly with the available space within the lower platform. Purple and orange colors indicate the porcupine quill and muscle tissue, respectively. Set-up (A) was utilized when we penetrated the porcupine quill into muscle tissue to a depth up to 10 mm. As the thickness of muscle tissue was <10 mm, we rotated the tissue vertically within the lower grips to allow penetration in the transverse direction. Set-up (B) was used to adequately compare data from the tests with gelatin gel and muscle tissue. This comparison was useful to examine how barbs generate mechanical adhesion with tissue by examining quills following retrieval. To minimize any movement of muscle tissue, which was not under compression, we used thicker muscle tissue (i.e. chicken breast). Since the quill was consistently covered by tissue when 10 mm was used as a penetrating depth, obscuring observation of barbs, a penetrating depth of 4 mm was used. The penetrating depth of all tests with set-up (B) was 4 mm. The test with porcine skin was performed with the set-up (A) as the skin was <10 mm thick. Furthermore, to study mechanisms of tissue adhesion with porcine skin, 4 mm was used as a penetrating depth. (note: we utilized set-up (A) for generating the data in Figures 1, 8, and 10. We used set-up (B) for the data in Figures 5, 6, 9, and 11. It is important to consider that the differences in models impacted the force profiles and puncture and penetration forces. In set-up (A), quill removal from tissue did not extend beyond zero in the force-extension curve. In set-up (B) where tissue was not in compression (likely mimicking how quills penetrate tissue in nature), the quill is pulled beyond 0 when it is removed from tissue). (Adapted from (*5*))

The remainder of the test followed the procedure previously described for muscle tissue.

**Surface Characterization of the Quills**

The microstructures of the porcupine quills before and after penetration-retraction tests were examined with field-emission scanning electron microscope (FE-SEM, JEOL 5910) following a 30 nm-thick gold sputter coating. Light and fluorescence images were obtained with a Nikon Eclipse TE-2000-U microscope (Nikon Digital Sight DS-QiMC camera, Japan). The length of barbed region of each quill was examined with a dissecting optical microscope (SZ-6 PLUS, Cambridge Instruments) and optical digital images were obtained (IXY Digital, Canon, Japan).

**Histological Analysis**

The porcupine quill was penetrated into muscle tissue at a rate of 1 mm/sec until the force reached 0.2 N. The sample was then fixed by immersing it into 10% buffered formalin for 24 h. The fixed sample was washed with water and stored in 70% ethanol prior to embedding in paraffin. The sample was then dehydrated with 95% and 100% ethanol solutions and embedded in paraffin (Thermo Electron Shandon Excelsior tissue processor). 5-μm sections of embedded samples were obtained with a rotary microtome (Thermo Scientific Shandon Finesse ME+). Sections were stained with haematoxylin and eosin, cover-slipped with a xylene-based mounting medium, and the prepared slides were examined with a Nikon Eclipse TE-2000-U microscope (Nikon Digital Sight DS-QiMC camera, Japan).

**Micro-Computed Tomography (Micro-CT)**

The porcupine quill was penetrated into muscle tissue at a rate of 1 mm/sec until the force reached 0.2 N. The sample was then fixed by immersing it into 10% buffered formalin for 24 h. The fixed sample was washed with water and dehydrated. For each 25%, 50%, 75%, and 100% ethanol solutions, the sample was incubated for 30 min. The sample was then evaluated using a microtomographic imaging system (eXplore CT 120, Gamma Medica, Northridge, California). CT slices of the sample were acquired by using 1200 views with 25-μm isotropic voxels, a tube voltage of 80 kVp, 32 mA current, and 100 ms exposure time. The sample images were obtained to include the entire region of the quill and tissue. Images were reconstructed, filtered, and a specimen-

specific threshold was applied. The penetrating depth of the porcupine quill within tissue was computed by using a direct three-dimensional approach that does not rely on assumptions regarding the underlying structure.

**Fabrication of Polyurethane (PU) Quills and Quill-mimetic Needles**

Poly(dimethylsiloxane) (PDMS) pre-polymer was prepared by mixing the base material and curing agent in a 10:1 ratio. After vigorous mixing and degassing, PDMS molds of natural barbed and barbless quills were prepared by thermal curing at 70 °C overnight. To make quill-mimetic needle, a 25 gauge needle was inserted into the quill's base. After curing PDMS, the quill and needle were removed to produce PDMS molds. The polyurethane acrylate, which was mixed with 0.1% photo-initiator, was added into the PDMS molds. To fabricate a quill-mimetic needle, a 25 gauge needle was again inserted into the mold at this stage allowing the polyurethane to bond to the needle. The samples were placed in a vacuum desiccator in the dark to degas the samples for 1-2 hours. The samples were then cured under UV (254 nm) for 90 min and removed from the molds.

**Measurement of Penetration Force of PU Quills and Needles with Tissue**

A thick section of muscle tissue was prepared to fit with the available space between the lower grips of mechanical tester. The prepared tissue was placed between the grips without compression. The PU quill was fixed between the upper grips of mechanical tester and the tip adjusted to contact the tissue surface. The quill was penetrated into the muscle tissue to the desired depth, 4 mm, at a rate of 1 mm/sec. For the duration of all experiments, the tissue was kept moist with phosphate buffered saline. Each quill was used for a single measurement. The mean penetration force was measured from n=5 different samples.

The penetration force of quill-mimetic PU needle was examined with artificial skin (SynDaver Labs) that mimics the property of human skin. The fabricated PU needle was connected with a force gauge (Model FGV-5XY, Nidec-Shimpo Corp., Japan), and inserted manually into the skin tissue. The force gauge reads the required penetration force. Each needle was used at least 4 times. The mean penetration force was obtained from n=3 different samples.

**Fabrication of a Quill-mimetic Patch with a Hexagonal Array of PU Quills**

The tip (5 mm-length) of natural quills was replicated with a hex nut base and arranged in a hexagonal array with a silicone backing layer using 60 min epoxy glue. Following generation of PDMS molds of barbed or barbless quills, we followed the same procedure descried previously to produce replica molded PU quills. The 7 PU barbed/barbless samples were then assembled with silicone backing layer. The hex base of PU quills allowed for simple alignment of a hexagonal array. To ensure that the array was stable, another backing layer was attached to the assembled sample using 5 min epoxy glue. All PU quills within the patch were perpendicular to the backing layer.

**Measurement of Tissue Adhesion Force of Quill-mimetic Patch**

A modification of ASTM F2258-05 was used to measure the tissue adhesion force of quill-mimetic patches. A flat section of muscle tissue was affixed using cyanoacrylate glue to test fixtures (i.e. pin mount stub with diameter of 25.4 mm). The prepared tissue sample was mounted within the lower grips at the base of the mechanical tester. The quill-mimetic patch was glued onto another fixture, and the prepared patch was fixed between the upper grips of mechanical tester. The tips of quills within the patch were adjusted to contact the tissue surface. The patch was penetrated into the muscle tissue to a depth of 4 mm at a rate of 1 mm/sec and was pulled out at a rate of 0.033 mm/sec to study how the barbs function during removal from tissue. For the duration of all experiments, the tissue was kept moist with phosphate buffered saline. The mean tissue adhesion force was measured from n=5 different samples.

**Finite Element Analysis (FEA)**

For the finite element simulation, we employed a two-dimensional approximation of the geometry. We model the quill and barbs as a linear elastic material with Young's modulus E = 3.25 GPa and Poisson's ratio $\nu$ = 0.4 as determined from uniaxial tension experiments of quill tips. The porcine skin is modeled as a non-linear incompressible material using the inverse Langevin model (*21*, *22*) with an initial shear modulus $\mu$ = 0.165 MPa and locking stretch $\lambda_L$ = 1.81. Please see the details in SI text.

## Acknowledgments

We would like to thank Admet Inc. for generously providing an eXpert 760 mechanical tester that was instrumental for this work. This work was supported by National Institutes of Health grant GM086433 and the American Heart Association grant 0835601D to JMK, the National Science Foundation Grant NIRT 0609182 and National Institutes of Health grant DE013023 to RL, and the National Research Foundation of Korea Grant funded by the Korean Government (Ministry of Education, Science and Technology) [NRF-2010-357-D00277]. We would like to thank the National Science Foundation Graduate Research Fellowship program and the Hugh Hampton Young Memorial Fund for supporting JA and the MIT UROP program for supporting AK and RKR. We would also like to thank the China Scholarship Council and the National Natural Science Foundation of China (No: 50702043; 51072159), Program for New Century Excellent Talents in Universities (Chinese Ministry of Education, 2301G107aaa) for supporting DG. We thank Dr. E. O'Cearbhaill and Bryan Laulicht for helpful discussions.

## References


1. U. Roze, The North American Porcupine, *Cornell University Press* (2009).

2. J. Vincent, P. Owers, Mechanical design of hedgehog spines and porcupine quills, *Journal of Zoology* (1986).

3. T. A. Vaughan, J. M. Ryan, N. J. Czaplewski, Mammalogy, *Saunders College Publishing, Philadelphia* (2000).

4. A. Kurta, Mammals of the Great Lakes region, *Univ of Michigan Press, AnnArbor* (1995).

5. W. K. Cho *et al.*, Microstructured barbs on the North American porcupine quill enable easy tissue penetration and difficult removal, *Proceedings of the National Academy of Sciences* **109**, 21289–21294 (2012).

6. T. Azar, V. Hayward, Estimation of the fracture toughness of soft tissue from needle insertion, *Biomedical Simulation* (2008).

7. O. A. Shergold, N. A. Fleck, Experimental investigation into the deep penetration of soft solids by sharp and blunt punches, with application to the piercing of skin, *J Biomech Eng* **127**, 838–848 (2005).

8. O. A. Shergold, N. A. Fleck, Mechanisms of deep penetration of soft solids, with application to the injection and wounding of skin, *Proceedings of the Royal Society A: Mathematical, Physical and Engineering Sciences* **460**, 3037–3058 (2004).

9. S. Das, A. Ghatak, Puncturing of soft gels with multi-tip needles, *Journal of materials science* (2011).

10. A. A. Sharp, A. M. Ortega, D. Restrepo, D. Curran-Everett, K. Gall, In vivo penetration mechanics and mechanical properties of mouse brain tissue at micrometer scales, *IEEE Trans Biomed Eng* **56**, 45–53 (2009).

11. P. S. L. Anderson, M. LaBarbera, Functional consequences of tooth design: effects of blade shape on energetics of cutting, *J. Exp. Biol.* **211**, 3619–3626 (2008).

12. F. Maier, A. Bornemann, Comparison of the muscle fiber diameter and satellite cell frequency in human muscle biopsies, *Muscle Nerve* **22**, 578–583 (1999).

13. J. Ankersen, A. E. Birkbeck, R. D. Thomson, P. Vanezis, Puncture resistance and tensile strength of skin simulants, *Proc Inst Mech Eng H* **213**, 493–501 (1999).

14. C. Edwards, R. Marks, Evaluation of biomechanical properties of human skin, *Clin. Dermatol.* **13**, 375–380 (1995).

15. M. L. Reed, H. Han, L. E. Weiss, Silicon micro velcro, *Adv. Mater.* (1992).

16. P. Griss, P. Enoksson, G. Stemme, Micromachined barbed spikes for mechanical chip attachment, *Sensor Actuat A-Phys* (2002).

17. P. Forbes, The Gecko's Foot: Bio-Inspiration: Engineering New Materials From Nature Author: Peter Forbes, Publisher: WW Norton &, (2006).

18. A. Mahdavi *et al.*, A biodegradable and biocompatible gecko-inspired tissue adhesive, *Proceedings of the National Academy of Sciences* **105**, 2307–2312 (2008).

19. J. M. Karp, R. Langer, Materials science: Dry solution to a sticky problem.*Nature* **477**, 42–43 (2011).

20. M. Yang, J. D. Zahn, Microneedle insertion force reduction using vibratory actuation, *Biomed Microdevices* **6**, 177–182 (2004).

21. A. Cohen, A Padé approximant to the inverse Langevin function, *Rheologica Acta* (1991).

22. E. M. Arruda, M. C. Boyce, A three-dimensional constitutive model for the large stretch behavior of rubber elastic materials, *Journal of the Mechanics and Physics of Solids* (1993).